Variational Motion Design
for Adaptive Structures

Renate Sachse
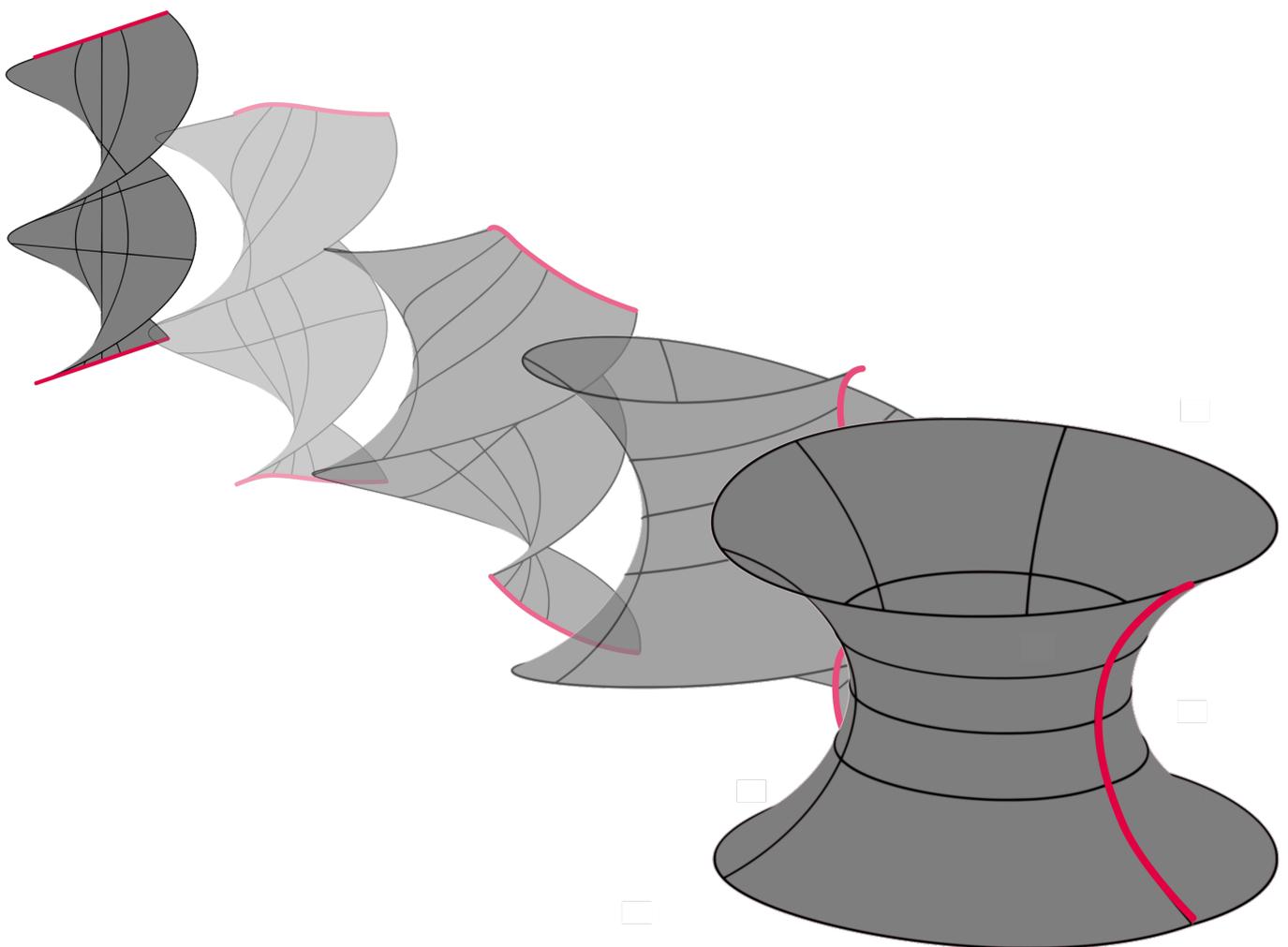
Variational Motion Design
for Adaptive Structures

von

Renate Sachse

Variational Motion Design
for Adaptive Structures

vorgelegt von

Renate Sachse

aus Stuttgart

Kurzfassung

In der gesellschaftlichen Debatte über zukünftige Querschnittsthemen spielen Nachhaltigkeit und Ressourceneffizienz eine zunehmend entscheidende Rolle. Im Bauwesen, aber auch in anderen Disziplinen wie dem Flugzeugbau oder der Raumfahrttechnik, bieten adaptive Strukturen das Potenzial, diesen Anforderungen gerecht zu werden. Während manche Tragwerke Kräfte und Verformungen aus sich verändernden Lasten unter weitestgehender Beibehaltung ihrer Form ausgleichen können, vollziehen andere Strukturen durch eine entsprechende Aktuierung erhebliche Geometrieänderungen, um sich an wechselnde Anforderungen während der Nutzung des Bauwerks anzupassen. Dies ist beispielsweise der Fall bei ausfahrbaren Stadiondächern oder bei Fassadenelementen, die sich je nach Stand der Sonne verformen und damit das Klima der Innenräume steuern können. Dabei muss die Struktur oft in der Lage sein große Deformationen ausführen zu können. Um dies zu ermöglichen, werden flexible Strukturen entworfen, die sich mit geringem Aufwand in eine bestimmte Richtung verformen können. Unabhängig von der Geometrie kann aber auch der Verformungsprozess an sich gezielt so gestaltet werden, um vorgegebene Anforderungen, wie zum Beispiel die Anforderung der Effizienz, zu erfüllen.

In dieser Arbeit wird ein neuartiger Ansatz zur Gestaltung adaptiver Strukturen vorgestellt und schrittweise entwickelt: die Methode des sogenannten Bewegungsentwurfs („Motion Design"). Ihr liegt die Tatsache zugrunde, dass je nach Steuerung der Aktuierung der gleiche Deformationszustand einer Struktur durch unterschiedliche Bewegungsabläufe erreicht werden kann. Die Methode des Bewegungsentwurfs ermöglicht es, optimale Bewegungen mit definierten Eigenschaften zwischen der Anfangsgeometrie und einer vorgegebenen deformierten Endgeometrie einer Struktur auf rein formalisierte Weise zu berechnen. Sie kann demzufolge angewendet werden, ohne dass umfassendes Ingenieursverständnis für die Lösungsfindung eingebracht werden muss. Dabei wird von quasi-statischem Verhalten ausgegangen, aber beliebig große Deformationen berücksichtigt.

Um die Effizienz einer Bewegung strukturmechanisch zu motivieren und zugleich auch mathematisch quantifizierbar zu machen, werden die sogenannten Deformationskosten als Zielgröße eingeführt. Diese sind abgeleitet von der dimensionslosen Größe der Transportkosten aus Bereichen wie der Biologie oder Robotik. Diese Transportkosten stellen ein Maß zur Quantifizierung der Energieeffizienz verschiedener Transportmethoden dar, wie zum Beispiel Gehen, Schwimmen, Fliegen eines Tieres oder Bewegung eines Fahrzeugs von einem zu einem anderen Ort. Im Kontext dieser Arbeit wird diese Größe hier auf flexible Strukturen übertragen. Dabei wird exemplarisch zunächst ein Energiekriterium auf Basis der inneren Energie verwendet. Um den gesamten Deformationsprozess berücksichtigen zu können, wird die interne Energie über den Deformationspfad integriert. Die Arbeitshypothese hierbei ist, dass es Aufwand erfordert Verzerrungsenergie in ein System einzubringen sowie die Struktur in einem verformten Zustand zu halten. Die so berechneten Deformationskosten ergeben dadurch ein geeignetes Maß für den

erforderlichen Aufwand, um eine Struktur in einen definierten Deformationszustand zu verformen. Sie stellen im Sinne der mathematischen Optimierung demnach die Zielfunktion für die Methode des Bewegungsentwurfs dar. Die Gültigkeit der mit dieser Funktion erhaltenen Bewegungen ist daher auf die Fälle limitiert, in denen diese Annahmen zutreffen.

Diese Problemstellung zeigt Analogien zum historischen Brachistochronenproblem, welches eine entscheidende Rolle bei der Entwicklung der Variationsrechnung einnahm. Deswegen basiert auch die Methode des Bewegungsentwurfs auf einer variationellen Formulierung mit den Deformationskosten als zugrunde liegendem Funktional und dem Verschiebungsfeld als gesuchter Funktion. Einer der entscheidenden Aspekte dieser Arbeit ist demzufolge die Diskretisierung dieses Bewegungspfades, also letztlich des Deformationsprozesses. Mithilfe der hier vorgestellten Methodik wird der gesamte Bewegungspfad durch eine Lösung eines einzigen nichtlinearen Problems berechnet und nicht mehr inkrementell, wie es bei einer klassischen nichtlinearen Strukturanalyse üblich ist. Durch den speziellen Aufbau des Funktionals, beziehungsweise der Zielfunktion, können im Rahmen eines Optimierungsalgorithmus analytische Sensitivitäten berechnet werden. Bei Verwendung der Verzerrungsenergie in den Deformationskosten werden dafür lediglich Größen benötigt, die ohnehin bereits in Finite-Elemente-Programmen zur Verfügung stehen, wie zum Beispiel die diskreten inneren Kräfte und die Tangentensteifigkeitsmatrix.

Die Methode des Bewegungsentwurfs wird zunächst anhand von einigen Beispielen verifiziert, deren Lösung bereits bekannt ist. Zusätzlich werden Strukturen untersucht, die durch Instabilitätsphänomene, wie zum Beispiel Durchschlagen, gekennzeichnet sind. Dies ermöglicht einen innovativen Bewegungsentwurf für adaptive Strukturen, bei dem Instabilitäten auch gezielt zum Zwecke der Effizienz genutzt werden können, anstatt sie zu vermeiden. Darüber hinaus wird die Anwendbarkeit auf den Entwurf dehnungsloser Verformungen von Schalen demonstriert. Die vorgestellte Methode eignet sich demnach besonders gut für die Identifizierung und den Entwurf kinematischer und energieminimaler Bewegungsmechanismen, was das Potenzial für die Anwendung bei wandelbaren Strukturen aufzeigt.

Mithilfe der statischen Gleichgewichtsbedingungen werden in einem Rückrechnungsschritt die erforderlichen Lasten berechnet, um auch optimale nicht-kinematische Bewegungen effizient zu realisieren. Das setzt zunächst die Annahme voraus, dass eine Aktuierung prinzipiell an jedem Freiheitsgrad möglich ist. Für Strukturen, bei denen die Aktuierung, wie in der Baupraxis üblich, nur durch bestimmte Lastfälle ermöglicht wird, werden entsprechende Nebenbedingungen in das Optimierungsproblem des Bewegungsentwurfs eingebracht („Constrained Motion Design"). Dadurch wird erreicht, dass allein die vorgegebenen zugelassenen Lasten zur Durchführung der optimierten Bewegung verwendet werden. Auch hier beweisen numerische Experimente die Anwendbarkeit dieser erweiterten Methode des Bewegungsentwurfs unter Berücksichtigung von Nebenbedingungen. Zusätzlich wird eine Aktorelementformulierung vorgestellt, die einfach in die Berechnungsmethode integriert und somit auch als spezieller Lastfall zur Aktuierung

betrachtet werden kann. Außerdem können auch andere Arten von Nebenbedingungen eingebracht werden, wie zum Beispiel die Einhaltung einer positiv definiten Tangentensteifigkeitsmatrix während der gesamten Deformation. Auf diese Weise wird beim Bewegungsentwurf automatisch sichergestellt, dass die optimierte Bewegung in einem lastkontrollierten Prozess stabil ausgeführt werden kann.

Abschließend werden zusätzliche Erweiterungsmöglichkeiten der Methode des Bewegungsentwurfs beziehungsweise Kombinationen mit anderen Methoden zur Effizienzerhöhung von adaptiven Strukturen untersucht. Beispielsweise kann auch die Form der noch undeformierten Struktur deutlich zur Effizienz der Bewegung beitragen. Deswegen wird auch der Einfluss einer Formoptimierung der Anfangsgeometrie analysiert. Mithilfe von geeigneten Zielfunktionen kann dadurch eine weitere Reduktion der Deformationskosten und somit eine noch nachhaltigere und ressourceneffizientere Gestaltung von adaptiven Strukturen erreicht werden. Während die Art der Aktuierung zunächst immer vorgegeben war, kann auch sie in den Entwurfsprozess mit einbezogen werden. Dafür wird der Bewegungsentwurf mit etablierten Methoden zur Aktorplatzierung kombiniert. Auf diese Weise kann die Position der effizientesten Einzellasten für eine energieminimale Bewegung bestimmt werden. Zusätzlich werden unterschiedliche Modifikationen der zugrunde liegenden Zielfunktion, also der Deformationskosten, im Rahmen der Methode aufgezeigt. Unter anderem kann auf einfache Weise die Bewegung mit der kürzesten Deformationstrajektorie berechnet werden. Dies ist der Ausgangspunkt für die Vorstellung eines inkrementellen Verfahrens für den Bewegungsentwurf, welches sich auch für komplexere Problemstellungen eignet und dessen Wirkprinzip exemplarisch an einer biologischen Struktur gezeigt wird.

Abstract

In the social debate on future cross-cutting subjects, sustainability and efficiency of material resources play an increasingly decisive role. In civil engineering and other disciplines, such as aviation or aerospace, adaptive structures offer the potential to meet these requirements. While some structures are able to compensate for forces and deformations from varying loads mostly retaining their shape, other structures undergo substantial shape changes via actuation to adapt to alternating requirements during usage of the building. This is, for example, the case with retractable stadium roofs or with façade elements, which can deform depending on the position of the sun and, thus, control the climate of the interior. In doing so, the structure must often be able to carry out large deformations. For this purpose, flexible structures are designed, which are capable of deforming in a certain direction with little effort. Regardless of the geometry, however, the deformation process itself can also be designed to meet predetermined requirements, such as the requirement for efficiency.

In this thesis, a novel approach for the design of adaptive structures is presented and gradually developed: the so-called method of motion design. It is based on the observation that, depending on the control of the actuation, the same deformation state of a structure can be reached through various motion processes. The method of motion design allows to calculate optimal deformation paths with defined properties between the initial geometry and a given deformed end geometry of a structure in a purely formalized way. It can hence be applied without the need for a profound engineering understanding of the solution process. Quasi-static behavior is assumed, but large deformations are taken into account.

In order to motivate the efficiency of a movement and to make it mathematically quantifiable, the so-called cost of deformation is introduced as a target value. It is derived from the dimensionless quantity cost of transport from disciplines such as biology or robotics. This cost of transport represents a measure to quantify the energy efficiency of different transport methods, such as walking, swimming, flying of an animal or moving of a vehicle from one place to another. In the context of this work, this measure is transferred to flexible structures, where an energy criterion based on the strain energy is first exemplarily employed. In order to consider the entire deformation process, the internal energy is integrated over the deformation path. The applied working hypothesis is that inducing strain energy into a system and maintaining this internal strain state state requires effort. Thus, the cost of deformation calculated in this way provides a suitable measure of the effort required to deform a structure into a defined deformation state. Consequently, it represents the objective function used for the motion design method in terms of mathematical optimization. The validity of motions obtained with this function is therefore limited to cases, in which these assumptions apply.

This problem formulation shows clear analogies to the historical brachistochrone problem, which played a decisive role in the development of the calculus of variations. Hence, the method of motion design is developed based on a variational formulation using the

cost of deformation as underlying functional and the displacement field as the unknown function. One of the decisive features in this work is the discretization of this motion path, i. e., the deformation process. As a result of the presented methodology, the entire motion path is obtained by solving one nonlinear problem instead of applying an incremental procedure, as is usually the case in a classical nonlinear structural analysis. Due to the special structure of the functional, or objective function, respectively, analytical sensitivities can be calculated within an optimization algorithm. When using the strain energy in the cost of deformation, only quantities that are generally already available in finite element software, such as the discrete internal forces and the tangent stiffness matrix, are required.

The method of motion design is first verified using various examples whose solutions are already known. Additionally, structures characterized by instability phenomena, such as snap-through, are investigated. This allows an innovative motion design for adaptive structures, where instabilities can specifically be used for efficiency instead of avoiding them. Furthermore, the applicability to the design of inextensional deformations of shells is demonstrated. The presented method is, therefore, particularly well suited for identification and design of kinematic and energy-minimal motion mechanisms, which emphasizes the potential for application to deployable shape changing structures.

By means of the static equilibrium conditions, the required loads to also efficiently realize optimal non-kinematic motions are calculated in a postprocessing step. This a priori implies the assumption that any degree of freedom can be controlled and actuated. For structures, where actuation is only possible by certain load cases, as usual in practical applications, corresponding constraints are introduced into the optimization problem of motion design. This ensures that only specifically permitted loads are used to perform the optimized motion. Again, numerical experiments prove the applicability of this extended motion design method under consideration of constraints. In addition, an actuator element formulation is presented that allows an easy integration into the calculation method and can also be considered as a special load case for actuation. Furthermore, other types of constraints can be introduced, such as maintaining a positive definite tangent stiffness matrix during the entire deformation. In this way, the motion design method automatically ensures that the optimized motion can be performed in a stable manner within a load-controlled process.

Finally, additional enhancement possibilities of the motion design method or combinations with other methods to increase the efficiency of adaptive structures are investigated. For example, the shape of the yet undeformed structure also has an influence and can significantly contribute to the efficiency of the movement. Therefore, the potential of a shape optimization of the initial geometry is examined. With the help of suitable objective functions, a further reduction of the cost of deformation and, therefore, a more sustainable and resource efficient design of adaptive structures can be achieved. While the type of actuation has always been predefined at first, it can also be included in the design process. In this way, the most efficient position of point loads for actuation of an energy-minimal motion can be determined. Additionally, several modifications of the

underlying objective function within the method are demonstrated. Among other things, the motion with the shortest deformation trajectory can be calculated in a simple way. This represents the starting point for an incremental method for motion design, which is suitable for more complex problems, shown on the example of a biological structure.

„Der Weg ist das Ziel.“

Konfuzius
(Chinesischer Philosoph, 551-479 v. Chr.)

Danksagung

Die vorliegende Arbeit entstand während meiner Zeit als wissenschaftliche Mitarbeiterin am Institut für Baustatik und Baudynamik der Universität Stuttgart. Während dieser Zeit haben so viele Personen auf unterschiedlichste Art und Weise positiv zu dieser Arbeit beigetragen, dass diese Danksagung den meisten leider bei weitem nicht gerecht wird.

Der erste und besonders große Dank geht an meinen Doktorvater Prof. Dr.-Ing. habil. Manfred Bischoff – zunächst für die Möglichkeit zur Promotion, aber vor allem für die extrem geduldsame Unterstützung in allen Phasen dieser Doktorarbeit. Seine Begeisterung für die wissenschaftliche Arbeit sowie das Engagement und die Fähigkeit auch andere für die Wissenschaft zu beigestern haben auch mich in das "Team Baustatik" geführt. Das große Vertrauen in jeden einzelnen Mitarbeiter und die damit verbundenen Freiheiten haben mich stets sehr motiviert und mir erlaubt, mich während der gesamten Zeit fachlich sowie persönlich zu entwickeln. Gleichzeitig wusste ich aber immer, dass Hilfe und Rückendeckung sofort vorhanden sind, sobald sie erforderlich werden. Vielen Dank auch für die Vorbereitung auf alles, was danach in einer beruflichen Laufbahn auf uns zukommt und für das Nahebringen von Werten für gute Forschung und wissenschaftliche Praxis.

Des Weiteren danke ich Herrn Prof. Dr.-Ing. Kai-Uwe Bletzinger für das aufrichtige Interesse an meiner Arbeit und die Übernahme des Mitberichts. Ich habe mich besonders darüber gefreut, da wir schon in einer frühen Phase meiner Promotion Gedanken ausgetauscht hatten, die mich während der Bearbeitung positiv begleitet haben.

Zusätzlich möchte ich mich bei Herrn Prof. Dr.-Ing. Dr.-Ing. E.h. Dr. h.c. Ekkehard Ramm bedanken. Seine Nahbarkeit gegenüber uns Doktoranden und die Möglichkeit von zahlreichen Erfahrungen zu lernen und profitieren sind bei weitem nicht selbstverständlich. Mich haben unsere fachlichen Diskussionen immer sehr motiviert. Vielen Dank für die Hilfe und Geduld bei fachlichen, beruflichen und auch anderen einfach nur interessierten Nachfragen.

Ein weiterer Dank geht an Dr.-Ing. Malte von Scheven. Du hältst die Dinge am Institut in geregelten Bahnen und uns Doktoranden dabei den Rücken frei. Danke außerdem für das Beantworten tausender Fragen, das Einrichten zahlreicher von mir benötigter Technik und Software und deine allgemeine Unterstützung und Beratung.

Ich bin außerdem sehr dankbar für meine aktuellen und ehemaligen Kollegen, die ich während der Zeit am Institut kennenlernen durfte, und für die zahlreichen Freundschaften, die sich daraus entwickelt haben. Vielen Dank für wichtigen fachlichen Input im Rahmen zahlreicher Diskussionen, Abschlussarbeiten und Kooperationen. Danke auch für jegliche lustige, ernste, informative, motivierende und persönliche Gespräche in der Kaffeeküche, den Büros und an vielen anderen Orten. Auch in der Endphase dieser Arbeit konnte ich immer auf eure Unterstützung zählen, ob beim Korrekturlesen oder der fachlichen, organisatorischen und mentalen Prüfungsvorbereitung. Besonders

möchte ich meinem Bürokollegen Dr.-Ing. Bastian Oesterle danken, der mich schon während des Studiums betreut, mich zu einer möglichen Promotion beraten und auch meinen Weg dabei bis zum Ende freundschaftlich begleitet hat. Ich behalte meine Zeit am Institut durch das "Team Baustatik" immer in positiver Erinnerung.

Ich danke auch meiner engen Kooperationspartnerin Dr. Anna Westermeier. Mir hat unsere interdisziplinäre Arbeit viel Freude bereitet und du hast mir noch einen ganz anderen spannenden Aspekt unserer Forschung in der Mechanik gezeigt. Außerdem durfte ich während der gesamten Zeit Kollegen an anderen Instituten, Fakultäten und Universitäten kennenlernen. Mir haben unsere Gespräche und der Austausch über gemeinsame Herausforderungen und Unterschiede sehr gutgetan und ich bin froh, dass auch daraus für mich sehr wertvolle Freundschaften entstanden sind.

Nicht zuletzt aber im ganz Besonderen danke ich meiner gesamten Familie. Ohne euch wären mein Studium und diese Arbeit nicht möglich gewesen und ihr habt mich während der ganzen Zeit unterstützt. Danke, dass ihr immer und bedingungslos hinter mir steht!

Stuttgart, im Februar 2021   Renate Sachse

Contents

List of Figures

List of Abbreviations

Abbreviations

EAS .... Enhanced Assumed Strain

EP .... Equilibrium Point

HOT .... Higher-order terms

NURBS ...... Non-Uniform Rational B-Splines

PCC .... Piecewise Constant Curvature

Mathematical notations

$(\bullet)^{-1}$ .... Inverse of $(\bullet)$

$(\bullet)^{\mathrm{T}}$ .... Transpose of $(\bullet)$

$(\bullet)^{-\mathrm{T}}$ .... Transpose of the inverse of $(\bullet)$

$(\bullet \cdot \bullet)$ .... Scalar product of vectors or inner product of tensors

$(\bullet \times \bullet)$ ...... Cross product

$\mathrm{d}(\bullet)$ .... Infinitesimal quantity of $(\bullet)$

$\delta(\bullet)$ .... Variation of $(\bullet)$

$\Delta(\bullet)$ .... Incremental quantity of $(\bullet)$

$\mathrm{Im}(\bullet)$ .... Imaginary part of $(\bullet)$

$\mathrm{Div}(\bullet)$ .... Divergence of $(\bullet)$ in the reference configuration

$\mathrm{LIN}(\bullet)$ ..... Linearization of $(\bullet)$

$\frac{\mathrm{d}(\bullet)}{\mathrm{d}(\bullet)}$ .... Total derivative

$\frac{\partial(\bullet)}{\partial(\bullet)}$ .... Partial derivative

$\max(\bullet,\bullet)$ ..... Function that returns the larger value of the two scalars $(\bullet,\bullet)$

$\det(\bullet)$ .... Determinant of matrix $\bullet$

$\mathrm{tr}(\bullet)$ .... Trace of $(\bullet)$

$\bigcup$ .... Assembly operator

$\cup$ .... Union

$\cap$ .... Intersection

$\varnothing$ .... Empty set

Latin letters

a .... Point of differentiation

A .... Cross-sectional area

$\hat{\mathbf{b}}$ .... Vector of the external body forces

B_α .... Component of strain-displacement-operator of an actuator element associated with elogation parameter

$\mathbf{B}$ .... Strain-displacement-operator

$\mathbf{B}_\mathrm{d}$ .... Component of strain-displacement-operator of an actuator element associated with displacement degrees of freedom

c_i .... Complementarity parameter

C .... Constant

C_i .... Complementarity function associated with constraint i

$\mathbb{C}$ .... Material tensor of fourth order

$\mathrm{d}A,\ \mathrm{d}a$ .... Infinitesimal surface element in reference and current configuration

$\mathrm{dV},\ \mathrm{dv}$ .... Infinitesimal volume element in reference and current configuration

$\mathrm{d}\mathbf{X},\ \mathrm{d}\mathbf{x}$ ...... Infinitesimales line element in reference and current configuration

$\mathbf{d}$ .... Vector of element degrees of freedom in the spatial discretization

$\bar{\mathbf{d}}$ .... Vector of element degrees of freedom in the path discretization

D .... Displacement value

$\mathbf{D}$ .... Vector of total degrees of freedom in the spatial discretization

$\bar{\mathbf{D}}$ .... Vector of total degrees of freedom

e .... Element in finite element discretization

$\mathbf{e}_{1\text{–}3}$ .... Normalized basis vectors in Cartesian coordinate system

E .... Young's modulus

E_d .... Total Green-Lagrange strain in an actuator element

E_el .... Elastic Green-Lagrange strain in an actuator element

E_α .... Actuation strain

$\mathbf{E}$ .... Green-Lagrange strains

$\mathbf{f}_\mathrm{int,act}$ .... Vector of local actuator forces

$\mathbf{f}_{\text{int}}$, $\mathbf{f}_{\text{ext}}$ ...... Vectors of local internal and external forces

F .... Generalized function in functional

$\mathbf{F}$ .... Deformation gradient

$\mathbf{F}_{\text{int}}$, $\mathbf{F}_{\text{ext}}$ .... Vectors of global internal and external forces

g .... Constraint

$\mathbf{g}$ .... Vector of constraints

$\mathbf{g}_F$ .... Vector of constraints associated with constraints on forces

$\mathbf{g}_{\text{det}}$ .... Vector of constraints associated with constraints on the determinant of the stiffness matrix

$\mathbf{G}$ .... Matrix that comprises the first derivatives of constraints

h .... Distance to neighboring point

$\mathbf{H}_i$ .... Hesse matrix/second derivative of constraint i

$\mathbf{I}$ .... Identity tensor or identity matrix

J .... Functional

J_{u} .... Functional for the minimization of the deformation trajectory

J_{Π^j} .... Functional based on the internal energy with the exponent j

$J_{\Pi_{\text{act}}}$ .... Functional based on the actuation energy

$J_{\Pi_{\text{el}}}$ .... Functional based on the internal elastic energy

J_{Π} .... Functional based on the internal energy

$\hat{J}$ .... Extended functional

$\mathbf{J}$ .... Jacobian matrix

k .... Node in finite element discretization

$\mathbf{k}_{\text{act}}$ .... Stiffness matrix of an actuator element

$\mathbf{k}_{\text{e}}$ .... Elastic stiffness matrix of an element

$\mathbf{k}_{\text{eu}}$ .... Combination of the initial displacement stiffness matrix and the elastic stiffness matrix of an element

$\mathbf{k}_{\text{g}}$ .... Geometric or initial stress stiffness matrix of an element

$\mathbf{k}_{\text{u}}$ .... Initial displacement stiffness matrix of an element

$\mathbf{k}_{\text{T}}$ .... Tangent stiffness matrix of an element

$\mathbf{K}_{\text{e}}$ .... Elastic stiffness matrix

$\mathbf{K}_{\text{eu}}$ .... Combination of initial displacement stiffness matrix and elastic stiffness matrix

$\mathbf{K}_{\text{g}}$ .... Geometric or initial stress stiffness matrix

$\mathbf{K}_{\text{u}}$ .... Initial displacement stiffness matrix

$\mathbf{K}_{\text{T}}$ .... Tangent stiffness matrix

l_α	. . . .	Targeted length change of an actuator element
L	. . . .	Length
n	. . . .	Variational index
n_act	. . . .	Number of actuators
n_dof	. . . .	Number of degrees of freedom in the spatial discretization
$\bar{n}_\mathrm{dof}$	. . . .	Total number of degrees of freedom
$n_\mathrm{dof,nd}$	. . . .	Number of degrees of freedom per node of the spatial discretization
$n_\mathrm{disp,nd}$	. . . .	Number of displacement degrees of freedom per node of the spatial discretization
n_ele	. . . .	Number of finite elements in the spatial discretization
$\bar{n}_\mathrm{ele}$	. . . .	Number of finite elements in the path discretization
n_nd	. . . .	Number of nodes in the spatial discretization
$\bar{n}_\mathrm{nd}$	. . . .	Number of nodes in the path discretization
$n_\mathrm{nd,ele}$	. . . .	Number of nodes in one element of the spatial discretization
$\bar{n}_\mathrm{nd,ele}$	. . . .	Number of nodes in one element of the path discretization
n_s	. . . .	Degree of static indeterminacy
N	. . . .	Shape function of spatial discretization
$\bar{N}$	. . . .	Shape function of path discretization
$\mathbf{N}$	. . . .	Matrix of shape functions for the spatial discretization
$\bar{\mathbf{N}}$	. . . .	Matrix of shape functions for the path discretization
p	. . . .	Polynomial degree
P	. . . .	Point
$\mathbf{P}$	. . . .	First Piola-Kirchhoff stress tensor
$\mathbf{R}$	. . . .	Residual
s	. . . .	Arc length and deformation path
$\bar{s}$	. . . .	Normalized arc length
s_u	. . . .	Total arc length
$\mathbf{s}_\mathrm{u}$	. . . .	First partial derivative of total arc length
$\mathbf{S}_\mathrm{u}$	. . . .	Second partial derivative of total arc length
$\mathbf{S}$	. . . .	Second Piola-Kirchhoff stress tensor
t	. . . .	Time or pseudo-time (quasi-static problems)
$\bar{t}$	. . . .	Curve parameter of cycloid
$\mathbf{t}$	. . . .	Cauchy traction vector
$\hat{\mathbf{t}}$	. . . .	Prescribed traction vector
T	. . . .	Total required time

$\mathbf{u}$ .... Vector of displacement field

$\hat{\mathbf{u}}$ .... Vector of prescribed displacements

v .... Velocity

V .... Volume

$\mathbf{v}$ .... General vector

W_int .... Internal strain energy density

x .... Variable

$\mathbf{x}$ .... Position vector of a material point in the current configuration

$\mathbf{X}$ .... Position vector of a material point in the reference configuration

y .... General function

$\tilde{y}$ .... Neighboring function

Greek letters

α .... Elongation parameter of actuator element formulation

β .... Penalty parameter

Γ .... Boundary of domain

Γ_D .... Dirichlet boundary

Γ_N .... Neumann boundary

ε .... Multiplication factor of variation

λ .... First Lamé parameter

$\boldsymbol{\lambda}$ .... Vector of Lagrange parameters

μ .... Second Lamé parameter

ν .... Poisson's ratio

$\boldsymbol{\xi}$ .... Coordinates in natural element coordinate system of a spatial element

$\bar{\xi}$ .... Coordinates in natural element coordinate system of a path element

Π .... Potential energy

Π_ext .... External energy

Π_int .... Internal energy

Π_kin .... Kinetic energy

$\Pi_\mathrm{int,act}$ .... Actuation energy

$\Pi_\mathrm{int,el}$ .... Elastic part of the internal energy

$\boldsymbol{\sigma}$ .... Cauchy stress tensor

$\boldsymbol{\phi}$ .... Matrix of eigenvectors

Ω .... Domain

Indication of variables, super- and subscripts

$(\bar{\bullet})$ .... Variables referring to the path discretization

$(\bullet)_{\text{max}}$ .... Maximum value of quantity $(\bullet)$

$(\bullet)_e$ .... Quantity $(\bullet)$ associated with the spatial finite element e

$(\bullet)^e$ .... Quantity $(\bullet)$ associated with the path finite element e

$(\bullet)_k$ .... Quantity $(\bullet)$ evaluated at the node k of the spatial discretization

$(\bullet)^k$ .... Quantity $(\bullet)$ evaluated at the node k of the path discretization

$(\bullet)_a$ .... Quantity $(\bullet)$ associated with an active constraint

$(\bullet)_i$ .... Quantity $(\bullet)$ associated with an inactive constraint

$(\bullet)_h$ .... Discretized quantity of $(\bullet)$

$(\bullet)_{\text{md}}$ .... Quantity $(\bullet)$ associated with motion design

1

Introduction

1.1 Motivation and current developments

Nowadays, sustainability and energy efficiency play an increasingly important role in society and economy. Research, in particular, is continually progressing this aspect through new technologies and advances in a variety of disciplines. Especially the building industry, which is responsible for a significant part of the energy consumption as well as the exploitation of material resources, offers great potential in this respect. This includes, among other things, energy savings in indoor climate regulation, such as cooling or heating, but also the reduction of non-recyclable material in the supporting structure of a building. Moreover, by decreasing the amount of construction material, the embodied energy can be decreased. Hence, architects and engineers face the major challenge of designing exceptionally sustainable and extremely lightweight building structures. One promising approach to meet this requirement is the development of adaptive structures. These structures are able to optimally adapt to changing external conditions, typically by actively changing their shape. Two fundamentally different types of adaptive structures, both based on the working principle of geometry change, can be distinguished.

The first type of adaptive structure serves the purpose of accommodating to varying load cases. Usually, conservative structures are designed to guarantee the compliance with proofs in the ultimate limit state or in serviceability limit state for the "worst-case" load scenario. Therefore, the supporting structure needs to provide sufficient strength and stiffness and is over-dimensioned for most of the time. This leads to excessive use of material. In contrast, the geometry and stiffness of an adaptive structure are not designed for this "worst case" a priori, but rather comprise actuators that allow the structure to actively adjust to changing loads. This way, it can counteract resulting deformations and compensate vibrations to ensure serviceability. Furthermore, also internal forces can be manipulated and the stress distribution can be homogenized by

actuation. In doing so, the structure can be designed more slender, and eminent material savings can be achieved while maintaining its performance.

These adaptive structures usually contain sensors measuring changes in the external conditions or their influence onto the structure, such as the resulting internal reactions. It can then respond to the measurements by adjusting the appropriate actuators. In this case, the terms smart structures and shape control are very common. This first type of adaptive structures is, for example, treated in a general way in ZUK AND CLARK (1970), HOUSNER ET AL. (1997), SPENCER AND NAGARAJAIAH (2003), KORKMAZ (2011), SOBEK (2016) and SENATORE (2018). There exist several types of actuators for use in adaptive structures. In truss structures, discrete actuator elements are usually incorporated. Such elements can actively increase or decrease their length and, thus, deform the entire structure or only a part thereof. A continuous actuation is also possible and can be realized by e. g., piezoelectric or electroactive polymer actuators, as addressed in IRSCHIK (2002) and BAR-COHEN AND ANDERSON (2019), as well as shape-memory alloys, as addressed in a review by MOHD JANI ET AL. (2014). The actuator behavior is usually controlled through dedicated control algorithms, as described, for instance, in PREUMONT (2011). Besides, the question where to place the actuators for them to be most efficient plays a major role. The better the choice of the actuator location, the better the structure can be actuated, and the less energy is required for actuation. This task is usually investigated with the help of various optimization algorithms. Further literature and studies dealing with objectives and methods for different actuator placement strategies are provided by ABDULLAH ET AL. (2001), GUPTA ET AL. (2010), MASCHING AND BLETZINGER (2016), WAGNER ET AL. (2018) and REKSOWARDOJO ET AL. (2020). Examples for this type of adaptive structure are the so-called SmartShell, as presented in NEUHAEUSER ET AL. (2013) and illustrated in Figure 1.1a, the "infinitely stiff" cantilever beam introduced by SENATORE ET AL. (2018) as well as a highrise building, which serves as a demonstrator in a current collaborative research project dealing with such adaptive structures, as described in WEIDNER ET AL. (2018). All of these examples are characterized by the fact that only small displacements are necessary for the adaptation, and therefore geometrically linear analyses are sufficient for their investigation.

The situation is different for the second type of adaptive structures. Here, the structure is not intended to adapt to varying loads, but to changing requirements during its operation. To serve this purpose, the individual structural configurations usually differ significantly from each other, and actuation is therefore accompanied by major shape changes. This is often realized by designing deployable and retractable structures. Prominent examples are the opening and closing of roofs, especially stadiums roofs, such as the Commerzbank-Arena in Frankfurt, Germany (GÖPPERT AND STEIN 2007), shown in Figure 1.1b/c, or the folding and unfolding of adaptive bridges as, for example, real-

ized in the Kiel Hörn Footbridge in Kiel, Germany (KNIPPERS AND SCHLAICH 2000). In these cases, one single structure is designed to serve two purposes in two distinct configurations. Moreover, adaptive façade elements beyond conventional sun-blinds can be seen as another adaptive structure of this described second type. These can be closed and opened to regulate the interior climate and daylight intake of a building depending on the exterior weather conditions. Particularly this fact may significantly contribute to the building's energy efficiency (DEL GROSSO AND BASSO 2010). Realizations of such adaptive façades are e. g., the One Ocean Expo 2012 Pavilion in Korea (KNIPPERS ET AL. 2013) and the biomimetic façade elements Flectofin (LIENHARD ET AL. 2011) and Flectofold (KÖRNER ET AL. 2018). Furthermore, such adaptive structures play a role in other disciplines as well. One current research field is the shape change of morphing wings of airplanes, which is investigated, for example, in MAUTE AND REICH (2006), CAMPANILE (2006), SANTER AND PELLEGRINO (2009) and VASISTA ET AL. (2012) or the deployment of satellite structures in aerospace applications (PELLEGRINO 2015).

As already mentioned, the different geometric states of the second type of adaptive structures, e. g., the closed and opened state of a façade element, strongly deviate from each other. To enable this significant shape change, the structure must be designed accordingly. The most common approach to achieve variability in geometry is the targeted introduction of joints and hinges between stiff elements and the associated defined kinematics by unfolding, sliding and similar mechanisms. However, joints often represent particularly weak spots of the structure and may be prone to failure. Another strategy for geometrical variability is to use discrete systems with integrated actuators, as it has also been done in the first type of adaptive structures. In this case, however, they have to allow for large deformations. They take, for example, the form of trusses, as presented in SOFLA ET AL. (2009), tensegrity structures (KMET AND MOJDIS 2015; RAJA AND NARAYANAN 2009; SYCHTERZ AND SMITH 2018; VAN DE WIJDEVEN AND DE JAGER 2005; VEUVE ET AL. 2017) or lattice structures (FRIEDMAN AND IBRAHIMBEGOVIC

Figure 1.1: Examples for adaptive structures. a) SmartShell in Stuttgart (SOBEK (2016), © ILEK, Stuttgart). b) Open and c) closed roof of the Commerzbank-Arena in Frankfurt, Germany (GÖPPERT AND STEIN (2007), Photographer: Heiner Leiska).

2013). The individual actuator elements of these structures can change their length so that the entire geometry is adjusted in an intended manner. This stands in contrast to an alternative strategy, which is the design of continuous flexible and morphing structures. The fundamental idea in such structures is to incorporate an overall flexibility that is distributed throughout the entire structure. Consequently, it may undergo a smoothly distributed motion as in flexible and shape-changing shells, for example, in PAGITZ AND BOLD (2013) and PELLEGRINO (2015). In special cases, even pure bending deformations, so-called inextensional deformations, are possible. Moreover, there are approaches to combine discrete flexibility by joints with distributed structural compliance. These so-called compliant structures are characterized by continuous stiffness changes and a varying stiffness distribution within the structure, and, consequently, specific hinge zones are formed. The compliance enables an efficient deformation and is investigated in numerous research contributions such as in SIGMUND (1997), FRECKER ET AL. (1997), SAGGERE AND KOTA (1999), SAXENA AND ANANTHASURESH (2000), LU AND KOTA (2003), LAN AND CHENG (2008), HASSE AND CAMPANILE (2009), SANTER AND PELLEGRINO (2009) and MASCHING AND BLETZINGER (2016). The challenge here is that, despite its high degree of flexibility, the structure remains strong enough to withstand loads in all configurations. The concept of multi-stable compliant structures also represents a possibility to deal with this problem and, at the same time, to keep the configurations stable without continuously expending effort, as described in SANTER AND PELLEGRINO (2008), OH AND KOTA (2009) and ZHANG ET AL. (2017).

It has just been described that the design of compliant structures is concerned with satisfying demands on the structure in the individual geometric configurations, e.g., the open and closed state. Nevertheless, especially when large changes of the geometry are involved, the deformation process itself, i.e., the transition between these states, also has to meet specified requirements. However, an infinite number of different motions with different properties can be realized that all eventually reach the same final geometry, depending on how the actuators are controlled. Since the majority of motions cause stress in the structure and accordingly require energy, the motion that meets the prescribed requirements, such as efficiency, best can then be selected from this variety of possible motions. Particularly, the search for the most efficient motion motivates a closer look into movement mechanisms in nature, e.g., in plant motions (see KNIPPERS AND SPECK (2012), POPPINGA ET AL. (2016) and POPPINGA ET AL. (2020)). These are presumed to be governed by an efficiency principle and to require as little energy as possible. After gaining an understanding of the underlying movement mechanism of a chosen biological role model (as in CHARPENTIER ET AL. (2017), WESTERMEIER ET AL. (2018) and SACHSE ET AL. (2020)), the mechanism can be transferred to structural engineering and biomimetic structures can be developed, such as the already mentioned façade elements Flectofin or the Flectofold. However, the individual criteria for the mo-

tion in biological structures need to be thoroughly investigated. While aspects such as digestion or growth processes are important in nature, these factors do not play a role in architectural and engineering structures. Therefore, the underlying movement criteria of the biological structure and its biomimetic counterpart, i. e., the adaptive structure, may differ significantly. Apart from that, the geometry and the motion pattern strongly depend on the chosen biological role model. This flexibility in the specified requirements and the design leads to the desire for a more general method for the design of efficient motions in engineering structures.

Exactly this problem of finding optimal trajectories between an initial state and a target state regarding a prescribed objective is addressed in control theory, especially in optimal control (LIBERZON 2012; SARGENT 2000), and in motion planning of robots (CARBONE AND GOMEZ-BRAVO 2015; ELBANHAWI AND SIMIC 2014; LAVALLE 2006). The general procedure to design robots and their motions starts with trajectory planning. This can either be done in a purely geometrical fashion, or the dynamic behavior of the object can be taken into account in kinodynamic motion planning (KARAMAN AND FRAZZOLI 2010). To actually follow the planned trajectory, algorithms from control theory are used to calculate the required actuation. With the help of sensors and their feedback about the current state, deviations from the planned motion path can be corrected accordingly. Optimal trajectories between the initial and target states of, e. g., a robot can be calculated using methods of optimal motion planning and optimal control. They differ in the applied algorithms and the applicability of different constraints on the motion (BERGMAN AND AXEHILL 2018). However, most investigated and calculated structures in these research areas are characterized by a discrete kinematic mechanism and no (or little) elastic deformation. As a consequence, the problem formulation comprises fewer degrees of freedom than morphing continuous structures. In the field of continuum robotics and hyper-redundant manipulators with many actuatable degrees of freedom, such systems are planned and investigated (see, for example, CHIRIKJIAN AND BURDICK (1994), YEKUTIELI ET AL. (2005) and BIEZE ET AL. (2018)). A review of this field is given in RUS AND TOLLEY (2015). In these mostly linear robots, the inverse kinematics problem poses a particular challenge, where suitable geometric states are to be found for a given end tip location or for certain movements, such as grasping or wrapping. For this purpose, different geometric descriptions are used. Alongside continuous mechanical modeling of the beam-like structure, also several simplifications are typically made. For example, a piecewise constant curvature (PCC) model is introduced to capture the kinematics as described in WEBSTER AND JONES (2010). This allows the control of such systems and the solution of the inverse kinematics problem, where the required curvatures for a given end position are calculated. However, the applied methods highly depend on the specific robot and must be adapted to its characteristics in terms of form and actuation (RUS AND TOLLEY 2015). Due to the considerable num-

ber of involved degrees of freedom, the general realization of the desired motion remains the main difficulty. Mechanical quantities, such as strain and stress, can be calculated without any problems, but do not form the basis for an optimized motion. Nonetheless, planning and optimal control methods for continuous robots without restrictive simplifications in the kinematics remain a challenging research task.

However, there exist studies, where the mechanics and analysis of structures are combined with control and motion planning strategies, especially with regard to tensegrity structures (MASIC AND SKELTON 2005). On the one hand, robots are being constructed as tensegrity structures as in GRAELLS ROVIRA AND MIRATS TUR (2009). On the other hand, the methods in control theory are adapted to civil structures as in a deployable bridge (see VEUVE ET AL. (2017) and SYCHTERZ AND SMITH (2018)). Furthermore, IBRAHIMBEGOVIC ET AL. (2004) successfully combined an optimal control algorithm with nonlinear structural mechanics of a beam to achieve a deformed end configuration with certain properties.

To sum up, the first type of adaptive structure adjusts to different load cases through actuation. Since this is usually possible with relatively small deformations, it is mostly sufficient to assume a linear description of the underlying kinematics. However, this is no longer possible for the second type of adaptive structure, which adapts to changing requirements during operation. Because the shape has to adjust noticeably in this case, large deformations have to be taken into account. In order to design such compliant structures, a measure for their flexibility is optimized. This allows them to deform in a certain direction with little effort. But since the motion direction already needs to be predefined, the focus is laid on the design of the geometry rather than the motion. To design the motion itself to be efficient, a biomimetic approach can be followed, where biological motion mechanisms are transferred to adaptive structures. However, the underlying motion criteria might differ in the two scenarios. Moreover, the freedom in the design of the initial and end geometry, as well as the motion pattern, are limited due to the biological role model. Other methods that allow finding optimal motion paths between two given states of a structure are optimal control algorithms and motion planning. There are, in general, no restrictions on the individual states using these methods, but limitations arise regarding the manageable number of degrees of freedom. This does not pose a problem for typical applications in the field of robotics since the kinematics are usually clearly defined. Once a flexible and continuous structure is used, however, considerably more degrees of freedom are involved, and significant challenges in applying the methods arise. Therefore, the research in this area mostly concentrates on enabling the envisaged motions rather than optimizing them.

1.2 Objective and outline of this work

Based on the preceding observations, the objective of this thesis is to find a new method for designing optimal deformation trajectories between two (or more) predefined geometric states of a flexible structure. Therefore, a formalized optimization approach should be developed to identify optimal motions of any kind of flexible structure performing large elastic deformations, as occurring in architectural and civil engineering structures as well as other disciplines. In contrast to the existing concepts reviewed above, the focus here is not laid on the properties of the individual initial and target geometries of the structure, but the entire motion path is considered. In this context, it should become possible to plan the motion in advance without a control algorithm and related sensory equipment. The idea is to design optimal shape transitions based on a variational formulation, while taking geometrically nonlinear structural behavior into account. A quasi-static process is assumed such that no inertia effects are considered.

This thesis is structured as follows:

First, in *Chapter 2*, the historical background and developments as well as the mathematical foundations of the calculus of variations are presented. Due to its close correlation to the objectives in this work, the brachistochrone problem, being one of the first problems solved by variational principles, is employed to motivate the use of a variational approach.

In *Chapter 3*, the basics needed for the mechanical analysis of a structure are described. Therefore, the quantities and principles required for the understanding of the following chapters are explained in the context of continuum mechanics, and the finite element method is introduced as the method of choice for discretization and numerical solution.

Afterwards, the novel method of motion design is introduced in *Chapter 4*. At first, the problem statement and its basic assumptions are clarified, and the underlying objective function, i.e., the functional, is presented. The method is derived with the exemplary objective of minimizing the integral of the strain energy along the entire motion path, which represents a measure for the cost of deformation and serves as a proof of concept. Next, the motion design procedure is developed step by step by means of the calculus of variations. Motion design is based on a discretization of the motion path with finite elements, in addition to the usual spatial discretization, along with a Newton-Raphson solution algorithm, which is a second-order optimization scheme. Due to the path discretization, analytical sensitivities can be calculated by making use of standard components of the classical finite elements used for spatial discretization, e.g., the tangent stiffness matrix. The concept of the proposed method is first studied and verified through simple benchmarking examples, i.e., using problems with known analytical solutions. Next, additional numerical experiments, including instability phenomena and

inextensional deformations of shells, are investigated in order to gain a more profound understanding of the functional principle, beneficial features and further potential of the method.

In *Chapter 5*, the previously presented basic method of motion design is extended towards including additional constraints into the problem. After a short introduction into constraint enforcement techniques, various types of constraints that the resulting motion needs to satisfy are investigated. While it has previously been assumed that point loads could potentially be applied at every degree of freedom, this can now be restricted such that the optimized motion may only be realized with certain predefined load cases. The applicability of this constrained motion design approach is demonstrated with several numerical experiments. In order to also design motions of structures that include discrete actuator elements, an actuator element formulation is derived. It enables a straightforward integration into the motion design method. Apart from this, a positive determinant of the tangent stiffness matrix can be enforced throughout the motion, which is illustrated by the introduction of inequality constraints. This leads to the design of motions that remain stable during an entire load-controlled deformation process. Finally, it is shown that the different types of constraints can be combined within one motion design procedure.

Chapter 6 serves to demonstrate possibilities to combine motion design with other concepts to increase the efficiency of a flexible moving structure. For example, the initial geometry has a significant influence on the objective function. This is already studied in compliant structures, as described above. Therefore, motion design is combined with shape optimization of the initial geometry, and its positive influence is evaluated. Here, the focus is laid on the choice of possible objective functions. Furthermore, the most efficient load cases or actuator locations for the motion can be identified by means of existing methods for optimal actuator placement. Additionally, several modifications of the underlying objective function within the method are demonstrated and an approach for an incremental motion design procedure is presented.

Finally, the method of motion design as well as its further potentials are evaluated conclusively in *Chapter 7*, and the findings of this work are summarized.

<div style="text-align: right; font-size: 3em; font-weight: bold;">2</div>

Fundamentals of the Calculus of Variations

The goal of motion design, formulated in a more general way, is to find a trajectory or path between two states that minimizes a particular property of the entire motion. From this perspective, the objective recalls a historical and groundbreaking problem in the development of current methods in mechanics. In the year 1696, Johann Bernoulli (Figure 2.1a) posed a problem to the scientific community of that time. He asked for the curve of quickest descent, which went down in history as the brachistochrone problem, from the Greek word *brachistos* – shortest and *chronos* – time. The solutions submitted by important mathematicians formed the basis for today's calculus of variations and already contained first approaches to a kind of finite element method, which is today the method for the calculation of structures.

In this chapter, first, the brachistochrone problem and a short overview of the historical developments around the published task itself, the involved scientists and their solution approaches are given. Next, the problem is formulated and the functional of the brachistochrone is derived. In order to solve this problem, the basics of the calculus of variations are introduced and finally, the problem is solved analytically.

2.1 Historical background

Here, only a brief summary of the relevant and also interesting events around the brachistochrone problem during that time is given. More detailed information on the history and the individual approaches can be found in SUSSMANN AND WILLEMS (1997), KNOBLOCH (2012) and STEIN (2018).
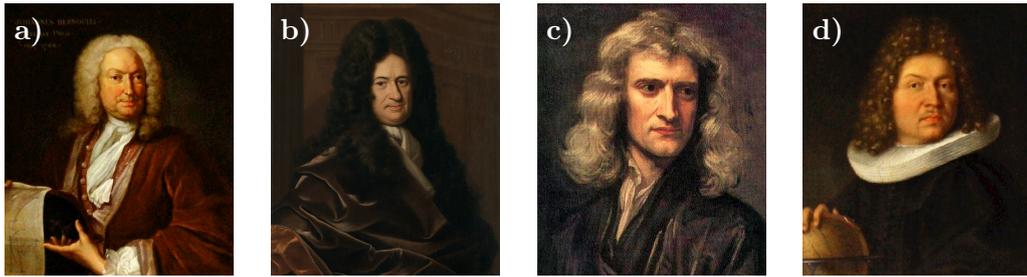
Figure 2.1: Involved scientists in the brachistochrone problem. a) Johann Bernoulli (1667-1748). b) Gottfried Wilhelm Leibniz (1646-1716). c) Isaac Newton (1643-1727). d) Jacob Bernoulli (1655-1705).

The occurrences began in the year 1696 with Johann Bernoulli's "Invitation to all mathematicians to solve a new problem" in Figure 2.2 (BERNOULLI 1696). He published it in the journal edited by Gottfried Wilhelm Leibniz (Figure 2.1b), the *Acta Eruditorum*:

"If in a vertical plane two points A and B are given, then it is required to specify the orbit AMB of the movable point M, along which it, starting from A, and under the influence of its own weight, arrives at B in the shortest possible time. So that those who are keen of such matters will be tempted to solve this problem, is it good to know that it is not, as it may seem, purely speculative and without practical use. Rather it even appears, and this may be hard to believe, that it is very useful also for other branches of science than mechanics. In order to avoid a hasty conclusion, it should be remarked that the straight line is certainly the line of shortest distance between A and B, but it is not the one which is traveled in the shortest time. However, the curve AMB – which I shall divulge if by the end of this year nobody else has found it – is very well known among geometers."
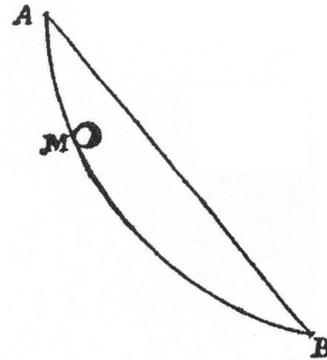
Figure 2.2: Johann Bernoulli's invitation to solve a new problem (BERNOULLI 1696).

In addition to the describing text, he also added a sketch, where he illustrated the problem. The task was to find the curve between two points A and B on which a mass point M requires the least time to move frictionlessly from A to B due to gravity.

Bernoulli has set the deadline for the publication of his solution to the end of the year. However, Leibniz answered him with a letter, where he explained that the problem "had attracted him against his will and that he hesitated because of its beauty like Eve before the apple" (KNOBLOCH 2012). At the same time, he also suggested him

to extend the deadline since the publications reach other countries with a delay of a couple of months. Bernoulli agreed with the proposal, reformulated and published the problem again. This time, his task reached more attention than before. Isaac Newton (Figure 2.1c), who received the problem half a year later, was taken by it. His solution was published anonymously in the journal *Philosophical Transactions* in January 1697 (ANONYMOUS 1697). Nevertheless, Johann Bernoulli directly identified the handwriting "from the claw of a lion (*ex ungue leonem*)" (KNOBLOCH 2012) as Newton's.

After the deadline expired, Leibniz published all the received solutions in the May issue of the *Acta Eruditorum* (LEIBNIZ 1697). Even though Johann Bernoulli introduced the brachistochrone problem as a "new problem", Leibniz discovered that it already had been solved by Galileo Galilei in the year 1638 in his *Discorsi* (GALILEI 1638). He discussed Galilei's solution along with a total of seven submitted solutions from famous mathematicians. Johann Bernoulli himself presented two solutions with geometrical and analytical ideas based on a light path in a medium with linearly increasing density. Due to Leibniz's confident request, Johann Bernoulli's always competing brother Jacob Bernoulli (Figure 2.1d) has also solved the brachistochrone problem using a first version of the calculus of variations. Leibniz published his own solution as well. It furthermore included a sketch of another idea, which he did not elaborate further due to the similarity to Jacob Bernoulli's approach. Additionally, the publication included two other solutions from Guillaume de l'Hôpital and Ehrenfried Walther von Tschirnhaus as well as Newton's solution, which was reprinted. Here, a special focus is put on the solution of Jacob Bernoulli and the sketched idea of Leibniz. Bernoulli had already broken down the problem into a discrete problem in order to get a finite number of problems of infinitesimal calculus. Furthermore, he introduced triangular test functions between neighboring points, as can be seen in his original illustration in Figure 2.3a. For the limit of the distance between the points converging to zero, the solution to the brachistochrone problem is a cycloid. Leonhard Euler took Bernoulli's solution as a basis and extended it to generalized functions using triangular test functions as well.

Figure 2.3: a) Original illustration from Jacob Bernoulli (LEIBNIZ 1697), b) Leibniz' original figure for his discrete solution (taken from STEIN (2018)), c) Illustration in Schellbach's publication SCHELLBACH (1851)

He presented his method in his book from 1744, where he introduced the calculus of variations (EULER 1744). The idea with the sketch from Leibniz (cf. Figure 2.3b) was not pursued, but it also contained the division of the continuous problem into a discrete one. Schellbach took up this idea again in 1851 and finally realized it (SCHELLBACH 1851). His solution, and therefore also Leibniz' idea, already revealed approaches to a kind of finite element method, which can be recognized in Figure 2.3c.

2.2 Formulation of the brachistochrone problem

The task, presented by Bernoulli, is to find a curve between two points A and B that minimizes the required time for a mass point to move from A to B under its own weight. To solve this minimization problem, a formula is needed that comprises the function for the curve $y(x)$ as well as the time T. This is achieved by taking the conservation of energy as a starting point. It requires that the potential energy $\Pi_{\text{pot},A}$ at point A equals the total energy, i.e., the sum of the kinetic energy Π_{kin} and potential energy Π_{pot}, throughout the entire motion

$$\Pi_{\text{pot},A} = \Pi_{\text{kin}} + \Pi_{\text{pot}} . \tag{2.1}$$

By using the definition for the kinetic energy and the potential energy

$$\Pi_{\text{kin}} = \frac{1}{2}mv^2, \tag{2.2}$$

$$\Pi_{\text{pot}} = mgy(x) , \tag{2.3}$$

including the mass m, the velocity v and the gravitational constant g, the conservation of energy can be transformed to

$$mgy_{\text{A}} = \frac{1}{2}mv^2 + mgy(x) \tag{2.4}$$

with y_{A} being the vertical coordinate of the starting point A and $mgy_{\text{A}} = \text{const.}$ defining the reference energy. This can then further be resolved for the velocity

$$v = \sqrt{2g\left(y_{\text{A}} - y(x)\right)} . \tag{2.5}$$

Another equation for the velocity is its definition as the derivative of the arc length s with respect to the time t

$$v = \frac{\mathrm{d}s}{\mathrm{d}t} . \tag{2.6}$$

The transformation and combination of these two definitions in eq. (2.5) and eq. (2.6) provides the infinitesimal time

$$\mathrm{d}t = \frac{1}{v}\,\mathrm{d}s = \frac{1}{\sqrt{2g\big(y_\mathrm{A} - y(x)\big)}}\,\mathrm{d}s\,, \tag{2.7}$$

and, therefore, the equation for the total required time T

$$T = \int_{s_\mathrm{A}}^{s_\mathrm{B}} \frac{1}{\sqrt{2g\big(y_\mathrm{A} - y(x)\big)}}\,\mathrm{d}s\,. \tag{2.8}$$

The arc length s still represents an unknown parameter in this equation. This is why it is calculated with the help of the Pythagorean theorem and the infinitesimal triangle in the curve as seen in Figure 2.4:

$$\mathrm{d}s = \sqrt{\mathrm{d}x^2 + \mathrm{d}y^2} = \sqrt{\left(\frac{\mathrm{d}x}{\mathrm{d}x}\right)^2 + \left(\frac{\mathrm{d}y}{\mathrm{d}x}\right)^2}\,\mathrm{d}x = \sqrt{1 + y'(x)^2}\,\mathrm{d}x\,. \tag{2.9}$$

Furthermore, this step also establishes a relationship between the arc length s, the curve $y(x)$ and the variable x as well as their infinitesimal increments. By application of the rules for the substitution of an integral, the total required time can finally be expressed as

$$T = \int_{s_\mathrm{A}}^{s_\mathrm{B}} \frac{1}{\sqrt{2g\big(y_\mathrm{A} - y(x)\big)}}\,\mathrm{d}s = \int_{x_\mathrm{A}}^{x_\mathrm{B}} \sqrt{\frac{1 + \big(y'(x)\big)^2}{2g\big(y_\mathrm{A} - y(x)\big)}}\,\mathrm{d}x\,. \tag{2.10}$$

Eq. (2.10) represents the functional of the brachistochrone problem. The peculiarity in this equation is that the variable itself is a function, namely the function of the solution
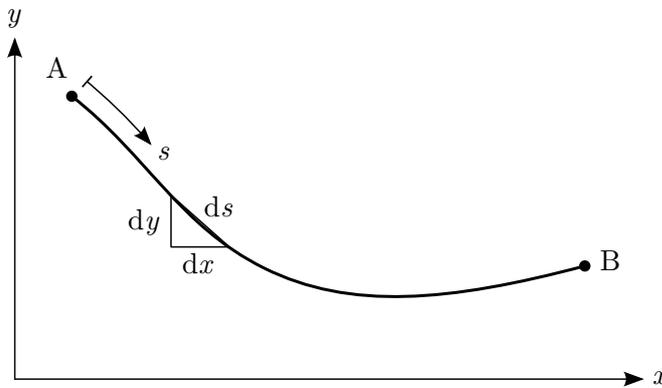
Figure 2.4: Arc length of the brachistochrone curve.

curve, which is to be found. In the meantime, the well-established method to solve this type of problem is the calculus of variations, which is presented in the following section.

2.3 Introduction to the calculus of variations

The calculus of variations is a mathematical tool that enables the calculation of extreme values of integral quantities. In the following, the basics of the calculus of variations are presented in order to solve the brachistochrone problem. For more detailed explanations, it is for example referred to ELSGOLC (1970), CLEGG (1970) and GELFAND AND FOMIN (2000).

The functional of the brachistochrone problem in eq. (2.10), which needs to be minimized, includes the classical characteristics of such functionals. A functional J is a function that does not only depend on a scalar parameter x, but also on a function $y(x)$ and its derivative $y'(x)$. The argument is, therefore, a function itself. In addition, it contains an integral and returns a scalar value. Even for multidimensional problems, the result remains scalar and the functional value for various functions can be compared directly. The generalized form of a simple functional J is

$$J\{y(x)\} = \int\limits_{x_A}^{x_B} F\left(x, y(x), y'(x)\right) \mathrm{d}x \to \min \tag{2.11}$$

with the boundary conditions

$$y(x_A) = y_A \,, \tag{2.12}$$
$$y(x_B) = y_B \,. \tag{2.13}$$

For the problem to be solvable the function $y(x)$ has to be differentiable twice between the bounds x_A and x_B. A neighboring function $\tilde{y}(x)$, as seen in Figure 2.5 is now introduced. It differs from the solution by the variation $\delta y(x)$ of the function $y(x)$, multiplied by a factor ε:

$$\tilde{y}(x) = y(x) + \varepsilon \delta y(x) \,. \tag{2.14}$$

The variation vanishes at the bounds and must also be twice differentiable. As a consequence, the neighboring function $\tilde{y}(x)$ fulfills the same boundary conditions as
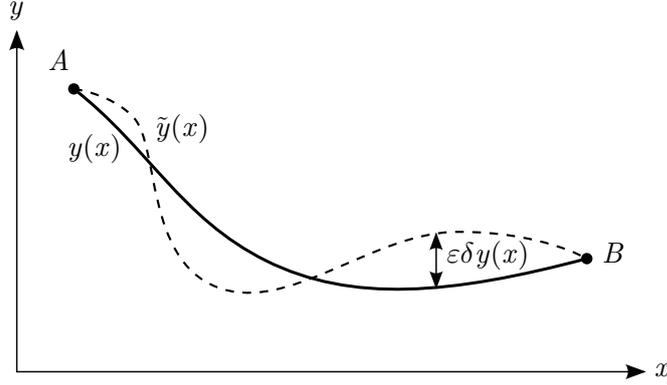
Figure 2.5: Neighboring function $\tilde{y}(x)$ with the variation $\delta y(x)$.

$y(x)$. The functional, depending on the neighboring function, is then defined as

$$J\{\tilde{y}(x)\} = J(\varepsilon) = \int_{x_A}^{x_B} F\left(x, y(x) + \varepsilon\delta y(x), y(x)' + \varepsilon\delta y'(x)\right) \mathrm{d}x\,. \tag{2.15}$$

As the function $y(x)$ represents the solution of the minimization problem, the minimum is found when $\varepsilon = 0$. The first derivative of the functional with respect to ε, evaluated at that point, should, therefore, be zero. It is defined as the variation δJ of the functional J and is calculated using the rules of differential calculus

$$\delta J := \left.\frac{\mathrm{d}J(\varepsilon)}{\mathrm{d}\varepsilon}\right|_{\varepsilon=0} = \lim_{\varepsilon \to 0} \frac{J\{\tilde{y}\} - J\{y\}}{\varepsilon} = 0\,. \tag{2.16}$$

As in differential calculus, the calculus of variations deals with the question of how a functional behaves in the vicinity of a point. The derivative of a function in differential calculus corresponds to the variation of a functional in the calculus of variation, which should be zero for extremal values. With the chain rule, it follows that

$$\delta J = \int_{x_A}^{x_B} \left[\frac{\mathrm{d}F\left(x, \tilde{y}(x), \tilde{y}'(x)\right)}{\mathrm{d}\varepsilon}\right] \mathrm{d}x = \int_{x_A}^{x_B} \left[\frac{\partial F}{\partial x}\frac{\partial x}{\partial \varepsilon} + \frac{\partial F}{\partial \tilde{y}}\frac{\partial \tilde{y}}{\partial \varepsilon} + \frac{\partial F}{\partial \tilde{y}'}\frac{\partial \tilde{y}'}{\partial \varepsilon}\right] \mathrm{d}x \tag{2.17}$$

and with the evaluation of the individual terms, the variation simplifies to

$$\delta J = \int_{x_A}^{x_B} \left[\frac{\partial F}{\partial y}\delta y + \frac{\partial F}{\partial y'}\delta y'\right] \mathrm{d}x\,. \tag{2.18}$$

To move the differential operator away from the variation, the second term is partially integrated

$$\int\limits_{x_\mathrm{A}}^{x_\mathrm{B}} \left[\frac{\partial F}{\partial y'} \delta y' \right] \mathrm{d}x = \left[\frac{\partial F}{\partial y'} \delta y \right]_{x_\mathrm{A}}^{x_\mathrm{B}} - \int\limits_{x_\mathrm{A}}^{x_\mathrm{B}} \left[\frac{\mathrm{d}}{\mathrm{d}x} \left(\frac{\partial F}{\partial y'} \right) \delta y \right] \mathrm{d}x \,. \tag{2.19}$$

Just like the variation, the boundary term also vanishes, which further simplifies the variation to

$$\delta J = \int\limits_{x_\mathrm{A}}^{x_\mathrm{B}} \left[\frac{\partial F}{\partial y} - \frac{\mathrm{d}}{\mathrm{d}x} \left(\frac{\partial F}{\partial y'} \right) \right] \delta y \, \mathrm{d}x \,. \tag{2.20}$$

Next, the fundamental lemma of the calculus of variations can be applied. It states that if a function $f(x)$ is continuous in the interval $x_\mathrm{A} \leq x \leq x_\mathrm{B}$ and if the condition

$$\int\limits_{x_\mathrm{A}}^{x_\mathrm{B}} f(x) \delta y(x) \, \mathrm{d}x = 0 \tag{2.21}$$

is valid for every continuously differentiable function $\delta y(x)$ with the boundary conditions $\delta y(x_\mathrm{A}) = 0$ and $\delta y(x_\mathrm{B}) = 0$, it follows that $f(x) = 0$ applies for the whole interval. This leads to the definition of Euler's equation

$$\frac{\partial F}{\partial y} - \frac{\mathrm{d}}{\mathrm{d}x} \left(\frac{\partial F}{\partial y'} \right) = 0 \,, \tag{2.22}$$

which was first introduced in Leonhard Euler's book from 1744 (EULER 1744). Expanding the second term

$$\frac{\mathrm{d}}{\mathrm{d}x} \left(\frac{\partial F}{\partial y'} \right) = \frac{\partial}{\partial x} \left(\frac{\partial F}{\partial y'} \right) \frac{\partial x}{\partial x} + \frac{\partial}{\partial y} \left(\frac{\partial F}{\partial y'} \right) \frac{\partial y}{\partial x} + \frac{\partial}{\partial y'} \left(\frac{\partial F}{\partial y'} \right) \frac{\partial y'}{\partial x} \tag{2.23}$$

leads to another form of Euler's equation

$$\frac{\partial F}{\partial y} - \frac{\partial^2 F}{\partial x \partial y'} - \frac{\partial^2 F}{\partial y \partial y'} y' - \frac{\partial^2 F}{\partial y'^2} y'' = 0 \,. \tag{2.24}$$

The function that satisfies this differential equation represents the solution to the variational problem. Like this, the minimization problem in eq. (2.11) is transformed into a partial differential equation. The constants that occur in the calculation can then be

solved by the application of the constraints

$$y(x_\text{A}) = y_\text{A} \,, \tag{2.25}$$

$$y(x_\text{B}) = y_\text{B} \,. \tag{2.26}$$

In most engineering applications, functionals come along with constraints. These are conditions that are imposed on the functions that occur in the functional, which have to be fulfilled by the solution either at the boundaries or in the entire domain. In the case of problems in mechanics, which are discussed in the course of this work, these can, for instance, represent geometric boundary conditions.

2.4 Solution to the brachistochrone problem

With the help of the introduced calculus of variations, a tool to solve minimization problems, such as the brachistochrone problem, is now available. In this chapter, the historical brachistochrone problem (cf. Figure 2.2) is solved analytically. It can be formulated with the previously derived functional in eq. (2.10) as

$$T = \int_{x_\text{A}}^{x_\text{B}} \sqrt{\frac{1 + \big(y'(x)\big)^2}{2g\big(y_\text{A} - y(x)\big)}} \, \mathrm{d}x \to \min .$$

The starting point for the solution is Euler's equation (2.24). As the functional only depends on the function $y(x)$ and its derivative $y'(x)$, but not on the variable x itself, Euler's equation can be further simplified to

$$\frac{\partial F}{\partial y} - \frac{\partial^2 F}{\partial y \partial y'} y' - \frac{\partial^2 F}{\partial y'^2} y'' = 0 \,. \tag{2.27}$$

The multiplication with $y'(x)$

$$\frac{\mathrm{d}y}{\mathrm{d}x} \left(\frac{\partial F}{\partial y} - \frac{\partial^2 F}{\partial y \partial y'} y' - \frac{\partial^2 F}{\partial y'^2} y'' \right) = \frac{\mathrm{d}}{\mathrm{d}x} \left(F - y' \frac{\partial F}{\partial y'} \right) = 0 \tag{2.28}$$

and a subsequent integration lead to the simplified Euler-equation

$$F - y' \frac{\partial F}{\partial y'} = C \,, \tag{2.29}$$

also called the Beltrami identity. Applying it to the functional of the brachistochrone problem yields

$$\sqrt{\frac{1 + y'^2}{2g(y_A - y)}} - y'\frac{y'}{\sqrt{2g(y_A - y)(1 + y'^2)}} = \frac{1}{\sqrt{2g(y_A - y)(1 + y'^2)}} = C_1 \,, \qquad (2.30)$$

which can be solved for y'

$$y' = \sqrt{\frac{1}{2gC_1^2(y_A - y)} - 1} = \sqrt{\frac{1 - 2gC_1^2(y_A - y)}{2gC_1^2(y_A - y)}} \,. \qquad (2.31)$$

To solve this differential equation, a substitution is necessary. A clever choice is a combination of trigonometric functions, such as

$$2gC_1^2(y_A - y) = \sin^2\left(\frac{\bar{t}}{2}\right) = \frac{1}{2}\left(1 - \cos(\bar{t})\right). \qquad (2.32)$$

The resulting equation for y

$$y = y_A - \frac{1}{2gC_1^2}\sin^2\left(\frac{\bar{t}}{2}\right) = y_A - \frac{1}{4gC_1^2}\left(1 - \cos(\bar{t})\right) \qquad (2.33)$$

represents the ansatz for y, which can then be inserted into eq. (2.31)

$$y' = \sqrt{\frac{1 - \sin^2\left(\frac{\bar{t}}{2}\right)}{\sin^2\left(\frac{\bar{t}}{2}\right)}} = \frac{\cos\left(\frac{\bar{t}}{2}\right)}{\sin\left(\frac{\bar{t}}{2}\right)} = \frac{\mathrm{d}y}{\mathrm{d}x} \qquad (2.34)$$

to enable the substitution

$$\mathrm{d}x = \frac{\sin\left(\frac{\bar{t}}{2}\right)}{\cos\left(\frac{\bar{t}}{2}\right)}\,\mathrm{d}y\,. \qquad (2.35)$$

Additionally, the derivative of y with respect to $\bar{t}$ is still required

$$\frac{\mathrm{d}y}{\mathrm{d}\bar{t}} = \frac{1}{2gC_1^2}\sin\left(\frac{\bar{t}}{2}\right)\cos\left(\frac{\bar{t}}{2}\right)\,. \qquad (2.36)$$

The transformation for $\mathrm{d}y$

$$\mathrm{d}y = \frac{1}{2gC_1^2}\sin\left(\frac{\bar{t}}{2}\right)\cos\left(\frac{\bar{t}}{2}\right)\mathrm{d}\bar{t} \qquad (2.37)$$

can now be inserted into eq. (2.35)

$$\mathrm{d}x = \frac{\sin\left(\frac{\bar{t}}{2}\right)}{\cos\left(\frac{\bar{t}}{2}\right)}\,\mathrm{d}y = \frac{\sin\left(\frac{\bar{t}}{2}\right)}{\cos\left(\frac{\bar{t}}{2}\right)}\frac{1}{2gC_1^2}\sin\left(\frac{\bar{t}}{2}\right)\cos\left(\frac{\bar{t}}{2}\right)\mathrm{d}t \tag{2.38}$$

$$= \frac{1}{4gC_1^2}\left(1-\cos(\bar{t})\right)\mathrm{d}\bar{t}\,. \tag{2.39}$$

As a result, the equation for x and y can be obtained by integration of eq. (2.39) and eq. (2.37).

$$y = y_\mathrm{A} - \frac{1}{2gC_1^2}\sin^2\left(\frac{\bar{t}}{2}\right) = y_\mathrm{A} - \frac{1}{4gC_1^2}\left(1-\cos(\bar{t})\right), \tag{2.40}$$

$$x = \frac{1}{4gC_1^2}\left(\bar{t}-\sin(\bar{t})\right) + C_2\,. \tag{2.41}$$

These equations are the solution to the brachistochrone problem in a parametric form and represent the equations of a general cycloid. A cycloid is defined as the trajectory of a point on a rolling circle. It must be noted that the variable $\bar{t}$ neither represents the time nor the arc length parameter s, but it is the angle through which a rolling circle has rotated, a point of which generated the curve $(x(\bar{t}),y(\bar{t}))$. However, the substitution in eq. (2.32) already required some knowledge about the solution.

The constants C_1, C_2 as well as the parameter value $\bar{t}_\mathrm{end}$ at point B are derived by the boundary conditions of the starting point A and the end point B

$$x(t = 0) = x_\mathrm{A}\,, \tag{2.42}$$

$$x(\bar{t} = \bar{t}_\mathrm{end}) = x_\mathrm{B}\,, \tag{2.43}$$

$$y(\bar{t} = \bar{t}_\mathrm{end}) = y_\mathrm{B}\,. \tag{2.44}$$

These boundary conditions represent nonlinear functions themselves that need to be solved iteratively. Only the condition $y(\bar{t} = 0) = y_\mathrm{A}$ is fulfilled by definition of the problem. Exemplary values are given for the starting point $x_\mathrm{A} = 1.0$, $y_\mathrm{A} = 5.0$ and the endpoint $x_\mathrm{B} = 10.0$, $y_\mathrm{B} = 2.0$ (calculated for simplicity with a rounded gravitational constant $g = 10$)

$$C_1 = 0.116 \qquad\qquad C_2 = 1.0 \qquad\qquad \bar{t}_\mathrm{end} = 4.05 \tag{2.45}$$

The corresponding curve with the prescribed points A and B is given in Figure 2.6.

The focus of this chapter was set on the calculus of variations, its historical development, its fundamentals and the solution of one of the best-known problems, the brachistochrone problem. First, the history of this problem was presented, where Johann Bernoulli,
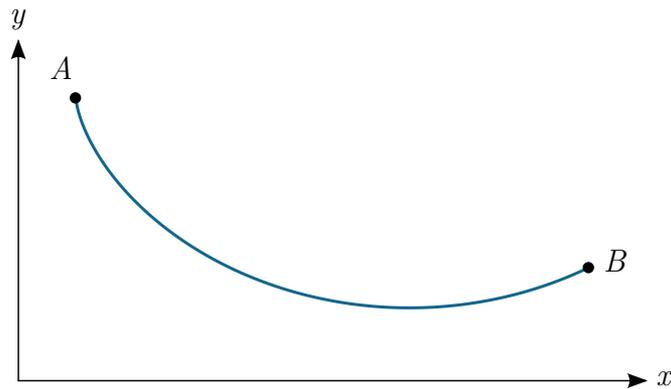
Figure 2.6: The cycloid as the solution of the brachistochrone problem.

Gottfried Leibniz and Jacob Bernoulli played a crucial role. The latter provided in his solution of the brachistochrone problem the basis for the development of the calculus of variations by Leonhard Euler. Thereupon, the functional of the brachistochrone problem was derived employing the conservation of energy. After the fundamentals of the calculus of variations were introduced and the derivation of Euler's equation was presented, the brachistochrone problem could be solved analytically with a differential equation.

This problem formulation of the brachistochrone can be taken as a simplified template for what is intended to be done in motion design. The goal is to find a path between two configurations, e. g., the points A and B or an open and a closed geometry of an adaptive element, that fulfills specified demands like minimization of the total required time, energy or effort for traversing from A to B, or any other objective for the entire path. In the case of the brachistochrone, it was solved with the calculus of variations. This method is also used for the motion design of structures, which will be explained in detail in Chapter 4. The two configurations are the initial geometry of the structure and a desired final geometry.

3

Fundamentals of Continuum Mechanics and Finite Element Formulation

This chapter deals with the fundamentals for the analysis of structures that are needed for the formulation of the motion design method. First, the boundary value problem is presented with basic concepts of continuum mechanics. This includes the kinematic equations, the relations to various stress measures, the constitutive equations as well as the governing equations for the static equilibrium of structures. Since an analytical solution to the resulting differential equations can only be found in exceptional cases, the finite element method is afterwards introduced as a numerical solution method. It is based on the division of both the solution and the structure into elements, the discretization. The finite element method nowadays represents the most widely used method for the solution of the governing equations for the analysis of structures.

3.1 Continuum mechanics and boundary value problem

Here, a brief introduction into the basics of nonlinear continuum mechanics is given. Furthermore, the boundary value problem as a starting point for further derivations is presented. Continuum solid mechanics describes the deformation of a solid body due to external forces and correlates this deformation and the strains with the resulting stresses by a material law. In the following, the kinematic equations, which describe the kinematics and deformation of a solid body in space, as well as the stress measures and material law, are described. Next, the static equilibrium equation together with the boundary conditions are presented. These equations represent the boundary value problem of solid mechanics. As its weak form is more accessible to methods of numerical

solution techniques, it is derived by the method of weighted residuals. This leads to the definition of the principle of virtual work. Alternatively, it can also be obtained from the minimum potential energy principle by a variational formulation.

This chapter is not intended to provide extensive insight into the topic, but rather to give an overview of the relevant quantities and equations for the investigations of this work. For further literature, the reader is referred to Marsden and Hughes (2012), Holzapfel (2010) and Belytschko et al. (2014).

3.1.1 Kinematics

In continuum mechanics, the correct representation of large deformations plays a substantial role. Here, the kinematic relationships that describe the deformation are presented here. Figure 3.1 shows a body in its reference configuration Ω with the boundary Γ and the deformed current configuration Ω_c. For the representation of the deformation process in the three-dimensional space, a Lagrangian point of view is usually chosen. In doing so, the kinematics and deformation of a body are described via the position of its material points throughout the deformation process.

The position of a material point is defined by the position vector $\mathbf{X}$ in the reference configuration and $\mathbf{x}$ in the current configuration, respectively. The displacement vector $\mathbf{u}$ represents the connection between these configurations and is calculated by the difference of their position vectors

$$\mathbf{u} = \mathbf{x} - \mathbf{X}.$$ (3.1)
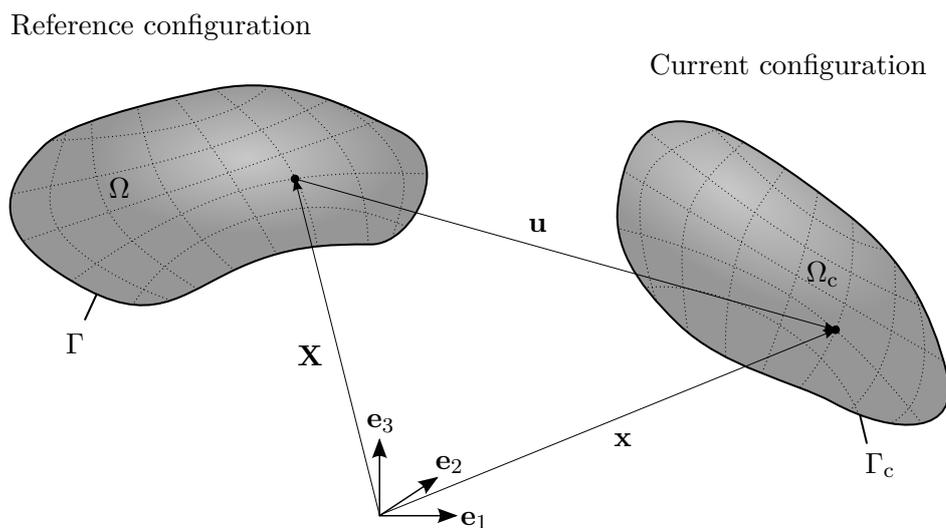
Figure 3.1: Reference and current configuration of a solid body in space.

In this work, the total Lagrangian approach is pursued, in which all quantities are defined with respect to the reference configuration. Therefore, the position vector $\mathbf{X}$ represents an independent variable and the problem is solved for the unknown displacements $\mathbf{u}$.

The fundamental quantity to describe the resulting strains in solid mechanics is the deformation gradient $\mathbf{F}$. It is defined as the partial derivative of the position vector in the current configuration with respect to the position vector in the reference configuration

$$\mathbf{F} = \frac{\partial \mathbf{x}}{\partial \mathbf{X}} = \mathbf{I} + \frac{\partial \mathbf{u}}{\partial \mathbf{X}} \tag{3.2}$$

with the identity tensor $\mathbf{I}$. It can also be interpreted geometrically as the factor of the length change of an infinitesimal line element between the two configurations, i.e.,

$$\mathrm{d}\mathbf{x} = \mathbf{F} \cdot \mathrm{d}\mathbf{X} \,. \tag{3.3}$$

Similarly, the relationship between infinitesimal volume elements can be established by the deformation gradient as

$$\mathrm{d}v = \det \mathbf{F} \, \mathrm{d}V = J \, \mathrm{d}V \,. \tag{3.4}$$

The transformation happens with the determinant of $\mathbf{F}$, the so-called Jacobian determinant J. In addition to the mapping of lengths and volumes, the deformation gradient also allows for the mapping of oriented infinitesimal area elements. These can be interpreted as vectors $\mathrm{d}\mathbf{A}$, which are defined as the area $\mathrm{d}A$ multiplied with the normal vector $\mathbf{N}$ onto the area. This leads to $\mathrm{d}\mathbf{A} = \mathrm{d}A\mathbf{N}$ for the reference configuration and $\mathrm{d}\mathbf{a} = \mathrm{d}a\mathbf{n}$ for the current configuration, respectively. The transformation can be conducted with Nanson's formula

$$\mathrm{d}\mathbf{a} = J\mathbf{F}^{-\mathrm{T}} \cdot \mathrm{d}\mathbf{A} \,. \tag{3.5}$$

Consequently, the deformation gradient plays a significant role as a strain measure. However, it is not invariant with respect to rigid body motions, which leads to the need for another strain measure. Since this work primarily deals with problems with large deformations, but small strains, the Green-Lagrange strain measure, a commonly used strain measure in solid mechanics, is chosen. With the help of the deformation gradient, the Green-Lagrange strains are defined as

$$\mathbf{E} = \frac{1}{2}(\mathbf{F}^{\mathrm{T}}\mathbf{F} - \mathbf{I}) \,. \tag{3.6}$$

When the nonlinear terms of the Green-Lagrange strains are neglected, they reduce to the common linear engineering strains.

3.1.2 Stress measures and constitutive laws

External forces and the resulting deformation lead to internal stresses. These can be correlated to the traction on an area element of a body by the Cauchy theorem

$$\mathbf{t} = \boldsymbol{\sigma} \cdot \mathbf{n} \,. \tag{3.7}$$

It includes the traction vector $\mathbf{t}$ acting on an area with the normal vector $\mathbf{n}$ and the Cauchy stress tensor $\boldsymbol{\sigma}$. The latter contains all the information about the internal stress state. In the case of the Cauchy stress tensor, this stress state is also referred to as the true stress state, because the involved quantities are related to the current configuration – the current force on the corresponding area element of the current configuration. Alternative stress measures refer to quantities of the reference configuration. The first Piola-Kirchhoff stress tensor $\mathbf{P}$, for example, maps the current force onto an area element in the reference configuration. It is derived with the help of Nanson's formula (eq. 3.5) from the Cauchy stress tensor

$$\mathbf{P} = J\boldsymbol{\sigma} \cdot \mathbf{F}^{-\mathrm{T}} \,. \tag{3.8}$$

Similarly, the second Piola-Kirchhoff stress tensor $\mathbf{S}$ additionally maps the force into the reference configuration and is related to the other stress measures by

$$\mathbf{S} = J\mathbf{F}^{-1} \cdot \boldsymbol{\sigma} \cdot \mathbf{F}^{-\mathrm{T}} = \mathbf{F}^{-1} \cdot \mathbf{P} \,. \tag{3.9}$$

The Cauchy stress tensor as well as the second Piola-Kirchhoff stress tensor are symmetric. This symmetry follows from the balance of angular momentum. Unlike the Cauchy stress, the values of the first and second Piola-Kirchhoff stress tensor can not directly be physically interpreted. A so-called push forward operation, a transformation of the quantities from the reference to the current configuration, is required to obtain the Cauchy stress and, therefore, the true stress state.

The relationship between the stress and the strain measures is established by the constitutive law, also known as material law. Despite the numerous stress and strain measures, however, they can not be combined arbitrarily. They form pairs that are energetically conjugated to each other. The value of the strain energy needs to be the same for every energetically conjugate pair of stress and strain measures. As already mentioned, the Green-Lagrange strain is chosen as strain measure in this work. The energetically conjugate stress measure is the second Piola-Kirchhoff stress tensor. They can, for example, be related by the linear elastic St. Venant-Kirchhoff material law

$$\mathbf{S} = \mathbb{C} : \mathbf{E} \tag{3.10}$$

with the fourth-order material tensor $\mathbb{C}$. It results from the internal strain energy density

$$W_{\mathrm{int}} = \frac{1}{2}\lambda(\operatorname{tr}\mathbf{E})^2 + \mu\mathbf{E} : \mathbf{E} \tag{3.11}$$

as the second derivative with respect to the Green-Lagrange strain

$$\mathbb{C} = \frac{\partial^2 W_{\mathrm{int}}(\mathbf{E})}{\partial\mathbf{E}\partial\mathbf{E}} \; . \tag{3.12}$$

Due to the symmetry of $\mathbf{S}$ and $\mathbf{E}$ as well as the use of an isotropic material, the material tensor $\mathbb{C}$ only contains two independent parameters. These are the Lamé parameters λ and μ, which correlate with the commonly used Young's modulus E and Poisson's ratio ν via

$$\lambda = \frac{E\nu}{(1+\nu)(1-2\nu)} \qquad \text{and} \qquad \mu = \frac{E}{2(1+\nu)} \; . \tag{3.13}$$

Beside the linear St. Venant-Kirchhoff material model, there also exist other, more complex, nonlinear hyperelastic material models. With the general concept of variational motion design being independent of the choice of the particular constitutive law, also such hyperelastic models could be used. However, these are not implemented within the scope of this work and, therefore, not further presented at this point.

3.1.3 Static equilibrium equation and boundary conditions

The initial boundary value problem of nonlinear solid mechanics can now be formulated with the help of the introduced kinematic and stress quantities. The equilibrium equation, which relates the external and internal forces acting on a body, forms the basis for the formulation. It can be derived from the balance of linear momentum. In this work, only static problems are considered. Thus, the inertia terms are neglected and the static equilibrium equation on the whole domain is

$$\operatorname{Div}\mathbf{P} + \hat{\mathbf{b}} = \mathbf{0} \, , \tag{3.14}$$

with the vector of the external body forces $\hat{\mathbf{b}}$. In addition to static equilibrium, initial and boundary conditions have to be satisfied. In static problems, the definition of boundary conditions is sufficient. They are applied on the boundary Γ of the domain, which is divided into the disjoint Neumann boundary Γ_{N} and Dirichlet boundary Γ_{D}

with the relations

$$\Gamma_{\mathrm{N}} \cup \Gamma_{\mathrm{D}} = \Gamma \qquad \text{and} \qquad \Gamma_{\mathrm{N}} \cap \Gamma_{\mathrm{D}} = \varnothing \,. \tag{3.15}$$

The Neumann boundary conditions are also referred to as traction boundary conditions. With the application of the Cauchy theorem (eq. 3.7) in the reference configuration and the given traction vector $\hat{\mathbf{t}}$, they take the form

$$\mathbf{P} \cdot \mathbf{N} = \hat{\mathbf{t}} \qquad \text{on } \Gamma_{\mathrm{N}} \,. \tag{3.16}$$

On the other hand, displacements are prescribed on the Dirichlet boundary

$$\mathbf{u} = \hat{\mathbf{u}} \qquad \text{on } \Gamma_{\mathrm{D}} \,. \tag{3.17}$$

The boundary conditions in eq. (3.16) and eq. (3.17), together with the static equilibrium in eq. (3.14), represent the boundary value problem. The combination of these three equations is considered as the strong form of the problem as it is enforced at every point of the entire domain.

3.1.4 Principle of virtual work and minimum potential energy principle

An analytical solution of the boundary value problem in its strong form can only be found in special cases. This leads to the need for a numerical solution method. The finite element method, which is further explained in Section 3.2, represents such a solution method, but it requires a weak form of the boundary value problem. The weak form can be derived from static equilibrium (eq. 3.14) and the Neumann boundary conditions (eq. 3.16) by applying the method of weighted residuals. In this method, the involved equations are cast into a residual form, multiplied with a test function $\delta\mathbf{u}$, the virtual displacements, and integrated over the domain

$$\delta\Pi = \int_{\Omega_0} (\mathrm{Div}\,\mathbf{P} + \hat{\mathbf{b}}) \cdot \delta\mathbf{u}\ \mathrm{d}\Omega + \int_{\Gamma_{\mathrm{N}}} (\hat{\mathbf{t}} - \mathbf{PN}) \cdot \delta\mathbf{u}\ \mathrm{d}\Gamma = 0 \,. \tag{3.18}$$

This is also the definition of the principle of virtual work. It states that a geometrically compatible virtual displacement field on a mechanical system in equilibrium does not cause any virtual work. Using partial integration, Gauss' divergence theorem, the transformation of the first to the second Piola-Kirchhoff stress and the definition of the Green-Lagrange strain, the principle of virtual work from eq. (3.18) can alternatively be

written as

$$\delta\Pi = \underbrace{-\int_{\Omega_0} \delta\mathbf{E} : \mathbf{S}\,\mathrm{d}\Omega}_{\delta\Pi_{\mathrm{int}}} + \underbrace{\int_{\Omega_0} \delta\mathbf{u} \cdot \hat{\mathbf{b}}\,\mathrm{d}\Omega + \int_{\Gamma_{\mathrm{N}}} \delta\mathbf{u} \cdot \hat{\mathbf{t}}\,\mathrm{d}\Gamma}_{\delta\Pi_{\mathrm{ext}}} = 0\,. \tag{3.19}$$

Here, the internal virtual work $\delta\Pi_{\mathrm{int}}$ and external virtual work $\delta\Pi_{\mathrm{ext}}$ can be identified.

Another derivation of equilibrium results from the minimum potential energy principle. It states that the total energy, i. e., the sum of the internal and the external energy, of a mechanical system becomes minimal in the state of equilibrium

$$\Pi_{\mathrm{tot}} = \Pi_{\mathrm{int}} + \Pi_{\mathrm{ext}} = \min\,. \tag{3.20}$$

With the definition for the internal and external energy

$$\Pi_{\mathrm{int}} = -\int_{\Omega} \frac{1}{2}\mathbf{S} : \mathbf{E}\,\mathrm{d}\Omega\,, \tag{3.21}$$

$$\Pi_{\mathrm{ext}} = \int_{\Omega} \mathbf{u} \cdot \hat{\mathbf{b}}\,\mathrm{d}\Omega + \int_{\Gamma_{\mathrm{N}}} \mathbf{u} \cdot \hat{\mathbf{t}}\,\mathrm{d}\Gamma \tag{3.22}$$

the potential energy, which needs to be minimized, can be derived as

$$\Pi_{\mathrm{tot}} = -\int_{\Omega} \frac{1}{2}\mathbf{S} : \mathbf{E}\,\mathrm{d}\Omega + \int_{\Omega} \mathbf{u} \cdot \hat{\mathbf{b}}\,\mathrm{d}\Omega + \int_{\Gamma_{\mathrm{N}}} \mathbf{u} \cdot \hat{\mathbf{t}}\,\mathrm{d}\Gamma = \min\,. \tag{3.23}$$

This is the functional of the potential energy and contains the typical main characteristics of a functional as explained in the previous chapter. One of them is the argument, which represents a function instead of a scalar parameter. In the case of the potential energy functional, this function, which needs to be solved for, is the displacement field $\mathbf{u}$. Following the methods of variational calculus, the variation with respect to the displacement $\mathbf{u}$ has to be zero

$$\delta\Pi_{\mathrm{tot}} = -\int_{\Omega} \delta\mathbf{E} : \mathbf{S}\,\mathrm{d}\Omega + \int_{\Omega} \delta\mathbf{u} \cdot \hat{\mathbf{b}}\,\mathrm{d}\Omega + \int_{\Gamma_{\mathrm{N}}} \delta\mathbf{u} \cdot \hat{\mathbf{t}}\,\mathrm{d}\Gamma = 0\,. \tag{3.24}$$

By a transformation of the variation in eq. (3.24), the equilibrium in eq. (3.14) and the Neumann boundary conditions in eq. (3.16) the boundary value problem can, in turn, be derived. In doing so, it can be seen that the Neumann boundary conditions are directly introduced into the minimum potential energy principle by taking the boundary term in the external energy into account. The Neumann boundary conditions are natural boundaries as they result automatically from the solution of eq. (3.24). The Dirichlet

boundary conditions, however, represent essential boundary conditions and need to be considered in the further derivation.

The derived variation in eq. (3.24) also corresponds to the principle of virtual work from eq. (3.19). The two principles are therefore equivalent, but with the condition that the minimum potential energy principle can only be derived for problems in which such a potential Π_{tot} actually exists. The principle of virtual work, on the other hand, can also be applied for problems without a potential, as in cases that include plasticity, frictional sliding or non-conservative loading. It is therefore more general.

Both derivations, however, lead to the weak form of the boundary value problem, where the equilibrium, as well as the Neumann boundary conditions, are fulfilled in an integral way. Furthermore, in the weak form, the highest degree of derivative reduces compared to the boundary value problem itself. This leads to lower requirements regarding the differentiability of the solution function $\mathbf{u}$ for a subsequent numerical solution. All in all, the weak formulation of the boundary value problem in solid mechanics can be reformulated in a compact manner as: Find the displacement field $\mathbf{u}$, representing the solution function, such that $\delta\Pi(\mathbf{u}) = 0$ for any test function $\delta\mathbf{u}$.

3.2 Spatial discretization and finite element formulation

The equations of the boundary value problem in the weak form are so far continuous. This means that a displacement field $\mathbf{u}$ is searched for that satisfies the weak form for any test function $\delta\mathbf{u}$. If such a displacement field is found, then the corresponding differential equations are fulfilled exactly at each material point. Since in the field of mechanics, an analytical solution can be found only in very few cases, numerical methods are applied for the solution of the underlying partial differential equations. In this work, the finite element method (FEM) is used to solve the boundary value problem or, in this case, the weak form of the boundary value problem from eq. (3.19) or eq. (3.24). In this numerical method, the domain, as well as the solution function, is discretized. Thus, the continuous function is converted into a discrete problem with a finite number of evaluation points, the nodes, where discrete unknown variables are defined and solved for by algebraic equations. Between these points, the values are interpolated and approximated by so-called shape functions. Within the scope of this work, displacement-based finite elements, where only the displacements $\mathbf{u}$ are the sought-after solution functions, are primarily used.

In this section, the discretization of the domain and the displacement field within the isoparametric concept is introduced. Next, the requirements for the shape functions to guarantee convergence of the finite element method are presented. Afterwards, the

chosen nonlinear solution technique, the Newton-Raphson method with a linearization of the residual, is described. Further literature on the finite element method is for example given in the textbooks by HUGHES (2000), ZIENKIEWICZ AND TAYLOR (2006) and BELYTSCHKO ET AL. (2014).

3.2.1 Isoparametric concept

As already mentioned, the basic idea of the finite element method is to transform the continuous problem into a discrete problem with a finite number of degrees of freedom. For this purpose, the domain Ω is divided into a finite number n_{ele} of subdomains Ω_e, the so-called finite elements

$$\Omega \approx \Omega_h = \bigcup_{e=1}^{n_{\mathrm{ele}}} \Omega_e \, . \tag{3.25}$$

Herein, Ω_h represents the discrete approximation of the whole domain by the subdomains Ω_e, which are assembled using the assembly operator $\bigcup$. Each finite element is defined by a number $n_{\mathrm{nd,ele}}$ of nodes per element. The individual elements are connected via these nodes that are shared by neighboring elements. Between the nodes, the nodal values of the discrete functions are interpolated by $n_{\mathrm{nd,ele}}$ shape functions N within the element. Consequently, the approximation of the unknown displacement field $\mathbf{u}$ within an element is

$$\mathbf{u}_e(\mathbf{X}) \approx \mathbf{u}_{e,h}(\mathbf{X}) = \sum_{k=1}^{n_{\mathrm{nd,ele}}} N_k(\mathbf{X}) \mathbf{d}_k = \mathbf{N}(\mathbf{X}) \mathbf{d}_e \, . \tag{3.26}$$

This defines a discrete approximation of the displacement field inside each element, the ansatz function. The vectors $\mathbf{d}_k$ are the nodal values of one element. In the case of the displacement approximation, they represent the nodal displacement values, the degrees of freedom, which are located at the nodes of the elements. The matrix $\mathbf{N}$ and the vector $\mathbf{d}_e$ collect the shape functions, or the degrees of freedom, respectively, of one element. Usually, the shape functions are defined in a natural coordinate system $\boldsymbol{\xi}$ of a single reference element or a group of reference elements, a so-called patch. The mapping between the natural coordinate system and the Euclidian coordinate system, in which the whole domain is defined, is represented by a Jacobian matrix $\mathbf{J}_e = \frac{\partial \mathbf{X}_e}{\partial \boldsymbol{\xi}}$. The approximation of $\mathbf{u}$ then transforms into

$$\mathbf{u}_{e,h}(\boldsymbol{\xi}) = \sum_{k=1}^{n_{\mathrm{nd,ele}}} N_k(\boldsymbol{\xi}) \mathbf{d}_k = \mathbf{N}(\boldsymbol{\xi}) \mathbf{d}_e \, . \tag{3.27}$$

In addition to the solution functions, the test functions also need to be discretized. In the Bubnov-Galerkin approach that is pursued in this work, the virtual displacements $\delta\mathbf{u}$ are approximated with the same shape functions

$$\delta\mathbf{u}_{e,h}(\boldsymbol{\xi}) = \sum_{k=1}^{n_{\mathrm{nd,ele}}} N_k(\boldsymbol{\xi})\delta\mathbf{d}_k = \mathbf{N}(\boldsymbol{\xi})\delta\mathbf{d}_e \,. \tag{3.28}$$

Finally, the geometry of the reference configuration is discretized as well. Within the isoparametric concept, this is performed with the same shape functions

$$\mathbf{X}_h(\boldsymbol{\xi}) = \sum_{k=1}^{n_{\mathrm{nd,ele}}} N_k(\boldsymbol{\xi})\mathbf{X}_k = \mathbf{N}(\boldsymbol{\xi})\mathbf{X}_e \,. \tag{3.29}$$

If these three discretizations of the displacement field, the virtual displacement field and the geometry are carried out, all further quantities, e. g., the strain and stress measures, can also be described in a discrete form. To obtain a system of equations that contains all degrees of freedom $\mathbf{D}$ of a given problem, the nodal values of the elements are assembled via the previously introduced assembly operator

$$\mathbf{D} = \bigcup_{e=1}^{n_{\mathrm{ele}}} \mathbf{d}_e \,. \tag{3.30}$$

The isoparametric concept builds the basis for most finite element formulations in scientific and commercial software. Especially the definition of the shape functions in the natural coordinate system, i. e., the parameter space, has proven to be efficient. It enables a simple description of distorted element shapes by the Jacobian and has advantages in numerical integration.

Special attention is also paid to the type of shape functions. Mainly Lagrange shape functions with trilinear or bilinear functions are widespread due to efficiency reasons. However, also shape functions of higher order are used, among others, in the field of p-FEM. In recent years, a strong development concerning the isogeometric concept, where Non-Uniform Rational B-Splines (NURBS) are used as shape functions, is recognizable (COTTRELL ET AL. 2009). These allow for a better approximation of the geometry as well as the solution functions attributable to a higher degree of continuity. The mentioned shape functions differ in efficiency, their approximation capability, polynomial degree and differentiability. Depending on the problem, they must meet specific requirements. Their continuity within and between the elements plays an important role, which will be explained in more detail in the next section.

3.2.2 Convergence requirements

In the previous section, the isoparametric concept within the finite element method was presented. Here, an approximated numerical solution of a differential equation is found by employing a discretization of the domain with finite elements. With the number of elements also the number of degrees of freedom increases. A numerical method is called convergent if the numerical solution approaches the analytical solution of the underlying differential equation. Thus, with a constant polynomial degree p, a more and more accurate solution and approximation are expected with an increasing number of degrees of freedom. The theorem of Lax-Wendroff states that convergence of a finite element method is ensured if it is consistent and stable. The first requirement, consistency, is guaranteed by completeness and compatibility. These two factors, in particular, impose requirements on the shape functions. A decisive factor here is the variational index n. It is defined as the highest derivative of the unknown function occurring in the weak form.

Completeness means that the shape functions are able to exactly reproduce functions up to a polynomial order of $p = n$.

Compatibility, on the other hand, requires at least C^n-continuity within the element and at least C^{n-1}-continuity between the elements.

A function, whose n^th derivative is continuous, is called C^n-continuous. For the most standard displacement-based elements, based on the principle of virtual work, the variational index is $n = 1$, as only first derivatives appear in the weak form. The shape functions should, therefore, contain at least linear polynomials. Additionally, C^0-continuity is required between the elements. The functions should thus have the same value at connecting nodes and along a connecting edge, but are allowed to have a kink at the element transition. The requirements on shape functions change according to the type of structural theory and, therefore, according to the weak form.

Stability is secured by a sufficient integration order and a regular element shape, which is characterized by a positive Jacobian determinant.

If the conditions for stability are not met, zero energy modes can occur. On the other hand, particularly the rule of sufficient integration order can be relaxed to avoid undesired unphysical effects, such as locking. More information on these effects can be found in BOFFI ET AL. (2013).

3.2.3 Discretized weak form, linearization and solution procedure

With the discretization and the shape functions, which satisfy the described require-
ments, an approximated solution of the weak form of the boundary value problem can
be found. In the following, tensor notation is replaced by matrix notation in a Voigt-
representation of the main quantities for an improved readability. For reasons of com-
prehensibility, the principle of virtual work (eq. 3.19) or the variation of the potential
energy (eq. 3.24) is repeated here in matrix notation:

$$\delta\Pi_{\text{tot}} = -\int_{\Omega} \delta\mathbf{E}^{\text{T}}\mathbf{S} \, d\Omega + \int_{\Omega} \delta\mathbf{u}^{\text{T}}\hat{\mathbf{b}} \, d\Omega + \int_{\Gamma_{\text{N}}} \delta\mathbf{u}^{\text{T}}\hat{\mathbf{t}} \, d\Gamma = 0 \,. \tag{3.31}$$

By applying the St. Venant-Kirchhoff material law from eq. (3.10), which establishes a
relationship between the Green-Lagrange strains and the second Piola-Kirchhoff stress
tensor, the following representation is obtained

$$\delta\Pi_{\text{tot}} = -\int_{\Omega} \delta\mathbf{E}^{\text{T}}\mathbf{C}\mathbf{E} \, d\Omega + \int_{\Omega} \delta\mathbf{u}^{\text{T}}\hat{\mathbf{b}} \, d\Omega + \int_{\Gamma_{\text{N}}} \delta\mathbf{u}^{\text{T}}\hat{\mathbf{t}} \, d\Gamma = 0 \,. \tag{3.32}$$

This is the variational formulation of the problem that is to be solved for the unknown
displacements. The solution is carried out with a transformation from the continuous
form into a set of algebraic equations by the discretization of the displacements (eq. 3.27)
and their variations (eq. 3.28).

Discretized form of the equilibrium equation

In order to obtain the discretized form of the equilibrium equation, the variations of the
discretized quantities are derived with the rules of calculus of variations. Due to the dis-
cretization, the nodal values of the displacements $\mathbf{d}$ represent the unknown parameters.
For the discretized virtual displacements, it therefore follows

$$\delta\mathbf{u} = \left(\frac{\partial\mathbf{u}}{\partial\mathbf{d}}\right)\delta\mathbf{d} = \mathbf{N}\delta\mathbf{d} \,, \tag{3.33}$$

$$\delta\mathbf{u}^{\text{T}} = \delta\mathbf{d}^{\text{T}}\left(\frac{\partial\mathbf{u}}{\partial\mathbf{d}}\right)^{\text{T}} = \delta\mathbf{d}^{\text{T}}\mathbf{N}^{\text{T}} \,. \tag{3.34}$$

The variation of the strains is also required for the first term, which contains the internal
virtual work. The strains depend in turn on the displacements and are derived with the

same rules

$$\delta \mathbf{E} = \left(\frac{\partial \mathbf{E}}{\partial \mathbf{d}}\right)\delta\mathbf{d} = \mathbf{B}\delta\mathbf{d}\,, \tag{3.35}$$

$$\delta \mathbf{E}^{\mathrm{T}} = \delta\mathbf{d}^{\mathrm{T}}\left(\frac{\partial \mathbf{E}}{\partial \mathbf{d}}\right)^{\mathrm{T}} = \delta\mathbf{d}^{\mathrm{T}}\mathbf{B}^{\mathrm{T}}\,. \tag{3.36}$$

The derivative of the strains with respect to the displacement values is defined as the strain-displacement-operator $\mathbf{B}$. The discretization also divides the integration domain. Therefore, the integration takes place on element level. Accordingly, the weak form of the boundary value problem is transformed into

$$\sum_{e=1}^{n_{\mathrm{ele}}} \left(\int_{\Omega_e} \delta\mathbf{d}^{\mathrm{T}}\mathbf{B}^{\mathrm{T}}\mathbf{C}\mathbf{E}\,\mathrm{d}\Omega - \int_{\Omega_e} \delta\mathbf{d}^{\mathrm{T}}\mathbf{N}^{\mathrm{T}}\hat{\mathbf{b}}\,\mathrm{d}\Omega - \int_{\Gamma_{\mathrm{N},e}} \delta\mathbf{d}^{\mathrm{T}}\mathbf{N}^{\mathrm{T}}\hat{\mathbf{t}}\,\mathrm{d}\Gamma \right) = 0\,. \tag{3.37}$$

The Dirichlet boundary conditions, which specify the displacements on the displacement boundary Γ_{D}, are introduced here by the choice of the ansatz functions. They are defined such that they satisfy the boundary conditions, i. e., $\delta\mathbf{d} = \mathbf{0}$ and $\mathbf{d} = \hat{\mathbf{d}}$ on Γ_{D}. As the nodal values of the displacements only contain discrete values and no functions, they can be extracted from the integrals

$$\sum_{e=1}^{n_{\mathrm{ele}}} \delta\mathbf{d}^{\mathrm{T}} \left(\underbrace{\int_{\Omega_e} \mathbf{B}^{\mathrm{T}}\mathbf{C}\mathbf{E}\,\mathrm{d}\Omega}_{\mathbf{f}_{\mathrm{int}}} \underbrace{- \int_{\Omega_e} \mathbf{N}^{\mathrm{T}}\hat{\mathbf{b}}\,\mathrm{d}\Omega - \int_{\Gamma_{\mathrm{N},e}} \mathbf{N}^{\mathrm{T}}\hat{\mathbf{t}}\,\mathrm{d}\Gamma}_{-\mathbf{f}_{\mathrm{ext}}} \right) = 0\,. \tag{3.38}$$

Herein, the internal and external forces on element level can be identified as

$$\mathbf{f}_{\mathrm{int}}(\mathbf{d}) = \int_{\Omega_e} \mathbf{B}^{\mathrm{T}}\mathbf{C}\mathbf{E}(\mathbf{d})\,\mathrm{d}\Omega\,, \tag{3.39}$$

$$\mathbf{f}_{\mathrm{ext}} = \int_{\Omega_e} \mathbf{N}^{\mathrm{T}}\hat{\mathbf{b}}\,\mathrm{d}\Omega + \int_{\Gamma_{\mathrm{N},e}} \mathbf{N}^{\mathrm{T}}\hat{\mathbf{t}}\,\mathrm{d}\Gamma\,, \tag{3.40}$$

which can be assembled via the assembly operator to the global vectors of internal and external forces

$$\mathbf{F}_{\mathrm{int}}(\mathbf{D}) = \bigcup_{e=1}^{n_{\mathrm{ele}}} \mathbf{f}_{\mathrm{int}}(\mathbf{d}) \qquad \text{and} \qquad \mathbf{F}_{\mathrm{ext}} = \bigcup_{e=1}^{n_{\mathrm{ele}}} \mathbf{f}_{\mathrm{ext}}\,. \tag{3.41}$$

The internal forces depend nonlinearly on the displacements, whereas the external forces are independent of the displacement field in a conservative loading situation. Similarly, the values on element level are assembled to the global vector of degrees of freedom $\mathbf{D}$. With these definitions, eq. (3.37) can be written, using the global vector of degrees of

freedom, as

$$\delta \mathbf{D}^{\mathrm{T}}(\mathbf{F}_{\mathrm{int}}(\mathbf{D}) - \mathbf{F}_{\mathrm{ext}}) = 0\,. \tag{3.42}$$

The values of the virtual nodal displacements $\delta \mathbf{D}$ may take any value. Therefore, the static equilibrium condition can be expressed in the discretized residual form as

$$\mathbf{R}(\mathbf{D}) = \mathbf{F}_{\mathrm{int}}(\mathbf{D}) - \mathbf{F}_{\mathrm{ext}} = \mathbf{0}\,, \tag{3.43}$$

and thus represents a set of nonlinear algebraic equations.

Linearization and system of equations

In this thesis, the Newton-Raphson method is applied for the solution of the nonlinear equation (3.43). It is an iterative method that is based on a linearization of the nonlinear algebraic equations of the residual and on a solution of the resulting linear system of equations. The unknown quantities, in this case the nodal displacements, are iteratively updated until a prescribed convergence criterion is met.

The starting point is the linearization of the residual. This corresponds to a Taylor series expansion with a truncation after the linear term, i.e.,

$$\mathrm{LIN}\,\mathbf{R} = \mathbf{R} + \frac{\partial \mathbf{R}}{\partial \mathbf{D}}\Delta\mathbf{D} = \mathbf{0}\,. \tag{3.44}$$

The required derivative of the residual is defined as the tangent stiffness matrix. As the external forces do not depend on the displacements in conservative loading situations, the derivative can be restricted to the internal forces. On element level, it follows for the element tangent stiffness matrix

$$\mathbf{k}_{\mathrm{T}} = \frac{\partial \mathbf{f}_{\mathrm{int}}}{\partial \mathbf{d}} = \int\limits_{\Omega_e} \left(\mathbf{B}^{\mathrm{T}}\mathbf{C}\mathbf{B} + \frac{\partial \mathbf{B}}{\partial \mathbf{d}}\mathbf{S}\right)\mathrm{d}\Omega\,. \tag{3.45}$$

Therein, two terms can be distinguished and interpreted. The first term

$$\mathbf{k}_{\mathrm{eu}} = \mathbf{k}_{\mathrm{e}} + \mathbf{k}_{\mathrm{u}} = \int\limits_{\Omega_e} \mathbf{B}^{\mathrm{T}}\mathbf{C}\mathbf{B}\,\mathrm{d}\Omega \tag{3.46}$$

is the combination of the elastic stiffness matrix $\mathbf{k}_{\mathrm{e}}$ and the so-called initial displacement stiffness matrix $\mathbf{k}_{\mathrm{u}}$. The elastic stiffness matrix corresponds to the stiffness of the undeformed reference configuration, whereas the initial displacement stiffness matrix includes the stiffness change resulting from the geometry change by deformation. The

second term

$$\mathbf{k}_{\mathrm{g}} = \int\limits_{\Omega_e} \frac{\partial \mathbf{B}}{\partial \mathbf{d}} \mathbf{S} \, \mathrm{d}\Omega \tag{3.47}$$

is called the geometric or initial stress stiffness matrix and takes the stiffness change due to the incorporated stresses in the structure into account.

The global tangent stiffness matrix is obtained from the element tangent stiffness matrices via the assembly operator

$$\mathbf{K}_{\mathrm{T}} = \bigcup_{e=1}^{n_{\mathrm{ele}}} \mathbf{k}_{\mathrm{T}} \,. \tag{3.48}$$

By insertion of the tangent stiffness into the linearization in eq. (3.44), the global linearized system of equations is derived

$$\mathbf{K}_{\mathrm{T}} \Delta \mathbf{D} = -\mathbf{R} \,. \tag{3.49}$$

This is the linear system of equations that needs to be solved in each iteration step within the Newton-Raphson method. The result is the numerically approximated displacement field for which the resulting internal forces equal the given external forces, i. e., the deformation satisfying the equilibrium conditions. The converged solution, therefore, corresponds to an equilibrium point (EP).

Solution techniques for quasi-static problems

For quasi-static problems, it is assumed that the load is applied so slowly that dynamic effects do not play a significant role. Usually, not only the final equilibrium point $\mathrm{EP}_{\mathrm{end}}$ of a structure under a certain load is relevant, but also the complete equilibrium path until the final load is reached is of interest. Furthermore, if only the end point $\mathrm{EP}_{\mathrm{end}}$ of the deformation is searched for, the Newton-Raphson method for solving the nonlinear equation (3.43) may diverge already in the case of moderately nonlinear problems. To improve convergence, the problem is typically solved incrementally. Here, additional equilibrium points EP_i are computed along the equilibrium path until the sought-after final equilibrium point is reached. The solution process is illustrated in Figure 3.2. For every increment, a converged equilibrium point EP_i is obtained iteratively with the Newton-Raphson method. This equilibrium point serves as the starting point, the predictor, for computation of the next point EP_{i+1}. With this procedure, the equilibrium path, and thus, the complete deformation process is successively determined. To describe the progress of the solution process, a scalar parameter, the so-called pseudo-time t is
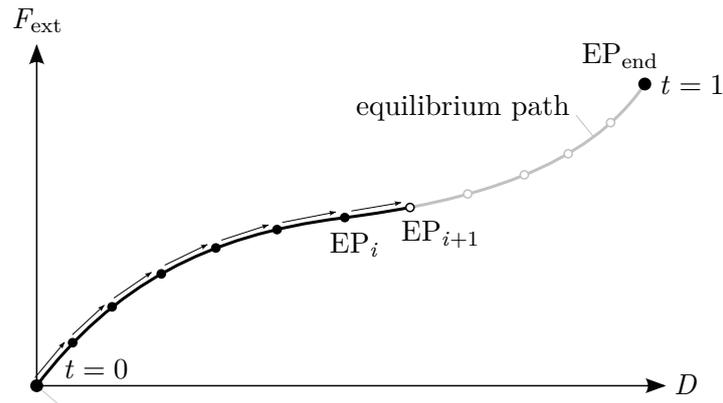
Figure 3.2: Illustration of the incremental determination of the equilibrium path.

introduced. It is zero ($t = 0$) at the beginning of the deformation and usually takes the value $t = 1$ at the end of the deformation.

There exist several path-following methods, where different incremental quantities are controlled throughout the solution process. In a load-controlled path-following method, the load is divided into increments, the load steps. For every load step, a corresponding equilibrium point is computed. Here, the pseudo-time is associated with a load factor, which describes the subsequent increase of the external load for the solution. On the contrary, in a displacement-controlled path-following method, it describes the controlled displacement degree of freedom. When using the arc length method for path-following, the arc length of the equilibrium path between the evaluated equilibrium points is controlled. However, these methods are not discussed further at this point. Similarly, there are much more elaborate techniques to obtain a good predictor state for the next load step. Nevertheless, again, the reader is referred to the corresponding literature for further details of such procedures (see HUGHES (2000), ZIENKIEWICZ AND TAYLOR (2006) and BELYTSCHKO ET AL. (2014)).

<div style="text-align: right; font-size: 4em; font-weight: bold;">4</div>

Motion Design as a Variational Formulation

In this chapter, the new method of motion design of structures is presented. First, the basic concept, including the approach and the assumptions for motion design, is elaborated. Based on that, the mathematical framework of the method is developed, starting with the functional and its variation. The solution methods that are used here are the same as for structural finite elements, but specific differences to this kind of problem need to be considered. Therefore, an additional discretization to the well-known spatial discretization with finite elements, the discretization of the motion path, is introduced. Also in the case of motion design, the Newton-Raphson method is chosen as solution procedure for the nonlinear algebraic equations. It requires a consistent linearization and leads to a linear system of equations that is to be solved in each iteration step. Furthermore, numerical experiments illustrate the working principle and allow for the interpretation of the potential of the motion design method.

4.1 Basic concept of motion design

Motion design is a method to calculate an optimal deformation path between two pre-scribed geometric configurations of a structure with respect to a given objective function. For further explanation, this is illustrated with an exemplary two-bar truss, forming a shallow arc (see Figure 4.1). It is supposed to deform from an initial configuration, shown in black, to a target configuration, shown in blue. In motion design, the optimal deformation trajectory (red) that connects these two geometries is searched for. This scenario is obviously inspired by the bi-stable setup of a snap-through problem. The blue target configuration, however, is not the stress-free snapped-through configuration of the black one, but deviates from it by a horizontal shift of the central node. At the
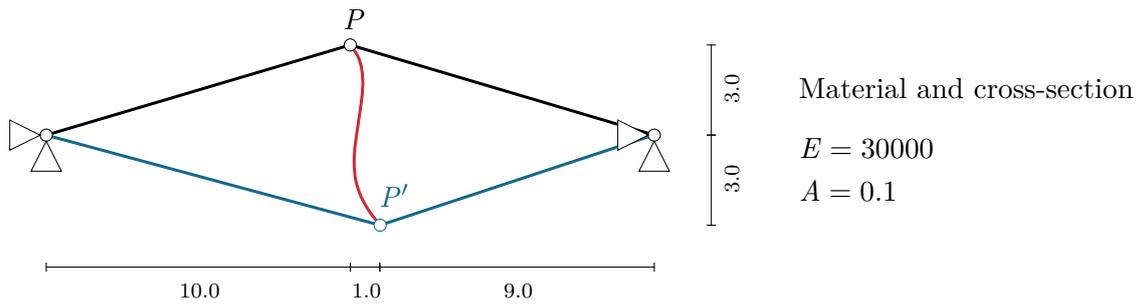
Figure 4.1: Illustration of the motion design concept with the example of a two-bar truss.

end of the deformation, the midpoint P should therefore have moved downwards and also sideways to the position P'.

This given task resembles a lot the brachistochrone problem, which was introduced in Chapter 2. The two geometric configurations at the start and the end of the deformation process correspond to the points A and B (see Figure 2.2). In the brachistochrone problem, the connection or path between these points that fulfills the prescribed requirement is searched for. This requirement, i. e., the functional, represented the minimization of the total time to traverse the connecting path. Also in the case of motion design, the curve between two configurations that minimizes a particular property is to be found. Due to this analogy, the same solution method, the variational calculus, is chosen for the development of the method of motion design. The underlying functional is presented in the following section.

The problem formulation does not include the equilibrium conditions. However, equilibrium is enforced within a post-processing step after the optimized deformation path has been found by motion design. With the resulting deformation, the internal forces can be calculated for the entire deformation process. To ensure equilibrium, these are then identified with the external forces, which in turn represent the loads required to realize the optimized deformation path obtained by motion design. One output of the method is, therefore, the evolution of the external loads throughout the deformation process that are required to follow the optimized motion trajectory.

In the exemplary two-bar truss from Figure 4.1, the structure contains two unconstrained degrees of freedom at the midpoint, the horizontal and the vertical displacement. It is therefore assumed that forces can be applied on both of them, i. e., a vertical point load as well as a horizontal point load, to reach the end configuration. More generally speaking, the basic motion design method is based on the assumption that a point force can potentially be applied at every degree of freedom. However, when considering real structures, e. g., in civil or aerospace engineering, there may be severe restrictions on the number of degrees of freedom to which external forces can actually be applied,

since some form of actuator is required at each such degree of freedom. This is why an extension of the basic motion design method will be introduced in Chapter 5, in which this limitation will be handled and resolved. Furthermore, the method and applications in this work are restricted to quasi-static problems, where inertia effects are neglected. The following contents in this chapter are closely related to the publication SACHSE and BISCHOFF (2020).

4.2 Formulation of the motion design functional

At the beginning of the motion design process, the objective function, i. e., the functional, needs to be defined. This functional defines the property that shall be assigned to the entire motion. A lot of possible objective functions can be specified. Keeping in mind that the method of motion design is developed to be applied for an efficient deformation or movement of adaptive structures, energy considerations represent a reasonable approach for a potentially suitable objective function. The advantage of such considerations regarding the energy is that they are also qualified for analyses of plant movements, as energy efficiency plays a crucial role in motions in nature.

For example, a measure for the effort to deform a structure can be defined and minimized with the presented motion design method. Such a measure is comparable to the dimensionless quantity *cost of transport* that is used in various disciplines like biology or robotics. It represents a measure to quantify the cost or energy efficiency of various transport methods, i. e., walking, swimming or flying of an animal or moving a vehicle from one location to another location. In this context, it is transferred to a *cost of deformation* for flexible structures, where also an energy criterion based on the internal strain energy is utilized. This cost of deformation is intended to represent a quantity for the required effort to deform a given flexible structure. It is defined in the following and taken as exemplary functional for the development of the motion design method in this section. In a next step, Euler's equation of a simple motion design problem is solved, following the approach of variational calculus.

4.2.1 Integrated internal energy as cost of deformation

One point that greatly contributes to a structure's efficiency is how much the material is stretched and, therefore, also stressed. The energy measure that gives a quantifiable information about this is the internal strain energy Π_{int} in eq. (3.21). However, the internal energy is path-independent and only depends on the current deformation of the structure. In order to still have a measure that takes the entire deformation process into

account, the integrated internal energy over the complete motion path s is chosen as the relevant objective function in this work. Thereupon, the functional to be minimized is

$$J = \int_s \Pi_{\text{int}} \, \mathrm{d}s \; \to \; \min . \tag{4.1}$$

If it is assumed that it requires effort to deform a structure and maintain the deformed configuration and the associated internal stress state, this functional in eq. (4.54) provides an intuitive measure for the described cost of deformation. Incidentally, it is pointed out that this functional serves as a proof of concept and can be replaced by other objectives for a designed motion.

With the definition of the internal energy by a conjugate pair consisting of the Green-Lagrange strain tensor $\mathbf{E}$ and the second Piola-Kirchhoff stress tensor $\mathbf{S}$, as well as the insertion of a linear elastic St. Venant-Kirchhoff material law for the assumption of small strains (but large displacements and rotations) in matrix notation, the functional follows as

$$J = \int_s \int_\Omega \frac{1}{2} \mathbf{E}^{\mathrm{T}} \mathbf{S} \, \mathrm{d}\Omega \, \mathrm{d}s = \int_s \int_\Omega \frac{1}{2} \mathbf{E}^{\mathrm{T}} \mathbf{C} \mathbf{E} \, \mathrm{d}\Omega \, \mathrm{d}s \; \to \; \min . \tag{4.2}$$

In the example of the two-bar truss, the point P follows the trajectory (red) until it arrives at the end position P', as can be seen in Figure 4.2a. Figure 4.2b shows a diagram, where the internal energy is plotted over the two displacement degrees of freedom D_1 and D_2. Here, the yet unknown trajectory of the point P (red) can be identified within the plane that is spanned by the axes D_1 and D_2. The corresponding internal energy throughout the entire deformation process is obtained by a projection of
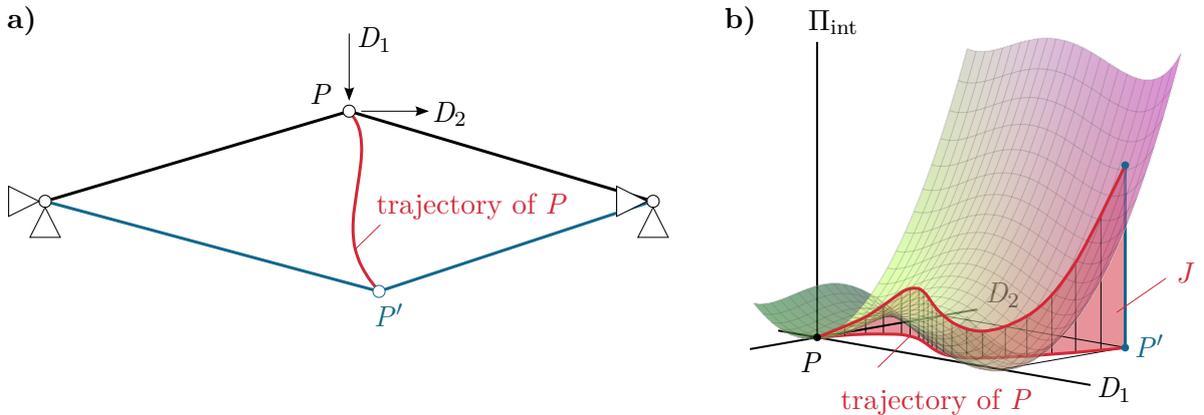
Figure 4.2: Exemplary two-bar truss. a) Initial and end configuration with trajectory of point P. b) Visualization of the functional.

the trajectory onto the plotted surface. The area that is spanned by the projection can then be identified as the value of the functional. Consequently, motion design aims at finding the trajectory that minimizes this area and, therefore, the cost of deformation.

4.2.2 Motion path and normalized arc length

The deformation is described by the displacement field $\mathbf{u}$ (cf. Figure 4.3). The length of the path, along which the internal energy of the structure is integrated, can be associated with the arc length of this displacement field of the underlying motion, which in turn is a function of the position $\mathbf{X}$ of the structure as well as the progress of the motion, the pseudo time t

$$\mathbf{u}(\mathbf{X},t) = \begin{bmatrix} u_1(\mathbf{X},t) \\ u_2(\mathbf{X},t) \\ u_3(\mathbf{X},t) \end{bmatrix}. \tag{4.3}$$

In order to consider the motion in its entirety within the functional, the internal energy is integrated over the deformation path s. This deformation path s represents a scalar measure that indicates how much the structure has already moved and deformed. Unlike the pseudo-time or the physical time t, it does not proceed independently, but is directly coupled to the deformation. Consequently, it is defined here as the arc length of the displacement field $\mathbf{u}(\mathbf{X},t)$. But since it still depends on the position $\mathbf{X}$, the mean value of the displacement arc length over the whole spatial domain Ω is employed. Based on the same derivation as in the brachistochrone problem (see Figure 2.4 and eq. (2.9)), an infinitesimal arc length can then be specified for a three-dimensional problem as

$$\mathrm{d}s = \frac{1}{V} \int_\Omega \sqrt{\mathrm{d}u_1^2 + \mathrm{d}u_2^2 + \mathrm{d}u_3^2}\, \mathrm{d}\Omega \tag{4.4}$$
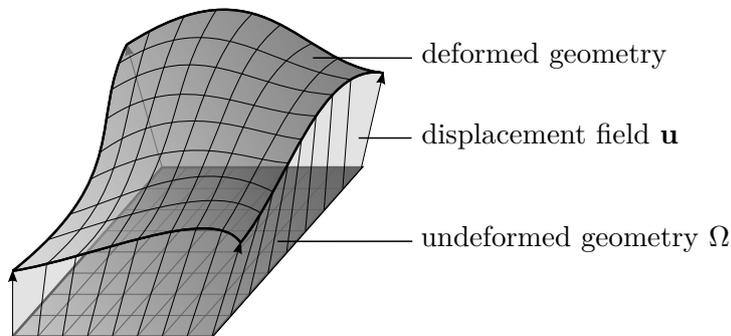
Figure 4.3: Illustration of the displacement field.

with V being the total volume of the domain, which can be integrated in order to obtain the total arc length $s_{\text{tot}} = \int \mathrm{d}s$. The arc length of the deformation of an initial geometry to a deformed end configuration strongly depends on how the resulting displacement field $\mathbf{u}$ changes throughout the motion. In the illustrating example of the two-bar truss, the arc length is calculated as follows: Because this problem involves only two degrees of freedom that are located at one node, the arc length represents the trajectory length of the point P multiplied by half of the length of the connecting bars. Accordingly, the arc length or trajectory of a direct connection between P and P' is different from one that takes a detour that might be beneficial for the functional value.

However, the internal energy is integrated over the arc length in the functional. As this arc length is initially unknown, the integration bounds are not fixed, but remain unknown, as it was the case in the brachistochrone problem. Therefore, another parameter must be introduced that indicates the motion progress, but provides fixed integration bounds. As has been discussed in Section 3.2, such a parameter indicating the motion progress is usually already known in quasi-static structural analysis, namely the pseudo-time t, which typically runs from $t = 0$ to $t = 1$. This idea is adopted in the context of motion design and the path parameter is re-defined as a normalized arc length of the deformation path. To distinguish the definition of the pseudo time in motion design from the real time or other definitions of the pseudo time in path-following methods, the normalized arc length is referred to as $\bar{s}$ in the following. At the beginning of the deformation, it is set to $\bar{s} = 0$ and it takes the value $\bar{s} = 1$ when the end configuration is reached. To also use this path parameter as integration parameter, a substitution becomes necessary

$$\int\limits_{0}^{s_{\text{u}}} (\dots)\, \mathrm{d}s = \int\limits_{0}^{1} (\dots)\frac{\mathrm{d}s}{\mathrm{d}\bar{s}}\, \mathrm{d}\bar{s} = \int\limits_{0}^{1} (\dots) s_{\text{u}}\, \mathrm{d}\bar{s}\,. \tag{4.5}$$

The mapping function s_{u} can be interpreted as a kind of velocity with respect to the path parameter $\bar{s}$ (instead of time t) and is, therefore, referred to as pseudo-velocity. It can be written in the following ways

$$\begin{aligned} s_{\text{u}} &:= \frac{\mathrm{d}s}{\mathrm{d}\bar{s}} = \frac{\frac{1}{V}\int_{\Omega} \sqrt{\mathrm{d}u_1^2 + \mathrm{d}u_2^2 + \mathrm{d}u_3^2}\, \mathrm{d}\Omega}{\mathrm{d}\bar{s}} \\[2mm] &= \frac{1}{V}\int\limits_{\Omega} \sqrt{\left(\frac{\mathrm{d}u_1}{\mathrm{d}\bar{s}}\right)^2 + \left(\frac{\mathrm{d}u_2}{\mathrm{d}\bar{s}}\right)^2 + \left(\frac{\mathrm{d}u_3}{\mathrm{d}\bar{s}}\right)^2}\, \mathrm{d}\Omega \\[2mm] &= \frac{1}{V}\int\limits_{\Omega} \sqrt{u_{1,\bar{s}}^2 + u_{2,\bar{s}}^2 + u_{3,\bar{s}}^2}\, \mathrm{d}\Omega\,. \end{aligned} \tag{4.6}$$

The minimization problem with the functional then transforms to

$$J = \int\limits_0^1 \int\limits_\Omega \frac{1}{2} \mathbf{E}^{\mathrm{T}} \mathbf{C} \mathbf{E} \, \mathrm{d}\Omega s_{\mathrm{u}} \, \mathrm{d}\bar{s} \; \rightarrow \; \min . \tag{4.7}$$

4.2.3 Solution of Euler's equation of a motion design problem

As has been done for the brachistochrone problem, the functional of motion design, where the internal energy is used as the cost of deformation in eq. (4.7), can also be solved by using Euler's equation from eq. (2.24). This shall be illustrated with a simple structure. However, the illustrating example of a two-bar truss from Figure 4.1 is not used here as the exemplary system. Due to the special character of the problem that incorporates snap-through in the deformation process, the optimal deformation path might not be smooth. Therefore, it is not ideally suited for an analytical solution. Instead, another example is introduced in Figure 4.4, which is more accessible to analytical solution techniques. The midnode P of the illustrated two-bar truss (black) is to be moved sideways to arrive at the prescribed end configuration (blue). Here, the horizontal degree of freedom is defined as the x-coordinate $D_1 = x$. The vertical displacement degree of freedom can then be described as a function of x as $D_2 = y(x)$. Based on these definitions, the solution curve, i.e., the trajectory of the point P, takes the form of a classical function.
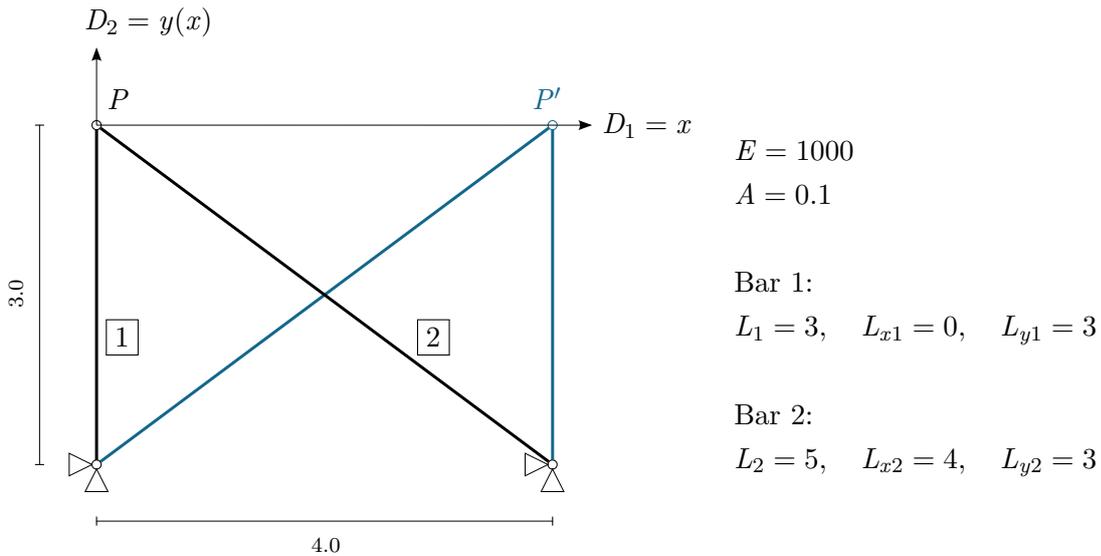
Figure 4.4: Illustrating example for the solution of Euler's equation for motion design.

With the Green-Lagrange strains of both bars

$$E_1 = \frac{1}{2} \frac{(L_{1x} + x)^2 + (L_{1y} + y(x))^2 - L_1^2}{L_1^2} \,, \tag{4.8}$$

$$E_2 = \frac{1}{2} \frac{(L_{2x} - x)^2 + (L_{2y} + y(x))^2 - L_2^2}{L_2^2} \,, \tag{4.9}$$

the internal energy can be determined for this example as

$$\Pi_{\text{int}} = \frac{1}{2} E_1 E E_1 A L_1 + \frac{1}{2} E_2 E E_2 A L_2 \,. \tag{4.10}$$

Due to the formulation of the degrees of freedom D_1 and D_2 as variable x and a function of this variable $y(x)$, the infinitesimal arc length can be computed in the same manner as in the brachistochrone problem as

$$\mathrm{d}s = \sqrt{\mathrm{d}x^2 + \mathrm{d}y^2} = \sqrt{\left(\frac{\mathrm{d}x}{\mathrm{d}x}\right)^2 + \left(\frac{\mathrm{d}y}{\mathrm{d}x}\right)^2}\,\mathrm{d}x = \sqrt{1 + y'(x)^2}\,\mathrm{d}x \,. \tag{2.9}$$

Mapping the parameter for the integration is not necessary in this case, as the integration domain of x from $x = 0$ to $x = 4$ is prescribed. The functional then results to

$$J = \int_0^4 \left(\frac{1}{2} E_1 E E_1 A L_1 + \frac{1}{2} E_2 E E_2 A L_2 \right) \sqrt{1 + y'(x)^2}\,\mathrm{d}x \,. \tag{4.11}$$

The general form of the used Euler's equation is repeated at this point for reasons of clarity and comprehensibility

$$\frac{\partial F}{\partial y} - \frac{\partial^2 F}{\partial x \partial y'} - \frac{\partial^2 F}{\partial y \partial y'} y' - \frac{\partial^2 F}{\partial y'^2} y'' = 0 \,. \tag{2.24}$$

Application of eq. (2.24) to eq. (4.11) leads to the strong form of motion design for the problem in Figure 4.4

$$
\begin{aligned}
& \left(E_1 EA \frac{L_{1y} + y(x)}{L_1} + E_2 EA \frac{L_{2y} + y(x)}{L_1} \right) \sqrt{1 + y'(x)^2} \\
& - \left(E_1 EA \frac{L_{1x} + x}{L_1} + E_2 EA \frac{-L_{2x} + x}{L_1} \right) \frac{y'(x)}{\sqrt{1 + y'(x)^2}} \\
& - \left(\left(E_1 EA \frac{L_{1y} + y(x)}{L_1} + E_2 EA \frac{L_{2y} + y(x)}{L_1} \right) \frac{y'(x)}{\sqrt{1 + y'(x)^2}} \right) y'(x) \\
& - \left(- \left(\frac{1}{2} E_1 EE_1 AL_1 + \frac{1}{2} E_2 EE_2 AL_2 \right) \frac{y'(x)^2}{\sqrt{(1 + y'(x)^2)^3}} \right. \\
& \left. + \left(\frac{1}{2} E_1 EE_1 AL_1 + \frac{1}{2} E_2 EE_2 AL_2 \right) \frac{1}{\sqrt{1 + y'(x)^2}} \right) y''(x) = 0 \,.
\end{aligned}
\tag{4.12}
$$

The resulting equation represents a differential equation, which can hardly be solved analytically. Therefore, the method of finite differences is used for obtaining a numerical solution. In this method, the domain of the variable x is divided into multiple parts and the differential quotient is replaced by a difference quotient. To get an approximated curve in a sufficiently high resolution, the domain is divided into 100 parts. Figure 4.5 shows the solution curve (red) on the real system (a) and in a scaled graph (b). The red solution curve is the trajectory of the midpoint P that minimizes the functional. To minimize the internal energy throughout the entire motion, it follows an unsymmetric S-shaped trajectory attributable to the initial unsymmetric configuration with different bar lengths.
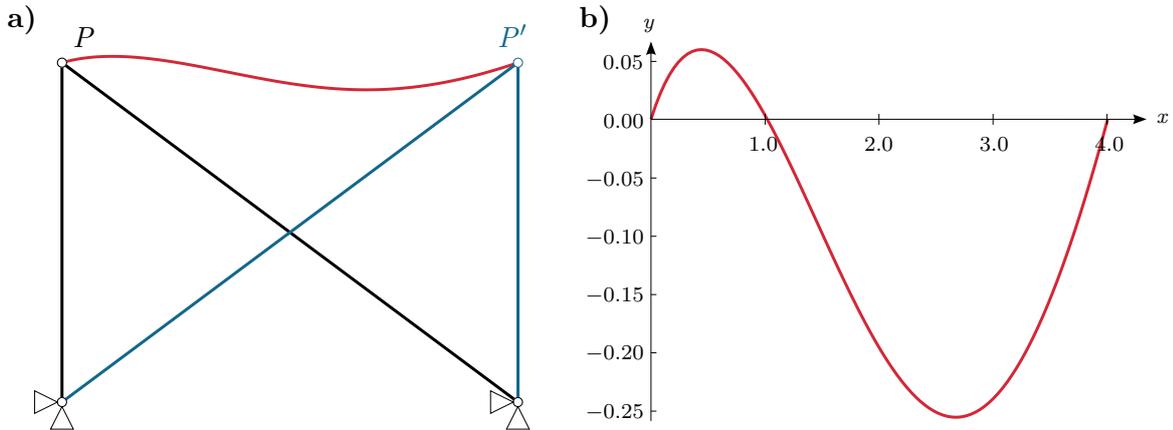
Figure 4.5: Solution curve of Euler's equation for motion design. a) Motion path illustrated a) in the structure and b) in a scaled graph.

4.3 First variation of the motion design functional

4.3.1 Continuous variation

Following the methods of variational calculus, the first variation of the motion design functional is derived. The Green-Lagrange strains $\mathbf{E}$ as well the pseudo-velocity s_{u} are functions of the unknown displacements. Therefore, the first variation is computed according to the chain rule with respect to these quantities and set equal to zero

$$\delta J = \int\limits_0^1 \left(\int\limits_\Omega \delta \mathbf{E}^{\mathrm{T}} \mathbf{C} \mathbf{E} \, \mathrm{d}\Omega s_{\mathrm{u}} + \int\limits_\Omega \frac{1}{2} \mathbf{E}^{\mathrm{T}} \mathbf{C} \mathbf{E} \, \mathrm{d}\Omega \delta s_{\mathrm{u}} \right) \mathrm{d}\bar{s} = 0 \,. \tag{4.13}$$

The next step is the introduction of the discretization. As this method is to be applied for motions of flexible structures, the geometry as well as the displacement field are spatially discretized with finite elements in the following.

4.3.2 Introduction of the spatial discretization

Spatial degrees of freedom

As in structural analyses, the obtained continuous variation in eq. (4.13), representing a differential equation, is solved with finite elements. The spatial discretization has already been introduced in Section 3.2 and is also applied at this point. However, there is a significant difference: In motion design, the displacement degrees of freedom are still functions of the normalized arc length $\bar{s}$, which describes the dependency of the deformation on the motion progress, i. e., the deformation path. The approximated semidiscrete displacement field obtained by the spatial discretization can then be written for one finite element as

$$\mathbf{u}_{e,h}(\boldsymbol{\xi},\bar{s}) = \mathbf{N}(\boldsymbol{\xi})\mathbf{d}_e(\bar{s}) \,. \tag{4.14}$$

The global spatial displacement degrees of freedom, which also still depend on the path parameter $\bar{s}$, are again obtained by an assembly operation

$$\mathbf{D}(\bar{s}) = \bigcup\limits_{e=1}^{n_{\mathrm{ele}}} \mathbf{d}_e(\bar{s}) \,. \tag{4.15}$$

This dependency on the normalized arc length also holds for the variations of the local and global degrees of freedom $\delta\mathbf{d}(\bar{s})$ and $\delta\mathbf{D}(\bar{s})$, respectively.

Pseudo-velocity

The definition of the pseudo-velocity from eq. (4.6) can also be expressed in a spatially discretized form. As it is defined for the entire spatial domain, not only for one finite element, the discretized infinitesimal arc length transforms into a function of the global degrees of freedom $\mathbf{D}(\bar{s})$. First, the lengths of the trajectories of the individual nodes of the spatial discretization are generated. According to eq. (4.6), the pseudo-velocity of one node then follows as

$$s_{\mathrm{u},k} = \sqrt{\sum_{i}^{n_{\mathrm{disp,nd}}} D_{ik,\bar{s}}(\bar{s})^2} \,, \tag{4.16}$$

with $n_{\mathrm{disp,nd}}$ being the number of displacement degrees of freedom per node. Simply building the mean value of all nodal displacement velocities results in a dependency of the spatial discretization. Therefore, a mean value, in this case the root mean square, of the nodal trajectory lengths is determined, taking into account the influence volume V_k of each individual node k, as illustrated in Figure 4.6. The root mean square can then be computed as

$$s_{\mathrm{u}} = \sqrt{\frac{1}{V} \sum_{k}^{n_{\mathrm{nd}}} V_k s_{\mathrm{u},k}^2} \,, \tag{4.17}$$

representing the spatially discretized pseudo-velocity. It can be seen in eq. (4.16) and eq. (4.17), that the pseudo-velocity depends on the derivative of the displacements and not on the displacements themselves. Thus, the variation needs to be considered with respect to the derivative of the global displacement degrees of freedom

$$\delta s_{\mathrm{u}} = \left(\frac{\partial s_{\mathrm{u}}}{\partial \mathbf{D}_{,\bar{s}}}\right)^{\mathrm{T}} \delta \mathbf{D}_{,\bar{s}} \,. \tag{4.18}$$

trajectory of node k

node k

influence volume V_k
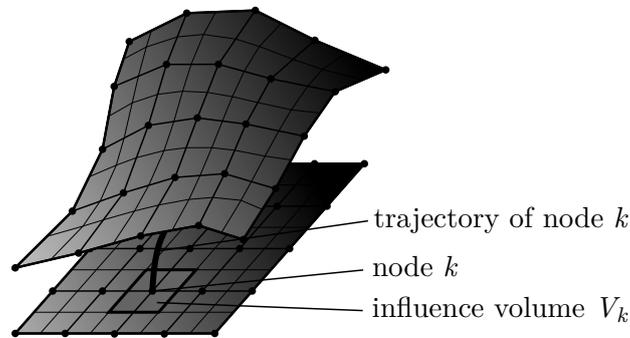
Figure 4.6: Illustration of a nodal trajectory and the influence volume.

It includes the gradient of s_u differentiated after the derivatives of the global displacements. For a concise notation, the following short notations for the derivatives of the pseudo-velocity with respect to the spatial parameters are introduced as

$$\mathbf{s}_\mathrm{u} := \frac{\partial s_\mathrm{u}^s}{\partial \mathbf{D}_{,\bar{s}}}\,, \tag{4.19}$$

$$\mathbf{S}_\mathrm{u} := \frac{\partial^2 s_\mathrm{u}^s}{(\partial \mathbf{D}_{,\bar{s}})^2}\,. \tag{4.20}$$

4.3.3 Semidiscrete variation with a discretization in space

The discretized variations derived above can now be inserted into the continuous variation from eq. (4.13). The spatially discretized variation then follows as

$$\delta J = \int\limits_0^1 \left(\sum_{e=1}^{n_\mathrm{ele}} \int\limits_{\Omega_e} \delta \mathbf{d}^\mathrm{T} \mathbf{B}^\mathrm{T} \mathbf{C} \mathbf{E}\, \mathrm{d}\Omega\, s_\mathrm{u} + \sum_{e=1}^{n_\mathrm{ele}} \int\limits_{\Omega_e} \frac{1}{2} \mathbf{E}^\mathrm{T} \mathbf{C} \mathbf{E}\, \mathrm{d}\Omega\, (\mathbf{s}_\mathrm{u} \delta \mathbf{D}_{,\bar{s}}) \right) \mathrm{d}\bar{s}\,, \tag{4.21}$$

with the strain-displacement-operator $\mathbf{B} = \partial \mathbf{E}/\partial \mathbf{d}$. Again, it has to be kept in mind that the displacement degrees of freedom $\mathbf{d} = \mathbf{d}(\bar{s})$ and their variations $\delta \mathbf{d} = \delta \mathbf{d}(\bar{s})$, included in the Green-Lagrange strains $\mathbf{E}$, are still functions of the path parameter $\bar{s}$. By rearranging the equation, the internal forces $\mathbf{F}_\mathrm{int}$ and the internal energy Π_int, both still continuous in $\bar{s}$ as well, can be identified and the variation results in

$$\delta J = \int\limits_0^1 \left(\delta \mathbf{D}^\mathrm{T} \mathbf{F}_\mathrm{int}\, s_\mathrm{u} + (\delta \mathbf{D}_{,\bar{s}})^\mathrm{T} \mathbf{s}_\mathrm{u} \Pi_\mathrm{int} \right) \mathrm{d}\bar{s}\,. \tag{4.22}$$

This represents the semidiscrete variation of the motion design functional.

4.4 Discretization of the motion path

The just derived semidiscrete variation of the motion design functional is already discretized in space. However, the spatial degrees of freedom $\mathbf{D}(\bar{s})$ are still functions of the path and still continuous in the deformation process, i. e., in the normalized path parameter $\bar{s}$. Therefore, a second discretization, the path discretization, is required for the development of the motion design method. It can also be denoted as a discretization of motion. Thus, the fully discretized variation is derived in the following.

4.4.1 Introduction of the path discretization

In the motion path discretization, the deformation path, parametrized by the normalized arc length $\bar{s} \in [0,1]$, is subdivided into $\bar{n}_{\text{ele}}$ path finite elements in the same manner as in the spatial discretization

$$\bar{s} \approx \bar{s}_h = \bigcup_{e=1}^{\bar{n}_{\text{ele}}} \bar{s}^e \,. \tag{4.23}$$

For distinction of the two discretizations, variables referring to the path discretization are marked with a bar $(\bar{\bullet})$. Furthermore, numberings are indicated with a superscript instead of a subscript. The elements are also defined by $\bar{n}_{\text{nd,ele}}$ nodes and the approximated quantities are interpolated between the nodes by shape functions $\bar{N}$ as in the spatial discretization. These shape functions can either be defined in the normalized parameter space $\bar{s} \in [0,1]$ or they can be transformed by a Jacobian. In this case, the approximated functions are the global spatial degrees of freedom $\mathbf{D}(\bar{s})$, which were, until now, still continuous in the path parameter $\bar{s}$. At this point, they are discretized in the motion:

$$\mathbf{D}^e(\bar{s}) \approx \mathbf{D}_h^e(\bar{s}) = \sum_{k=1}^{\bar{n}_{\text{nd,ele}}} \bar{N}^k(\bar{s})\bar{\mathbf{d}}^k = \bar{\mathbf{N}}(\bar{s})\bar{\mathbf{d}}^e \,. \tag{4.24}$$

Here, the vector $\bar{\mathbf{d}}_e$ comprises the local degrees of freedom, located at the nodes of one path element. The nodes of the path discretization represent the different deformed geometric configurations during the motion. This includes the initial geometry, intermediate deformed configurations and the end geometry. Consequently, in the motion discretization, the deformed configurations are interpolated by the shape functions throughout the deformation process. Therefore, the nodal degrees of freedom of the path discretization simply contain the global spatial degrees of freedom of the deformation state $\bar{s}^k$

$$\bar{\mathbf{d}}^k = \mathbf{D}^k = \mathbf{D}(\bar{s}^k) \tag{4.25}$$

and the vector of the local degrees of freedom for a path element results as

$$\bar{\mathbf{d}}^e = \begin{bmatrix} \mathbf{D}^1 \\ \mathbf{D}^2 \\ \vdots \\ \mathbf{D}^k \\ \vdots \\ \mathbf{D}^{\bar{n}_{\text{nd,ele}}} \end{bmatrix} \tag{4.26}$$

containing $\bar{n}_{\mathrm{nd,ele}}$ subvectors. The vector of the global degrees of freedom including both discretizations is obtained by assembly

$$\bar{\mathbf{D}} = \bigcup_{e=1}^{\bar{n}_{\mathrm{ele}}} \bar{\mathbf{d}}^e \tag{4.27}$$

and is constructed in this case of $\bar{n}_{\mathrm{nd}}$ subvectors

$$\bar{\mathbf{D}} = \begin{bmatrix} \mathbf{D}^1 \\ \mathbf{D}^2 \\ \vdots \\ \mathbf{D}^k \\ \vdots \\ \mathbf{D}^{\bar{n}_{\mathrm{nd}}} \end{bmatrix}, \tag{4.28}$$

where $\bar{n}_{\mathrm{nd}}$ is the total number of nodes in the motion path discretization. As a consequence, the number of total degrees of freedom results to

$$\bar{n}_{\mathrm{dof}} = \bar{n}_{\mathrm{nd}} \cdot n_{\mathrm{dof}} . \tag{4.29}$$

Accordingly, this path discretization is one-dimensional as it has only one direction, the motion progress from $\bar{s} = 0$ to $\bar{s} = 1$. When a natural coordinate $\bar{\xi}$ is used for the shape functions, a Jacobian $\bar{J} = \mathrm{d}\bar{s}/\mathrm{d}\bar{\xi}$ needs to be calculated for the derivatives. This happens in the same way as in the spatial discretization and is explained in Section 3.2. With an increasing number of degrees of freedom in space, the path forms a one-dimensional subspace within an n_{dof}-dimensional hyperspace. In general, various types of functions can be used for interpolation, such as Lagrange polynomials, B-splines or NURBS. Due to the presence of the arc length in the variation, first derivatives of the approximated functions are included in the variation and the variational index is $n = 1$. Therefore, at least C^0-continuous functions are required.

This motion path discretization is again visualized in the example of the two-bar truss as shown in Figure 4.7a. Here, the structure contains two displacement degrees of freedom D_1 and D_2, which are comprised in the vector $\mathbf{D}^k$ of the deformed configuration at the path node k

$$\mathbf{D}^k = \begin{bmatrix} D_1^k \\ D_2^k \end{bmatrix} . \tag{4.30}$$

The deformation path is exemplarily discretized with four elements and linear shape functions. As only the midpoint can move during the deformation, the trajectory of point P represents the deformation path and is, therefore, approximated with path

elements. The vectors of the degrees of freedom for all four path elements then follow as

$$\bar{\mathbf{d}}^1 = \begin{bmatrix} D_1^0 \\ D_2^0 \\ D_1^1 \\ D_2^1 \end{bmatrix} \qquad \bar{\mathbf{d}}^2 = \begin{bmatrix} D_1^1 \\ D_2^1 \\ D_1^2 \\ D_2^2 \end{bmatrix} \qquad \bar{\mathbf{d}}^3 = \begin{bmatrix} D_1^2 \\ D_2^2 \\ D_1^3 \\ D_2^3 \end{bmatrix} \qquad \bar{\mathbf{d}}^4 = \begin{bmatrix} D_1^3 \\ D_2^3 \\ D_1^{\mathrm{end}} \\ D_2^{\mathrm{end}} \end{bmatrix} \qquad (4.31)$$

and assembled to the global vector of degrees of freedom

$$\bar{\mathbf{D}} = \begin{bmatrix} D_1^0 & D_2^0 & D_1^1 & D_2^1 & D_1^2 & D_2^2 & D_1^3 & D_2^3 & D_1^{\mathrm{end}} & D_2^{\mathrm{end}} \end{bmatrix}^{\mathrm{T}}. \qquad (4.32)$$

In the initial configuration, the displacement values are zero ($D_1^0 = 0$ and $D_2^0 = 0$) and at least a part of the final displacements needs to be prescribed. Here, the values are given as $D_1^{\mathrm{end}} = 6$ and $D_2^{\mathrm{end}} = 1$. Thus, the end geometry is completely described and the internal energy of this configuration is fixed. The method for motion design aims to modify the displacements of the intermediate configurations such that the resulting area of the functional J illustrated in Figure 4.7b is minimized.

One issue with the motion design problem described so far is its potential ill-posedness for special cases. Within the path discretization, nodes may be located anywhere on the trajectory, while still approximating the same curve. This can easily be understood when imagining a trajectory in the form of a straight line. A similar issue is well-known, for instance, in shape optimization and form finding problems of thin-walled structures, where nodes can be dislocated in-plane without changing the geometry. Thus, the solution is not unique and the problem needs to be regularized. A corresponding regularization can be realized by either enforcing a uniform path element size or by
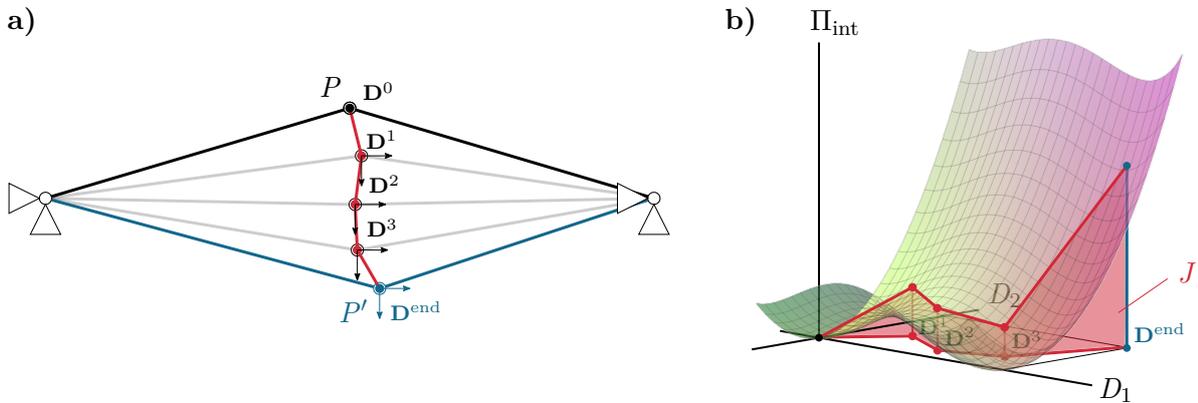
Figure 4.7: Exemplary two-bar truss with path discretization. a) Discretized motion path. b) Visualization of the discretized functional.

controlling the increments of a specified displacement degree of freedom throughout the deformation process. This aspect is further elaborated in the Section 4.5.3.

At first glance, the motion path discretization might resemble the approach of dynamic problems with space-time elements, where the time dimension is also discretized by finite elements. Nonetheless, on closer inspection, these two approaches are fundamentally different, since the arc length depends on the deformation of the structure, whereas time remains an independent and autonomous value. Another difference lies in the application of the two approaches. While space-time elements are mostly used to calculate and represent dynamic problems containing inertia effects, the motion path discretization is developed for quasi-static loading situations and static problems. This influences the required element size, as dynamic effects, which can potentially be missed by using a too coarse time discretization, do not play a role in motion design problems.

4.4.2 Path-discretized variation of the motion design functional

The semidiscrete variation in eq. (4.22) can now be fully discretized with the motion path discretization. It also includes the derivatives of the displacements with respect to the path parameter $\mathbf{D}_{,\bar{s}}$ and their variations $\delta\mathbf{D}_{,\bar{s}}$, which are calculated as

$$\mathbf{D}_{h,\bar{s}}^e = \bar{\mathbf{N}}_{,\bar{s}}\bar{\mathbf{d}}^e \tag{4.33}$$

$$\delta\mathbf{D}_{h,\bar{s}}^e = \bar{\mathbf{N}}_{,\bar{s}}\delta\bar{\mathbf{d}}^e \,. \tag{4.34}$$

The approximated functions $\mathbf{D}$, their variations $\delta\mathbf{D}$ and derivatives can now be inserted into the semidiscrete variation. By setting it to zero, the minimization problem of motion design follows as

$$\delta J = \sum_{e=1}^{\bar{n}_{\mathrm{ele}}} \int\limits_{\bar{s}_e} \left(\delta\bar{\mathbf{d}}^{\mathrm{T}}\bar{\mathbf{N}}^{\mathrm{T}}\mathbf{F}_{\mathrm{int}}s_{\mathrm{u}} + \delta\bar{\mathbf{d}}^{\mathrm{T}}\bar{\mathbf{N}}_{,\bar{s}}^{\mathrm{T}}\mathbf{s}_{\mathrm{u}}\Pi_{\mathrm{int}} \right) \mathrm{d}\bar{s} = 0 \,. \tag{4.35}$$

Transforming the equation by removing the discrete variables $\delta\bar{\mathbf{d}}$ from the integral and applying the discrete fundamental lemma of variational calculus yields the local residual $\mathbf{r}_{\mathrm{md},e}$ of motion design for each path element

$$\mathbf{r}_{\mathrm{md}}^e(\bar{\mathbf{d}}) = \int\limits_{\bar{s}_e} \left(\bar{\mathbf{N}}^{\mathrm{T}}\mathbf{F}_{\mathrm{int}}s_{\mathrm{u}} + \bar{\mathbf{N}}_{,\bar{s}}^{\mathrm{T}}\mathbf{s}_{\mathrm{u}}\Pi_{\mathrm{int}} \right) \mathrm{d}\bar{s} \,. \tag{4.36}$$

It has to be noted that this local residual is defined for the whole spatial domain, but only on one path element. Through assembly

$$\mathbf{R}_{\mathrm{md}} = \bigcup_{e=1}^{\bar{n}_{\mathrm{ele}}} \mathbf{r}_{\mathrm{md}}^{e}\,, \tag{4.37}$$

the total residual $\mathbf{R}_{\mathrm{md}}$ for the entire motion path is obtained, which is set equal to zero

$$\mathbf{R}_{\mathrm{md}}(\bar{\mathbf{D}}) = \mathbf{0}\,. \tag{4.38}$$

This represents the nonlinear residual equation that needs to be solved in motion design. The solution process is explained in the following section.

4.5 Solution procedure for motion design problems

The resulting discretized residual of motion design in eq. (4.38) was just derived from the functional and its variation. This nonlinear equation resembles a lot the residual equation for equilibrium in eq. (3.43), which has been solved with the Newton-Raphson method. Because of the similarity of both residual equations, the solution of the motion design problem is obtained with the same method. The following derivations are closely related to those in Section 3.2. Consequently, the nonlinear residual equation is solved iteratively by linearization and repeated solution of the resulting linear system of equations until convergence is reached.

4.5.1 Linearization and global system of equations

The residual is linearized by carrying out a Taylor series expansion and truncating it after the linear term

$$\mathrm{LIN}\,\mathbf{R}_{\mathrm{md}} = \mathbf{R}_{\mathrm{md}} + \frac{\partial \mathbf{R}_{\mathrm{md}}}{\partial \bar{\mathbf{D}}} \Delta \bar{\mathbf{D}} = \mathbf{0}\,. \tag{4.39}$$

In the equilibrium residual, the gradient with respect to the discrete displacement parameters represents the tangent stiffness matrix $\mathbf{K}_{\mathrm{T}}$ of the structure. Here, a different residual is differentiated with respect to different displacement parameters and the gradient in eq. (4.39) can, therefore, not be interpreted as a stiffness. However, there are familiar terms due to the relatedness of some expressions. As the global spatial displacement parameters depend on the parameters of the path discretization, the chain rule is

applied for the terms

$$\frac{\partial \mathbf{F}_{\text{int}}}{\partial \bar{\mathbf{d}}} = \frac{\partial \mathbf{F}_{\text{int}}}{\partial \mathbf{D}} \frac{\partial \mathbf{D}}{\partial \bar{\mathbf{d}}} = \mathbf{K}_{\text{T}} \bar{\mathbf{N}} , \tag{4.40}$$

$$\frac{\partial \Pi_{\text{int}}}{\partial \bar{\mathbf{d}}} = \frac{\partial \Pi_{\text{int}}}{\partial \mathbf{D}} \frac{\partial \mathbf{D}}{\partial \bar{\mathbf{d}}} = \mathbf{F}_{\text{int}} \bar{\mathbf{N}} , \tag{4.41}$$

$$\frac{\partial s_{\text{u}}}{\partial \bar{\mathbf{d}}} = \frac{\partial s_{\text{u}}}{\partial \mathbf{D}_{,\bar{s}}} \frac{\partial \mathbf{D}_{,\bar{s}}}{\partial \bar{\mathbf{d}}} = \mathbf{s}_{\text{u}} \bar{\mathbf{N}}_{,\bar{s}} , \tag{4.42}$$

$$\frac{\partial \mathbf{s}_{\text{u}}}{\partial \bar{\mathbf{d}}} = \frac{\partial \mathbf{s}_{\text{u}}}{\partial \mathbf{D}_{,\bar{s}}} \frac{\partial \mathbf{D}_{,\bar{s}}}{\partial \bar{\mathbf{d}}} = \mathbf{S}_{\text{u}} \bar{\mathbf{N}}_{,\bar{s}} . \tag{4.43}$$

The gradient on path element level, representing a Hessian matrix for motion design $\mathbf{k}_{\text{md}} = \frac{\partial \mathbf{r}_{\text{md}}^{e}}{\partial \bar{\mathbf{d}}}$, then follows as

$$\mathbf{k}_{\text{md}}^{e} = \int\limits_{\bar{s}^{e}} \left(\bar{\mathbf{N}}^{\text{T}} \mathbf{K}_{\text{T}} s_{\text{u}} \bar{\mathbf{N}} + \bar{\mathbf{N}}^{\text{T}} \mathbf{F}_{\text{int}} \mathbf{s}_{\text{u}} \bar{\mathbf{N}}_{,\bar{s}} + \bar{\mathbf{N}}_{,\bar{s}}^{\text{T}} \mathbf{s}_{\text{u}} \mathbf{F}_{\text{int}} \bar{\mathbf{N}} + \bar{\mathbf{N}}_{,\bar{s}}^{\text{T}} \Pi_{\text{int}} \mathbf{S}_{\text{u}} \bar{\mathbf{N}}_{,\bar{s}} \right) \mathrm{d}\bar{s} . \tag{4.44}$$

By standard assembly operations, the Hessian matrix on the global level $\mathbf{K}_{\text{md}}$ is determined

$$\mathbf{K}_{\text{md}} = \bigcup_{e=1}^{\bar{n}_{\text{ele}}} \mathbf{k}_{\text{md}}^{e} . \tag{4.45}$$

These definitions lead to the linearized system of equations

$$\mathbf{K}_{\text{md}} \Delta \bar{\mathbf{D}} = -\mathbf{R}_{\text{md}} . \tag{4.46}$$

Within the framework of the Newton-Raphson method, this linearized system of equations is built and solved in each iteration until the parameters do not show a significant change anymore, the residual norm is close to zero and thus, convergence is reached. Note that with this system the entire problem is solved monolithically, instead of incrementally proceeding along the path. On convergence of the iterative solution method, all intermediate configurations along the path are obtained in one go.

This system depends on the employed spatial finite element formulation as it includes the tangent stiffness matrix of the structure and the internal forces. However, all ingredients can be combined in a modular manner. Thus, it does not pose any problem to use various element types, like mixed elements or elements with isogeometric spatial discretizations. Additionally, also the matrix $\bar{\mathbf{N}}$ with the shape functions for the path discretization can include any shape functions, not only linear Lagrange polynomials, as displayed

in Figure 4.7a, but also B-splines. These can often better approximate the path with fewer points and therefore save degrees of freedom, which is attributable to their higher continuity.

Furthermore, the question may arise whether the method of motion design could also be carried out with independent and constant path increments, i.e., not considering the displacement arc length. This would then resemble the time incrementation within space-time finite elements. However, such an approach would fundamentally affect the structure of the functional. In particular, the internal energy would not be integrated over the arc length s of the displacement field anymore, as it has been the case in eq. (4.54), but directly over a dimensionless path parameter. In other words, the mapping function s_u would therefore not be included in the functional and the path parameter would represent a totally independent path discretization instead. Due to its constant and independent definition, this dimensionless parameter would not contain any information about the actually covered deformation of the structure per path element. However, since it is integrated over this parameter, the odd result would be a motion that is squeezed into just one single path element, while the remaining path elements would not contribute to the motion anymore. Of course, this would also lead to a minimization of the functional. Still, the fundamental goal of motion design would not be met, because the path increments would not adequately resolve the motion. Therefore, the arc length with its real information about the deformation must be included in order to obtain physically meaningful results.

4.5.2 Verification and interpretation of resulting optimized motions

This section serves as proof of concept for demonstrating the effectiveness of the path discretization as well as for verifying and understanding the resulting motions. To keep things simple, the example setups already introduced before will be revisited.

Path-discretized brachistochrone problem

The principle of path discretization can also be applied to the solution of the brachistochrone problem, which was presented in Section 2.2 and already solved analytically with Euler's equation in Section 2.4. The obtained result now serves as a reference solution. The solution of the brachistochrone problem represents a special case of motion design. Since no spatial discretization is required, the motion design problem and the application of the path discretization simply reduces to a finite element solution of the underlying variational formulation. In this case, the unknown approximated functions

are the coordinates x and y of the solution curve. This requires the functional, i.e., the total required time in eq. (2.11), to be formulated in a parametric form

$$T = \int_{s_A=0}^{s_B} \frac{1}{\sqrt{2g\left(y_A - y(s)\right)}}\, \mathrm{d}s\,, \tag{4.47}$$

The parameter s again represents the path parameter, while the upper integration bound, i.e., the length of the resulting curve, is unknown. Therefore, the mapping parameter $\bar{s}$, the normalized arc length, is used and the mapping function is derived for the brachistochrone problem as

$$s_u = \sqrt{x'(\bar{s})^2 + y'(\bar{s})^2}\,. \tag{4.48}$$

Inserting this into the functional yields

$$T = \int_0^1 \sqrt{\frac{x'(\bar{s})^2 + y'(\bar{s})^2}{2g\left(y_A - y(\bar{s})\right)}}\, \mathrm{d}\bar{s}\,. \tag{4.49}$$

The variation of this functional is formulated with respect to the unknown functions $x(\bar{s})$ and $y(\bar{s})$ as well as their derivatives and is set to zero:

$$\delta T = \int_0^1 \left(\sqrt{\frac{x'^2 + y'^2}{8g\left(y_A - y\right)^3}}\, \delta y + \frac{x'\delta x' + y'\delta y'}{\sqrt{2g\left(y_A - y\right)\left(x'^2 + y'^2\right)}}\, \delta x' \right) \mathrm{d}\bar{s} = 0\,. \tag{4.50}$$

It represents the weak form of the brachistochrone problem. The next steps follow the standard procedure of a finite element formulation. First, a discretization for x and y as well as their variations δx and δy are introduced

$$x \approx x_h = \bar{\mathbf{N}}\mathbf{x}\,, \qquad\qquad \delta x \approx \delta x_h = \bar{\mathbf{N}}\delta\mathbf{x}\,, \tag{4.51}$$

$$y \approx y_h = \bar{\mathbf{N}}\mathbf{y}\,, \qquad\qquad \delta y \approx \delta y_h = \bar{\mathbf{N}}\delta\mathbf{y}\,, \tag{4.52}$$

where the matrix $\bar{\mathbf{N}}$ contains the path element shape functions and the vectors $\mathbf{x}$, $\mathbf{y}$, $\delta\mathbf{x}$ and $\delta\mathbf{y}$ comprise discrete nodal values of the unknown functions x and y, respectively. In this case, all functions are discretized with the same number of finite elements and shape functions, following the Bubnov-Galerkin approach. Inserting the discretization

into the variation yields the discretized weak form of the brachistochrone problem

$$\delta T = \int\limits_0^1 \left(\sqrt{\frac{(\bar{\mathbf{N}}'\mathbf{x})^2 + (\bar{\mathbf{N}}'\mathbf{y})^2}{8g\big(y_A - \bar{\mathbf{N}}\mathbf{y}\big)^3}} \bar{\mathbf{N}}\delta\mathbf{y} + \frac{\bar{\mathbf{N}}'\mathbf{x}\bar{\mathbf{N}}'\delta\mathbf{x} + \bar{\mathbf{N}}'\mathbf{y}\bar{\mathbf{N}}'\delta\mathbf{y}}{\sqrt{2g\big(y_A - \bar{\mathbf{N}}\mathbf{y}\big)\big((\bar{\mathbf{N}}'\mathbf{x})^2 + (\bar{\mathbf{N}}'\mathbf{y})^2\big)}} \right) \mathrm{d}\bar{s} = 0 \,. \tag{4.53}$$

By moving the vectors $\delta\mathbf{x}$ and $\delta\mathbf{y}$ out of the integral and applying the discrete form of the fundamental lemma of the calculus of variations, a residual equation is obtained. After linearization, it can be solved iteratively using the Newton-Raphson method for the nodal values $\mathbf{x}$ and $\mathbf{y}$, which provide an approximation for the solution functions x and y in a parametric form. Here, path discretization does not represent a deformation path, of course, but instead the required trajectory of the mass point to minimize the required time to move from A to B.

Starting point of the solution process is the predictor, which represents in this and the following cases a simple linear interpolation between the points A and B or between the initial and end configuration, respectively. During the iterations within the Newton-Raphson scheme, this linear curve converges towards the illustrated solution curve. Figure 4.8a shows the solution curve with a path discretization with linear Lagrange shape functions and 15 elements. As the parametrization of the curve, and thus, the placement of the nodes along the solution curve, is not unique, equal length of the path elements is enforced to regularize the problem formulation. The additional constraint is enforced by Lagrange multipliers. This aspect is further elaborated in Section 4.5.3. It can be seen that the solution with finite elements and linear shape functions approximates well the exact reference curve (grey) obtained in Section 2.4, but, due to the C^0-continuous linear shape functions, it still contains kinks. The number of degrees of freedom is twice the number of internal nodes (x- and y-coordinate at each node). An improvement of the approximation is possible by using an interpolation with B-spline-functions. This can be seen in Figure 4.8b, where the solution for a discretization with two path ele-
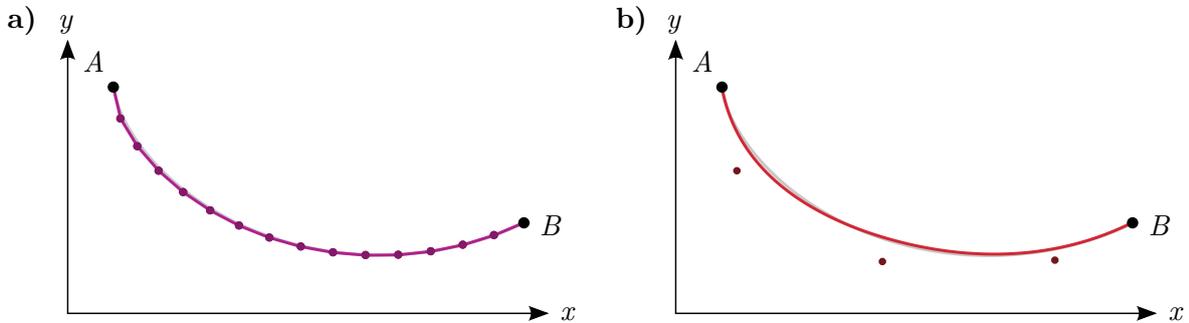
Figure 4.8: Solution to the brachistochone problem with finite elements. Solution curve with a) linear Lagrange shape functions and b) B-splines.

ments and cubic shape functions is illustrated. The higher continuity enables a better approximation without kinks and fewer internal nodes, thus resulting in fewer degrees of freedom.

Study on a kinematic bar structure with rigid body rotations

The new variational approach for motion design, especially the influence of the path discretization, is now studied on a simple bar structure. Specifically, one single truss element (Young's modulus $E = 100000$, cross-section area $A = 1$, length $L = \sqrt{2}$) is modeled and supported at one node (see Figure 4.9). The other node remains unconstrained such that the structure can perform a kinematic motion, i.e., a rigid body rotation around the supported node. In this example, the vertical displacement of the second node is prescribed and also controlled throughout the motion to assure the required regularization. Furthermore, the horizontal displacement remains variable during the motion as well as in the target configuration. Thus, it can adapt such that a quarter circle can be followed. Accordingly, the exact analytical solution of the presented motion design method with the underlying functional represents a circular trajectory of the moving point. This motion does not cause any deformation of the bar, no internal energy is built up, and consequently, the functional value of the optimized motion corresponds to $J = 0$, which is to be expected for a pure rigid body movement. Therefore, the analytical solution of motion design is known for this example and the setup can be interpreted as a benchmark test.
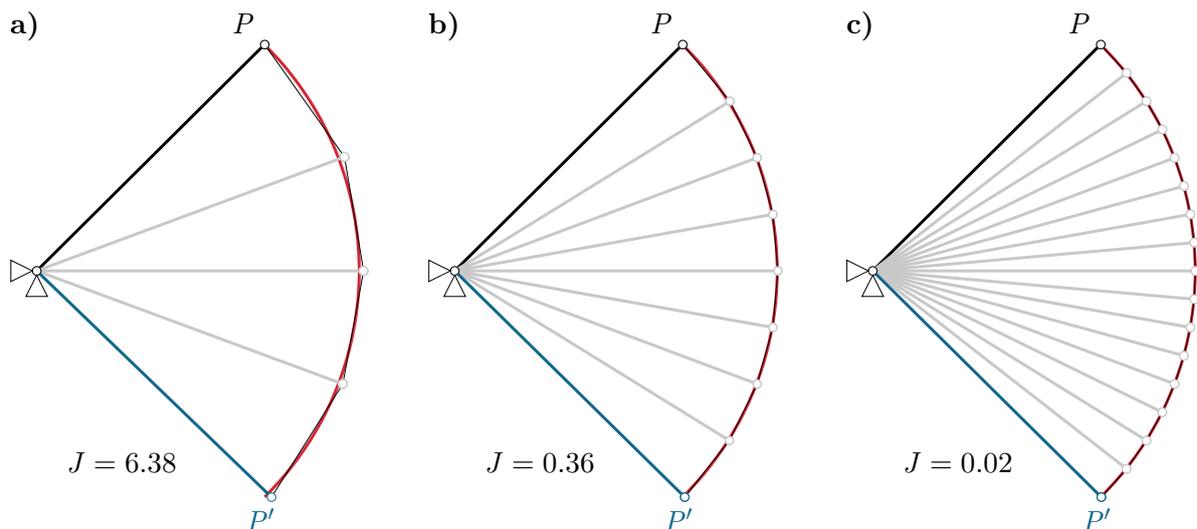
Figure 4.9: Convergence study of the path discretization. Motion path discretized with a) four, b) eight and c) sixteen elements.

Resulting motions with different path discretizations are illustrated in Figure 4.9a-c, where the path discretization is refined from left to right. All motions are computed with path elements approximated by linear shape functions. It can be observed that the unsupported node in the intermediate configurations does not lie directly on the exact trajectory (red). This especially happens when using a coarse discretization, since the minimum of the internal energy over the motion path is only fulfilled in an integral way. However, a finer discretization using more path elements leads to a better approximation of the exact solution curve, the prescribed arc. Also, it can be seen that the functional value converges to zero with an increasing number of path elements.

This qualitative convergence study illustrates the approximation behavior of the motion path discretization. It is further extended and supported by a quantitative analysis in Section 4.7.5, while other kinematic structures are investigated in Section 4.7.1.

Comparison with the semi-analytical solution obtained by Euler's equation

In Section 4.2.3, the motion design problem was solved semi-analytically for a simple example with two bars (see Figure 4.4). The strong form of the motion design functional of this example was calculated by Euler's equation and solved numerically by finite differences. In doing so, a reference solution was obtained. At this point, this shall be compared to the solution obtained with the presented motion design method.

For this purpose, the path is discretized by five, ten and twenty elements with linear Lagrange shape functions. As the points of the path discretization can be placed anywhere on the trajectory and still approximate the same curve, the distance between the
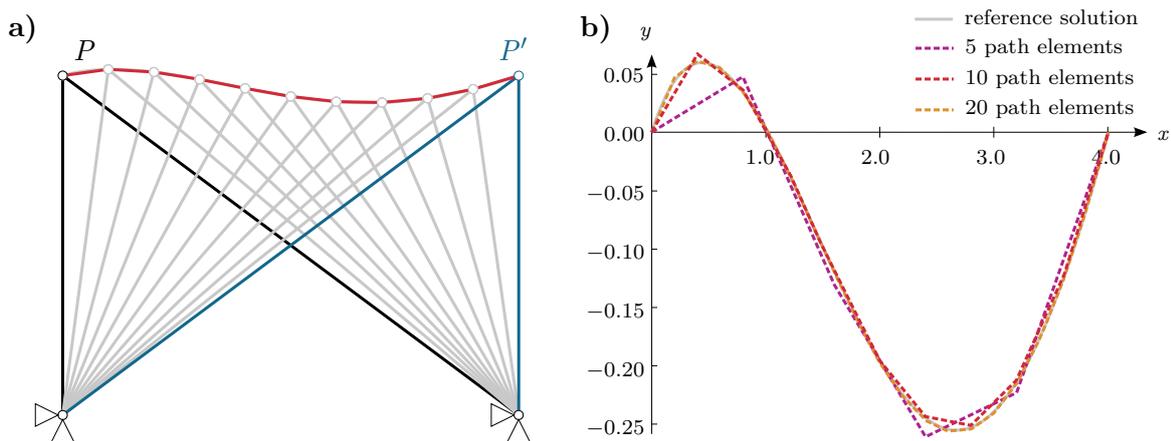
Figure 4.10: Comparison of numerical motion design solutions to the analytical reference curve. Discretized motion path illustrated a) in the structure and b) in a scaled graph.

points in the x-direction, the horizontal displacement of the midpoint, is fixed while the vertical displacement can be varied.

It can be seen in Figure 4.10 that the point P follows the same trajectory as in the reference solution for every path discretization. The more path elements are used, the better the reference solution is approximated. This serves as a qualitative verification of convergence of the proposed motion design method. A quantitative convergence study of this structure will be carried out in Section 4.7.5.

Optimized motion of the exemplary two-bar truss

At the beginning of this chapter, the illustrating example of a two-bar truss was introduced in Figure 4.1. To solve this problem using the motion design method, the path is discretized with 14 linear finite elements. As already indicated in the brachistochrone problem in Subsection 4.5.2, a predictor needs to be chosen for the solution process. The simplest possible choice of a predictor represents a linear interpolation between the initial and final geometry as seen in Figure 4.11a, whereas other predictors may also be selected. Since one evaluation of the problem results in the entire path, the predictor must also correspond to a complete motion. The linearly interpolated motion yields a functional value of $J = 491$.

Using the motion design method, an optimized motion path is found within nine iterations and a convergence tolerance of 10^{-8} in the L_2-norm of the residual in the Newton-Raphson loop, while equal length of the path elements is enforced by Lagrange multipliers. In terms of the integrated internal energy, it is apparently more advantageous to first enforce a purely vertical snap-through, followed by a horizontal movement (as opposed to following the straight path of the linear predictor motion), as is illustrated in Figure 4.11b. The functional value reduces to $J = 183$. This is visualized in the two diagrams in Figure 4.11c/d. In the three-dimensional plot, which has already been introduced in Figure 4.2b and Figure 4.7b, the internal energy is plotted over the two spatial degrees of freedom. Here, the two different midpoint trajectories of the predictor motion as well as the optimized motion are identified in the D_1-D_2-plane. The resulting spanned areas between these trajectories on the bottom plane and their corresponding internal energy represent the values of the functional. The plot demonstrates the difference between the two motions: The spanned area of the optimized motion is much smaller than the area of the predictor motion, thus illustrating the decrease of the functional value. Furthermore, the diagram in Figure 4.11d shows a projection of these surfaces, where the internal energy is plotted versus the respective total arc length. It can be seen that the total arc length of the two motions differ because the midpoint trajectories vary in their lengths. However, even though the arc length of the optimized

motion is larger than in the predictor motion, this proposed detour actually leads to a smaller accumulated internal energy throughout the motion. Therefore, the motion design method yields an optimized motion in a purely formalized way without the need to put any engineering expert knowledge into the analysis.

The snap-through characteristics can also be detected in the progress of the internal energy for the final solution. After snap-through, the internal energy vanishes, because the length of the bars now matches the length in the initial configuration. Since the whole end geometry is prescribed, the last value of the internal energy is the same in the predictor state and the solution state. With the method for motion design, it is not possible to influence the internal energy in the end configuration (in case it is fully prescribed), but only what happens until the desired end configuration is reached.

In order to realize the prescribed deformation that results from motion design, in practice, forces need to be applied. These are evaluated after convergence from the internal forces and equilibrium of internal and external forces. This means that for the particular case considered so far, where a point load can potentially be applied at every degree of freedom, the equilibrium conditions are not needed for the solution of the motion de-
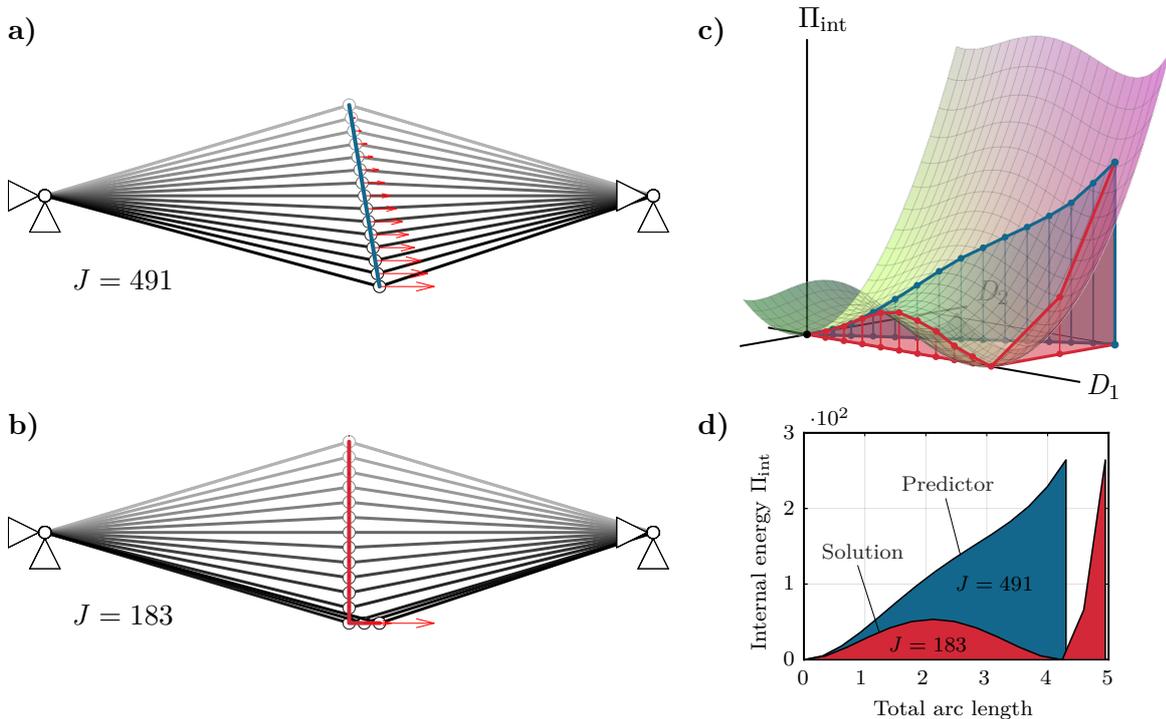
Figure 4.11: Solution of the illustrating two-bar truss. a) Predictor motion. b) Optimized motion. Visualization of the functional in c) a three-dimensional plot and d) as a projection in form of a plot of the internal energy over the total arc length.

sign problem. The equilibrium equations are only used for post-processing of the nodal forces.

4.5.3 Convergence aspects of motion design problems

The derived nonlinear problem needs to be solved iteratively. In motion design, the degrees of freedom are all spatial degrees of freedom in every single configuration. Some configurations are known, such as the initial, starting geometry and at least a part of the final, target geometry. The displacements of the deformed intermediate configurations and eventually the rest of the target geometry are solved for in one step. As was already presented in the current and previous sections, the entire motion is obtained by one monolithic solution of the nonlinear problem. Therefore, the predictor describes an entire motion path between a known initial geometry and a (partly) prescribed end geometry.

Due to these characteristics of motion design problems, two aspects regarding the problem definition and the convergence behavior arise. There is a need for a regularization of the problem and, furthermore, a method to improve the convergence behavior of the Newton-Raphson method is required.

Regularization of the motion path discretization

In all three problems solved in Section 4.5.2, the path elements discretize either the trajectory of a mass point moving from A to B (brachistochrone problem) or the trajectory of a point in a spatially discretized deformable structure. As was already mentioned in Section 4.4, the nodes of the path discretization can be placed at every point on the resulting trajectory while still approximating the same curve. The parametrization of the curve, and thus, the placement of the nodes along this curve, is not unique, which can be visualized with the example of a straight one-dimensional line. This leads to an ill-posed problem. Therefore, motion design problems need to be regularized by additional control procedures. Either the progression of one (or multiple) spatial degrees of freedom can be prescribed by e.g., constant increments between the deformed configurations throughout the deformation process, or equal lengths of the path elements can be enforced with the help of the Lagrange multiplier method. Even though this effect was explained on problems, where only one trajectory had to be discretized, it also holds for multi-dimensional problems.

Convergence behavior of the Newton-Raphson method

Due to the additional path discretization in motion design problems, a large number of variables, i.e., the displacement (spatial) degrees of freedom in every intermediate load configuration as described in Section 4.4, is usually involved. This may lead to an inferior convergence behavior compared to other nonlinear problems, such as geometrically nonlinear static analyses. As the difference between the predictor motion and the final result may also be significant, the solution process sometimes suffers from convergence problems and the Newton-Raphson method occasionally diverges after several iterations. Furthermore, there is no straightforward analogy to incremental-iterative solution procedures with the option to decrease the size of the increments (such as the load step size in nonlinear analyses) to improve convergence behavior.

This aspect is elaborated here, and various methods that will be applied in this work for improving the convergence behavior are presented. These can be combined for an efficient solution procedure depending on the specific underlying problem. However, the methods discussed here only represent an extraction of many other possible methods that can reach and improve the convergence behavior of motion design problems.

Fewer degrees of freedom by path approximation with B-splines

It was observed that motion design problems with fewer degrees of freedom show improved convergence behavior. As the motion design method is primarily intended to provide information on the conceptual design of an adaptive structure, a coarse discretization of the spatial domain and the path is often appropriate. However, the coarseness has its limits, because a certain accuracy of the solution is required in motion design, too. One way of reducing the number of degrees of freedom and still achieve a good approximation of continuous deformation processes is to approximate the motion path
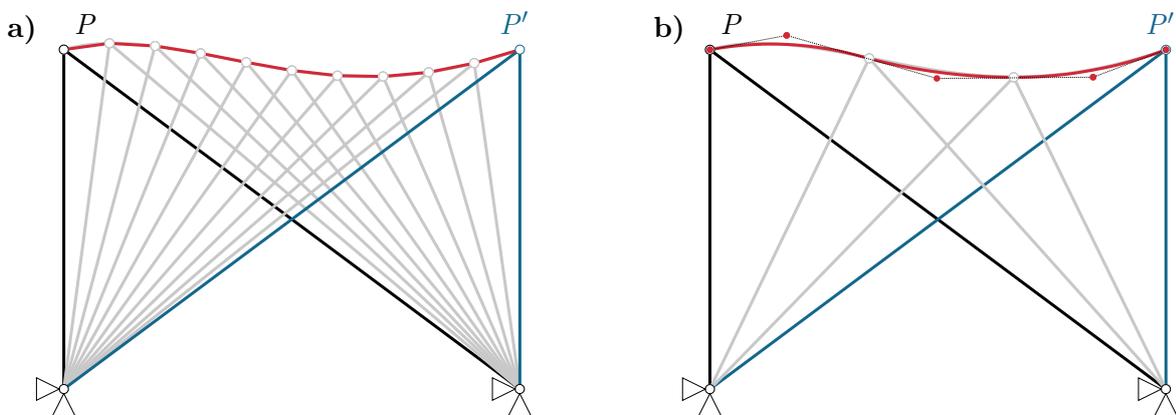
Figure 4.12: Different path discretizations with a) linear elements and b) B-splines.

by B-spline functions, as has already been mentioned in Section 4.4. This is illustrated in Figure 4.12, where the motion path is approximated with either ten linear elements (a) or with three cubic elements described by B-spline functions (b). In the latter case, the reference solution is well approximated by only three control points, which results in only six variables in total compared to 18 variables in the approximation with ten linear elements.

Better predictor based on a preanalysis

The number of required iterations in a solution process of a nonlinear problem often severely depends on the quality of the first guess, the predictor. One way of improving the convergence behavior, therefore, lies in the improvement of the predictor. Since a linear interpolation (which is typically chosen as predictor here due to its simplicity) between the initial and end configuration might represent an unphysical motion, a preceding geometrically nonlinear analysis can be carried out instead. The loads needed for this nonlinear analysis are received by a post-processing step, where the internal forces in the prescribed deformed end configuration are first calculated and then set as external forces. The resulting equilibrium path represents the deformation for a linear incremental increase of the forces. Nonetheless, to approach a feasible motion, this obtained deformation can be used as a predictor. It is most probably different from the force evolution in an optimized deformation path but might be closer to the solution path due to the improved physical plausibility of the predictor motion.

Hierarchically improved predictor from solution with coarse path discretization

The methods described until now are based on the reduction of variables and the improvement of the predictor. Now both methods are combined within a hierarchical approach. Here, the motion is first coarsely discretized by a small number of path elements, which already improves the convergence behavior. However, the path might still be too coarsely approximated. Afterward, the solution of the first motion design is
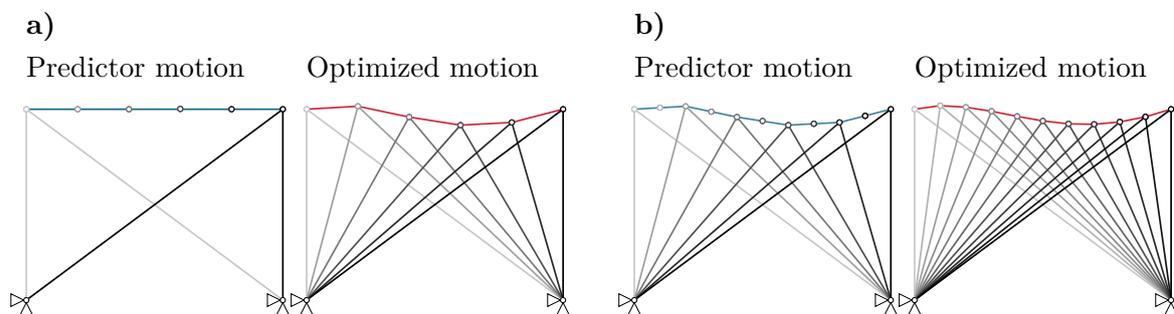
Figure 4.13: Illustration of the hierarchically improved predictor with a) first and b) second step.

interpolated and used as a predictor for a subsequent motion design with a finer path discretization, as seen in Figure 4.13. This process can be repeated several times, depending on the desired smoothness of the resulting deformation path. More generally, a hierarchically modified predictor improves convergence.

Modification of the Newton-Raphson method with a relaxation factor

Alternatively to reducing the number of variables or improving the predictor, the Newton-Raphson method as such can be modified. One way is to apply a relaxation factor that prevents an off-shooting from a possible solution in those iterations, where the norm of the residual increases. This method is presented in ALBANESE AND RUBINACCI (1992) and further investigated and developed in FUJIWARA ET AL. (1993).

4.6 Generalized motion design for any objective function

So far, the minimization of the internal energy integrated along the path, as presented in Section 4.2, was used as a proof of concept for the proposed motion design framework. However, in principle, any functional or objective function can be used and incorporated into this method in a straightforward manner. Here, a general quantity F, which is a function of the displacement field $\mathbf{u}$ and is to be minimized over the motion, is introduced. The minimization problem with the general functional then follows as

$$J = \int_s F(\mathbf{u}) \, \mathrm{d}s \; \rightarrow \; \min. \tag{4.54}$$

The problem can be solved in the same manner as with the exemplary objective function containing the internal energy. Introducing the pseudo-velocity and the spatial discretization as well as the motion path discretization yields the variation

$$\delta J = \sum_{e=1}^{\bar{n}_{\mathrm{ele}}} \int_{\bar{s}_e} \left(\delta \bar{\mathbf{d}}^{\mathrm{T}} \bar{\mathbf{N}}^{\mathrm{T}} F_{,\mathbf{D}} s_{\mathrm{u}} + \delta \bar{\mathbf{d}}^{\mathrm{T}} \bar{\mathbf{N}}_{,\bar{s}}^{\mathrm{T}} \mathbf{s}_{\mathrm{u}} F \right) \mathrm{d}\bar{s} = 0 \tag{4.55}$$

with the partial derivatives of the chosen quantity with respect to the spatial degrees of freedom $F_{,\mathbf{D}}$. Linearization leads to the residual vector of one path element

$$\mathbf{r}_{\mathrm{md},e}(\bar{\mathbf{d}}) = \int_{\bar{s}_e} \left(\bar{\mathbf{N}}^{\mathrm{T}} F_{,\mathbf{D}} s_{\mathrm{u}} + \bar{\mathbf{N}}_{,\bar{s}}^{\mathrm{T}} \mathbf{s}_{\mathrm{u}} F \right) \mathrm{d}\bar{s} \tag{4.56}$$

and the Hessian matrix for motion design

$$\mathbf{k}_{\text{md},e} = \int\limits_{\bar{s}_e} \left(\bar{\mathbf{N}}^{\text{T}} F_{,\mathbf{D},\mathbf{D}} s_{\text{u}} \bar{\mathbf{N}} + \bar{\mathbf{N}}^{\text{T}} F_{,\mathbf{D}} s_{\text{u}} \bar{\mathbf{N}}_{,\bar{s}} + \bar{\mathbf{N}}_{,\bar{s}}^{\text{T}} s_{\text{u}} F_{,\mathbf{D}} \bar{\mathbf{N}} + \bar{\mathbf{N}}_{,\bar{s}}^{\text{T}} F \mathbf{S}_{\text{u}} \bar{\mathbf{N}}_{,\bar{s}} \right) \mathrm{d}\bar{s} \,. \tag{4.57}$$

With this procedure, the nonlinear problem and the linearized system of equations for any objective function can be built. The minimized quantity must depend on the displacements to apply this method for motion design as derivatives need to be calculated. However, they could as well be calculated numerically. Using other optimization algorithms asides the classical Newton-Raphson approach, the residual and its derivative can be used as analytical sensitivities, i. e., the gradient and Hessian matrix, for an optimization of the motion.

In many cases and problem types, stresses or strains represent a reasonable choice for the measure F. These are calculated in an analysis anyway and are therefore readily available in standard finite element codes.

4.7 Numerical experiments

To further verify the method of motion design and demonstrate its potential, numerical experiments are carried out and presented in this section. Different kinds of problems are investigated. Kinematic structures with rigid body motions serve as verification of the method, while more complex problems that incorporate instability phenomena or inextensional deformations of shell structures highlight the capabilities and future potential of the presented method.

As already mentioned in the previous section, the corresponding quantities of various available finite element formulations can simply be plugged into the system of equations for motion design without additional effort. Therefore, also various element types (e. g., truss, shell, 2D and 3D continuum elements) are used in the following numerical experiments.

4.7.1 Rigid body motions as benchmark for motion design

In Section 4.5.2, one exemplary numerical solution has already been compared with the analytical reference solution obtained by applying Euler's equation to the functional for motion design. However, there are no established benchmark tests yet for such a problem formulation. In order to generate further benchmark problems for quantitative verification of the resulting motions, rigid body motions of kinematic structures can

be investigated. Here, motions can be performed that work purely by a kinematic movement without any distortions and, thus, without any internal energy. Therefore, the integrated internal energy, i. e., the value of the functional, is also expected to be zero. As a consequence, it is anticipated that the new motion design method should be able to formally identify these "optimal" solutions in the case of kinematic structures. This hypothesis is examined in the following experiments below.

Kinematic truss system

The first example is a kinematic truss system with four nodes, three bars and two supports, as shown in Figure 4.14a. This kinematic system allows for a purely energy-free rigid body movement during which the lengths of the bars do not change. However, it strongly depends on the problem formulation and the prescribed end geometry whether the rigid body motion can actually be obtained. If the whole end geometry is fixed, it might not correspond to a configuration that can be attained without any length changes of the bars except for special configurations such as the mirroring of the geometry. Accordingly, the final geometry must be given a certain level of freedom to adjust and meet the expectation of a rigid body motion. Pretending that the target configuration is unknown, it is sufficient to specify only the vertical displacement of the second node. The other displacements are expected to adjust to allow the kinematic movement and, therefore, to minimize the functional of motion design.

To perform a motion design, the path is discretized by 14 elements and approximated by shape functions with polynomial degree $\bar{p} = 1$. This results in $\bar{n}_{\mathrm{dof}} = 42$ degrees of freedom. For regularization, as explained in Section 4.5.3, the increments of the vertical displacement of the second node are prescribed throughout the motion. The intentionally naive first guess, the predictor motion, is a linear interpolation between the initial and the prescribed end configuration for the upper left node, while the upper right node does not move at all, as seen in Figure 4.14b. As this motion obviously does not represent a rigid body motion, forces are needed to enforce it, which are shown as red arrows. In the case of only one predefined end displacement, the predictor appears to be far off the expected solution and the functional takes the value of $J = 12843$.

Figures 4.14c and Figures 4.14d show a comparison of eight snapshots, i. e., every second intermediate configuration, of the converged optimized motion and the predictor motion. It can be seen that the solution obtained from motion design reflects the expected rigid body motion despite the naive predictor. Furthermore, the correct final configuration is adjusted such that the bars do not undergo any length changes. The functional value of the optimized motion reduces to $J = 0.05$, which is not precisely zero. The reason for that lies in the error from the chosen, rather coarse path discretization with 14 linear

elements. In the exact rigid body motion, the second point ought to move along a perfect arc. However, this arc is approximated by linear elements in the discrete motion design solution. Therefore, a small length change of the bars occurs between two nodes of the path discretization. By refining the motion with more path elements, as seen in Figure 4.15a/b, the approximation quality increases and the value of the functional approaches zero as can be expected by a well-posed finite element formulation.
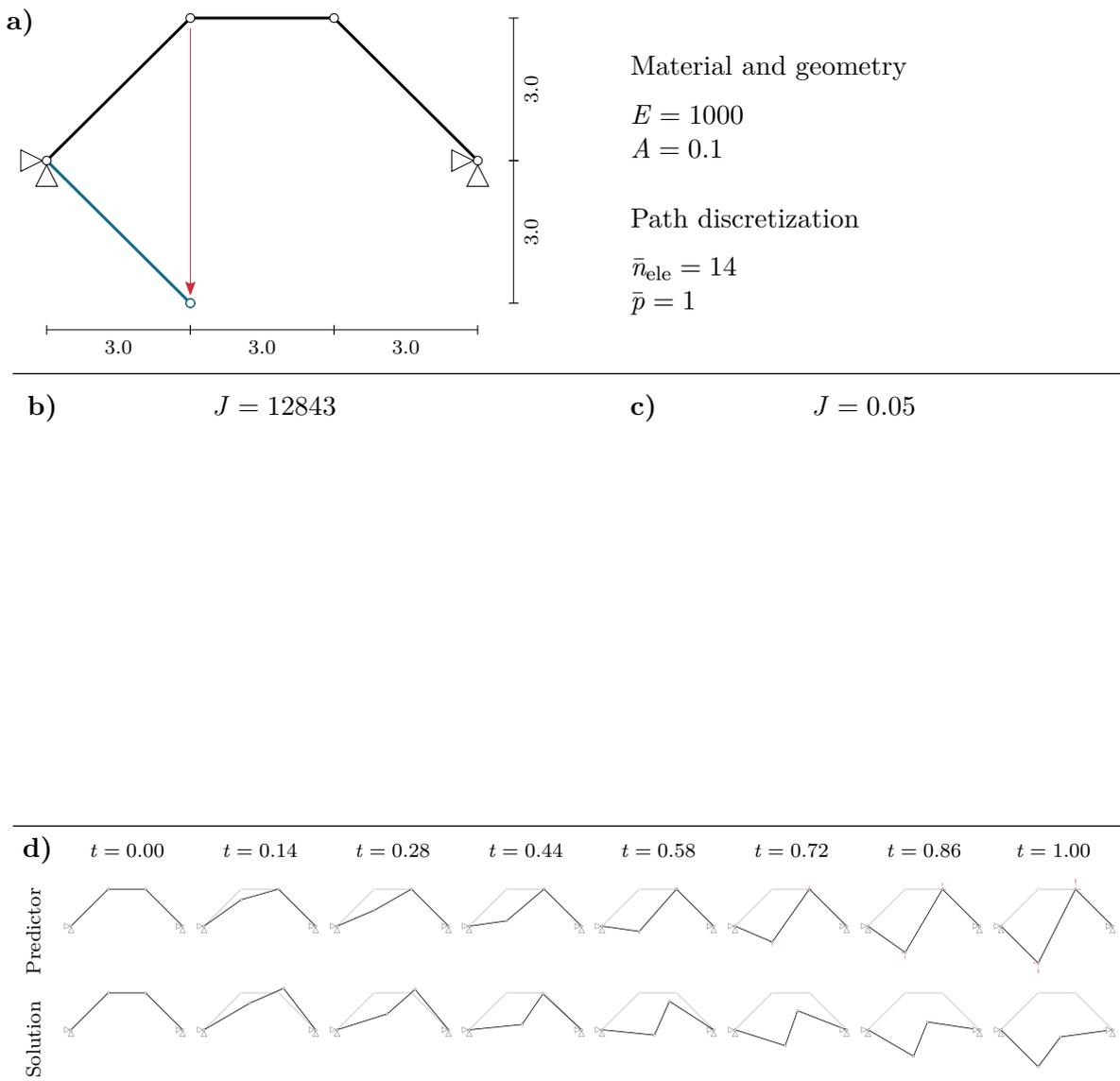
Figure 4.14: Kinematic bar structure for benchmarking. a) Problem setup. b) Predictor motion. c) Optimized motion. d) Sequence of the two motions. An animation of the motion can be found in the digital version of this work.

a) $J = 0.0028$ **b)** $J = 0.00015$ **c)** $J = 0.00013$

$\bar{n}_{\text{ele}} = 28,\ \bar{n}_{\text{dof}} = 84$ $\bar{n}_{\text{ele}} = 56,\ \bar{n}_{\text{dof}} = 168$ $\bar{n}_{\text{ele}} = 10,\ \bar{p} = 3,\ \bar{n}_{\text{dof}} = 42$

Figure 4.15: Convergence study for the kinematic truss structure. Path discretization with a) 28 elements with linear Lagrange shape functions, b) 56 elements with linear Lagrange shape functions and c) 10 elements with B-spline shape functions.

Alternatively, the path can also be approximated by higher-order shape functions enabling an even better approximation of the arc. This can be done by either Lagrange shape functions or B-spline shape functions, both of them meeting different continuity requirements. However, the path discretization with higher-order shape functions is carried out in the following with B-splines. Here, the path is approximated with cubic B-splines. Like this, the functional value reduces drastically with fewer required degrees of freedom compared to a path discretization with linear elements. This qualitative convergence study of the path discretization and its influence, therefore, explains the slight inaccuracy of the functional value obtained initially.

Kinematic folding motion with quadrilateral elements

Another kinematic structure, as shown in Figure 4.16a, is examined in the next example. Here, four square discs are supported and connected by hinges either on the upper or on the lower corner in such a way that they can perform a fold-like motion. This enables mirroring of the geometry solely by rigid body translations and rotations. Every disc is discretized by only one displacement-based 4-node quadrilateral element with bilinear shape functions (Q1-element). This very coarse discretization is adequate as no distortions of the elements and, therefore, no strains or stresses are expected in the solution. In this case, the path is approximated by six quadratic elements with B-spline shape functions. Again, the target geometry is assumed to be unknown. Only the vertical displacement of the upper second and fourth node is prescribed and the vertical displacement increments of these nodes are controlled during the deformation process. Therefore, the predictor of the motion as a linear interpolation between the initial and end configuration exhibits an unphysical movement with self-penetration of the elements, see Figure 4.16b.

Applying the method of motion design for this problem, the physically expected kinematic motion without any internal energy is found (see Figure 4.16c). Specifically, the functional value of the optimized motion takes a value of $J = 0.03$, thus being close to zero and only a fraction of the initial, very naive estimation of $J = 41244$.

The motion design of the two exemplary kinematic structures proves that the proposed new method finds the expected rigid body movements, which minimize the internal energy over the motion path. The displacement values of the degrees of freedom that are not prescribed or controlled during the motion adjust such that the kinematic motion is performed. This even holds for cases, where the predictor or first guess, a linear interpolation of the motion, turns out to be far off the actual solution.
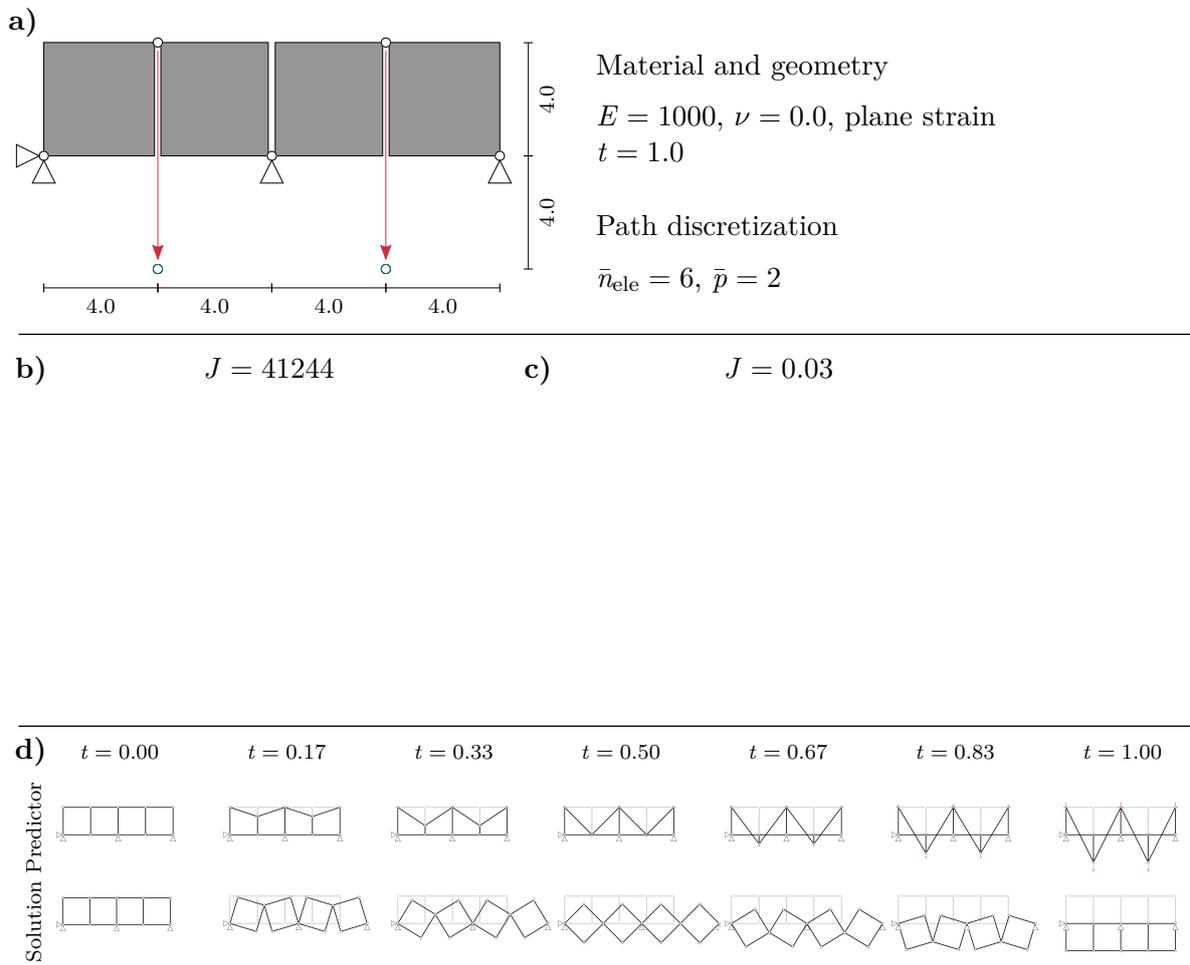
Figure 4.16: Kinematic folding motion with Q1-elements. a) Problem setup. b) Predictor motion. c) Optimized motion. d) Sequence of the two motions. An animation of the motion can be found in the digital version of this work.
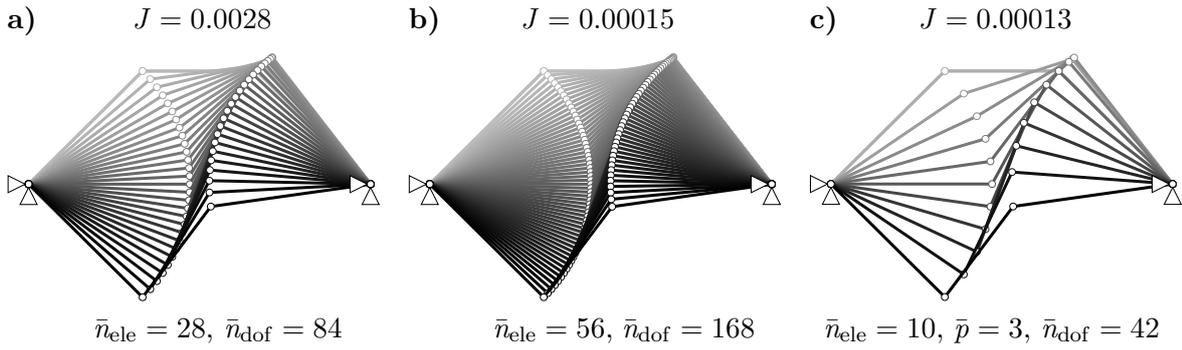
4.7.2 Exploring motions with instability problems

Another interesting aspect to further understand and validate the properties of the proposed motion design method is the analysis of structures and motions where instability phenomena such as snap-through or bifurcation can occur. Thus, various structures with potential instabilities are investigated. The first example, a shallow arc modeled with two bars undergoing a snap-through process, has already been presented during the derivation of the method in the current chapter (cf. Figure 4.11). The following numerical experiments aim to further establish an understanding of the method concerning instability problems.

Motion design with multiple snap-through processes

Since a snap-through phenomenon with bar elements has already been investigated in detail, a study on the combination of several interdependent snap-through processes is carried out at this point. The combination of three pairs of hinged bars, shown in Figure 4.17a, represents a system for which the equilibrium path may exhibit multiple limit points, i. e., horizontal tangents, where snap-through occurs.

Two shallow arcs with bar cross-sections A_1 are modeled separately. The midpoints of these serve as supports for a third shallow arc with larger cross-sections A_2. For the motion of interest, the midpoint of this third arc is to be moved downwards. This vertical displacement also represents the controlled degree of freedom for motion design. All three shallow arcs can, therefore, potentially undergo a snap-through. To enhance the convergence behavior, the predictor is calculated and updated hierarchically from a solution obtained with a coarse path discretization, as it was explained in Section 4.5.3. A first solution is calculated with eight linear path elements and then further refined in two additional motion design steps to obtain a solution with 32 path elements. Thus, the linear interpolation between the initial and the end geometry with this final number of elements does not represent the actual predictor motion because of the application of the hierarchically modified predictor strategy. However, the solution is compared to a linear interpolation between the initial and a mirrored geometry, as seen in Figure 4.17b, which is expected to represent a better approximation than the naive linear interpolation of only the upper central node to its target position. This results in a motion dominated by global snap-through.

The result of motion design provides a different type of motion, as can be seen in Figure 4.17c. When the two lateral structures do not perform the snap-through simultaneously, the upper arc does not show a pronounced snap-through deformation and internal energy can thus be "saved". This effect can also be detected in the progress

of the internal energy over the total arc length, which is plotted in Figure 4.17d. The bulges in the diagram indicate the snap-through processes during the deformation. The resulting end configuration is found to be the horizontally mirrored geometry, which reduces the internal energy back to zero. The value of the functional decreases significantly from $J = 440$ to $J = 11$, as is illustrated in Figure 4.17d as well (note the two different scales of the y-axis in the plot of the internal energy).
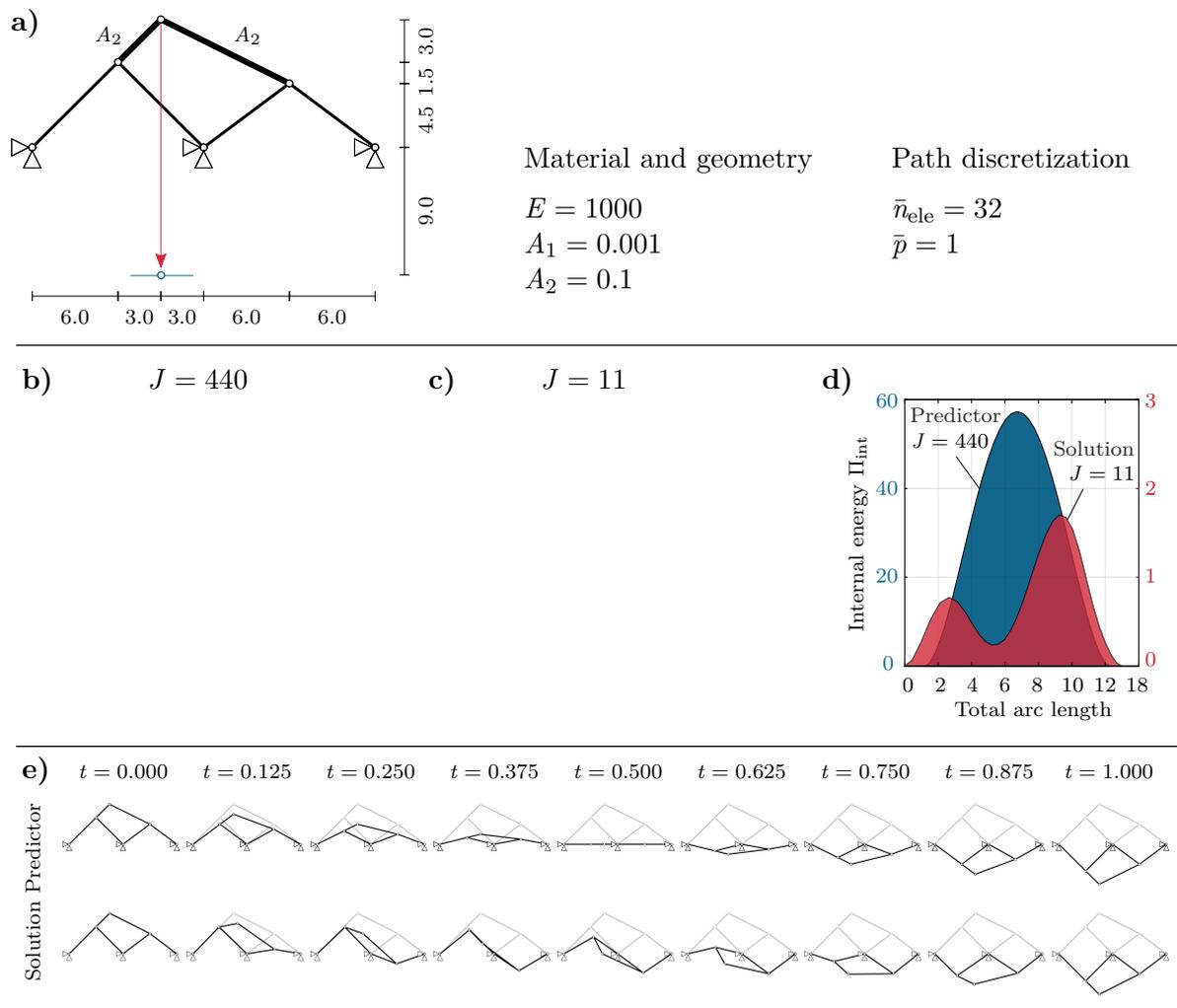
Figure 4.17: Motion design with a combination of multiple snap-throughs. a) Problem setup. b) Linear interpolation. c) Optimized motion. d) Functional visualization with a plot of the internal energy over the total arc length. e) Sequence of the two motions. An animation of the motion can be found in the digital version of this work.

Motion design in a bifurcation problem

In addition to a snap-through problem, a bifurcation problem is now analyzed. Sticking to simple truss examples, such phenomena can also be investigated by a two-bar structure. In the shallow arc examples presented up to now, only limit points are present, which induce a snap-through deformation while the midpoint is moved downwards. However, if the height-to-total-span ratio of such a structure exceeds a value of $\sqrt{2}/2$, an additional critical point, a bifurcation point, occurs before the limit point (snap-through) is reached. Therefore, a higher arc with a ratio of 2/3 is modeled as illustrated in Figure 4.18a. The midpoint shall be moved downwards to arrive in a mirrored, vertically flipped geometry.

The motion path is discretized by twenty linear elements, where the vertical displacement increments during the motion of the midpoint are controlled. For the vertically flipped geometry as target configuration, the linear interpolation describes a purely vertical snap-through motion (see Figure 4.18b). Indeed, this happens to represent a stationary point for the functional of motion design. However, it provides a relative maximum of J, not a minimum, meaning that it is a worst-case scenario. This can be detected by a slight modification of the predictor and an observation of the functional value throughout the iterations. Therefore, the predictor needs to be modified significantly to improve convergence of the motion design algorithm to the desired solution. Due to the system symmetry, the direction in which the modification of the predictor is applied, plays a crucial role in the solution. It determines whether the midpoint moves to the left or the right side. For example, instead of a linear interpolation, a combination of the primary path – up to the critical point – followed by an arbitrarily chosen branch of the secondary equilibrium path, describing the deformation after buckling of the structure, can be used as predictor.

The optimized motion found on the basis of this predictor is shown in Figure 4.18c and yields a functional value of $J = 779$, which is reduced significantly compared to the value of $J = 1449$ obtained from the linear interpolation, the worst-case scenario mentioned above. But it is also superior to the value $J = 845$ obtained for the improved predictor based on the secondary path (see Figure 4.18d), which confirms the virtue of the method of motion design.

It can be observed, however, that the maximum value of the internal energy during deformation is higher for the optimized motion than for the secondary path (diagram in Figure 4.18f). The fact that the functional value is still lower for the optimized motion follows from two aspects: During the first phase of the deformation process, the internal energy value is higher in the predictor than in the optimized motion and the deformation path is slightly longer. These aspects are dominant and lead to the reduction of the

functional value, even though the maximum value of internal energy is higher in the optimized solution.

Yet an alternative predictor is the so-called critical path, as illustrated in Figure 4.18e. It is defined as the path that connects configurations for which the determinant of the stiffness matrix is zero, i.e., $\det \mathbf{K}_T = 0$. It leads to a functional value of $J = 956$,

a)

Material and geometry

$E = 10000$
$A = 0.1$

Path discretization

$\bar{n}_{\mathrm{ele}} = 20,\ \bar{p} = 1$

f)

Linear interpolation
$J = 1449$

Critical path
$J = 958$

Secondary path
$J = 845$

Solution
$J = 779$

Internal energy Π_{int}

Total arc length

b) $J = 1449$ **c)** $J = 779$ **d)** $J = 845$ **e)** $J = 958$
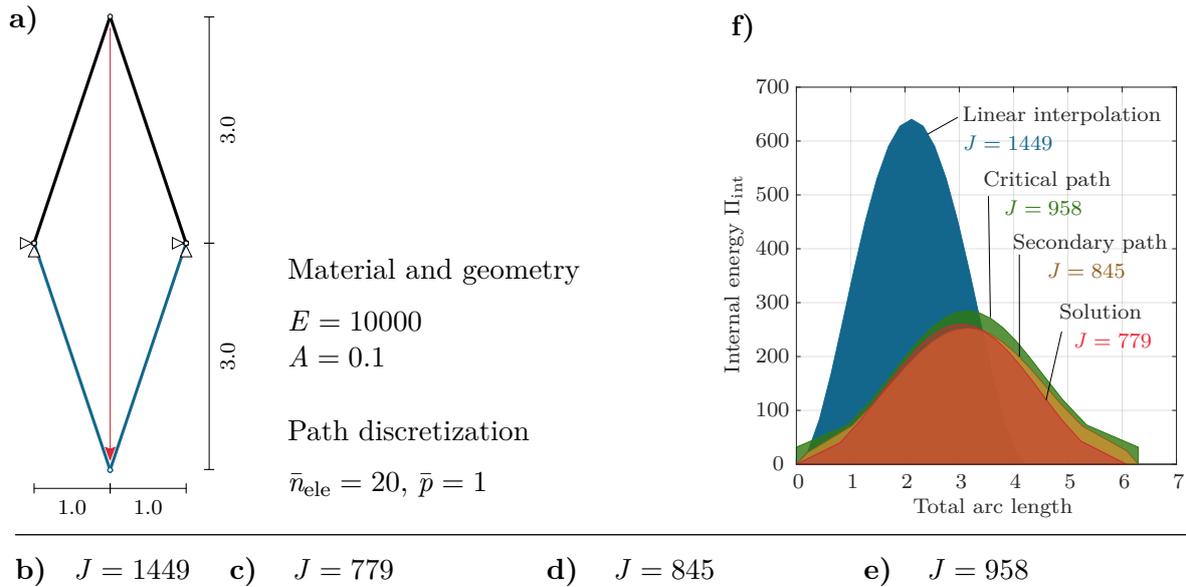
Figure 4.18: Analysis of a two-bar truss with bifurcation and motion design. a) Problem setup. b) Linear interpolation. c) Optimized motion. d) Secondary path. e) Critical path. f) Functional visualization with a plot of the internal energy over the total arc length. An animation of the motion can be found in the digital version of this work.

which is worse than both the optimal solution and the solution obtained from following the secondary path. Nevertheless, it would also be a valid predictor for obtaining convergence of the motion design algorithm.

A main difference between the different paths are the required loads for the resulting deformation. The linear interpolation as well as the secondary path are equilibrium paths for loading by a sole vertical force at the midnode and therefore do not allow horizontal loading. On the other hand, the optimized motion requires a vertical as well as a horizontal force to follow the path. These forces are recovered after the optimized path is found. This also holds for the case of the critical path, where again two forces are needed.

Snap-through of a curved arc

The last example with a snap-through phenomenon is a shallow arc, which is modeled as a two-dimensional continuum structure under plane strain conditions using quadrilateral finite elements, as shown in Figure 4.19a. The fully prescribed end geometry is the artificially chosen (approximately) mirrored geometry of the initial configuration. The path is discretized by five cubic elements with B-spline functions as shape functions and the vertical displacement of the midpoint is controlled for motion design.

First, purely displacement-based bilinear quadrilateral elements are used for spatial discretization. The predictor motion is again a linear interpolation between the initial and end configuration and represents a symmetric snap-through-dominated motion (see Figure 4.19b).

With this problem setup and element type, an antisymmetric swaying motion is found by the new motion design approach, as can be seen in Figure 4.19c. It decreases the value of the functional from $J = 1263$ to $J = 144$. In this symmetric example, the horizontally mirrored deformation is equivalent to the calculated solution and there is no preferred side for the lateral motion. The resulting motion to the right is only attributable to numerical imperfections.

Nonetheless, it is well-known that displacement-based finite elements suffer from locking. As a consequence, this effect is also incorporated into the resulting motion computed by motion design using these elements. Usually, the effects of locking become apparent as too small displacements due to an artificially increased tangent stiffness or oscillations in the affected stress measures. However, as the deformed configuration is prescribed in motion design, locking effects do not results in the displacement values being too small, but in the predicted forces required to realize this deformation being too large. The influence of locking on the resulting motion is exemplarily studied here by applying

quadrilateral elements with an Enhanced Assumed Strain (EAS) formulation, proposed by SIMO AND RIFAI (1990). In the EAS-element formulation, shear locking and volumetric locking can be effectively treated by adding four strain parameters per element. The resulting stiffness matrix and internal forces of this element formulation can again simply be plugged into the derived system of equations for motion design. Solving this system results in a different optimized motion that is not affected by locking phenomena and is illustrated in Figure 4.19d. Already in the snapshots of the motion, the difference in the results obtained with finite elements that suffer from locking and locking-free elements is visible, although the overall character of the motion seems to be similar. Even though locking is not dominant in this example, it can be observed that the EAS-elements exhibit more bending throughout the motion. The artificial energy that results from locking effects increases the internal energy along the path and acts as a penalty for bending modes. In slightly simplified terms, locking causes an unphysical penalization of bending deformations attributable to the occurrence of so-called parasitic stresses. When the penalization of bending due to the artificial stiffness is eliminated by using a locking-free element formulation, the finite elements can undergo a physically more meaningful motion including more pronounced bending deformations. Locking-free element formulations avoid this penalty and the value of the functional of an optimized motion with these elements decreases significantly from $J = 144$ to $J = 58$.
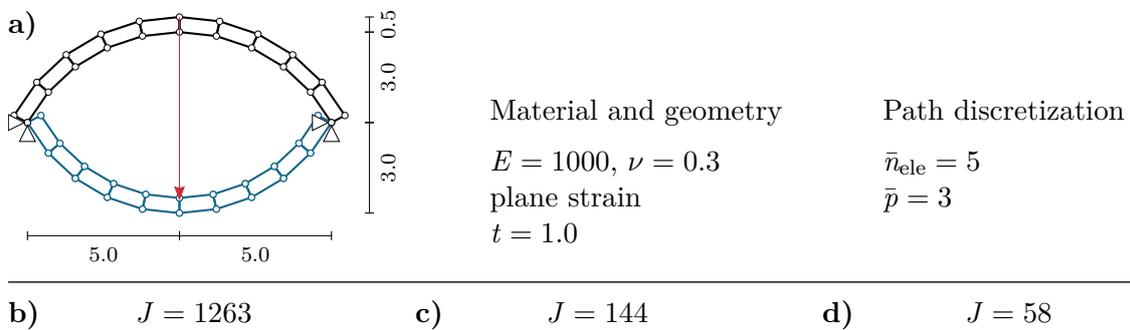
Figure 4.19: Arc with quadrilateral elements and the influence of locking on motion design. a) Problem setup. b) Linear interpolation. c) Optimized motion. d) Optimized locking-free motion. An animation of the motion can be found in the digital version of this work.

The proposed motion design method automatically makes full use of such an improvement in finite element modeling. For example, in the given scenario, a further improved motion is found that is not affected by spurious locking phenomena.

Shear locking effects play a more significant role in more slender structures and the penalization for bending modes throughout the deformation increases. It might also increase to such an extent that even completely different motions are found by motion design. A similar effect has been observed for shape optimization problems for locking-free elements and elements affected by locking in CAMPRUBÍ ET AL. (2004). It can be attributed to the shifted stiffness and energy relationship between membrane, shear and bending modes. However, it is essential to point out that this is not a weakness of the corresponding motion design or shape optimization methods, but is entirely connected to the employed finite element formulation.

4.7.3 Specification of intermediate configurations

Beyond the possibility to specify initial and target configuration, also intermediate configurations can be included as an objective for motion design. Figure 4.20a shows a three-dimensionally curved cantilever beam, discretized by trilinear volume elements (i. e., 8-node hexahedra).

In addition to the end configuration, two intermediate configurations are defined and the motion design process is carried out in three stages. This procedure is used due to the relatively large amount of variables and the expected non-smooth deformation result. In problems with fewer degrees of freedom, such a procedure might not be needed to reach convergence.

First, a cantilever with a tip that is rotated by 90° around the z-axis is specified as end geometry (Configuration 1). The path is approximated with B-spline shape functions and three quadratic elements. For stabilization, the displacement in the y-direction of a node at the cantilever tip is controlled. A first motion design (Stage 1) is carried out to find a motion between the initial configuration and Configuration 1.

In the next stage, Configuration 1, which was previously defined as end configuration, is set as an intermediate configuration. The newly defined end configuration represents a straight beam (Configuration 2), but this end geometry has to be reached by going through the (now intermediate) Configuration 1 first. The path discretization now changes, as more elements are added. Thus, the entire motion path is now approximated with $3 + 3 = 6$ quadratic elements. In this case, the C^1-continuity of the path discretization is reduced to a C^0-continuity at the node, where Configuration 1 is set to enable a kink in the motion path. The resulting motion of the second motion design

phase is shown in Figure 4.20b, Stage 1 + Stage 2. Nonetheless, it is also possible to maintain the continuity of the motion path discretization. This would significantly affect the designed motion and its smoothness as no kink is enforced anymore. Then, the interpolatory property of B-spline functions needs to be considered.

The final stage can be carried out in the same manner. While now Configuration 1 and Configuration 2 are defined as detours, Configuration 3 is set as end configuration. The path discretization is now built up by $3 + 3 + 3 = 9$ elements. The solution of a third

Material and geometry

$E = 1000$
$\nu = 0.0$

Path discretization

Stage 1	Stage 2	Stage 3
$\bar{n}_{\mathrm{ele}} = 3$	$\bar{n}_{\mathrm{ele}} = 3 + 3 = 6$	$\bar{n}_{\mathrm{ele}} = 3 + 3 + 3 = 6$
$\bar{p} = 2$	$\bar{p} = 2$	$\bar{p} = 2$
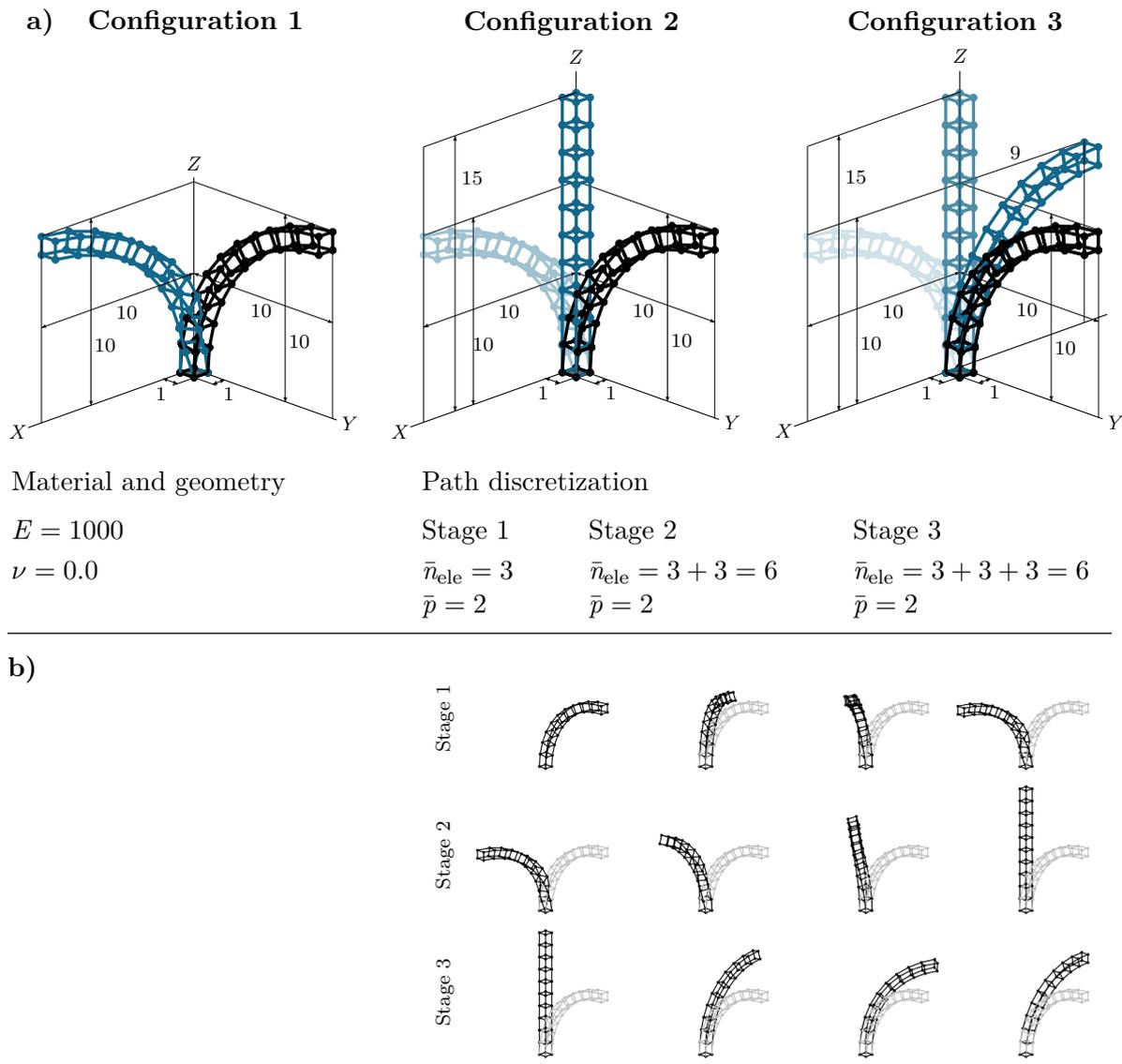
Figure 4.20: Specification of intermediate configurations on a volume cantilever beam. a) Problem setup. b) Illustration of total and sequential motion. An animation of the motion can be found in the digital version of this work.

motion design and the optimized motion consisting of Stage 1, Stage 2 and Stage 3 are given in Figure 4.20b.

4.7.4 Inextensional deformations of shells

Motion design can also be performed with shells. One particularly attractive option in this context is a modification of the functional by replacing the total internal energy by the membrane energy only. From a mechanical point of view, this provides an opportunity to compute motions that try to avoid membrane strains during deformation while bending deformation remains without any penalization. The results are then characterized by nearly inextensional deformations or even purely inextensional deformations, if the geometry is able to perform this kind of motion. Inextensional deformations of surfaces are defined as deformations that preserve lengths and angles of infinitesimal line elements at each point. Gaussian curvature remains constant during inextensional deformations. For thin shells (and beams), inextensional deformations can also be classified as pure bending deformations.

In the following examples, isogeometric Kirchhoff-Love elements, as presented in KIENDL ET AL. (2009), are used. However, as only the membrane energy is considered in the functional, the employed stiffness matrix for the system of equations for motion design corresponds to the tangent stiffness matrix of a membrane element formulation.

It has to be noted that these elements still suffer from membrane locking, although by integrating the internal energy, strain oscillations are leveled out to a certain extent. However, when recovering the forces required to realize the resulting deformation, the effect of membrane locking emerges in the form of much higher loads that are required to enable the prescribed displacements, which are attributable to artificial stiffening effects.

Deformation of a cantilever beam

Typically, thin developable structures with Gaussian curvature being equal to zero can undergo inextensional deformations, e.g., bending of a cylinder to a flat plane. Due to the Gaussian curvature that is equal to zero, the geometry can deform to another geometry with the Gaussian curvature being zero again, while the midsurface does not have to undergo any length changes.

The deformation of a cantilever beam illustrated in Figure 4.21a represents the same phenomenon in a simple two-dimensional configuration. The left side is clamped and

the final location of the tip is prescribed in the target configuration. It is defined in a way that allows the final configuration to form a perfect half-circle.

Initially, the beam is discretized with only two quadratic isogeometric elements to improve convergence due to the low number of degrees of freedom. The path is discretized by two quadratic elements with B-spline shape functions. Starting again with a linear predictor (see Figure 4.21b), the inextensional deformation is actually found by motion design, i.e., the straight cantilever is bent to a half-circle while preserving its length as illustrated in Figure 4.21c.

However, despite the good geometry approximation by NURBS shape functions, this finite element mesh is too coarse to provide reasonable results in terms of stress and

a)

6.4

10.0

1.0

Material and geometry	Path discretization
$E = 1000$	$\bar{n}_\mathrm{ele} = 2$
$\nu = 0.0$	$\bar{p} = 2$
$t = 0.1$	

b) $\quad J = 1132$ **c)** $\quad J = 4.8$ **d)** $\quad J = 0.01$
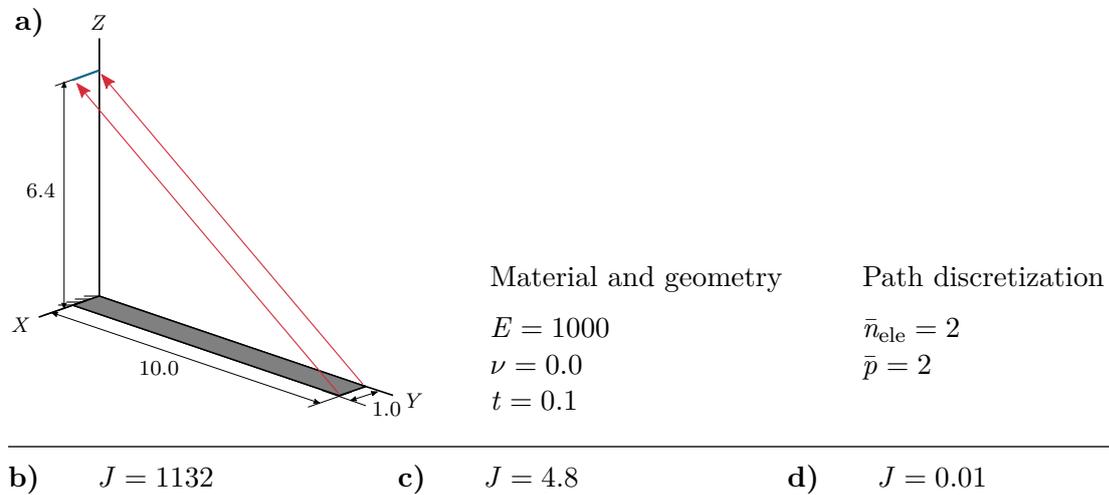
Figure 4.21: Motion design of a cantilever with shell elements and corresponding inextensional deformations. a) Problem setup. b) Linear interpolation. c) Optimized motion. d) Refined optimized motion. An animation of the motion can be found in the digital version of this work.

strain and, thus, the internal energy. Therefore, the geometry is better approximated with twelve quadratic isogeometric shell elements in the following. The motion that is obtained in the previous motion design with only two shell elements is used as a predictor for the next motion design with a refined mesh. The resulting motion still resembles the inextensional deformation (see Figure 4.21d) that is found in the previous motion design analysis with a coarse mesh. However, the functional value decreases from $J = 1132$ in the linear interpolation to $J = 4.8$ and further to $J = 0.01$ with the refined mesh.

In this numerical experiment, it has to be noted that the solution is not unique. Any deformed geometry having the same cantilever length as the original flat configuration (with the restriction of the position of the nodes at the tip) can be reached by an inextensional deformation. Accordingly, the described problem is ill-posed, attributable to the uniaxially curved geometry. Nonetheless, it regularizes itself and one valid solution is found with apparently no numerical problems. This can be traced back to the applied displacement-based standard Galerkin finite element formulation without any measures to avoid locking. For the problem at hand, the effect of membrane locking plays a significant role. For the given discretization with 12 quadratic elements, the effect is not very strong. However, the corresponding parasitic non-zero membrane strains are large enough to have a regularizing effect on the process of motion design.

Transformation of a helicoid to a catenoid

Another classical inextensional deformation is the transformation of a helicoid to a catenoid, as shown in Figure 4.22a. It is a rare example from the field of analytical differential geometry for which an analytical solution for large inextensional deformations exists in the case of Gaussian curvature being non-zero. Like the cantilever beam bent to a semi-circle, also these geometries allow for an inextensional deformation, which is, however, far less intuitive. First, the helicoid is discretized with 4×4 cubic isogeometric shell elements with B-spline shape functions.

For the target geometry, not the whole catenoid is prescribed, but only the final position of the upper and lower edges (*A*-*B*,*C*-*D*). The path is again coarsely discretized with two quadratic elements and B-spline shape functions. For motion design, the vertical displacement of a point at the upper edge *C*-*D* is controlled.

Since the final geometry is, therefore, only vaguely defined, the predictor, which again has been chosen based on a linear interpolation of the prescribed displacement values (see Figure 4.22b), must be characterized as a relatively poor first guess with partly even unphysical deformation states. Nonetheless, the solution of this motion design problem determines not only the correct inextensional deformation, but also the correct final geometry, the catenoid, as shown in Figure 4.22c. The value of the functional is reduced

from $J = 591$ to $J = 0.2$, which is almost zero and corresponds to the expected final result in accordance with possible discretization inaccuracies.

a)

Material and geometry

$E = 1000$
$\nu = 0.0$
$t = 0.1$

Path discretization

$\bar{n}_{\mathrm{ele}} = 2$
$\bar{p} = 2$

b) $\quad J = 591$

$t = 0.0 \quad t = 0.2 \quad t = 0.4 \quad t = 0.6 \quad t = 0.8 \quad t = 1.0$

c) $\quad J = 0.2$

$t = 0.0 \quad t = 0.2 \quad t = 0.4 \quad t = 0.6 \quad t = 0.8 \quad t = 1.0$
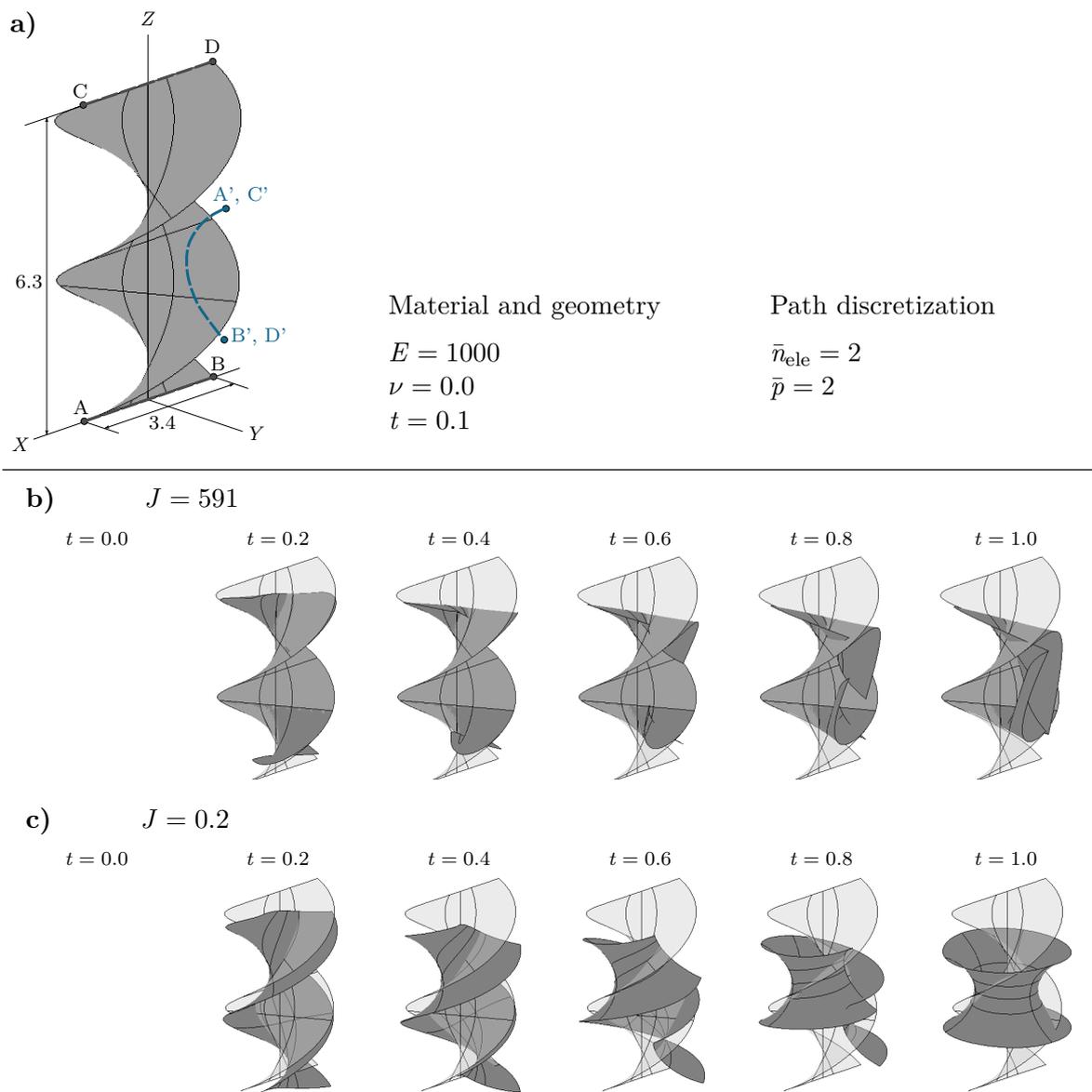
Figure 4.22: Transformation from a helicoid to a catenoid with a motion design analysis. a) Problem setup. b) Linear interpolation. c) Optimized motion. An animation of the motion can be found in the digital version of this work.

4.7.5 Path refinement and convergence studies

In addition to the already presented numerical experiments, convergence studies regarding path discretization shall be carried out at this point by uniformly increasing the number of path elements. Selected benchmark problems, which were already investigated in the previous sections, are exemplarily chosen and re-used for this purpose. In some cases, for example for the kinematic arc, a qualitative study of this type has already been carried out. Truss structures have deliberately been chosen over shell or continuum element formulations to eliminate the influence of spatial discretization.

First, two kinematic benchmark examples, specifically the kinematic single supported bar from Section 4.5.2 and the kinematic truss structure of Section 4.7.1, are further investigated. For both structures, the analytic solution of the internal energy over the motion path is zero, i.e., $J = 0$. The convergence diagrams for two different polynomial degrees of the path discretization are shown in Figure 4.23. Here, the order of convergence is observed to be $\mathcal{O}(\bar{h}^{2(p+1)})$ with $\bar{h}$ being the characteristic path element length. However, such kinematic structures represent special cases, which is why also structures that incorporate elastic deformations during the motion process are studied. For this purpose, the example of the two-bar truss that was first solved semi-analytically in Section 4.2.3 is taken up again. While a qualitative study of the motion path approximation was already carried out in Section 4.5.2, it is quantitatively evaluated here. The same is done with the truss system including multiple snap-throughs from Section 4.7.2. Reference solutions are obtained with a very fine path discretization and are then compared to the results with fewer motion path elements. It can be seen from the convergence diagrams in Figure 4.24 that the functional value converges in these non-kinematic cases with order $\mathcal{O}(\bar{h}^{2p})$, if uniform mesh refinement is applied. A more
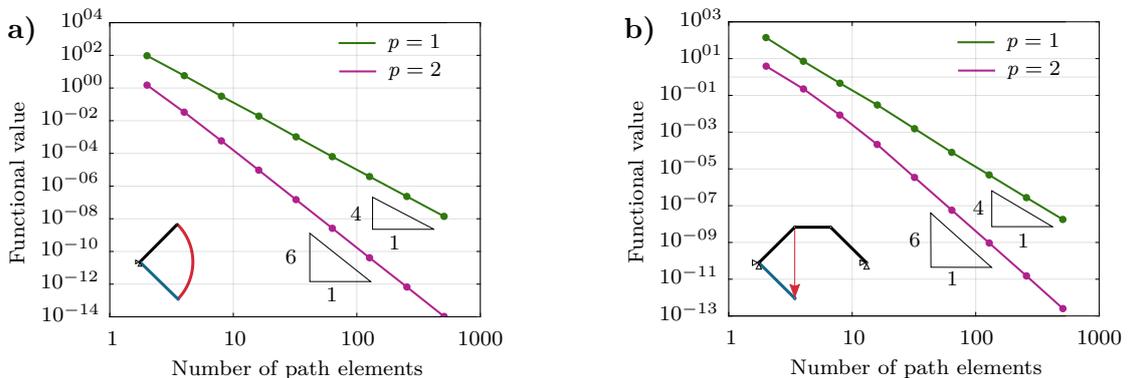
Figure 4.23: Convergence study of the path discretization on different kinematic examples. Convergence diagram for a) the kinematic arc motion and b) the kinematic truss system.
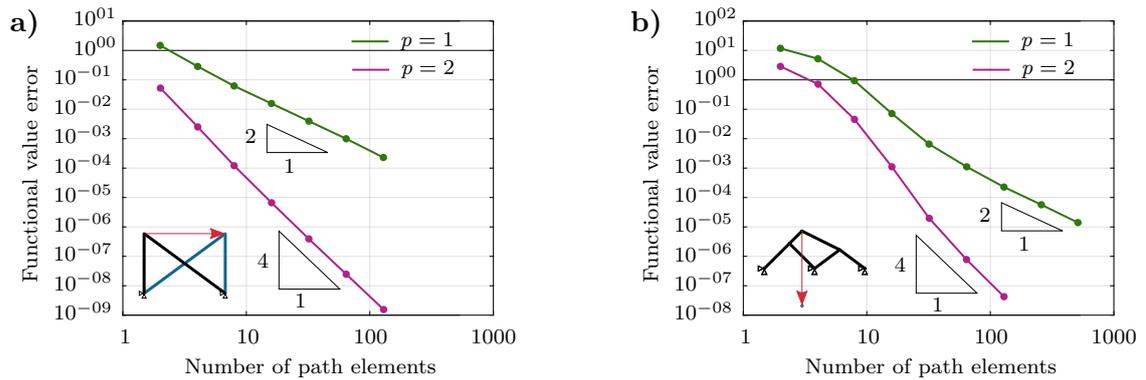
Figure 4.24: Convergence study of the path discretization on different non-kinematic examples. Convergence diagram for a) the semi-analytic reference problem and b) the instability problem with multiple snap-throughs.

detailed analysis of the mathematical background and, therefore, of the reasons for the observed convergence orders is beyond the scope of this thesis.

4.8 Interim conclusion on the motion design method

In this chapter, the theoretical foundation and algorithmic building blocks of the novel motion design method have been presented. Motion design allows to compute an optimal deformation path between two prescribed geometrical configurations of a structure and the evolution of the required loads to realize this optimized motion. First, the basic concept was introduced, including the assumptions and the functional that represents the quantity referred to as cost of deformation. This functional serves as proof of concept for the motion design method, but may also be replaced by a different objective function. In order to be able to consider the entire motion in this functional, the relevant measure is integrated over the deformation path. Here, with a focus on structural analysis, this measure represents the internal strain energy.

A decisive point in the development of the motion design method is the additional discretization of the motion path. In order to map the progress of the motion to a scalar quantity, the path parameter is introduced. It represents the arc length of the displacement field. As the resulting displacement field is initially unknown, a normalized arc length is proposed. Furthermore, its dependency on spatial discretization is removed by using the quadratic mean value of the arc length of the nodal trajectories. This discretization is always one-dimensional, and its nodes represent different deformed states throughout the deformation process, which are interpolated by suitable shape functions over the entire motion.

This leads to a system of equations whose solution directly incorporates all deformation states. Thus, the motion path is not solved iteratively, as usual in nonlinear structural analyses, but in just one step as a whole. This comes with the price of a large number of degrees of freedom that are solved for in the process. However, the method is intended to provide more of a first concept design. For this reason, the application of a coarse mesh in the spatial discretization as well as the path discretization is usually sufficient. The solution then serves as a basis for further, more in-depth analyses.

Since up to now the equilibrium conditions have not yet been considered in the method, their satisfaction must be ensured at the end by a post-processing step. For this purpose, the internal forces are calculated from the resulting displacement field and, therefore, the required external forces for the system to be in equilibrium can be identified. However, this procedure of first ignoring equilibrium conditions and then computing the required external forces by a post-processing is based on the assumption that a force can potentially act on every degree of freedom, which can be a limiting factor for structures in practice. In the following chapter, this observation will be taken up and, among several extensions of the method, suitable measures to deal with structures in which only a limited number of degrees of freedom can actually be actuated will be developed.

5

Constrained Motion Design Problems

As presented in Chapter 4, the motion design method incorporates the underlying assumption that a discrete point load can potentially be applied at any degree of freedom. This is illustrated with a new exemplary truss structure consisting of three bars in Figure 5.1a ($E = 30000$, $A = 0.1$). The vertical displacement of the unsupported midpoint is prescribed such that it moves downward and a snap-through deformation behavior may occur. There are three spatial degrees of freedom D_1, D_2 and D_3 that are not constrained by supports. A basic motion design procedure with 16 linear path elements and a control of the displacement D_2 is carried out. Figure 5.1b shows the solution to such an unconstrained motion design. As can be observed, the resulting optimized deformation path can only be realized by applying all possible non-zero point loads F_1, F_2 and F_3 associated with the degrees of freedom. Therefore, one goal of unconstrained motion design is to calculate how non-zero forces evolve independently from each other during the deformation process to enable an optimized motion.

Nevertheless, it is quite likely in various real applications that not all forces are at disposal for designing an optimized motion. For such cases, an extended approach re-
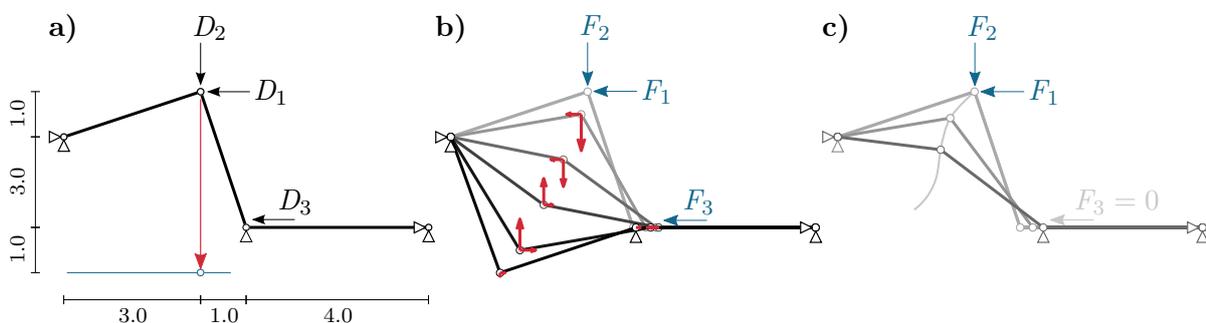
Figure 5.1: Illustrating truss example for constrained motion design. a) Problem setup. b) Unconstrained optimized motion. c) Principle of constrained motion design for discrete loads.

ferred to as constrained motion design will be proposed in the following. This allows for limiting the number of non-zero point loads that may be applied in order to follow the optimal deformation trajectory. When such constraints are taken into account, the minimal value of the employed functional is generally increased compared to the functional value obtained by an unconstrained motion design. For the presented exemplary system, this would mean that an optimal motion with respect to the given functional is to be computed, where e.g., the loads F_1 and F_2 can adjust freely, while F_3 must be zero throughout the entire deformation path (see Figure 5.1c). Consequently, and in contrast to the unconstrained motion design, the method of constrained motion design aims at calculating how selected non-zero forces need to evolve to follow an optimized deformation path.

In addition to point loads, further load cases can be considered. Hence, the discrete nodal forces may incorporate dependencies as it is the case in e.g., line loads or surface loads. Moreover, some adaptive structures contain actuator elements that are able to potentially induce a motion as well.

However, if the designed motion is to be enabled only with prescribed loads or load cases, this represents an additional constraint for the resulting optimized deformation path. Constraints can be introduced into the main functional by various constraint enforcement methods. Therefore, in this chapter, such methods are first presented along with complementing methods for numerical differentiation. Using these techniques, the motion design method is extended in such a way that the resulting motion is realized only by prescribed loads or discrete actuator elements. For the latter, an actuator element formulation is introduced, allowing a straightforward combination with the existing motion design method. Furthermore, also other, more complex constraints may be introduced in this manner, such as the stabilization of a motion by enforcing a positive determinant of the structural stiffness matrix. This procedure, as well as a combination of both classes of constraints, is presented in this chapter. The following contents are based on the publication SACHSE ET AL. (2021a).

5.1 Enforcing constraints in an optimization problem

When equality constraints need to be considered in an optimization problem, it can be reformulated as follows:

Find the minimum of the functional J subject to the constraints $g_i = 0$.

This affects the minimum that is to be found by the solution procedure, and therefore, the constraints already have to be included in the functional. Furthermore, certain constraints can only be formulated as inequality conditions. There exist several methods to enforce such constraints in an optimization problem. Here, the basics of the Lagrange multiplier and the penalty method are presented. For further information beyond the basics and other constraint enforcement methods, the reader is, for example, referred to BELYTSCHKO ET AL. (2014) or NOCEDAL AND WRIGHT (2006).

5.1.1 Lagrange multiplier method

Within the Lagrange multiplier method, additional variables, the so-called Lagrange multipliers λ_i, are introduced for each constraint g_i. The constraints are appended to the functional and multiplied with the corresponding Lagrange multiplier. By collecting these additional variables and the constraints in the vectors $\boldsymbol{\lambda}$ and $\mathbf{g}$, respectively, the extended functional follows as

$$\hat{J}(\mathbf{D},\boldsymbol{\lambda}) = J(\mathbf{D}) + \boldsymbol{\lambda}^{\mathrm{T}}\mathbf{g}(\mathbf{D}) \to \text{stat.} \tag{5.1}$$

The stationary value of the functional subject to the prescribed constraints represents a saddle point. Specifically, the solution is a minimum with respect to the primary variables $\mathbf{D}$ and a maximum with respect to the additional variables $\boldsymbol{\lambda}$. At the stationary point, the derivatives with respect to all variables vanish and, with the definition $\frac{\partial J}{\partial \mathbf{D}} = \mathbf{R}$, they can be expressed as

$$\frac{\partial \hat{J}}{\partial \mathbf{D}} = \frac{\partial J}{\partial \mathbf{D}} + \boldsymbol{\lambda}^{\mathrm{T}}\frac{\partial \mathbf{g}}{\partial \mathbf{D}} = \mathbf{R} + \boldsymbol{\lambda}^{\mathrm{T}}\frac{\partial \mathbf{g}}{\partial \mathbf{D}} = \mathbf{0}\,, \tag{5.2}$$

$$\frac{\partial \hat{J}}{\partial \boldsymbol{\lambda}} = \mathbf{g} = \mathbf{0}\,. \tag{5.3}$$

For an application of the Newton-Raphson method as iterative nonlinear solution scheme, the linearization is required and obtained through a truncated Taylor series expansion as

$$\mathbf{R} + \boldsymbol{\lambda}^{\mathrm{T}}\frac{\partial \mathbf{g}}{\partial \mathbf{D}} + \frac{\partial \mathbf{R}}{\partial \mathbf{D}}\Delta\mathbf{D} + \boldsymbol{\lambda}^{\mathrm{T}}\frac{\partial^2 \mathbf{g}}{\partial \mathbf{D}\partial \mathbf{D}}\Delta\mathbf{D} + \frac{\partial \mathbf{g}}{\partial \mathbf{D}}\Delta\boldsymbol{\lambda} = \mathbf{0}\,, \tag{5.4}$$

$$\mathbf{g} + \frac{\partial \mathbf{g}}{\partial \mathbf{D}}\Delta\mathbf{D} = \mathbf{0}\,. \tag{5.5}$$

For better readability, no Newton iteration index is used and the abbreviations

$$\mathbf{G}_i = \frac{\partial g_i}{\partial \mathbf{D}} \qquad \text{and} \qquad \mathbf{H}_i = \frac{\partial^2 g_i}{\partial \mathbf{D}\partial \mathbf{D}} \tag{5.6}$$

are introduced. The equations (5.4) and (5.5) can then be summarized in the following linearized system of equations to be solved in each Newton step:

$$\begin{bmatrix} \mathbf{K} + \lambda_i \mathbf{H}_i & \mathbf{G}^{\mathrm{T}} \\ \mathbf{G} & \mathbf{0} \end{bmatrix} \begin{bmatrix} \Delta \mathbf{D} \\ \Delta \boldsymbol{\lambda} \end{bmatrix} = - \begin{bmatrix} \mathbf{R} + \boldsymbol{\lambda}^{\mathrm{T}} \mathbf{G} \\ \mathbf{g} \end{bmatrix}, \tag{5.7}$$

where $\mathbf{G}$ is a matrix that comprises the first derivatives $\mathbf{G}_i$ in its rows and the gradient of $\mathbf{R}$ is defined as the matrix $\mathbf{K} = \frac{\partial \mathbf{R}}{\partial \mathbf{D}}$. With this procedure, as many equations as variables are at hand and the system can, therefore, be solved for all unknowns, the primary variables $\mathbf{D}$ and the Lagrange multipliers $\boldsymbol{\lambda}$. The Lagrange multiplier method has the advantage that the constraints are satisfied exactly, but of course, this comes at the price of additional variables and an indefinite system matrix.

5.1.2 Penalty method

Another constraint enforcement approach is the penalty method. Just as for the Lagrange multiplier method, the functional needs to be extended. However, in the case of the penalty method, no additional variables are introduced. Instead, the square of the constraints is multiplied by a so-called penalty parameter β, which typically represents a large positive number. With this modification, the stationary value of the functional remains a minimum, but now the constraints are only approximately satisfied due to the penalty term. The total functional then transforms into

$$\hat{J} = J + \frac{1}{2} \beta \mathbf{g}^{\mathrm{T}} \mathbf{g}. \tag{5.8}$$

Again, the minimum is characterized by a vanishing first derivative:

$$\frac{\partial \hat{J}}{\partial \mathbf{D}} = \mathbf{R} + \beta \mathbf{g}^{\mathrm{T}} \mathbf{G} = \mathbf{0}. \tag{5.9}$$

After linearization for applying the Newton-Raphson method as iterative solution scheme, the following linearized system of equations is obtained:

$$(\mathbf{K} + \beta \mathbf{G}^{\mathrm{T}} \mathbf{G} + \beta g_i \mathbf{H}_i) \Delta \mathbf{D} = -(\mathbf{R} + \beta \mathbf{g}^{\mathrm{T}} \mathbf{G}). \tag{5.10}$$

Here, no additional variables are introduced and the system of equations preserves its original size. However, the constraints are not satisfied exactly and, both the solution accuracy and the conditioning of the system matrix strongly depend on the chosen penalty parameter β.

There also exist other ideas for constraint enforcement that combine the advantages of both methods presented above, e. g., the augmented Lagrangian method. These methods are described in more detail in Nocedal and Wright (2006), for example. However, these are not used within this work and, therefore, not further discussed at this point.

5.1.3 Treatment of inequality constraints

Up to now, the constraints took the form of equality conditions and could easily be formulated in residual form. But also constraints, where a quantity is enforced to remain positive or negative are possible. Such inequality conditions can, in general, be expressed as

$$g_i \geq 0 \,. \tag{5.11}$$

Here, it has to be considered that some constraints might already be automatically satisfied, whereas others have to be enforced. Therefore, it has to be distinguished between the active and inactive set of constraints. One way of dealing with such conditions is an iterative scheme, where an assumed active set is validated and updated after each solution of the constrained minimization problem. Another approach is the direct integration of an active set strategy into the nonlinear problem formulation. Using the Lagrange multiplier method, so-called Karush-Kuhn-Tucker conditions form the basis of this approach

$$g_i \geq 0 \,, \qquad\qquad \lambda_i \geq 0 \,, \qquad\qquad g_i \lambda_i = 0 \,. \tag{5.12}$$

They state that either the active constraint g_i or the Lagrange multiplier λ_i is zero, and consequently, the product of both definitely is. This means that the Lagrange multiplier takes a positive value if the corresponding constraint needs to be enforced or equals zero for an inactive constraint. The Karush-Kuhn-Tucker conditions equations can alternatively be expressed compactly as a semi-smooth equation by means of the so-called nonlinear complementarity function

$$C_i = \lambda_i - \max\left(0, \lambda_i - c g_i\right) = 0 \,, \tag{5.13}$$

which is mathematically equivalent to the Karush-Kuhn-Tucker conditions in eq. (5.12). The complementarity parameter c has to be positive and regularizes the non-smooth constrained optimization problem. Also in the resulting system of equations, one has to distinguish between active and inactive constraints. The appropriate vectors and matrices are denoted with the subscript a for active and i for inactive, respectively. Building the variation and linearization yields the following extended system of equations

to be solved in each (semi-smooth) Newton step:

$$
\begin{bmatrix} \mathbf{K} + \lambda_i \mathbf{H}_i & \mathbf{G}_a^T & \mathbf{G}_i^T \\ \mathbf{G}_a & \mathbf{0} & \mathbf{0} \\ \mathbf{0} & \mathbf{0} & \mathbf{I} \end{bmatrix} \begin{bmatrix} \Delta \mathbf{D} \\ \Delta \boldsymbol{\lambda}_a \\ \Delta \boldsymbol{\lambda}_i \end{bmatrix} = - \begin{bmatrix} \mathbf{R} + \boldsymbol{\lambda}^T \mathbf{G} \\ \mathbf{g}_a \\ \boldsymbol{\lambda}_i \end{bmatrix} .
\tag{5.14}
$$

This linear system of equations must be complemented by an update formula based on eq. (5.12) to consider possible changes in the active set during the Newton iterations.

5.1.4 Methods of numerical differentiation

For the constraint enforcement with either method presented in Section 5.1.1, 5.1.2 and 5.1.3, derivatives of the constraint equations are required. Depending on the problem, an analytical derivative of the constraints is difficult to elaborate or sometimes even impossible to derive. To circumvent this problem of analytical derivatives, they can also be calculated numerically. For this purpose, the exemplary function to be differentiated $f(x)$, is evaluated at different points and the resulting function values are compared. There exist various types of numerical differentiation. All methods are based on a Taylor series expansion around a point a. For the simple forward difference, this yields

$$
y(x) = \sum_{n=0}^{\infty} \frac{y^{(n)}(a)}{n!} (x - a)^n = y(a) + \frac{y'(a)}{1}(x - a) + \frac{y''(a)}{2}(x - a)^2 + \dots \, .
\tag{5.15}
$$

The Taylor series expansion of a neighboring point with the distance h is

$$
y(x + h) = \sum_{n=0}^{\infty} \frac{y^{(n)}(a)}{n!} (x + h - x)^n = y(x) + \frac{y'(x)}{1}h + \frac{y''(x)}{2}h^2 + \dots
\tag{5.16}
$$

or in a simplified and approximated way

$$
y(x + h) \approx y(x) + h \cdot y'(x) + \mathrm{HOT} \, .
\tag{5.17}
$$

In numerical methods for differentiation, these equations are transformed with respect to the first derivative to get an approximation. However, two different errors can arise due to numerical issues. The *truncation error* is caused by cutting off higher-order terms of the Taylor series expansion, whereas the *substractive cancellation error*, on the other hand, arises due to the subtraction of two almost equal floating point numbers. With the methods presented in the following, only an appropriate approximation of the first derivative is obtained. Nonetheless, it is also possible to compute the second derivative of a function, but only with substantially higher errors.

Forward and backward difference method

Both the forward and backward difference method compare the value of $y(x)$ with the value at a neighboring point at a distance h. In a forward difference method, the distance h is added to x

$$y'(x) \approx \frac{y(x+h) - y(x)}{h} \,,$$
(5.18)

whereas the distance is substracted in the backward difference method

$$y'(x) \approx \frac{y(x) - y(x-h)}{h} \,.$$
(5.19)

With both methods, an approximation of the first derivative is obtained, but it still incorporates both types of errors.

Central difference method

For the central difference method, the function is evaluated at two points: One point where h is added and one point where h is subtracted. The distance between these points then corresponds to $2h$ and the derivative approximation from a Taylor series expansion is

$$y'(x) \approx \frac{y(x+h) - y(x-h)}{2h} \,.$$
(5.20)

This method enables a better approximation of the derivative than those of the forward and backward difference method. However, it still contains the truncation error as well as the subtractive cancellation error.

Complex step derivative

In MARTINS ET AL. (2003) the so-called complex step derivative is presented, where the distance h is added in the complex direction, i. e., the imaginary part. The Taylor series

expansion then follows as

$$y(x + ih) = \sum_{n=0}^{\infty} \frac{y^{(n)}(x)}{n!} (ih)^n \tag{5.21}$$

$$= y(x) + \frac{y'(x)}{1} ih + \frac{y''(x)}{2} (ih)^2 + \frac{y'''(x)}{6} (ih)^3 + \dots \tag{5.22}$$

$$= y(x) + \frac{y''(x)}{2} (ih)^2 + i \left(\frac{y'(x)}{1} h - \frac{y'''(x)}{6} h^3 \right) + \dots \, . \tag{5.23}$$

The first derivative only appears in the imaginary part. If the imaginary part is resolved after the derivative, it results in

$$y'(x) \approx \frac{\text{Im}(y(x + ih))}{h} \, . \tag{5.24}$$

In the first derivative, the subtractive cancellation error is, thus, completely avoided, since the expression does not contain any subtraction. The truncation error remains, but h can freely be chosen.

Directional derivative and complex step directional derivative

The directional derivative $y'_{\mathbf{v}}(\mathbf{x})$ of a function $y(\mathbf{x})$ describes the change of the function value at a point $\mathbf{x}$ in the direction of a vector $\mathbf{v}$. It can be expressed via the gradient and a scalar multiplication

$$y'_{\mathbf{v}}(\mathbf{x}) = \frac{\partial y(\mathbf{x})}{\partial \mathbf{x}} \cdot \mathbf{v} \, . \tag{5.25}$$

To evaluate this specific expression numerically, each partial derivative has to be numerically differentiated. However, the directional derivative can also be calculated and approximated in a forward difference approach as

$$y'_{\mathbf{v}}(\mathbf{x}) \approx \frac{y(\mathbf{x} + h\mathbf{v}) - y(\mathbf{x})}{h} \, . \tag{5.26}$$

Comparing both equations, eq. (5.25) and eq. (5.26), it can be concluded that the numerical directional derivative is advantageous regarding numerical efficiency whenever a gradient vector needs to be multiplied with a vector $\mathbf{v}$ in the further process. By using the directional derivative in these cases, only one additional evaluation into the direction $\mathbf{v}$ is required instead of a differentiation with respect to every entry of $\mathbf{x}$

$$\frac{\partial y(\mathbf{x})}{\partial \mathbf{x}} \cdot \mathbf{v} \approx \frac{y(\mathbf{x} + h\mathbf{v}) - y(\mathbf{x})}{h} \, . \tag{5.27}$$

Moreover, the directional derivative can be calculated as a complex step derivative

$$y_{\mathbf{v}}'(\mathbf{x}) \approx \frac{\mathrm{Im}(y(\mathbf{x} + ih\mathbf{v}))}{h} \,. \tag{5.28}$$

5.2 Restricting the motion to specified load cases

Using the constraint enforcement methods introduced above in combination with the procedures for numerical differentiation, the basic motion design method can be extended by the constraint that the sought-after motion should be realized with only a certain number and specific type of load cases. In the following, the strategy for introducing this condition into the basic motion design method is presented, including the restrictions that arise for prescribing the target configuration of the motion. Afterward, this is further illustrated with numerical experiments.

5.2.1 Equality constraints for unloaded degrees of freedom

For the derivation of the method of constrained motion design, the assumption holds that only external point loads, and not entire load cases, can be applied to the deforming structure. According to the defined constraint, they should only be placed at prescribed locations of the structure that are associated with specific degrees of freedom. Accordingly, also an internal force can only occur at these loaded degrees of freedom due to equilibrium, which must be included at this point. Following the motion design approach, these can freely evolve and adjust during the deformation process. On the other hand, the internal forces at the unloaded degrees of freedom are supposed to continually remain zero. This condition can be expressed as a set of equality constraints on the motion.

As the described constraints must hold for the entire motion, they are introduced for each configuration during the deformation process, i. e., the intermediate as well as the target configuration. They, therefore, represent pointwise constraints, which are not included in the integral of the main functional and can be expressed in a general way as

$$\mathbf{g} = \begin{bmatrix} \mathbf{F}^1 & \mathbf{F}^2 & \ldots & \mathbf{F}^k & \ldots & \mathbf{F}^{\bar{n}_{\mathrm{nd}}} \end{bmatrix}^{\mathrm{T}} \,. \tag{5.29}$$

Here, the vectors $\mathbf{F}^k$ gather the internal forces of the degrees of freedom, where no load is applied, for each load configuration or node of the motion path discretization $\bar{k}$. When using a path discretization with an approximation by B-spline shape functions,

these constraints should not be imposed on the control points but on the deformation path itself. For this reason, the constraints are enforced at collocation points, which are located on the path. In this case, Greville points are used.

For the system presented in Figure 5.1c with 16 linear path elements, the internal force at the degree of freedom number 3 must be zero in every path increment. Consequently, the vector of constraints can be written as

$$\mathbf{g} = \begin{bmatrix} F_3^2 & F_3^3 & F_3^4 & \dots & F_3^{16} \end{bmatrix}^{\mathrm{T}} . \tag{5.30}$$

The internal force F_3^1 of the initial configuration is suspended as the initial configuration is always assumed to be load-free. If load cases act on multiple nodes or degrees of freedom, such as distributed line loads or surface loads, the discrete forces of the individual degrees of freedom directly depend on each other through a scaling factor. In such cases, a master degree of freedom is selected and the associated forces are coupled to the load value of this master degree of freedom. Applying the Lagrange multiplier method as presented in Section 5.1.1 yields the extended system of equations for this type of constrained motion design problems as

$$\begin{bmatrix} \mathbf{K}_{\mathrm{md}} + \lambda_i \mathbf{H}_i & \mathbf{G}^{\mathrm{T}} \\ \mathbf{G} & \mathbf{0} \end{bmatrix} \begin{bmatrix} \Delta \bar{\mathbf{D}} \\ \Delta \boldsymbol{\lambda} \end{bmatrix} = - \begin{bmatrix} \mathbf{R}_{\mathrm{md}} + \boldsymbol{\lambda}^{\mathrm{T}} \mathbf{G} \\ \mathbf{g} \end{bmatrix} . \tag{5.31}$$

Here, the matrix $\mathbf{G}$ contains the first derivatives of all constraints, whereas the Hessian matrix $\mathbf{H}_i$ represents the second derivative of the ith constraint. This means that the constraints, i.e., the corresponding internal forces $\mathbf{F}^k$, need to be differentiated twice with respect to all degrees of freedom: those of the spatial discretization as well as those of the path discretization.

The internal force at a degree of freedom j in the load configuration $\bar{k}$ only depends on the displacements, i.e., the spatial degrees of freedom, at the associated path node. However, the tangent stiffness matrix $\mathbf{K}_{\mathrm{T}}^k$ already incorporates the first derivative of the internal forces with respect to the relevant degrees of freedom. This circumstance can be exploited at this point. Accordingly, if only one component $\mathbf{F}_j^k$ of the total internal force vector $\mathbf{F}^k$ is differentiated, the derivative is provided by the associated column $\mathbf{K}_j^k$ of the stiffness matrix. Consequently, the vector $\mathbf{G}_i$ of first derivatives of the ith constraint g_i follows as

$$\mathbf{G}_i = \frac{\partial g_i}{\partial \mathbf{D}^k} = \frac{\partial F_j^k}{\partial \mathbf{D}^k} = \mathbf{K}_j^k . \tag{5.32}$$

Additionally, the second derivative of the ith constraint is required for the Hessian matrix $\mathbf{H}_i$. In this case, this represents the derivative of the associated column of the stiffness

matrix. Usually, the relevant column of the stiffness matrix $\mathbf{K}_j$ has to be differentiated with respect to each degree of freedom. This yields for the Hessian matrix of the ith constraint

$$\mathbf{H}_i = \frac{\partial \mathbf{K}_j^k}{\partial \mathbf{D}^k} \, . \tag{5.33}$$

However, the analytical derivative of the tangent stiffness matrix can only be calculated in special cases. Using a numerical differentiation scheme as presented in Section 5.1.4, the tangent stiffness has to be evaluated multiple times to either get an approximation of the derivative or the exact derivative using complex step approximation (MARTINS ET AL. 2003). This might not be efficient in terms of the calculation time. Nonetheless, as only the column j of the stiffness matrix needs to be differentiated, the derivative of the entire stiffness matrix can be calculated and the corresponding degree of freedom can subsequently be extracted by a scalar product with a unit vector $\mathbf{D}_j$ in the direction of j

$$\mathbf{H}_i = \frac{\partial \mathbf{K}_j^k}{\partial \mathbf{D}^k} = \frac{\partial \mathbf{K}^k}{\partial \mathbf{D}^k} \cdot \mathbf{D}_j \, . \tag{5.34}$$

In this way, the derivative in eq. (5.33) is transformed into a directional derivative in eq. (5.34), which was described in Section 5.1.4. Thus, the advantage of using numerical differentiation regarding numerical efficiency becomes apparent. Instead of differentiating a single column of the stiffness matrix with respect to all degrees of freedom and consequently evaluating it as many times for numerical differentiation, the whole stiffness matrix now only has to be computed one additional time in the direction of $\mathbf{D}_j$. In order to increase accuracy, the numerical derivative is determined with the help of the complex step approximation. As already explained, the deviation is executed in the complex direction and, therefore, the first derivative can be calculated numerically exact.

The derivatives of the system in Figure 5.1 for the first ($i = 1$) constraint $F_3^2 = 0$ are exemplarily presented in the following. In this case, the relevant spatial degree of freedom is $j = 3$. Thus, the first derivative can be extracted from the total stiffness matrix of the current load configuration $\bar{k} = 2$, where it represents the third column

$$\mathbf{G}_1 = \frac{\partial F_3^2}{\partial \mathbf{D}^2} = \mathbf{K}_3^2 \, . \tag{5.35}$$

The Hessian matrix contains the entire stiffness matrix of the second configuration and can be calculated with the help of a directional derivative

$$\mathbf{H}_1 = \frac{\partial \mathbf{K}^2}{\partial \mathbf{D}^2} \cdot \mathbf{D}_3 \,. \tag{5.36}$$

With these derivatives, the extended system of equations from eq. (5.31) can be generated and solved. Thus, an optimized motion can be found, which is realized exclusively by the defined loads or load cases. The result is the deformation path and the development of the load case amplitudes during the motion.

5.2.2 Restrictions for the prescribed end geometry

In the basic motion design method, either the entire end geometry or only parts of it have to be prescribed. This is similar for constrained motion design problems, but with one important restriction: As equilibrium should be fulfilled throughout the entire motion only with the available loads, this should also be the case for the prescribed end geometry. There are two different strategies to guarantee that this condition is actually satisfied, depending on the number of given end displacement values:

- If the entire end geometry is prescribed, an optimization is carried out prior to the motion design process, where a new end geometry is computed. The objective function to be minimized is the difference between the target and the current geometry with the constraint that the appropriate forces must be equal to zero.

- Another possibility is to prescribe only a part of the end geometry. Like this, the rest of the geometry can adjust freely to meet the condition of equilibrium with the available loads. The maximum number of prescribed values of displacement degrees of freedom strongly depends on the number of load cases. It is not possible to prescribe more displacement values than load cases, whereas fewer are generally possible.

5.2.3 Solution and interpretation of the results

Taking into account the described restrictions for the target geometry, the extended system of equations, as introduced in eq. (5.31), can be solved. In doing so, an optimized motion path is obtained, while considering the given constraints of an equilibrium state with only the available loads or load cases. The results for the example in Figure 5.1 with a varying number of permitted loads and load cases are summarized in Figure 5.2.

If loads can be applied on every degree of freedom, no constraints are enforced and the solution is identical to the result from an unconstrained motion design. This is illustrated in Figure 5.2a, which is similar to the motion in Figure 5.1b. It can be seen in the load-displacement curves of all three discrete point loads in Figure 5.2b that they take non-zero values during the deformation process to realize the calculated optimal deformation path. This motion yields a minimized functional value of $J = 600$. When one load is suspended, this optimal deformation path cannot be followed anymore since all three possible point loads are required for keeping an equilibrium state in these deformed configurations. Therefore, a different motion is to be found that is enabled by the remaining loads. The new constrained optimized motion is illustrated in Figure 5.2c and the corresponding load-displacement curves in Figure 5.2d. Moreover, as only the vertical displacement of the target geometry is prescribed, the horizontal displacement adapts such that the additional constraint is met. The introduction of constraints also influences the minimum of the functional and its value increases to $J = 607$. If only one load case is permitted, as shown with the case of two dependent loads $F_1 = F_2$ (see Figure 5.2e and f), the result is identical to an equilibrium path obtained by a nonlinear static analysis with either the arc length method or a displacement-controlled algorithm. This motion does not represent a "design" in this case because there is no other equilibrium path (except in the special case of the existence of secondary paths) under only one possible given load case.
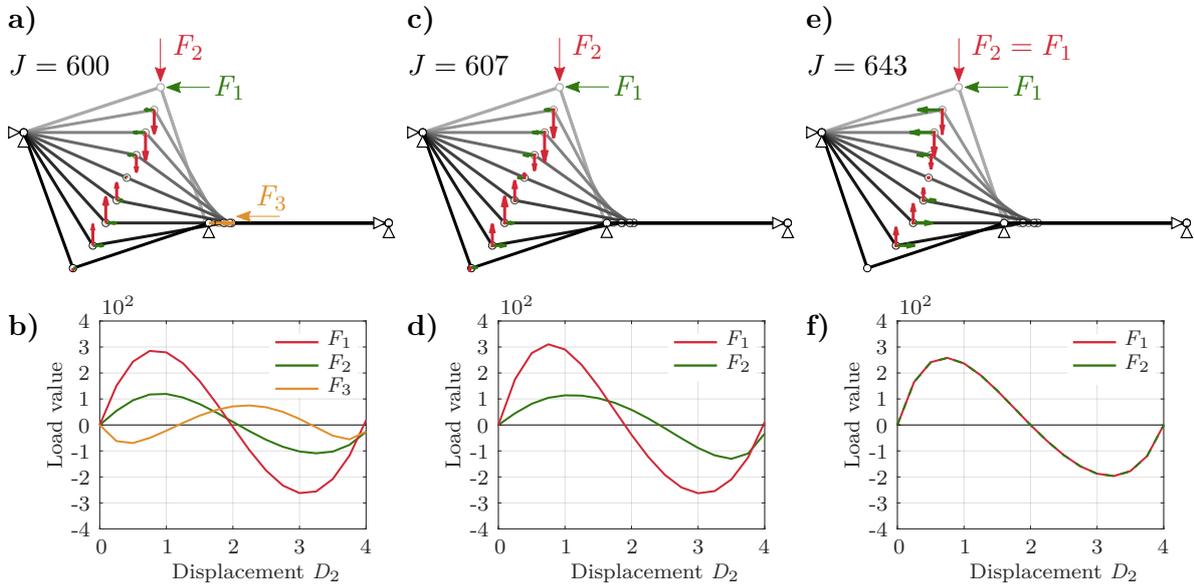
Figure 5.2: Solutions of the illustrating example with different numbers and types of load cases. a) Unconstrained motion with all possible point loads and b) load-displacement curves. c) Constrained motion with two independent loads and d) load-displacement curves. e) Constrained motion design with two dependent loads and f) load-displacement curves.

5.2.4 Numerical experiments for motion design with restricted load cases

Constrained motion design with multiple snap-through processes

To prove the applicability of the presented method, several numerical experiments are carried out. First, an example is presented, which was already previously studied in Section 4.7.2 in order to demonstrate the difference between unconstrained and constrained motion design. Three two-bar trusses are combined into one truss structure, whereby the upper two-bar truss with a larger cross-sectional area, and, therefore, also a higher stiffness, is supported by two other two-bar trusses (see Figure 4.17). For the motion, the vertical displacement of the upper node in the end configuration is prescribed and also controlled throughout the deformation. The result of an unconstrained motion design procedure with a path discretization with 16 linear elements is already shown in Figure 4.17c but is depicted again at this point with the corresponding point loads in Figure 5.3a. As already described in Section 4.7.2, the value of the functional decreases compared to a simple linear interpolation between the initial and end configuration when the lateral two-bar trusses perform a consecutive snap-through. The functional value for this motion is $J = 11.1$. To realize this optimal motion, point loads need to be applied on all six degrees of freedom, which can be seen in the load-displacement curves (green) in Figure 5.3c.

For a constrained motion design, now, only two point loads, a vertical and a horizontal load at the upper node are permitted to be applied. This results in four constraints per configuration, which enforce the remaining internal forces at the unloaded degrees of freedom to become zero. Solving the extended system of equations leads to the modified motion illustrated in Figure 5.3b. The end geometries of the unconstrained and constrained motion design variants vary slightly, but the vertical displacement of
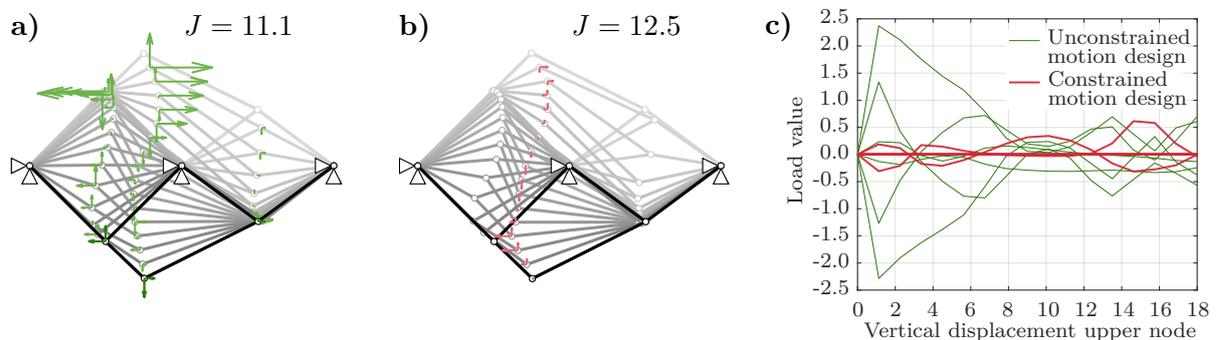
Figure 5.3: Combination of multiple snap-throughs with a) unconstrained motion design and b) constrained motion design. c) Corresponding load-displacement curves.

the upper node coincides in both cases, as this represents the prescribed displacement value. Furthermore, it can be seen that retaining the last equilibrium state requires lower forces in constrained motion design. Due to the additional constraints, the value of the functional increases to $J = 12.6$, i. e., by approximately 12,5 %. The two resulting motions from unconstrained and constrained motion design resemble each other, especially regarding the overall motion pattern with the consecutive lateral snap-through processes. However, the required loads differ and there is a significant difference in the magnitude of the forces. The loads to follow the constrained motion are much lower than the initial loads of the unconstrained motion design (see Figure 5.3c).

To sum up, the restriction to realize the motion with only two point loads instead of all six possible point loads leads to a slight increase of the functional value, while achieving a similar appearance of the motion in this particular scenario. Furthermore, the required absolute load values become much smaller even though the number of loads is decreased by four.

Snap-through of a shallow arc

The next problem is again the shallow arc, which has already been presented in a different form in the previous chapter in Section 4.7.2. The arc is modeled with displacement-based quadrilateral elements, as illustrated in Figure 5.4a, and is to be deformed such that it ends up in an approximately mirrored position. For this deformation, only the three visualized point loads may be applied. The end configuration differs slightly from the previously defined end configuration in Figure 4.19a to better illustrate the effect of the applied loads.

Since the target geometry is chosen artificially and is not based on real deformation results of an analysis with defined load cases, point loads have to be applied at every degree of freedom to guarantee equilibrium in the prescribed end geometry, see Figure 5.4b. This stands in contrast to the constraint that the motion shall now be realized with the three prescribed point loads only. Therefore, the end geometry has to be modified, as explained in Section 5.2.2. In this example, the complete geometry is prescribed and not only a part of the displacement values. Thus, an optimization of the final geometry is carried out prior to motion design. Here, the final nodal displacements represent the variables and the displacement difference between the prescribed and obtained geometry is minimized subject to the constraint that equilibrium is obtained only with the available loads. The resulting geometry differs noticeably from the prescribed geometry, as displayed in Figure 5.4c.

This newly obtained geometry is then set as the end configuration for motion design. The deformation path is discretized by 24 linear elements, and an unconstrained motion
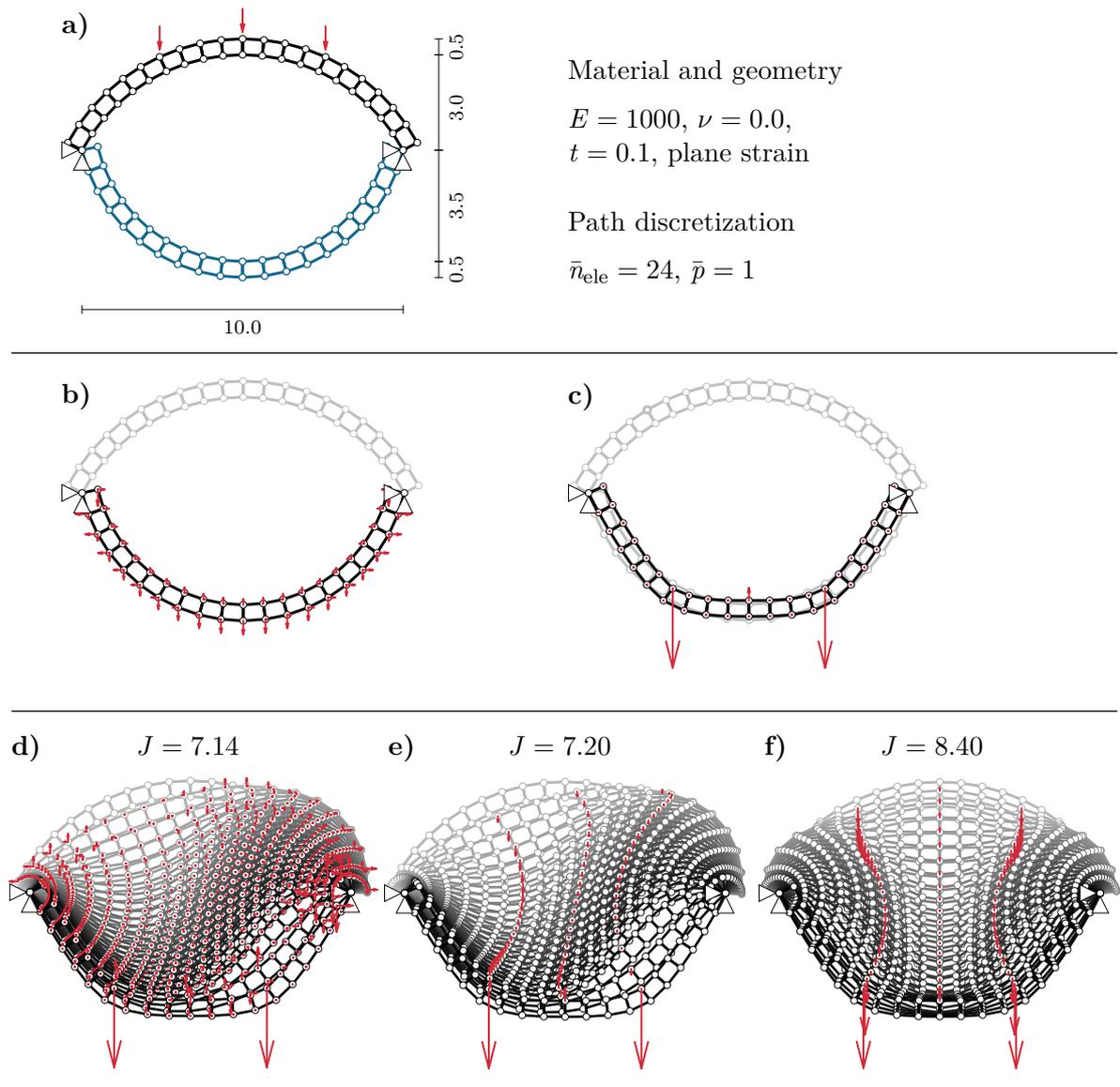
Figure 5.4: Constrained motion design of a shallow arc with three point loads. a) Problem setup. b) Prescribed end geometry. c) Modified end geometry. d) Unconstrained motion. e) Constrained motion. f) Deformation obtained by a static nonlinear analysis.

design yields the motion in Figure 5.4d with a functional value of $J = 7.14$. It is found again that a successive snap-through of the lateral parts of the structure leads to a decrease of the functional value compared to a simple linear interpolation. However, even though the end geometry can be reached only with the three prescribed loads, forces are applied at the other degrees of freedom throughout the motion to realize the resulting optimized deformation path, because this is favorable concerning the integrated internal energy. This result is different from the motion that is obtained by constrained

motion design, as illustrated in Figure 5.4e. Here, only the three prescribed point loads are applied to the structure and during the entire deformation process. Therefore, also the intermediate configurations are in an equilibrium state with the available loads. The functional value increases only slightly to $J = 7.20$, which is attributable to the additional constraints.

This result from motion design is compared to a classical static nonlinear analysis in Figure 5.4f, where the loads required for the end configuration are applied. The solution is calculated with the help of the arc length method as path-following technique within 24 steps. As all three forces are increased and decreased uniformly, a symmetric snap-through now appears, and the resulting deformation varies significantly from the deformation obtained by motion design. Furthermore, the functional takes a value of $J = 8.40$, which is higher than those from both unconstrained as well as constrained motion design. Thus, even though the constraints increase the cost of deformation, it is still lower than for the conventional approach of a static nonlinear analysis. This is the consequence of enabling an independent evolution of the different loads or load cases throughout the deformation process, which is only made possible by the new motion design procedure and its ability to identify a more efficient motion.

5.3 Actuator elements

Referring to the previous chapter, one possible load case can also be the actuation of discrete actuator elements in a truss structure. Actuator elements are able to contract or expand and thus, enforce a deformation of the entire system. To include such elements into the motion design method, a new actuator element formulation is introduced. Afterwards, it is combined with the previously presented algorithm building blocks of the motion design method.

5.3.1 Actuator element formulation

The basis of the actuator element is formed by a regular two-dimensional truss element with a vertical and horizontal displacement degree of freedom at each node (cf. Figure 5.5a). The actuator element, however, also allows for an independent elongation or contraction. This is depicted by an additional parameter α, which represents a factor for the targeted actuator element elongation, as can be seen in Figure 5.5b.
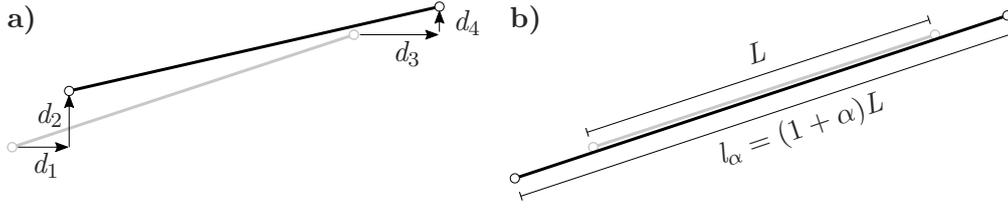
Figure 5.5: Parameter in the actuator element formulation. a) Displacement degrees of freedom. b) Elongation parameter.

In an actuator element, the total strain E_d consists of two parts: the elastic strain E_{el} and the strain resulting from the actuation E_α

$$E_d = E_{el} + E_\alpha \,. \tag{5.37}$$

The total strain E_d can be obtained by the usual displacement degrees of freedom and the actuation strain E_α is determined with the additional elongation parameter α. This allows the elastic strain to be evaluated. The stresses are calculated based on the elastic strain contribution only. Thus, the internal elastic energy is given by simply applying the linear elastic St. Venant-Kirchhoff material law as

$$\Pi_{int,el} = \int_\Omega \frac{1}{2} E_{el} \mathbf{C} E_{el} \, d\Omega = \int_\Omega \frac{1}{2} (E_d - E_\alpha) \mathbf{C} (E_d - E_\alpha) \, d\Omega \,. \tag{5.38}$$

Taking this as a basis, the internal forces can be derived, thus yielding for a single actuator element

$$\mathbf{f}_{int} = \int_{\Omega_e} \mathbf{B}^T \mathbf{C} (E_d - E_\alpha) \, d\Omega \,. \tag{5.39}$$

The strain-displacement-operator $\mathbf{B}$ is defined as the derivative of the elastic strain with respect to the unknown parameters and is divided into two parts: the derivative with respect to the local displacement degrees of freedom $\mathbf{d}$ and the derivative with respect to the elongation parameter α. This results in

$$\mathbf{B} = \begin{bmatrix} \mathbf{B}_d \\ B_\alpha \end{bmatrix} \qquad \text{with} \qquad \mathbf{B}_d = \frac{\partial E_d}{\partial \mathbf{d}} \qquad \text{and} \qquad B_\alpha = -\frac{\partial E_\alpha}{\partial \alpha} \,. \tag{5.40}$$

Consistent linearization of the global residual equation for equilibrium yields the stiffness matrix. The local stiffness matrix for the actuator element follows as

$$\mathbf{k}_{act} = \begin{bmatrix} \mathbf{B}_{d,d}^T \mathbf{C} E_{el} + \mathbf{B}_d^T \mathbf{C} \mathbf{B}_d & B_\alpha \mathbf{C} \mathbf{B}_d \\ \mathbf{B}_d^T \mathbf{C} B_\alpha & B_{\alpha,\alpha} \mathbf{C} E_{el} + B_\alpha \mathbf{C} B_\alpha \end{bmatrix} = \begin{bmatrix} \mathbf{k}_{dd} & \mathbf{k}_{d\alpha} \\ \mathbf{k}_{d\alpha}^T & \mathbf{k}_{\alpha\alpha} \end{bmatrix} \,. \tag{5.41}$$

It includes the tangent stiffness matrix $\mathbf{k}_{\mathrm{dd}}$ of a regular truss element in the upper left corner. The global stiffness matrix can be obtained by usual assembly operations for n_{ele} elements. These operations can be applied separately for the different stiffness components

$$\mathbf{K}_{\mathrm{dd}} = \bigcup_{e=1}^{n_{\mathrm{ele}}} \mathbf{k}_{\mathrm{dd}}\,, \qquad \mathbf{K}_{\mathrm{d}\alpha} = \bigcup_{e=1}^{n_{\mathrm{ele}}} \mathbf{k}_{\mathrm{d}\alpha}\,, \qquad \mathbf{K}_{\alpha\alpha} = \bigcup_{e=1}^{n_{\mathrm{ele}}} \mathbf{k}_{\alpha\alpha}\,, \tag{5.42}$$

which results in the global linearized system of equations

$$\begin{bmatrix} \mathbf{K}_{\mathrm{dd}} & \mathbf{K}_{\mathrm{d}\alpha} \\ \mathbf{K}_{\mathrm{d}\alpha}^{\mathrm{T}} & \mathbf{K}_{\alpha\alpha} \end{bmatrix} \begin{bmatrix} \Delta\mathbf{d} \\ \Delta\boldsymbol{\alpha} \end{bmatrix} = \mathbf{F}_{\mathrm{int}} - \mathbf{F}_{\mathrm{ext}}\,. \tag{5.43}$$

If the elongation or contraction of one or multiple actuators is given, this can then be treated as an inhomogeneous Dirichlet boundary condition, i.e., by prescribing the respective elongation parameter. The same procedure can also be regarded as a load case with an actuation load vector extracted from eq. (5.39):

$$\mathbf{f}_{\mathrm{int,act}} = -\int_{\Omega_e} \mathbf{B}^{\mathrm{T}}\mathbf{C}E_\alpha\,\mathrm{d}\Omega\,. \tag{5.44}$$

Thereupon, the resulting displacements are solved for. This procedure is demonstrated in the following example: a statically determinate structure, which has already been introduced in Figure 5.1. The left bar (marked in red) is now replaced by an actuator element that is to be shortened by 50 %. Thus, the elongation parameter for this element is set to the value $\alpha = -0.5$. The other two elements still represent regular truss elements. With the system of equations in eq. (5.43) and a load-controlled geometrically nonlinear analysis, the resulting nodal displacements can be computed. The solution is shown in Figure 5.6a. It can be observed that only the actuator element experiences a length change while the other two bars undergo a purely kinematic deformation and keep their initial lengths. When replacing one truss element by an actuator element in this statically determinate structure, no constraints are imposed on the remaining structure. Due to that, the actuator element reaches exactly the targeted length change of 50 %. The total strain, therefore, only contains a contribution of the actuation strain and the elastic strain is exactly zero (E_{el}). However, such a constraint-free shortening of the actuator element is only possible to a certain extent and strongly depends on the structure.

In contrast to that, another structure is investigated, in which only one more bar with the same cross-sectional area and material properties has been added (cf. Figure 5.6b). This results in a statically indeterminate system with the degree $n_{\mathrm{s}} = 1$. The same
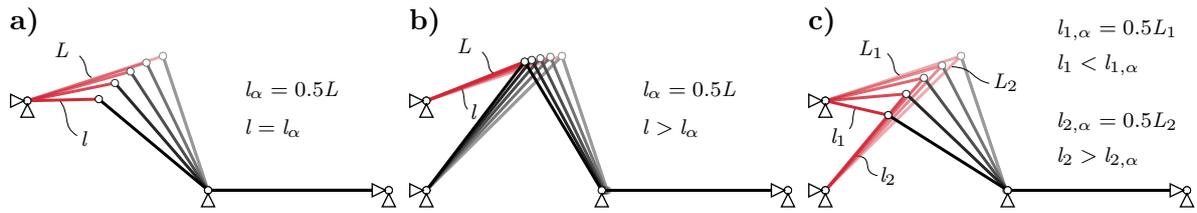
Figure 5.6: Actuator length change as load case and the resulting deformation of a) a statically determinate structure with one actuator element, b) a statically indeterminate structure with one and c) two actuator elements.

actuator element as before is now shortened with the same targeted length change of 50%, thus resulting again in an elongation parameter $\alpha = -0.5$. Due to the static indeterminacy of the structure in combination with the position of the single actuator element, its length change encounters resistance by the rest of the structure. Thus, the actuator cannot shorten anymore without causing stress in the other truss elements. Consequently, it does not reach the targeted length change as specified. This can also be explained using the different stiffness components. As the elongation parameter is specified, the actuation strain is similar as in the actuator element of the statically determinate structure. However, due to the resistance of the other bars, the elastic strain takes a non-zero value. This results in a different total strain than in the previous example. The deformed structure is illustrated in Figure 5.6b.

When a second actuator element replaces one regular truss element, a constraint-free actuator length change as well as a kinematic motion is again generally possible. The resulting deformation is displayed in Figure 5.6c. It appears that the truss elements still perform a kinematic motion. However, the length changes of both actuators do not match this specific motion, creating constraints in the actuators and leading to different length changes than prescribed. Therefore, the kinematic motion is not possible with the given actuator combination and the prescribed elongation parameters of both $\alpha = -0.5$ as displayed in Figure 5.6c. This short study shows that the combination of actuators, their elongation parameters and the static indeterminacy of the structure are crucial for the feasibility of a constraint-free kinematic motion.

These examples illustrate the expected structural behavior and deformation results in a qualitative manner. Accordingly, the actuator element formulation presented here is suitable for structural analyses with such actuators.

5.3.2 Motion design with actuator elements

The introduced actuator element formulation allows an easy implementation into the motion design method. For this purpose, the elongation parameters α_i for every actuator

element i are discretized over the motion path as it has been done with the displacement degrees of freedom. Thus, the elongation parameters α_i (as part of the solution vector) are directly solved for while optimizing the motion. Again, this is the same process as for the displacement degrees of freedom. Therefore, the elongation parameters vary according to the optimized motion and their evolution throughout the deformation process represents an output of the motion design method. This is again illustrated with the same example as given in Figure 5.1, the same prescribed vertical displacement value of the second node D_2 and a path discretization with twenty linear path elements. With the presented actuator element formulation, the basic motion design method already includes the actuator load case, i.e., without applying any constraints. However, to ensure that only the actuator is used to realize the optimized motion without any discrete point loads, these point loads are enforced to be zero at every degree of freedom (see Section 5.2).

First, the statically determinate structure with one actuator element is investigated and shown in Figure 5.7a. Here, a purely kinematic motion of the rest of the structure is obtained, which can be identified by the functional value being zero. This motion minimizes the functional, which is defined as the integral of the elastic energy of the regular truss elements. The main output of motion design is the evolution of the elongation parameter throughout the deformation process. Thus, the actuator length change, i.e., the elongation parameter, adapts to the optimized motion as can be seen in the plot of the elongation parameter over the displacement D_2 in Figure 5.7a (bottom). This
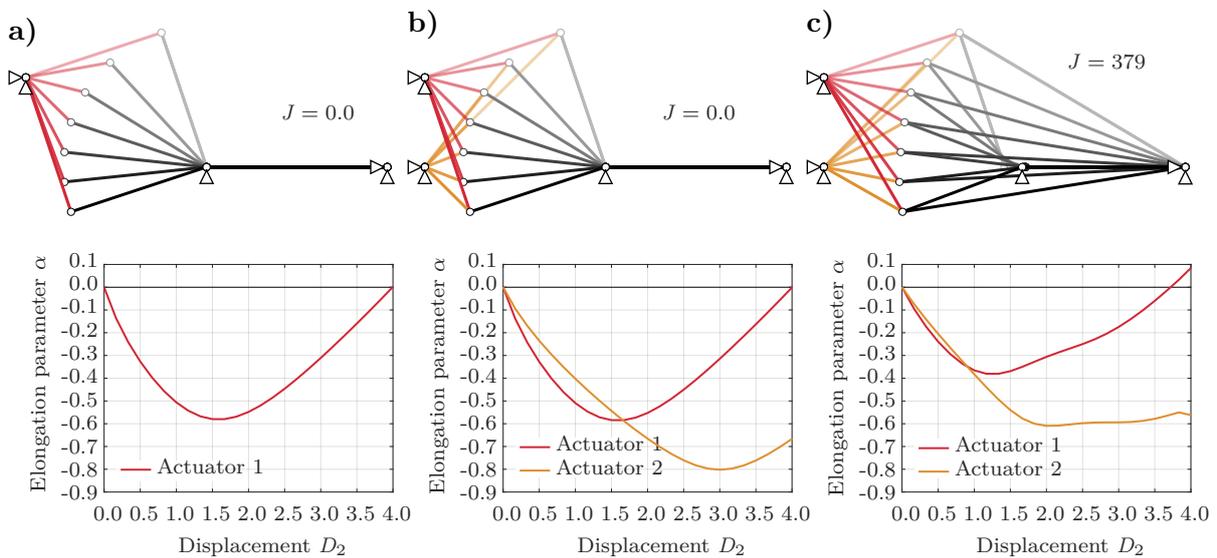
Figure 5.7: Motion design with actuator elements on a) a statically determinate structure, b) a statically indeteterminate structure (degree $n_s = 1$) with two actuator elements and c) a statically indeteterminate structure (degree $n_s = 2$) with two actuator elements.

can also be observed in the statically indeterminate structure (degree $n_s = 1$) with two actuator elements as illustrated in Figure 5.7b. In this case, a suitable combination of the elongation parameters of both actuator elements is found by the motion design method such that a purely kinematic motion is obtained. Again, this results in a functional value of $J = 0.0$. The beginning of the motion is different from the motion in Figure 5.6c. While the elongation parameters of both trusses (i. e., the two load cases) uniformly and synchronously increase in such a static nonlinear analysis, they can evolve independently in the designed motion, thus, enabling the minimization of the motion design functional.

To also perform a motion design for a motion incorporating elastic energy, and therefore with an expected functional value greater than zero, another structure with a second additional truss element is studied (cf. Figure 5.7c). This modification raises the degree of static indeterminacy to $n_s = 2$ and leads to a slightly different motion with different evolutions of both elongation parameters. However, the other bars cannot perform a pure rigid body motion anymore, but build up internal stress throughout the motion. This is the main difference compared to the two previous motion designs and leads to a functional value of $J = 379$.

5.3.3 Bridge structure with a traveling load

To show the potential of a combination of motion design with actuator elements, a more complex example is presented in the following. A bridge is modeled as a truss structure, as shown in Figure 5.8. Actuator elements are installed in the entire lower chord, thus resulting in a total of ten such elements. In this example, a parallel actuation mechanism is employed. This means that in addition to the actuator element, a regular, passive truss element is installed at the same place. As a result, this passive element is automatically stressed when the actuator changes its length. This leads to constraints
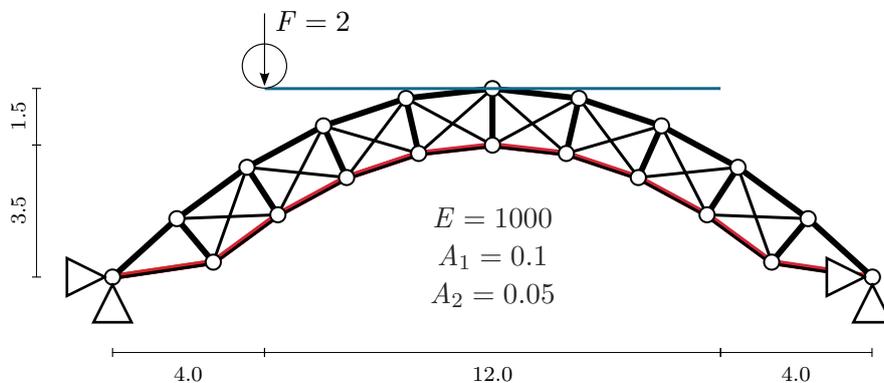
Figure 5.8: Problem setup for a bridge structure with traveling load.
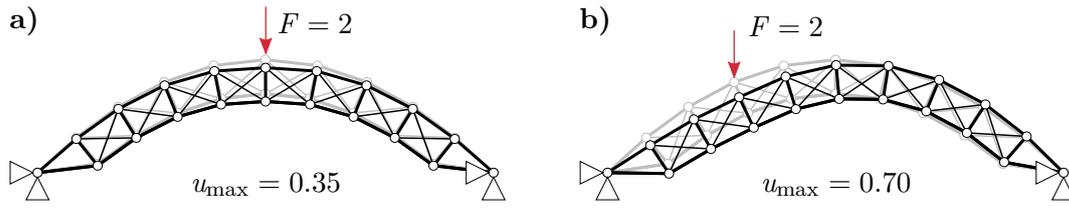
Figure 5.9: Bridge structure with traveling load. a) Deformation due to static central loading. b) Deformation due to static lateral loading.

during actuation, but represents an option to reflect the resistance of the actuator itself against a length change. The top chord and the vertical struts have a cross-sectional area of $A_1 = 0.1$, while the diagonals as well as the actuator elements and the passive truss elements in the lower chord are built of elements with half the cross-section, i. e., $A_2 = 0.05$.

The bridge is loaded by a load F, traveling from left to right. It is to be applied to the structure such that the loading point always remains at the same height throughout the entire motion, as indicated in Figure 5.8. In order to realize this task, the structure has to adapt and undergo large deformations. The required motion should be solely enabled by the actuators in the lower chord, while also bearing the traveling load. To obtain an estimation of the effect of the magnitude of the applied load, the passive structure without actuation is first loaded centrally and then laterally with a static point load. The deformed configurations can be seen in Figure 5.9a und Figure 5.9b, respectively. In both cases, significant nodal displacements of $u_{\max} = 0.35$ and $u_{\max} = 0.70$ are observed due to the static load.

To find a suitable motion for the traveling load and to make the deformation process as efficient as possible, motion design is carried out in two stages, see Figure 5.10. The initial configuration of the bridge is the symmetric, unloaded state. The two motion stages are not solved separately but by one single motion design procedure. However, they differ in the controlled and prescribed displacement values described in the following. Stage 1 of the motion represents the "picking up" of the point load on the left side. Therefore, the structure needs to deform sideways until the fourth node of the top chord (marked in blue) arrives at the starting point of the traveling load. For motion design, the vertical and horizontal end position of this node are prescribed, and its horizontal displacement value is controlled throughout the motion of the first stage (Configuration 0 to Configuration 5, cf. Figure 5.10a). In Stage 2, the load travels from the left side to the midnode of the top chord. To guarantee that it always remains at the same vertical position, the vertical displacements of the nodes of the top chord are prescribed in a sequential way throughout the configuration: First, the vertical displacement of the fourth node are prescribed, second, the vertical displacements of the fourth and fifth node is prescribed, third, the vertical displacement of the fifth node is prescribed and so

forth (cf. Figure 5.10b, marked in blue). In the motion design problems described up to now, at least one end displacement value is prescribed for the motion and one degree of freedom is controlled throughout the entire motion. This is not the case in Stage 2, but the nodes with specified vertical displacement values change in every configuration. However, these specifications still stabilize the motion and, therefore, the motion design procedure. Furthermore, the traveling load is applied to every node reaching this spe-
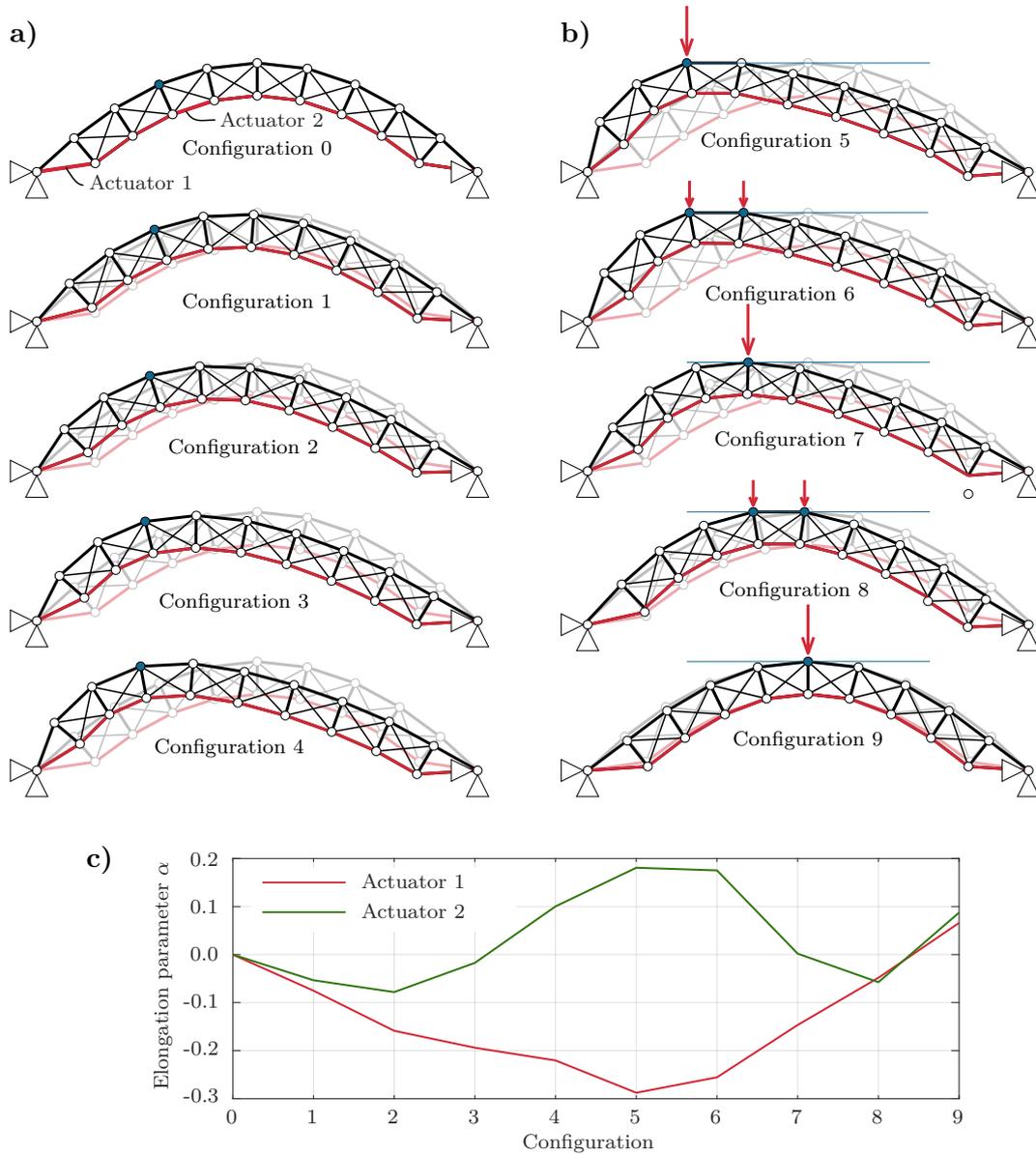
Figure 5.10: Optimized motion of the bridge structure with traveling load. a) Stage 1: Optimized motion for preparation. b) Stage 2: Optimized motion during load travel. c) Exemplary evolution of the actuator length change during the motion.

cific vertical position. If two nodes are placed at the same height, the load is split and distributed onto both nodes. The application of these point loads is also included as a constraint on the motion as described in Section 5.2.

An alternative approach to design a motion is to find the geometry for every single configuration separately with the specific constraints, i.e., displacement values and loading, by an optimization minimizing the internal energy. These optimized configurations can then be connected, thus generating an entire motion. These connected optimized geometries are then used as predictor for motion design. Figure 5.10a and Figure 5.10b show the optimized motion that results from the solution of the motion design problem including Stage 1 and Stage 2. Because of the applied constraints on the admissible point loads, the deformation is solely realized by the actuators. Furthermore, potential displacements due to the loading are compensated such that the point load can be kept at exactly the same height during the entire travel. The deformation to the right side is obtained by symmetry. Using the motion design method, the functional value reduces from $J = 103.2$ in the predictor (connection of energy-minimal configurations) to $J = 68.0$, i.e., by 34 %. This is due to the fact that the entire motion is considered in the objective function and not only in separate configurations.

An output of the method are the targeted actuator length changes in the form of the elongation parameters required to realize the optimal motion. Their evolution is exemplarily illustrated in Figure 5.10c for the first (Actuator 1) and fourth actuator (Actuator 2) of the lower chord (marked in Configuration 0). It can be seen that the elongation parameters do not increase monotonously as it would be the case in a nonlinear static analysis, but can also decrease during the process and develop independently.

Therefore, the motion design method allows to design efficient motions that are realized solely by actuator elements. The same advantages of the method as already described in Chapter 4, such as finding the most efficient motion by taking into account the entire deformation process, are also valid for these kinds of structures including actuator elements.

5.4 Stabilization of a motion

In addition to the presented constraints regarding admissible load cases for the optimized motion, other constraints can be applied to motion design problems, too. One possibility is to enforce a stabilized motion, where no structural instabilities occur during the deformation. Instability phenomena, such as bifurcation or snap-through, are usually initiated by critical points such as bifurcation points or limit points, respectively, and followed by unstable equilibrium path segments. An indication for the presence of

a critical point is given by the determinant of the structural tangent stiffness matrix. In quasi-static problems, it is zero when a critical point is reached and becomes negative when this point is passed. If this happens, the deformed structure is in an unstable equilibrium state. It has to be noted that this represents the trivial case. Further considerations need to be made when the passing of multiple critical points is expectable.

5.4.1 Introducing the determinant of the tangent stiffness matrix as inequality constraint

The basic method for motion design again marks the starting point for constrained motion design, however, now with different constraint types. To prevent that the structure follows an unstable equilibrium path after traversing a critical point, a constraint has to be applied on the determinant of the tangent stiffness matrix $\mathbf{K}_\mathrm{T}$. However, there is a significant difference compared to the constraints that were used in the previous section. Here, the determinant shall not take a specific value, but it is required to remain positive to stabilize the deformed configurations. By applying this, the following of unstable deformation paths during the motion is avoided. Therefore, the constraints can be formulated and summarized in a vector for all load configurations k, i. e.,

$$\mathbf{g} = \begin{bmatrix} \det \mathbf{K}^2 & \det \mathbf{K}^3 & \dots & \det \mathbf{K}^k & \dots & \det \mathbf{K}^{\bar{n}_\mathrm{nd}} \end{bmatrix}^\mathrm{T}, \tag{5.45}$$

where each entry i of the vector $\mathbf{g}$, i. e., each constraint g_i, needs to fulfill the inequality condition

$$g_i = \det \mathbf{K}_i \geq 0 \,. \tag{5.46}$$

Again, the initial configuration is excluded. Using a path discretization with B-splines, the constraints are again enforced at the Greville collocation points that are located on the deformation path, as has been discussed in Section 5.2.

The general approach for enforcing such inequality constraints with Lagrange multipliers was presented in Section 5.1.3. With the help of the Karush-Kuhn-Tucker conditions in eq. (5.12) and the complementarity function in eq. (5.13), the extended system of equations for motion design problems and this type of constraints can be formulated as

$$\begin{bmatrix} \mathbf{K}_\mathrm{md} + \lambda_i \mathbf{H}_i & \mathbf{G}_\mathrm{a}^\mathrm{T} & \mathbf{G}_\mathrm{i}^\mathrm{T} \\ \mathbf{G}_\mathrm{a} & \mathbf{0} & \mathbf{0} \\ \mathbf{0} & \mathbf{0} & \mathbf{I} \end{bmatrix} \begin{bmatrix} \Delta \mathbf{D} \\ \Delta \boldsymbol{\lambda}_\mathrm{a} \\ \Delta \boldsymbol{\lambda}_\mathrm{i} \end{bmatrix} = - \begin{bmatrix} \mathbf{R}_\mathrm{md} + \boldsymbol{\lambda}^\mathrm{T} \mathbf{G} \\ \mathbf{g}_\mathrm{a} \\ \boldsymbol{\lambda}_\mathrm{i} \end{bmatrix} \,. \tag{5.47}$$

Herein, a distinction is made between active and inactive constraints and hence, the active set strategy is taken into account. Also in this case, the derivatives of the constraints, i.e., the determinants of the tangent stiffness matrices in the corresponding deformation states, are required. Clearly, this is a non-trivial task and the derivative can typically not be calculated analytically for complex structures. Nevertheless, they can be derived numerically with the methods described in Section 5.1.4. In particular, the complex step approximation allows to compute the exact first derivative. In this way, the matrices $\mathbf{G}_{\mathrm{a}}$ and $\mathbf{G}_{\mathrm{i}}$ can be evaluated.

Nonetheless, the second derivatives cannot be calculated in this way without substantial numerical errors and a significant loss of numerical efficiency, which is attributable to the large number of required function evaluations. One way of circumventing these problems is to avoid the calculation of the second derivative by simply suspending it. This leads to a modified system of equations without the Hessian matrix $\mathbf{H}_i$, viz.

$$
\begin{bmatrix} \mathbf{K}_{\mathrm{md}} + \cancel{\lambda_i \mathbf{H}_i} & \mathbf{G}_{\mathrm{a}}^{\mathrm{T}} & \mathbf{G}_{\mathrm{i}}^{\mathrm{T}} \\ \mathbf{G}_{\mathrm{a}} & \mathbf{0} & \mathbf{0} \\ \mathbf{0} & \mathbf{0} & \mathbf{I} \end{bmatrix} \begin{bmatrix} \Delta\mathbf{D} \\ \Delta\boldsymbol{\lambda}_{\mathrm{a}} \\ \Delta\boldsymbol{\lambda}_{\mathrm{i}} \end{bmatrix} = - \begin{bmatrix} \mathbf{R}_{\mathrm{md}} + \boldsymbol{\lambda}^{\mathrm{T}}\mathbf{G} \\ \mathbf{g}_{\mathrm{a}} \\ \boldsymbol{\lambda}_{\mathrm{i}} \end{bmatrix} . \tag{5.48}
$$

Thus, the Newton-Raphson method is transformed into a modified Newton-Raphson solution scheme, in which the problem is not consistently linearized. This may affect the convergence behavior of the nonlinear problem. It is expected to have an inferior, no longer quadratic convergence behavior, as compared with the complete system of equations including the Hessian matrix. Nevertheless, the convergence behavior is expected to remain acceptable, since $\mathbf{K}_{\mathrm{md}}$ is still updated in each iteration. Due to the correct residual, the solution still converges to the correct minimal solution, but usually with an increased number of iterations. Alternatively, another possibility to set up the system of equations with consistent linearization is to calculate the second derivative exactly with hyper-dual numbers as proposed by FIKE AND ALONSO (2011).

To demonstrate the stabilization of motions, two simple two-bar structures incorporating snap-through phenomena as well as bifurcation points are presented in the following.

5.4.2 Numerical experiments with stabilized motions

Snap-through problem in a shallow two-bar truss

The method of stabilized motion design is first investigated on the example of an unsymmetric two-bar truss, as shown in Figure 5.11a. The asymmetry is chosen to avoid numerical instabilities in the calculation, attributable to multiple possible solution curves. Here, no constraints are enforced regarding the loads. Thus, two point loads can be

applied on the midnode in vertical as well as in horizontal direction. This corresponds to an unconstrained motion design, the result of which is shown in Figure 5.11b for a path discretization with ten elements and the vertical displacement of the midnode being controlled. The sign of $\det \mathbf{K}_\mathrm{T}$ is indicated in the background of the illustrated motion. When the structure is deformed in such a way that the midnode is located in the red zone, the determinant becomes negative. In the unconstrained motion design solution, the node traverses this "unstable" region. This is also visible in the plot of the determinant of the stiffness matrix over the displacement D_2 in Figure 5.11c. Between vertical
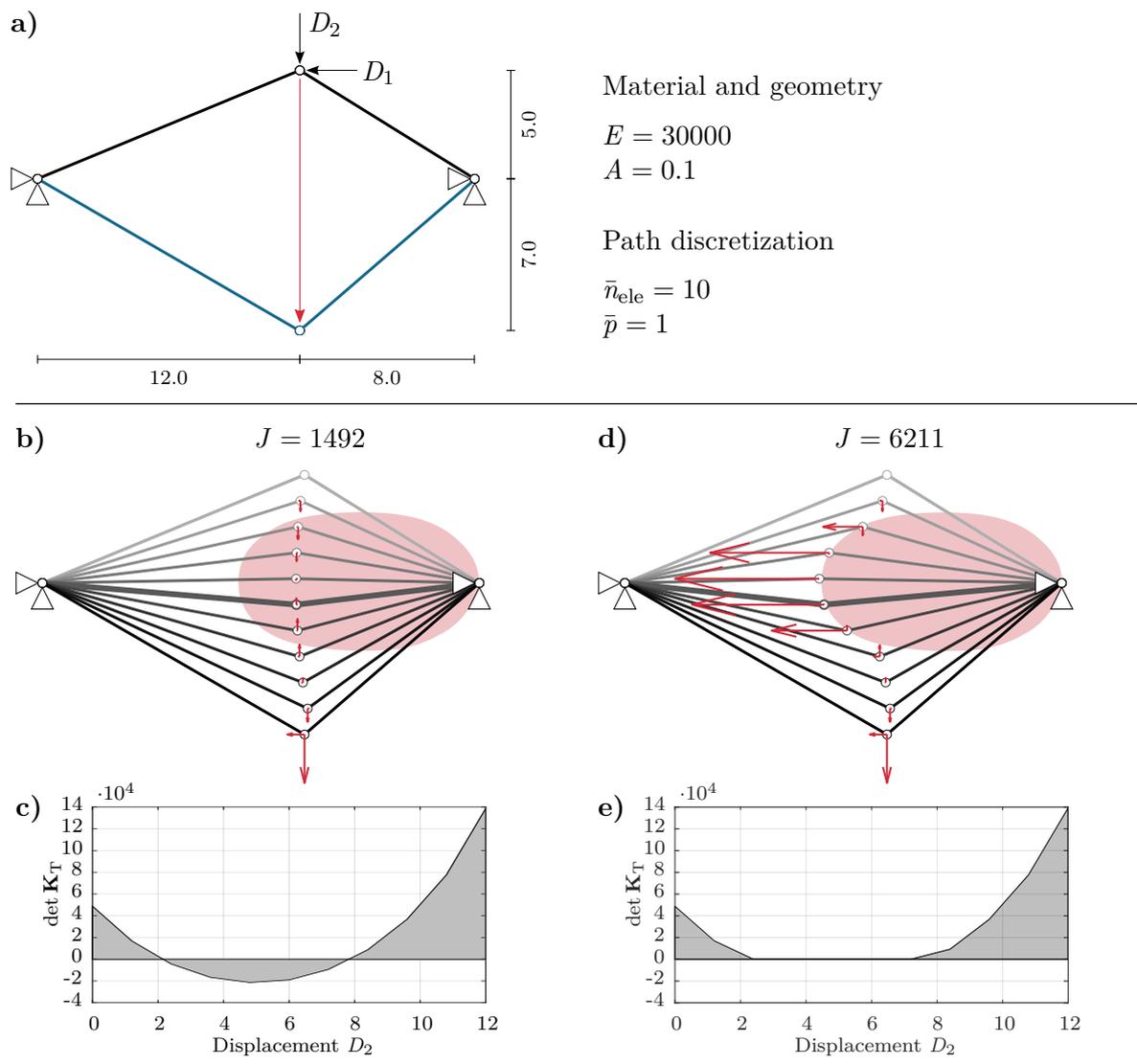
Figure 5.11: Unsymmetric stabilized two-bar truss. a) Problem setup. b) Unconstrained unstable optimized motion and c) plot of the stiffness matrix determinant. d) Stabilized motion and e) plot of the stiffness matrix determinant.

displacement values of $D_2 \approx 2$ and $D_2 \approx 8$, the determinant takes a negative value, which is equivalent to an unstable deformation state in a load-controlled process.

In the constrained motion design variant with a stabilized motion (see Figure 5.11d) on the other hand, the trajectory of the midnode only "touches" the zone where the determinant would become negative. It can also be seen that the magnitude of the forces, especially the horizontal point load at the midnode, changes in order to follow the alternative deformation path. The motion design functional itself, i.e., the minimum of the cost of deformation, stays the same, but its value increases drastically from $J = 1492$ to $J = 6211$ due to the necessary detour. However, a stabilization and a positive determinant are ensured throughout the entire motion (cf. Figure 5.11e). This is achieved by the initial stress stiffness and geometrical stiffness as introduced in Section 3.2. In a typical snap-through process, this part of the stiffness becomes negative and compensates the elastic and initial displacement stiffness contributions. This is further investigated in detail for the intermediate configuration highlighted in bold in Figure 5.11b/d. It represents an unstable deformation state in the unconstrained motion design variant, but a stable deformation state in the constrained motion design variant. The associated displacement values of the midpoint are for the unconstrained motion

$$D_{\text{instab}} = \begin{bmatrix} 0.38 \\ 6.00 \end{bmatrix} \tag{5.49}$$

and for the stabilized motion

$$D_{\text{stab}} = \begin{bmatrix} 2.88 \\ 6.00 \end{bmatrix} . \tag{5.50}$$

The tangent stiffness matrices evaluated at these deformation states then are

$$\mathbf{K}_{\text{T,instab}} = \begin{bmatrix} 380.82 & 14.05 \\ 14.05 & -49.40 \end{bmatrix} , \qquad \mathbf{K}_{\text{T,stab}} = \begin{bmatrix} 532.95 & 26.43 \\ 26.43 & 1.31 \end{bmatrix} . \tag{5.51}$$

Here, it can already be seen that an instability phenomenon is involved in the unconstrained tangent stiffness matrix: One of the main diagonal entries takes a negative value, whereas both are positive in the tangent stiffness matrix of the stable deformation state. This becomes even more obvious in the spectral decompositions

$$\mathbf{K}_{\text{T,instab,eig}} = \begin{bmatrix} 381.28 & 0.00 \\ 0.00 & -49.86 \end{bmatrix} \qquad \mathbf{K}_{\text{T,stab,eig}} = \begin{bmatrix} 534.26 & 0.00 \\ 0.00 & 10^{-8} \end{bmatrix} , \tag{5.52}$$

where the eigenvalues can be found in the diagonal entries. The matrices of the corresponding eigenvectors are

$$\boldsymbol{\phi}_{\text{T,instab,eig}} = \begin{bmatrix} 1.00 & -0.03 \\ 0.03 & 1.00 \end{bmatrix}, \qquad \boldsymbol{\phi}_{\text{T,stab,eig}} = \begin{bmatrix} 1.00 & -0.05 \\ 0.05 & 1.00 \end{bmatrix}. \qquad (5.53)$$

Since the determinant represents the product of the eigenvalues, its value and sign can be directly determined by this spectral representation. In the unstable deformation state, $\det \mathbf{K}_{\text{T}}$ becomes negative due to a negative eigenvalue, whereas it is practically zero in the stable state due to a zero eigenvalue, respectively. Therefore, it becomes obvious that the deformation state of the stabilized motion represents a limit state.

The tangent stiffness matrices in both representations consist of two different parts: the elastic stiffness combined with the initial displacement stiffness $\mathbf{K}_{\text{eu}}$ and the initial stress stiffness $\mathbf{K}_{\text{g}}$ as introduced in Section 3.2. These parts can also be transformed into the eigenvector basis of the total stiffness matrices, thus allowing for a better comparison of the different stiffness parts. The elastic and initial displacement stiffness for both cases can then be written as

$$\mathbf{K}_{\text{eu,instab,eig}} = (\boldsymbol{\phi}_{\text{T}}^{\text{T}} \mathbf{K}_{\text{eu}} \boldsymbol{\phi}_{\text{T}})_{\text{instab,eig}} = \begin{bmatrix} 435.61 & 0.00 \\ 0.00 & 4.48 \end{bmatrix}, \qquad (5.54)$$

$$\mathbf{K}_{\text{eu,stab,eig}} = (\boldsymbol{\phi}_{\text{T}}^{\text{T}} \mathbf{K}_{\text{eu}} \boldsymbol{\phi}_{\text{T}})_{\text{stab,eig}} = \begin{bmatrix} 537.88 & 0.00 \\ 0.00 & 3.63 \end{bmatrix}, \qquad (5.55)$$

and do not differ significantly in their magnitude. However, it can be noted that the second main diagonal entry is much lower than the first main diagonal entry. Compared to that, the initial stress stiffness matrices are

$$\mathbf{K}_{\text{g,instab,eig}} = (\boldsymbol{\phi}_{\text{T}}^{\text{T}} \mathbf{K}_{\text{g}} \boldsymbol{\phi}_{\text{T}})_{\text{instab,eig}} = \begin{bmatrix} -54.34 & 0.00 \\ 0.00 & -54.34 \end{bmatrix}, \qquad (5.56)$$

$$\mathbf{K}_{\text{g,stab,eig}} = (\boldsymbol{\phi}_{\text{T}}^{\text{T}} \mathbf{K}_{\text{g}} \boldsymbol{\phi}_{\text{T}})_{\text{stab,eig}} = \begin{bmatrix} -3.63 & 0.00 \\ 0.00 & -3.63 \end{bmatrix}. \qquad (5.57)$$

Especially in these matrices, the difference between the two displacement states can be identified: The absolute values of the initial stress stiffness in the stabilized state are significantly smaller. The sum of the two stiffness parts results in the total tangent stiffness matrix in a decomposed form in eq. (5.52):

$$\mathbf{K}_{\text{T,instab,eig}} = \mathbf{K}_{\text{eu,instab,eig}} + \mathbf{K}_{\text{g,instab,eig}}, \qquad (5.58)$$

$$\mathbf{K}_{\text{T,stab,eig}} = \mathbf{K}_{\text{eu,stab,eig}} + \mathbf{K}_{\text{g,stab,eig}}. \qquad (5.59)$$

For the unstable state, the bottom right entry of $\mathbf{K}_{\mathrm{eu,instab,eig}}$ is completely compensated by the corresponding entry in $\mathbf{K}_{\mathrm{g,instab,eig}}$, such that it becomes negative in the total stiffness matrix $\mathbf{K}_{\mathrm{T,instab,eig}}$. This results in the negative determinant, which in turn indicates an unstable deformation state. On the other hand, this particular entry is also compensated by the initial stress stiffness in the stabilized motion, but only to such an extent that it becomes zero, thus representing a limit state of the deformation. The reason for this behavior lies in the sign and magnitude of the normal forces in both bars

$$N_{1,\mathrm{instab,eig}} = -292 \qquad\qquad N_{1,\mathrm{stab,eig}} = -753 \qquad\qquad (5.60)$$

$$N_{2,\mathrm{instab,eig}} = -301 \qquad\qquad N_{2,\mathrm{stab,eig}} = 512 \,. \qquad\qquad (5.61)$$

In the unstable state, only compression forces occur and have a destabilizing effect on the structure, which can be detected in the initial stress stiffness. However, in the stable state, this effect is compensated by the occurrence of both compressive as well as tensile forces. The initial stress stiffness, therefore, does not comprise the discussed large negative value.

To sum up, this example nicely illustrates that the new motion design approach can be extended with inequality constraints such that a stable motion path is guaranteed. This way, a snap-through process could be stabilized even in a load-control problem setting. Of course, it should be emphasized that the employed strain measure plays a decisive role in the analyzed values.

Stabilization of a two-bar truss with bifurcation

In order to also investigate the stabilization in bifurcation problems, a high two-bar truss is studied next (see Figure 5.12a). This problem was already described in Section 4.7.2, where different solutions and equilibrium paths were compared. The midnode shall again be moved downwards in order to arrive in a mirrored end configuration.

Figure 5.12b shows the solution from unconstrained motion design. Again, the red zone indicates the sign of the determinant of the tangent stiffness matrix $\det \mathbf{K}_{\mathrm{T}}$. If the midnode is located in this zone, the determinant becomes negative and the deformed structure is characterized by an unstable equilibrium state with the corresponding external forces. However, another white zone ($\det \mathbf{K}_{\mathrm{T}} \geq 0$) is located within the unstable region. This is a result of the limit point that is only reached after the bifurcation point has been passed. The two resulting negative eigenvalues of the tangent stiffness matrix, again indicating an unstable deformation state, compensate each other. Therefore, the determinant becomes positive again, although no stable state has been reached. In the

a)

3.0

3.0

1.0   1.0

Material and geometry

$E = 10000$, $A = 0.1$

Path discretization

$\bar{n}_{\mathrm{ele}} = 20$, $\bar{p} = 1$

b) $J = 779$

d) $J = 907$

c)

e)
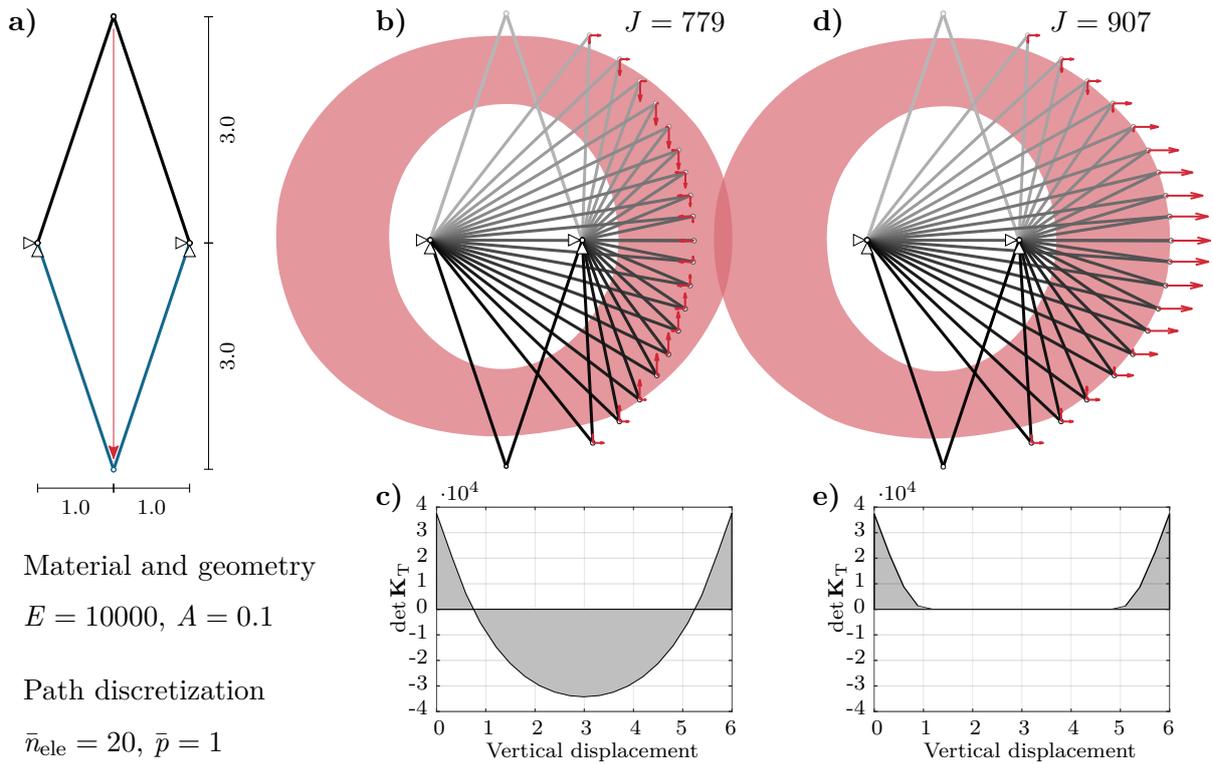
Figure 5.12: High two-bar truss with a bifurcation point and an unstabilized and stabilized motion. a) Problem setup. b) Unconstrained optimized motion and c) plot of the stiffness matrix determinant. d) Stabilized motion and e) plot of the stiffness matrix determinant.

unconstrained motion design solution, the unstable region is traversed by the deformation path, also depicted by the progress of the stiffness determinant in the corresponding diagram in Figure 5.12c.

Applying the inequality constraint $\det \mathbf{K}_{\mathrm{T}} \geq 0$ results in the motion that can be seen in Figure 5.12d, where the red zone is again only "touched" by the midnode, but not traversed. The constraint of enforcing a positive stiffness determinant (cf. Figure 5.12e) can, therefore, also be successfully applied to problems where bifurcation phenomena can occur.

Stabilization of a motion with specific load cases

Up to now, the two constraint types of enabling an optimized motion only by prescribed load cases (equality constraints) and of stabilizing the motion by enforcing a positive stiffness determinant (inequality constraints) were treated separately. However, they can also be combined. The vector **g** that gathers all constraints then contains entries with

the internal forces $\mathbf{g}_F$ as well as entries with the determinant of the stiffness matrix $\mathbf{g}_{\text{det}}$, and therefore results in

$$\mathbf{g} = \begin{bmatrix} \mathbf{g}_F \\ \mathbf{g}_{\text{det}} \end{bmatrix}. \tag{5.62}$$

As a consequence, the resulting system of equations is further expanded. This is shown in the following using the system from Figure 5.1a that has already been presented as an illustrating example for constrained motion design problems. It is already known at this
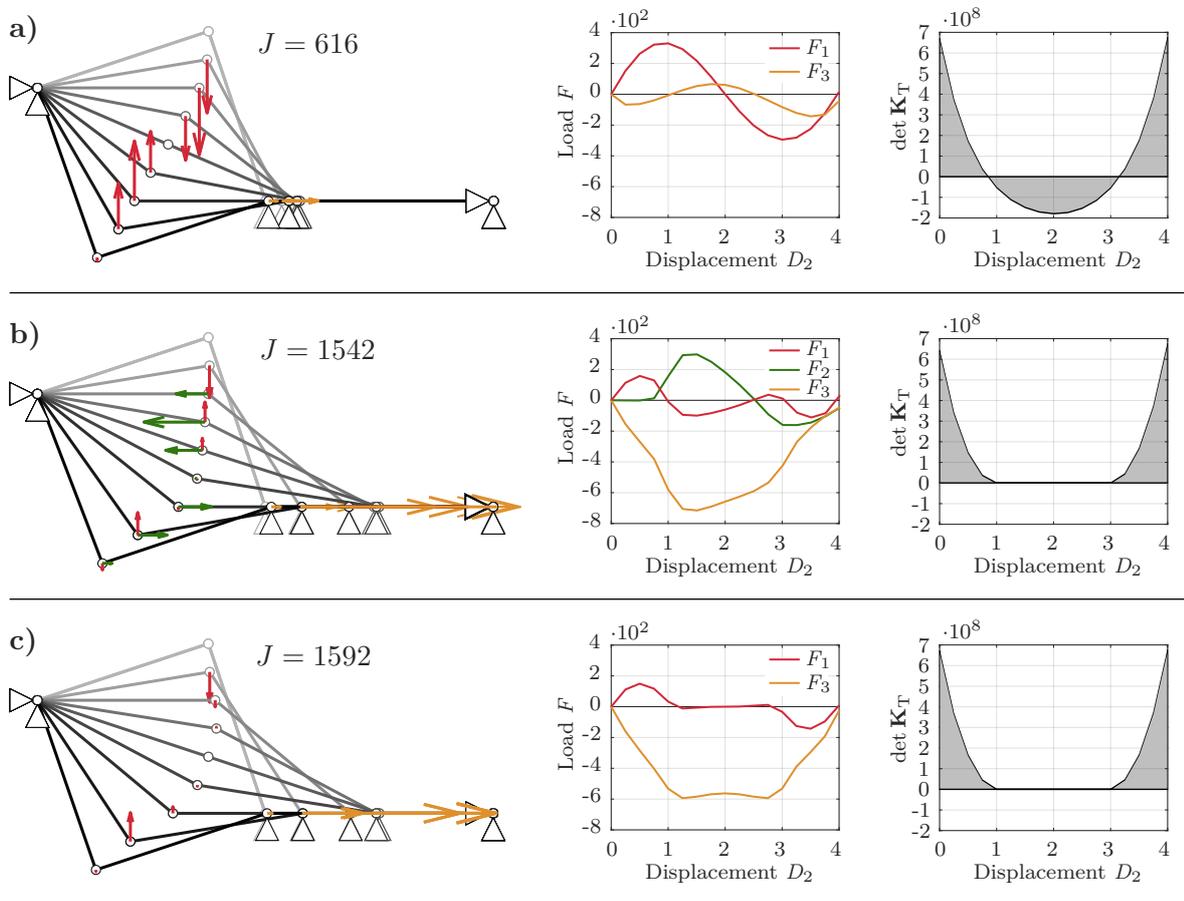
Figure 5.13: Constrained motion design on an exemplary system with different types of constraints as well as their combination. a) Optimized motion from a motion design with prescribed loads with load-displacement curves and plot of the stiffness determinant. b) Stabilized motion with load-displacement curves and plot of the stiffness determinant. c) Stabilized motion with prescribed loads with load-displacement curves and plot of the stiffness determinant.

point that unconstrained motion design yields the functional value $J = 600$, as shown in Figure 5.2a, which represents the reference value for the following modifications.

First, one load, the horizontal force at the free midnode, is suspended and a constrained motion design is carried out. This leads to the motion in Figure 5.13a. Due to the constraint, the value of the functional increases to $J = 616$. Secondly, all possible forces may again be applied, but a positive determinant of the stiffness matrix is enforced to find a stabilized motion. Again, a different motion is found (see Figure 5.13b) and the functional value increases significantly to $J = 1582$. In this structure, the horizontal bar is activated much more in the form of a high compressive force to reduce the snap-through effect of the two other bars. This result incorporates the same considerations about the initial stress stiffness as in the previous example of a shallow two-bar truss. Finally, both constraints can be combined. The result is a stable motion that always retains a positive determinant of the stiffness matrix, but is also realizable with only two point forces, as illustrated in Figure 5.13c.

5.5 Interim conclusion on constrained motion design

Based on the basic motion design method presented in Chapter 4, it has been shown in this chapter that constraints can be applied to the optimized motion with conventional constraint enforcement methods, e.g., with Lagrange multipliers or the penalty method for equality constraints as well as inequality constraints. The required derivatives are obtained either analytically or with different types of numerical differentiation. The latter enables certain freedom in the choice of the desired constraints. Previously, point loads were potentially necessary at every degree of freedom for realizing the resulting deformation. Here, the basic method could be extended by constraints such that only certain load cases enable the optimized motion. This makes it more applicable to real actuation situations. Such situations also include the actuation by actuator elements. For this reason, an actuator element formulation has been derived based on the targeted length change as an additional parameter, which allows for an easy integration into the motion design procedure. Numerical experiments showed the general applicability and that the conditions on the applied loads can be met. The minimal cost of deformation increases due to these constraints, as is to be expected.

Additionally, inequality constraints can be used to stabilize the resulting motion. Enforcement of a positive determinant of the tangent stiffness matrix throughout the entire deformation yields a motion that always remains stable within a load-controlled process. In complex structures, the high values of the determinant within the resulting system of

equations may lead to its ill-conditioning and numerical instabilities during the solution procedure. However, the simple examples demonstrate the principle feasibility.

It was further shown that it is possible to combine these two classes of constraints. Moreover, also other types of constraints are conceivable, e. g., to guarantee the compliance with strength conditions or stability conditions of the structure throughout the entire deformation process.

6

Further Potentials of Motion Design

So far, the basic motion design method as well as the constrained motion design method have been presented. While the first enables the design of the most efficient motion between two prescribed geometric states of a structure, the latter allows to realize the resulting optimized motion with specific load cases only. These two variants of the motion design approach can be treated as a basis for further extensions and modifications that follow the principal idea of this work of designing the most efficient movement.

In addition to the motion itself, the initial geometry plays a significant role and can be modified in this sense to reach the prescribed end geometry more efficiently. Another idea worth investigating is to integrate the choice of the actuating loads into the optimization procedure. In doing so, the loads that enable the most efficient motion can be explicitly selected. Moreover, it should be pointed out once more that the method has so far been developed using a functional based on the internal energy. However, the internal energy in the functional can also be modified or replaced by other quantities, thus, opening up the method for further possibilities and applications in terms of the objective to be minimized. These points are addressed in this chapter and potential extensions are described.

6.1 Combination of motion design with a shape optimization of the initial geometry

6.1.1 Motivation

In the present work, the focus is on designing a motion between two geometric states in such a way that it is as efficient as possible. For this purpose, the optimal individual deformation states, including parts of the final deformed configuration, are computed.

However, the shape of the initial configuration was never part of the motion design process so far, although it also significantly influences the efficiency of the motion and its cost of deformation. Therefore, not only the motion itself can be designed to be efficient, but also the initial geometry can be shaped accordingly in order to meet the requirement of motion efficiency and achieve further energy savings. This requires the initial geometry to be optimized for flexibility or, in kinematic structures, for motility. In doing so, the structure is made capable of carrying out large elastic deformations with the lowest possible deformation costs, which is a similar concept as in the design of compliant structures.

6.1.2 Objective functions for the design of compliant structures

The design and shape optimization of compliant structures represents an established field of research, where the choice of a suitable objective function is crucial. Some selected approaches are briefly explained in the following.

In Lan and Cheng (2008) and Masching and Bletzinger (2016), the displacement of a selected point reflects the compliance of the structure: the greater the displacement value of this point due to a given load case, the more flexible the structure. Accordingly, the goal of optimization is to maximize this specific displacement value. Moreover, also displacement differences to a desired deformation state subject to a load are used as objective function in Saggere and Kota (1999), Lu and Kota (2003) and Santer and Pellegrino (2009). In Hasse and Campanile (2009), the eigenvalues of the stiffness matrix with their associated eigenvectors are employed for a quantitative statement about the required energy. On the other hand, Frecker et al. (1997) and Saxena and Ananthasuresh (2000) pose additional demands on further properties of compliant structures. Besides flexibility, sufficient system stiffness is required such that the structure is able to bear loads. The latter is achieved by a minimization of the internal energy due to a given load.

However, the described objective functions are not suitable for the combination with motion design due to the different problem formulation. Instead of a load case, displacement values for the targeted deformed state are given, which means that the motion design problem formulation already meets the desired displacement values by definition. Moreover, there is no particular load case defined under which the displacement can be maximized, but instead, the evolution of the required loads for the deformation represents an output of the method. Furthermore, exploring detours to achieve optimal deformation costs is one of the essential benefits of motion design. In case specific directions of the deformation towards a particular displacement value are included in the

objective function, this strength may get lost, and different approaches than those of compliant structures need to be followed.

6.1.3 Minimization of the internal energy in the end configuration

Since displacement values instead of load cases are prescribed in motion design, minimal internal energy in the end configuration does not guarantee a high stiffness anymore. Here, it rather means that the structural elements exhibit low strains when having deformed to the desired configuration, which is also the goal of motion design. Therefore, the minimization of the internal energy in the end configuration is investigated as the quantity to be minimized for shape optimization of the initial geometry. Consequently, the initial configuration, for which the deformed target configuration exhibits the least internal energy, is searched for. The potential for possible energy savings is studied by employing several examples earlier presented in this thesis.

Kinematic structure

First, the structure from Figure 4.14, where the vertical displacement of the second node was specified such that it could be reached through a kinematic mechanism, is re-examined. It was used to verify the working principle of the motion design method. However, not every displacement state of this structure can be accessed by a rigid body mechanism. This occurs, for example, when the final position of the second node is prescribed differently than in the original problem. Figure 6.1a shows such a situation, where the given end configuration cannot be reached by a kinematic motion.

such that it cannot move along the arc shown in Figure 6.1a. Accordingly, motion design results in a motion with a non-zero functional value and point loads are required for its realization (cf. Figure 6.1b).
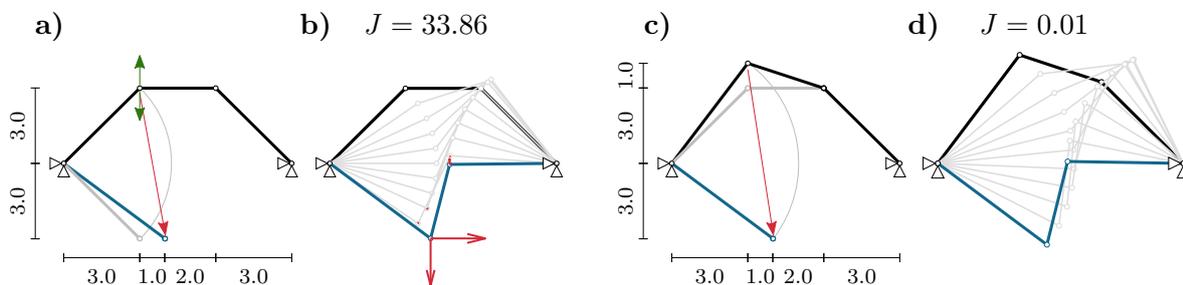
Figure 6.1: Shape optimization of a kinematic structure. a) Non-optimized initial geometry with problem setup and b) resulting non-kinematic motion. c) Optimized initial geometry and d) resulting kinematic motion.

Therefore, a shape optimization procedure is carried out, where the vertical coordinate of the second node remains variable. A built-in unconstrained optimization algorithm from Matlab (MATHWORKS, INC. 2018), based on a quasi-Newton procedure, is applied for this purpose. Depending on the problem formulation, constrained optimization algorithms may also be employed if the solution is not unique. In this case, the solution to the optimization problem results in the new initial geometry illustrated in Figure 6.1c. With this modified initial geometry, the target position of the second node is again located on an arc and it can, therefore, be reached by a kinematic mechanism (see Figure 6.1d). Certainly, the choice of the design variables plays a significant role. If, for example, the coordinates of the third node were chosen to remain variable, no rigid body motion could be achieved.

Application to inextensional deformations

Next, the objective function of minimizing the internal energy in the end configuration is applied to the design of inextensional deformations of shells, which were already investigated in Section 4.7.4. When using the membrane energy instead of the entire internal energy in the underlying functional, such deformations can also be considered as a kind of kinematic motion. Consequently, the objective function for the shape optimization of the initial geometry now changes to minimizing the membrane energy of the structure in the target configuration.

For studying the potential of such a shape optimization of the initial geometry with regard to inextensional deformations, the cantilever beam from Figure 4.21 is reconsidered. The initial geometry is a flat cantilever that is to be deformed into a half-circle. In the preceding example, the final configuration was only partly prescribed, and an inextensional deformation could be followed. Now, precisely the resulting deformed end
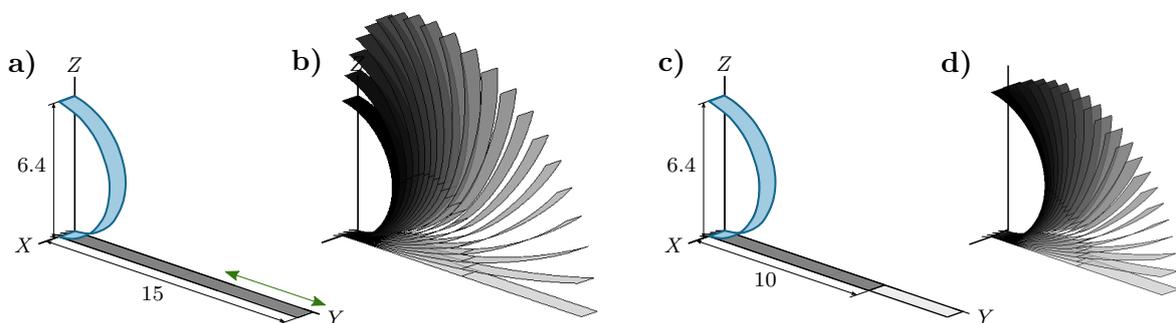
Figure 6.2: Shape optimization of a shell structure to deform by inextensional deformations. a) Geometry of long cantilever and b) resulting non-inextensional deformation. c) Cantilever with matching initial length for d) an inextensional deformation.

geometry from Figure 4.21c obtained by motion design is to be reached. It is, therefore, completely prescribed. For shape optimization, the cantilever length is set as a design variable. Accordingly, a length value of $L = 10$ as in Figure 4.21a represents the expected solution. However, to show the working principle of shape optimization, an increased cantilever length of $L = 15$ is used as starting value, which is shown in Figure 6.2a. Motion design with this geometry yields a motion that does not represent an inextensional deformation (cf. Figure 6.2b). In contrast, a shape optimization of the initial geometry with the objective to minimize the membrane energy leads to the given length of the original example, as is illustrated in Figure 6.2d. Therefore, the expected inextensional deformation can be obtained by motion design (illustrated in Figure 4.21c and again in Figure 6.2d).

This demonstrates that the chosen objective function is particularly useful for kinematic motions and inextensional deformations, especially when initially incompatible initial and target geometries are prescribed. By such an optimization step, the initial geometry can be adapted in such a way that kinematic mechanisms and inextensional deformations are potentially enabled and can, therefore, be computed by the motion design method.

Non-kinematic motion of a bridge structure

In the following, the minimization of the internal energy in the end configuration is further examined as objective function for the shape optimization of structures performing non-kinematic motions. For this purpose, a simple bridge truss structure is modeled as shown in Figure 6.3a. An initially flat bridge is to be deformed to a curved shape. The targeted vertical displacements of the upper chord are pre-defined, while the displacement of the bottom chord may be adapted. The end geometry is, therefore, not completely prescribed. A basic motion design of this problem with five linear path elements and the vertical displacement of the midnode of the upper chord is carried out first. It yields the deformation in Figure 6.3b with a functional value of $J = 6.84$.

For shape optimization, the horizontal coordinates of the bottom chord nodes are set as design parameters. This way, the angles of the diagonal truss elements are implicitly left variable. In order to guarantee a practicable truss structure as an outcome of shape optimization, the change in the horizontal coordinates compared to the starting geometry is limited to ± 0.5. Moreover, also symmetry of the structure is enforced. Applying the constrained optimization algorithm to minimize the internal energy in the end configuration yields the optimized initial geometry, and a subsequent motion design procedure leads to the optimized motion in Figure 6.3c. It can be observed that it exhibits a lower functional value of $J = 5.46$ than the motion in Figure 6.3b, which can be attributed to the optimized geometry. Thus, the cost of deformation can be

a)

Material and geometry	Path discretization
$E = 1000$	$\bar{n}_{\mathrm{ele}} = 5$
$A = 0.1$	$\bar{p} = 1$

b) $\quad J = 6.84$ **c)** $\quad J = 5.46$ **d)** $\quad J = 5.41$
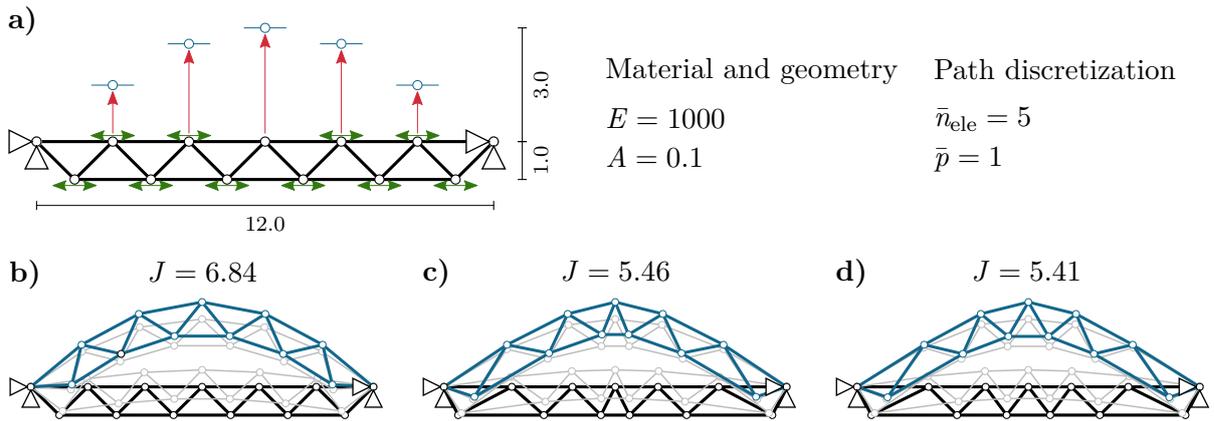
Figure 6.3: Shape optimization of a truss structure. a) Problem setup. b) Non-optimized initial geometry and resulting optimized motion. c) Optimized initial geometry by minimizing the internal energy at the target geometry and resulting deformation. d) Optimized initial geometry by minimizing the cost of deformation and resulting deformation.

improved, even though not the entire path is considered in the objective function of the shape optimization problem.

To evaluate the effect of the applied objective function, i.e., the minimization of the internal energy in the target geometry, on the cost of deformation, a reference solution is calculated. For this purpose, a further shape optimization is carried out, in which the cost of deformation is directly used as objective function. This involves an additional motion design step with the varying geometry each time the objective function is computed. By doing this, different nodal coordinates are obtained, thus leading to a different deformed configuration and a slightly reduced cost of deformation of $J = 5.41$, as shown in Figure 6.3d. It can, therefore, be concluded that by minimizing the internal energy in the target configuration, the cost of deformation is reduced, but not yet minimized in this example. However, the difference between the resulting costs of deformation is not crucial. The reason for this lies in the type of motion: The internal energy is monotonically increasing, and thus, the last energy level represents a decisive factor for the cost of deformation. Even though the differences between the motions of the three bridge geometries, especially of the two optimized geometries, are not substantial, this example shows the general applicability of such an additional shape optimization.

Influence of the objective function in a snap-through problem

A more significant difference between the two objective functions used to optimize the initial configuration for motion design can be detected in structures undergoing snap-through. For this purpose, a similar problem setup as in the illustrating example for

motion design from Figure 4.1 is given in Figure 6.4a. The midnode of the symmetric two-bar truss shall again be moved downwards and to the side. However, the targeted displacements are increased in this case to highlight the difference between the results. A motion design yields the optimized motion in Figure 6.4b (black) with $J = 775$. It shows the same motion pattern as the original illustrating example.

The design variable for the optimization of the initial geometry is the horizontal coordinate of the midnode. If both coordinates are left variable and the problem is not constrained, one outcome may be the trivial solution, where the optimized initial configuration corresponds to the target configuration. However, this is excluded by choosing the design variable as described above and prescribing the vertical component of the node. Solving the optimization task of minimizing the internal energy in the prescribed target configuration leads exactly to its mirrored geometry as starting geometry. This ensures that the element lengths are equal in both configurations. The internal energy is zero in the end configuration, which represents an optimum of the shape optimization problem. Nevertheless, it is also clear that a transition from the initial geometry to the final geometry cannot occur without introducing strain and stress to the structure.

A motion design with this initial geometry provides the expected snap-through behavior, shown in Figure 6.4b (red). But even though the initial geometry is optimized, the cost of deformation yields a larger value of $J = 798$ for the resulting motion compared to the first optimized motion.

Again, a reference value is computed by using the cost of deformation as objective function. Using this objective function for shape optimization of the initial geometry leads to a significant reduction of the functional value of the resulting optimized motion to $J = 708$ (cf. Figure 6.4b – green). This is the case even though the target configuration is not stress-free, as shown in Figure 6.4c.
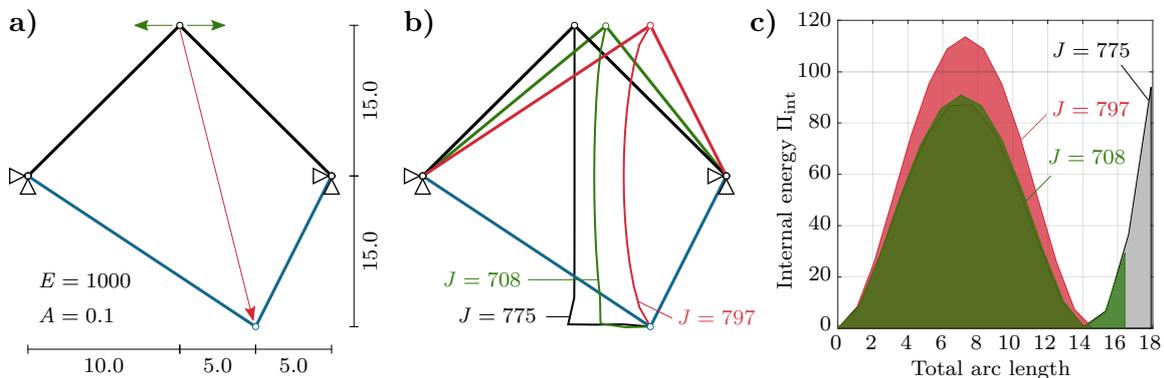
Figure 6.4: Shape optimization of the initial geometry in a snap-through problem. a) Problem setup. b) Different motion paths for varying initial geometries. c) Visualization of the functional value for the illustrated motions.

6.1.4 Conclusions

It has been shown that shape optimization of the initial geometry for motion design can lead to additional savings in the cost of deformation. Moreover, the motion design method has the potential to be applied to the design of compliant structures. However, the commonly used objective functions are not applicable here, as they often imply a certain direction of motion. This is precisely what is to be avoided in the motion design method in order not to restrict the solution space of possible optimized motions and to benefit from advantageous detours. However, the minimization of the internal energy in the target configuration of the deformation represents an adequate choice for the objective function for the intended purpose. It is particularly suited to design structures that can potentially perform kinematic mechanisms or inextensional deformations. Furthermore, this objective function may also be employed to design structures for non-kinematic motions. However, it is not as effective as using the cost of deformation directly as objective function, since in the latter, the entire deformation path is considered in the optimization.

Nevertheless, because an entire motion design must be carried out for each evaluation of the objective function, the last option turns out to be numerically inefficient. This reduction in efficiency can be limited by various measures for improving the predictor. The better the first guess, the fewer iterations are needed. Accordingly, the result of a preceding motion design with the original initial geometry can be used as a predictor for the subsequent motion designs. This reduces the number of required iterations to evaluate the objective function within the optimization iterations of motion design. Besides, it is possible to heuristically adjust and approximate the motion path of a slightly modified initial geometry based on an already calculated optimized motion. This way, the cost of deformation can be approximated without performing an additional motion design. These are strategies that can be applied to improve the predictor and, therefore, the convergence behavior and efficiency of the optimization using the cost of deformation as objective function.

Generally speaking, both studied objective functions, i.e., minimization of the internal energy in the target configuration and minimization of the cost of deformation, may be applied to optimize the initial geometry and improve the potential to reduce cost of deformation. Depending on the specific application, it needs to be evaluated, which objective function might best serve the desired purpose of the structure.

6.2 Choice of efficient actuation

6.2.1 Motivation

In the constrained motion design method presented in Chapter 5, the type and location of the loads and actuators were already given. However, this choice of actuation is decisive for the efficiency of the movement: The better the choice of the actuator locations, the less energy is needed for adaptation. In some applications, this choice is part of the design process and can still be flexibly adapted. In such cases, an additional optimization procedure can be employed to get the best possible placement of the applied point loads and actuators for the least increase of the functional value due to the constraints. The placement of the actuators already plays a major role in the efficiency of adaptive structures and represents an active field of research. The optimal actuator locations are usually calculated by using various optimization algorithms, where the correct choice of the objective function is a major challenge, as addressed in GUPTA ET AL. (2010). While ABDULLAH ET AL. (2001) used a genetic optimization algorithm for efficient structural vibration control, WAGNER ET AL. (2018) optimized towards an optimal ability to compensate perturbing factors using greedy and inverse greedy algorithms. Large deformations were already accounted for in MASCHING AND BLETZINGER (2016), where the actuation efficiency was optimized and included in the shape optimization of shells. In a similar approach, a multi-objective optimization was carried out to increase the response to loads for truss structures in REKSOWARDOJO ET AL. (2020). However, the listed references represent only an extraction of this field of research and are not intended to be exhaustive. In this section, an inverse greedy algorithm as well as a greedy algorithm are applied to find the optimal placement of possible point loads and actuator elements to realize the most efficient motion by the motion design method. The findings and examples are only schematically described in this section while being published in SACHSE ET AL. (2021b), together with more detailed explanations and more numerical examples.

6.2.2 Efficient load placement

Application of the inverse greedy algorithm

For the efficient placement of loads, it is assumed that only point loads are applied to the structure and that they can generally be placed at every degree of freedom. To choose the most efficient loads that are relevant for the specific deformation of the structure into its target configuration, an inverse greedy algorithm is applied in this work as introduced in KRUSKAL (1956) and also used in WAGNER ET AL. (2018). Using

this algorithm for motion design problems results in the following procedure: First, all possible point loads at every degree of freedom can be applied for the optimized motion. Thus, there are no constraints regarding the number of allowed point loads and an unconstrained motion design is carried out, thus, yielding a minimum of the functional value. Afterwards, multiple constrained motion design computations are executed, where the point load at each degree of freedom is suspended separately. The increase of the functional value attributable to the additional constraints is monitored for every load suspension. The load that causes the least deterioration in the objective value is then removed from the permitted load spectrum. This process is repeated until the desired number of loads is reached. The procedure is demonstrated in the following example of a statically indeterminate extended two-bar truss in Figure 6.5a. Here, two shallow arcs are connected by a very stiff element, modeled with a much larger cross-sectional area. For motion design, the upper midpoint is to be moved downwards, i. e., its vertical displacement is prescribed and controlled throughout the motion. There are four degrees of freedom in total: a horizontal and a vertical degree of freedom located at the upper as well as the lower midpoint. First, point loads can potentially be applied to all of them. However, in this example, only the two most relevant forces need to be chosen.
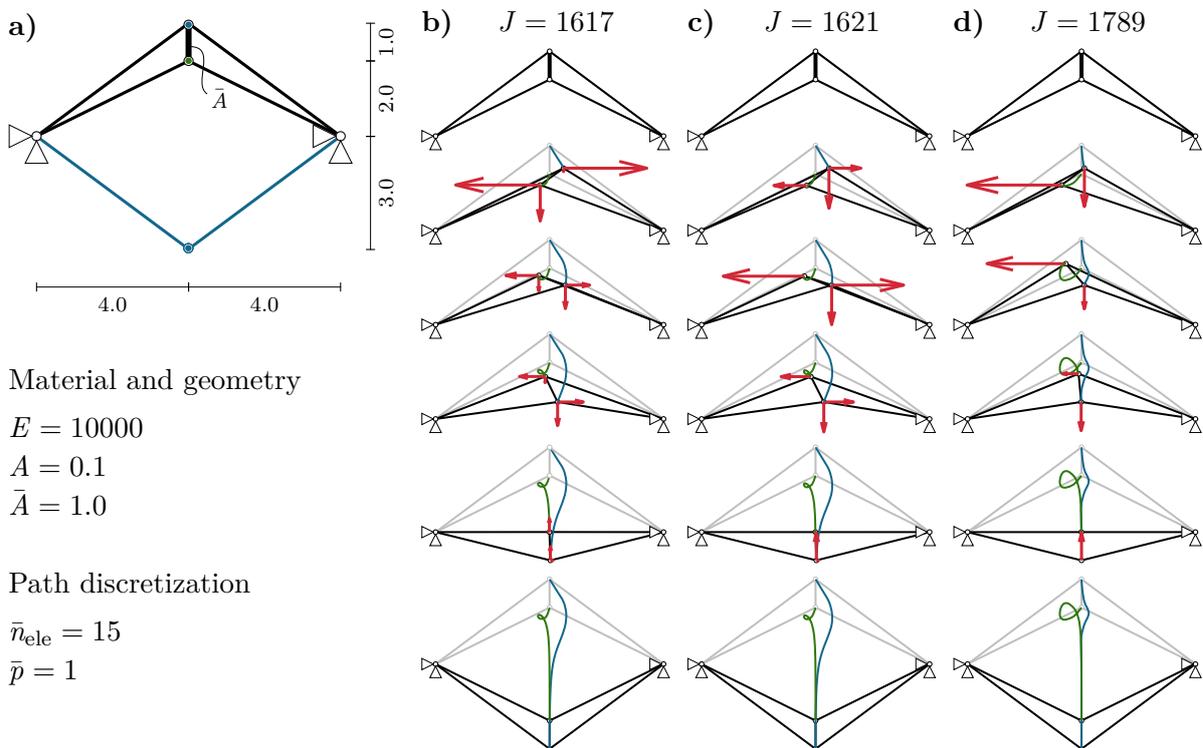
Figure 6.5: Load placement in an illustrating extended two-bar truss. a) Problem setup. Optimized motion with b) four point loads, c) three point loads and d) two point loads.

First, an unconstrained motion design is carried out and an optimized motion is found with a functional value of $J = 1617$. Here, the upper node first rotates around the lower node and then further moves downwards. Like this, the connecting bar encounters only minimum strains and a significant increase in internal energy due to its higher stiffness is avoided. This motion requires all four possible point loads to realize the calculated deformation, as illustrated in Figure 6.5b.

Afterwards, every load is removed separately and a constrained motion design is carried out for each load suspension. The load suspension that causes the least deterioration in the functional value is then saved. In the given example, the vertical force at the lower node has the least influence on the functional value. It increases by less than 1% from $J = 1617$ to $J = 1621$ when this load is removed. The resulting motion is illustrated in Figure 6.5c. It can be seen that the shape of the motion and the trajectory of both midpoints during deformation do not change significantly, even though only three forces instead of four are applied. This step is repeated, but now only the three remaining loads are suspended separately. Again, the force combination with the least increase in the functional value is chosen, as shown in Figure 6.5d. Now, a significant change can be observed in the trajectory of the two moving points and the functional value increases to $J = 1789$, i. e., by approximately 11% compared to the unconstrained motion design. However, the overall motion pattern stays the same.

The described inverse greedy algorithm represents a possibility to find the position of the most relevant point loads to perform an efficient motion or deformation between two prescribed geometries. In this way, it is possible to further improve the functional value compared to simply working with predefined loads in a constrained motion design.

Morphing cantilever as numerical experiment

A more complex example of a morphing cantilever is studied to show the potential of the load placement procedure. The structure is a hook-shaped cantilever that shall be deformed such that the endpoints arrive at the prescribed location, as illustrated in Figure 6.6a. The goal is to find an efficient motion in which the relevant nodes end up at the specified location and which can be performed by only four point loads – the ones perceived as being most effective for the assigned task. The method of motion design guarantees that the prescribed displacement values are met while the restriction to only a specific number of loads is achieved by constrained motion design. To choose the most efficient motion, the inverse greedy algorithm is applied. The defined goal can only be reached by combining these methods.

The cantilever, which is fixed at the bottom, is modeled with 16 displacement-based Q1-elements. This results in a total of 34 nodes, 64 unsupported degrees of freedom and,

therefore, 64 different point loads that may be applied. The motion path is discretized by 18 linear elements. Application of the described methods yields the location of the four most relevant point loads for an optimized motion, i. e., the loads that cause the least deterioration of the functional value, and their evolution throughout the deformation process. The result is illustrated in Figure 6.6b. Four point loads concentrated at two nodes are found to be most efficient for a minimization of the functional value and meet the requirement of the targeted end location of the cantilever tip. The resulting functional value, the integrated internal energy over the deformation path, is $J = 569$.

This solution is compared to the deformation resulting from a geometrically nonlinear analysis in Figure 6.6c, where the calculated points loads with their value from the end configuration are applied incrementally to the structure. It can be seen that even though the deformed end geometry remains the same due to the prescribed final load values, a completely different motion pattern is followed until this configuration is reached. This is attributable to the different evolution of the loads during the process. In standard
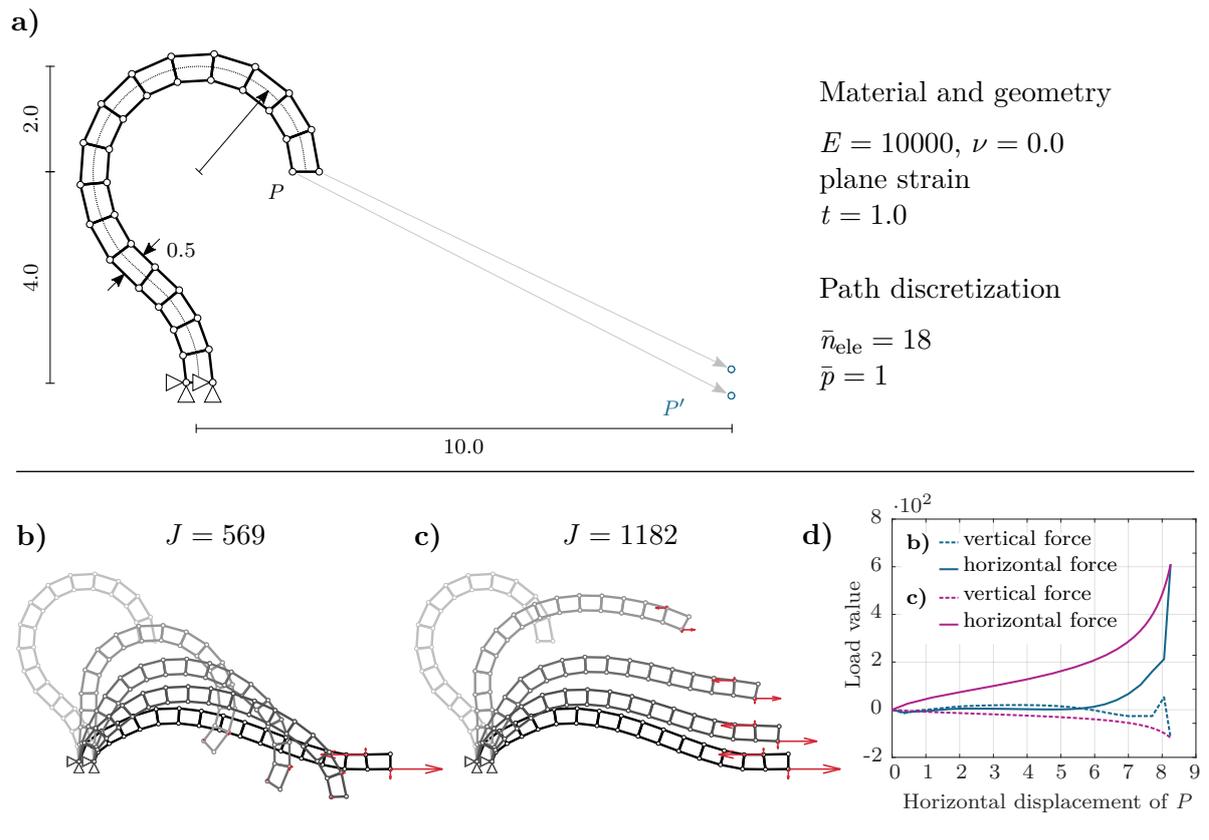
Figure 6.6: Motion design and load placement in a morphing cantilever. a) Problem setup. b) Solution of a constrained motion design with load placement. c) Deformation obtained by a nonlinear analysis. d) Load-displacement curves at point P.

nonlinear analysis, all loads are increased simultaneously and uniformly, whereas in motion design, all loads can be increased and also decreased independently from each other. This effect can also be observed in the load-displacement diagram in Figure 6.6d, where the horizontal and vertical force at point P are plotted over the horizontal displacement. As the same end geometry is reached, the load-displacement-curves join at the same point at the end of the deformation. The resulting deformation due to a uniform increase of loads obtained by structural analysis results in a functional value of $J = 1182$. This is significantly higher than the value obtained by motion design. Therefore, this independent evolution of the applied loads leads to the different motion patterns and to a lower cost of deformation, thus, demonstrating the potential of motion design again.

6.2.3 Efficient actuator placement

In the previous section, the optimal position of point loads to achieve given displacement values of the deformed geometry in an efficient way has been sought after. In reference to that, also the optimal location of actuators in a truss structure can be found. Here, a serial actuation framework is applied, which stands in contrast to the parallel actuation framework introduced in Section 5.3.3. While in the latter, a regular truss element is placed at the same location as the actuator element, this is not the case in serial actuation, but the actuator stands on its own. When the elastic energy over the deformation path is minimized, the energy due to the length changes of the actuators does not count towards the objective function. As a result, they can freely expand without any "penalization" in the optimization process. This complies with the case that no structural element is present at the position of the actuator. Thus, if a critical number of actuators is reached, a kind of rigid body motion, a kinematic mechanism, can be performed, which represents a minimum of the objective function with the value zero. Therefore, two issues are approached here: First, the minimum number and positions of the actuators are determined in order to achieve the specified displacement values by a kinematic mechanism. And secondly, the optimal placement of actuators for a minimum of the elastic energy to reach the end geometry through a non-kinematic mechanism is identified.

Minimum number of actuators for a kinematic mechanism

Whether such a described kinematic mechanism is possible strongly depends on the structure, or rather on its degree of static indeterminacy n_s, the number and location of the actuators as well as the number of prescribed displacement values in the end configuration. This is studied on truss structures with different degrees of static indeterminacy $n_\mathrm{s} = 1$, $n_\mathrm{s} = 3$ and $n_\mathrm{s} = 5$, as shown in Figure 6.7a.

The critical number of required actuators to exactly reach all prescribed displacement values with a kinematic mechanism is calculated using a brute force search combined with a greedy algorithm. The greedy algorithm represents the contrary of the inverse greedy algorithm, i. e., the number of actuators is stepwise increased and only those with the least increase in the objective function are saved. When combining both algorithms, the brute force search first identifies all actuator layouts that are able to exactly reach the prescribed end displacements. Based on these possible actuator layouts satisfying the problem definition of motion design, the number of actuators is stepwise increased within the greedy algorithm until a kinematic mechanism is found. There often exist several actuator combinations with the same number of actuators that enable a kinematic motion. Figure 6.7b and Figure 6.7c show kinematic mechanisms as a result of actuator placement for the three investigated trusses. Furthermore, two different scenarios with only one or three prescribed vertical displacement values are compared. The actuator layout for a specific number of actuators n_{act} for a kinematic mechanism is not unique. Therefore, only exemplary layouts are displayed in Figure 6.7. There also exist other actuator combinations that fulfill the defined requirement.

In all mechanisms, the elastic energy as well as the functional value are zero and an elastic-energy-free motion is possible. It can be observed in all exemplary mechanisms that the length of the standard truss elements is the same in the initial and the end geometry. Moreover, the number of actuators n_{act} to enable such a motion strongly depends on the topology of the structure. There is no obvious coherence between the
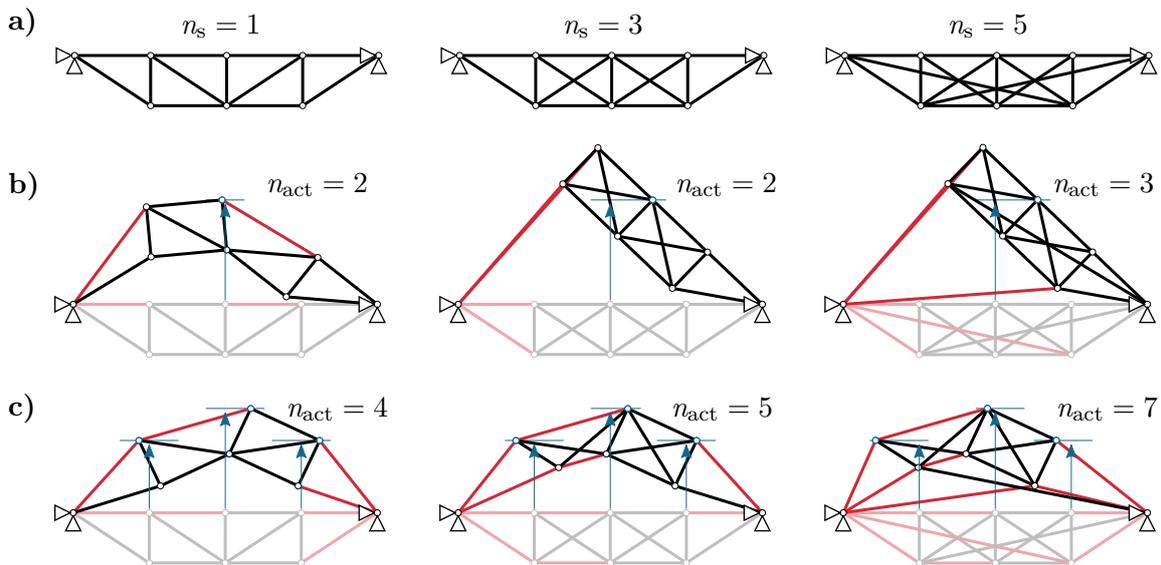
Figure 6.7: Actuator placement for kinematic mechanisms. a) Investigated structures with different degrees of static indeterminacy. Resulting actuator locations (red) for b) one and c) three prescribed end displacements.

degree of static indeterminacy and the required number of actuators. In contrast to this, however, it can be stated that the more displacement values are specified, the more actuators are needed to comply with the values.

Actuator placement for non-kinematic motions

If there are not enough actuators available to allow for a kinematic motion, it is an option to select those that still enable the most efficient motion regarding the underlying objective function, i.e., the integrated elastic energy. The inverse greedy algorithm used in the load placement algorithm is not suitable due to multiple independent kinematic motions when using too many actuator elements. Therefore, again, a combination of a brute force algorithm and a greedy algorithm is applied. The approach is illustrated in Figure 6.8 with the already introduced truss structure ($n_\mathrm{s} = 3$, three prescribed displacement values) and is explained in the following:

1. First, the number of actuators is successively increased and all combinations are explored until the specified end displacements are met.

2. If there are enough actuators such that the end displacement specifications can be fulfilled, the combination with the lowest objective function value and, thus, the most efficient motion is selected. This is shown in Figure 6.8a. The end displacement values are fulfilled exactly with three actuators. From all combinations of three actuators (only exemplary combinations are shown here), the most efficient with the lowest functional value of $J = 135$ is chosen.

3. In case more actuators are admissible, the actuator combination chosen in step 2 is used as a basis and the remaining elements are tested as actuators one after
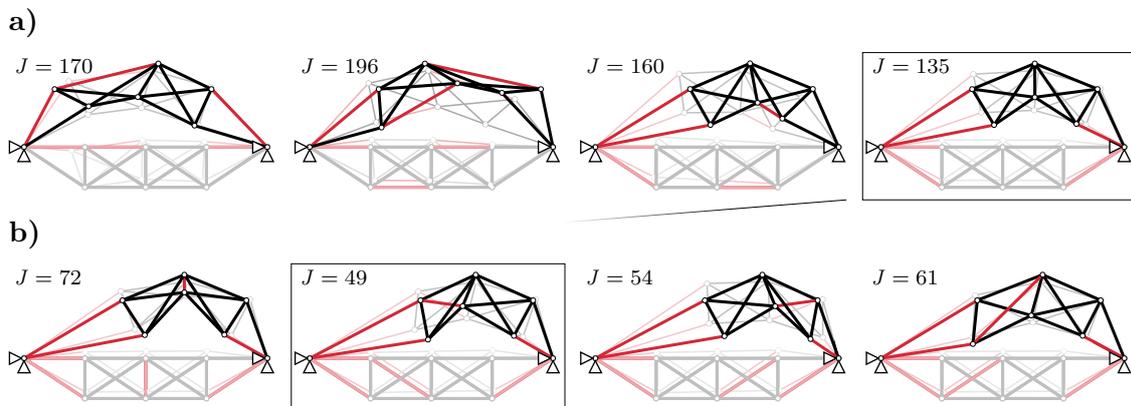
Figure 6.8: Actuator placement for a minimization of the integrated elastic energy with a) three actuators and b) four actuators.

the other. Again, the most efficient actuator combination is then identified (cf. Figure 6.8b). This step is repeated until the prescribed number of actuators is reached.

This procedure is used to determine the optimal actuator placement for the most efficient motion with respect to the required elastic energy.

6.2.4 Conclusions

In this short study, well-established algorithms for actuator placement have been used for the choice of an efficient actuation in motion design problems. For the choice of the most efficient point loads, an inverse greedy algorithm is applied, where a basic motion design procedure represents the starting point with all possible loads. By gradually removing the discrete forces and, thus, extending the number of constraints for the motion, the value of the objective function increases. Nevertheless, it has been shown on a simple illustrating example that the overall optimal motion pattern obtained by a basic motion design could be preserved.

As an alternative to using only point loads to realize a motion, also actuators can be used in truss structures. The placement of these actuators can be carried out in a similar manner. To this end, a combination of a brute force and a greedy algorithm has been used and demonstrated using a truss structure as an example. It was successfully shown that algorithms for the optimal selection of loads and actuators for the realization of an efficient motion can be combined with the method of motion design. This not only allows for designing the most efficient motion based on given loads, but also for the integration of the choice of these load cases or actuators into the design process in order to make the motion even more efficient.

6.3 Playground for variants of the underlying motion design functional

6.3.1 Motivation

The entire method of motion design was developed and presented with the exemplary functional of the internal energy being integrated over the motion:

$$J_\Pi = \int_s \Pi_{\text{int}} \, \mathrm{d}s \,, \tag{6.1}$$

which represents a measure for the introduced cost of deformation. This quantity contains relevant information about the energy state within the structure and, thus, already meets various possible requirements of adaptive structures. It can also be easily adapted to individual needs. For example, the membrane energy has already been isolated to calculate inextensional deformations of shells. In the same way, individual stress or strain components could be weighted differently for either a higher or lower penalization. For all these variants, analytical derivatives can be calculated with quantities readily available within in a regular nonlinear finite element code. However, Section 4.6 already shows that various other functionals can be applied, while still using the same method and solution principles. Generally speaking, it is assumed that a selected quantity, besides the internal energy, is integrated over the entire motion path in order to obtain a measure that contains information about the complete deformation process. The quantity only must be twice differentiable with respect to the degrees of freedom of the structure. These derivatives can either be calculated analytically or numerically, which allows a certain flexibility in the choice of the underlying quantity. This modification of the functional has already been investigated to some extent in Section 4.7.4, where the internal energy was replaced by the membrane energy for the calculation of inextensional deformations of shells. In the following, some more ideas and approaches based on potential modifications of the underlying functional are presented.

6.3.2 Minimization of the actuator energy

In Section 5.3 and Section 6.2 actuator elements were applied for the actuation of an adaptive structure. When designing such structures, further energy considerations are possible. The formulation of the total internal energy

$$\Pi_{\text{int}} = \underbrace{\int_\Omega \frac{1}{2} E_{\text{el}}^{\text{T}} \mathbf{C} E_{\text{el}} \, \mathrm{d}\Omega}_{\Pi_{\text{int,el}}} + \underbrace{\int_\Omega \left(E_{\text{el}}^{\text{T}} \mathbf{C} E_\alpha + \frac{1}{2} E_\alpha^{\text{T}} \mathbf{C} E_\alpha \right) \mathrm{d}\Omega}_{\Pi_{\text{int,act}}} \tag{6.2}$$

allows for separating the elastic energy

$$J_{\Pi_{\text{el}}} = \int_s \Pi_{\text{int,el}} \, \mathrm{d}s \,, \tag{6.3}$$

which was used as underlying functional for the designed motions with actuator elements so far. Alternatively, also the actuation energy can be extracted and chosen as the

functional to be minimized:

$$J_{\Pi_{\text{act}}} = \int_s \Pi_{\text{int,act}} \, \mathrm{d}s\,. \tag{6.4}$$

Both energies integrated over the deformation path may represent feasible measures for the cost of deformation. The actuation energy can be included into the motion design procedure without any numerical differentiation, as all required derivatives are already at hand.

For demonstrating the general applicability, the truss system from Section 6.2 with a degree of static determinacy of $n_{\text{s}} = 3$ and three prescribed end displacement values is used. In this example, an actuator placement for the most efficient actuator locations was already carried out based on the motion design functional with the elastic energy $J_{\Pi_{\text{el}}}$. This yields the actuator layout displayed in Figure 6.9a with the optimized value of $J_{\Pi_{\text{el}}} = 49$ for the integrated elastic energy and the relatively large non-optimized value of $J_{\Pi_{\text{act}}} = 9757$ for the integrated actuator energy. Consequently, in order to achieve the lowest possible elastic strains in the truss throughout the motion, considerable elongations of the actuators are necessary. Alternatively, an actuator placement procedure based on the integrated actuation energy can now be performed in the same way. Figure 6.9b shows the resulting – and significantly diffferent – optimized actuator layout with the corresponding values for the integrated energies. It can be observed that significantly lower actuator elongations are required, which also becomes apparent in the reduction of the integrated actuation energy to $J_{\text{act}} = 403$. On the contrary, the elastic energy increases as it no longer represents the quantity that is minimized.

In order to compare the two different functionals with the same actuator layout, a motion design based on the integrated elastic energy is carried out on this system. Even though

a)

Minimized elastic energy

min $J_{\Pi_{\text{el}}} = 49$

$J_{\Pi_{\text{act}}} = 9757$

b)

Minimized actuation energy

$J_{\Pi_{\text{el}}} = 136,\quad$ min $J_{\Pi_{\text{act}}} = 403$

Minimized elastic energy

min $J_{\Pi_{\text{el}}} = 115,\quad J_{\Pi_{\text{act}}} = 628$

c)
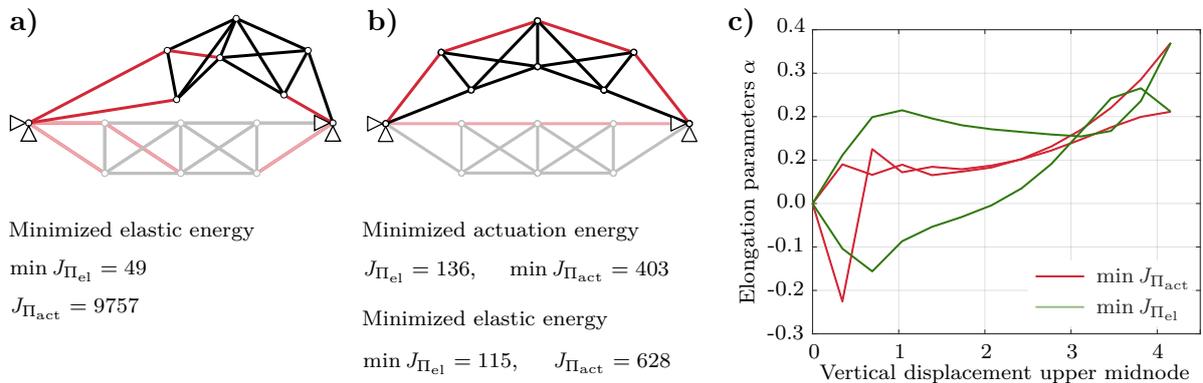
Figure 6.9: Truss structure with optimized actuator layout based a) on the elastic energy and b) on the actuator energy integrated over the motion path. c) Evolutions of elongation parameters throughout the motion for the system in b.

only three displacement values are given, the end configuration is identical. However, the motion path towards the end configuration differs. This can also be observed in the different evolution of the targeted actuator elongations throughout the motion in Figure 6.9c and is also reflected by the varying energy values.

Therefore, utilizing of the actuation energy in the underlying functional for motion design is generally possible. This results in different actuator layouts when used in an optimal actuator placement procedure.

6.3.3 Working with motion stages and energy levels

In some cases, motions consist of multiple motion stages. The fact that the motion design method can handle this has been shown with a three-dimensional cantilever example in Figure 4.20. Depending on the application, one of the stages may also include a rigid body motion of already pre-stressed structures due to previous motion stages, e.g., in deployed satellites that only need to change their orientation. However, if such structures undergo simple translatory or rotational movements, the internal energy and thus the cost of deformation accumulates within the method of motion design, which might not be desirable. Such deformations can generally be treated separately from the presented method, but if it is intended to integrate them into the motion design process, energy levels can be introduced.

The working principle is explained using a simple kinematic bar structure. Similar to the example in Figure 4.9, a bar is fixed on one node while the other node can move freely (see black bar in Figure 6.10a). The final position (blue) of this node is completely prescribed. Although the system itself is kinematic, this final position cannot be reached by a rigid body motion. The trajectory in Figure 6.10a (red) shows the result of a
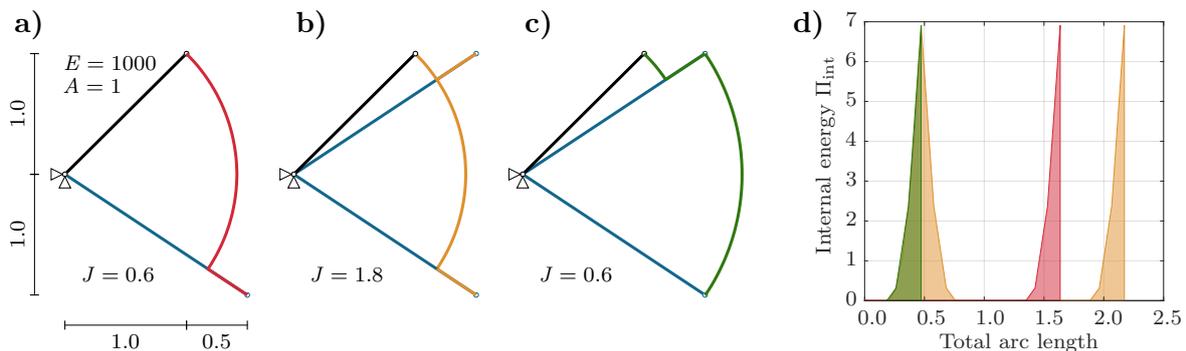
Figure 6.10: Working with energy levels. a) Usual motion design to final configuration. b) Usual motion design with intermediate configuration. c) Motion design with intermediate configuration and an additional zero-energy level. d) Diagram of the internal energy for all resulting motions.

standard motion design. First the free node is moved along an arc around the fixed node without introducing any internal energy into the bar. By applying external loads at a suitable point, the bar is then stretched to its final position.

In a next case, an intermediate state shall also be passed, as displayed in Figure 6.10b. Standard motion design yields the orange trajectory. In order to keep the integrated internal energy low, the node is again moved along the arc wherever possible, since the internal energy then corresponds to zero and is, therefore, not added to the cost of deformation.

In the last case (cf. Figure 6.10c), the intermediate state is again reached first. At this point, however, the concept of energy levels comes into play: the bar can "lock" its length such that it does not require any further effort to maintain the internal stress state. Accordingly, the energy level is then newly initialized for the subsequent motion stage. The continuation of the motion then corresponds again to a rigid body motion with the node of the extended bar moving along a different, larger arc (green). The differences between the three approaches are clearly visible in Figure 6.10d, where the internal energy is plotted over the total arc length.

Which technique is preferable strongly depends on the underlying problem. If the energy state can be locked, corresponding energy levels can be introduced into the procedure. However, if it requires substantial effort to maintain the stress state, it might still be advantageous to proceed with the regular motion design method.

6.3.4 Minimizing the displacement trajectory

Another objective when designing a motion might also be to find the shortest deformation path. The length of this path, however, is already implicitly included in the regular motion design functional through the integration over the entire motion. Because of this integration and an accompanying substitution, the total arc length s_{tot} is introduced in eq. (4.4) and represents the arc length of the displacement field. Thus, the objective of finding the shortest deformation path can be fulfilled with the trivial functional

$$J_{\text{u}} = \int_s \mathrm{d}s = \int_0^1 (\ldots) s_{\text{u}} \, \mathrm{d}\bar{s} \, . \tag{6.5}$$

As can be expected, if the lengths of the displacement trajectories are minimized, the solution corresponds to the linear interpolation between the initial and the target configuration, i.e., the direct connection. This is demonstrated on a simple cantilever truss structure in Figure 6.11a. It is to be deformed into a curved shape, which is first completely prescribed. In most numerical experiments, the linear interpolation has already
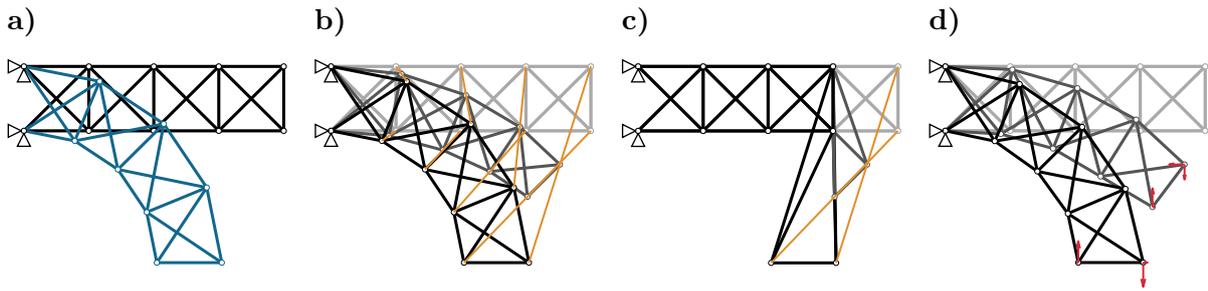
Figure 6.11: Exemplary truss structure and motions with minimized displacement trajectory. a) Problem setup. b) Optimized motion with a completely prescribed end configuration, c) with a partly prescribed end configuration and d) with a partly prescribed end configuration and constraints regarding applied loads.

been used as predictor. As this is also the case here, the solution and optimized motion in Figure 6.11b is directly found without any iterations. Figure 6.11c shows that the same applies when only a part of the end displacement values are prescribed, e. g., solely the end position of the cantilever tip nodes, even if the resulting motion seems to be unphysical. However, high forces must be applied for each node to be moved or kept in place. But there is again the possibility to impose additional constraints on the allowed loads as presented in Section 5.2. As a result, the shortest path to the end configuration that can be followed with the specified loads is searched for. To demonstrate this, it is assumed in a next step that loads can only be applied to the two nodes at the cantilever tip. Finally, iterations become necessary to obtain the solution, since the linear interpolation fulfills the condition of minimizing the deformation path, but not the given constraints. The converged solution for this problem is shown in Figure 6.11d.

6.3.5 Homogenizing the stress state throughout the motion

A further conceivable requirement for an adaptive structure might also be to homogenize the stress state or, similarly, the internal energy state. The envisaged homogenization restricts stress peaks or large energy changes during the motion. This can be achieved by only a slight modification of the original function, i. e., by squaring the internal energy value within the integration over the motion path:

$$J_{\Pi^2} = \int_s \Pi_{\text{int}}^2 \, \mathrm{d}s \,. \tag{6.6}$$

When using this function, locally high energy values are more emphasized and, therefore, reduced within the optimization. In general, also higher exponents would be possible, which would lead to an even more pronounced homogenization. However, at a certain
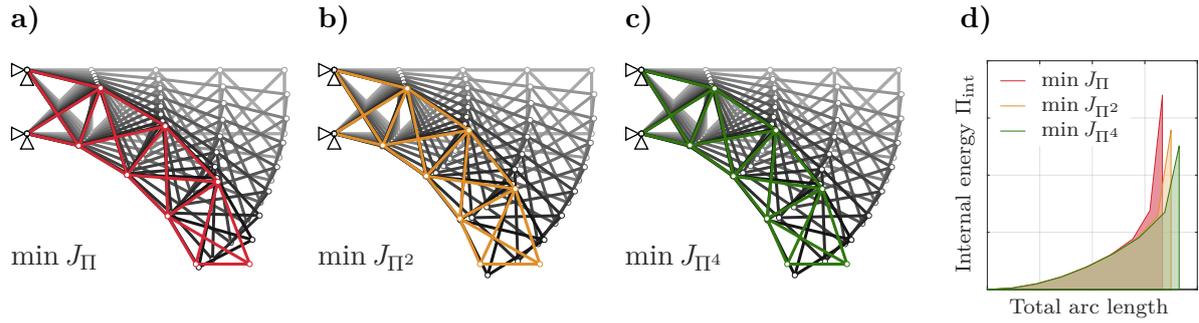
Figure 6.12: Optimized motions of the exemplary truss structure of a) a motion design based on the regular functional, b) with a square of the internal energy and c) with the exponent 4 of the internal energy within the integration over the motion path. d) Diagram of the internal energy for all motions.

point, the calculated values become very large and potentially lead to an ill-conditioned system of equations.

The working principle of this alternative functional is again shown on the truss cantilever problem from Figure 6.11a, where only the end positions of the tip nodes are prescribed. A regular motion design without exponentiation of the internal energy yields the optimized motion in Figure 6.12a. Applying the modified functional from eq. (6.6) results in the deformation shown in Figure 6.12b. Even if the exponent is increased to 4 (functional J_{Π^4}, leading to the motion in Figure 6.12c), there seems to be no significant difference to the other two motions. However, this becomes more obvious in Figure 6.12d, which shows the development of the internal energies for the three different cases. The larger the exponent in the integral, the larger the spanned area, i.e., the value for J_Π, but the maximum local energy value is reduced for the sake of homogenization. A homogenization over the motion can thus be achieved and large energy differences are avoided.

This approach of exponentiation also allows for another variant: Above, only the energy peaks within the motion were homogenized. However, if the exponentiation is drawn into the integral over the domain Ω, local stress or energy peaks throughout the spatial domain can also be compensated.

6.3.6 Incremental motion design approach for complex problems

The findings from the previous two subsections can be used to develop an incremental motion design process. Thereby, it is made use of the fact that a function with an exponent zero returns the value one and the same function with the exponent one yields the function itself. In terms of motion design, this means that if the quantity, namely the internal energy, within the integral over the motion path is taken to the power of zero, the functional for the minimization of the motion path length (see Section 6.3.4)

emerges. On the other hand, if the exponent is one, this results in the regular functional for motion design. Therefore, the internal energy is now exponentiated with a general factor j:

$$J_{\Pi^j} = \int_s \Pi_{\text{int}}^j \, \mathrm{d}s \qquad \text{with} \qquad j \in [0,1] \, . \qquad (6.7)$$

The procedure starts with a exponent of $j = 0$ and, thus, the trivial and already known optimization solution of a linear interpolation between the initial and end configuration is obtained. Starting from this, an incremental method can be developed by stepwise increasing the exponent j from zero to one, analogous to the pseudo-time in a nonlinear load-controlled analysis. Accordingly, the application of an exponent in between these values leads to an intermediate solution between the linear interpolation and the targeted solution of motion design. However, it is important to note that the individual solutions do not correspond to equilibrium points, which are successively connected to an equilibrium path, but to entirely optimized motions that are based on these varying objective functions. Through the incremental increase of j, the preceding optimized motion can be used as predictor for the following solution step. This gradually approximates the predictor to the sought-after motion and the solution procedure converges better or even converges at all.

This is again demonstrated on the truss structure from Figure 6.11a with prescribed vertical displacements of the cantilever tip. Figure 6.13 shows different solution steps with different exponents. The first predictor in Figure 6.13a is the linear interpolation between the initial state and the prescribed end values. When using an exponent of $j = 0.1$, the resulting motion already seems more physically meaningful, but it still maintains a rather linear appearance, as it can be seen in Figure 6.13b. With the exponent $j = 0.5$, the motion already resembles the final solution to a large extent, as illustrated in Figures 6.13c and d. Especially for the first, low exponents, considerable changes in the resulting motions have been observed, whereas for exponents above $j =$

a)   b)   c)   d)

$\min J_{\Pi^0}$ $\min J_{\Pi^{0.1}}$ $\min J_{\Pi^{0.5}}$ $\min J_{\Pi^1}$

Figure 6.13: Incremental motion design. a) Optimized motion for $j = 0.0$, b) for $j = 0.1$, c) for $j = 0.5$ and d) for $j = 1.0$

0.5, the final solution is already recognizable and fewer iterations per solution step are necessary.

The described approach of an incremental solution procedure also allows for the design of motions for more complex structures that might experience convergence problems in the regular motion design method. As an example, the motion of the carnivorous Venus flytrap, which has been investigated, for instance, in FORTERRE ET AL. (2005) and SACHSE ET AL. (2020), is taken up at this point. Plants that actively move mostly do so by changing the hydraulic pressure, the so-called turgor pressure, in certain motor cells. This causes a volume change of these cells, thus, leading to strains, stresses and a consequential overall shape change. In order to speed up the prey-catching, the Venus flytrap employs a snap-through mechanism to invert the curvature of its doubly curved trap geometry, as can be seen in Figure 6.14a and Figure 6.14b. In this study, a motion design is intended to be used for a hypothesis test. If the motion found in a purely numerical way corresponds to the motion observed in nature, it can be assumed that the internal energy, or any other utilized functional, also represents the driving force for the plant motion. Particularly when studying plants, the assumption of controlling all degrees of freedom is not a restriction and the basic motion design is suitable. This is due

a)

c)

e)

b)

Material and geometry

$E = 10$, $\nu = 0.0$, $t = 0.1$

Path discretization

$\bar{n}_{\mathrm{ele}} = 8$, $\bar{p} = 2$

d)

$\bar{t} = 0.00$ $\bar{t} = 0.25$ $\bar{t} = 0.50$ $\bar{t} = 0.75$ $\bar{t} = 1.00$

Figure 6.14: Hypothesis test for the snapping motion of the Venus flytrap. a) Open and b) closed state of real plant (©PBG Freiburg). c) Problem setup with open configuration, d) motion sequence and e) resulting closed configuration in the motion design procedure. An animation of the motion can be found in the digital version of this work.

to the fact that the motion can be realized by applying the strain state via targeted and directed turgor pressure. For motion design, one trap lobe is modeled with 5x5 Kirchhoff-Love shell elements with cubic NURBS shape functions. The geometry was taken from a 3D-scan of an exemplary real trap and then idealized, as illustrated in Figure 6.14c. The symmetry axis is fixed. Moreover, the material behavior is also an idealization and an isotropic, elastic constitutive model is applied. Eight solution steps are specified for the incremental procedure. In order to incorporate the observation regarding the solution step size, the exponent is not increased linearly, but it doubles with each step. Only the end position of the two marked nodes is prescribed and equal path element size is enforced for regularization, which results in the motion in Figure 6.14d and the end configuration in Figure 6.14e. This is already quite similar to the motion of the real plant. However, to obtain more profound insights, further measures should be taken to bring the model closer to the actual physiology and behavior of the plant. For example, a multilayer shell can be employed in a simple way and would be more in line with the real structure. Furthermore, the internal energy could be treated anisotropically. The cells in the plant have a tubular shape, which allows for an easier elongation in the longitudinal direction than in the radial direction. This could easily be considered in the functional by weighing the strain in this longitudinal direction. When using a weighting factor lower than one, the elongation would be penalized less and thus represent a more realistic actuation. This approach also allows for simulating anisotropic surface actuators.

6.3.7 Conclusions

In this section, modifications and variants of the underlying functional for motion design have shortly been presented and studied. Originally, a functional with the internal energy being integrated over the deformation path was used as proof of concept for the development of the method in Chapter 4. However, it was shown that, in general, also other variants besides the functional based on the internal energy are possible. This involves the integrated actuation energy or the utilization of energy levels within the motion. Furthermore, a minimization of the deformation trajectory length could easily be achieved by a trivial functional with the integrand being one. This also represented the starting point for a newly developed incremental motion design procedure, which allows for the design of motions for more complex structures and also enables to study motions of real structures. In this case, it was exemplarily applied for a hypothesis test of a biological structure, the Venus flytrap.

When numerical differentiation is used, almost arbitrary types of functionals can be used, which are based, for example, on other structural parameters, such as forces. In

general, also constraints as discussed in Chapter 5 can be combined with all functionals. Depending on the application, it has to be decided about the most relevant criteria for the motion and the functional has to be selected based on these.

7

Conclusions and Outlook

In certain structural engineering applications, adaptive structures need to perform large deformations. In order to enable the deformation process itself to contribute to the efficiency of the structure, the method of motion design has been proposed and developed in this work. It represents a new approach for the design of optimal motions between an initial and a target geometry of flexible and continuously deformable structures. The method is suitable for quasi-static loading processes and takes geometrically nonlinear deformation behavior into account. Furthermore, the individual geometric configurations are predetermined and exclusively the deformation process itself as well as its properties are regarded. For this purpose, a measure for the cost of deformation has been introduced, where a selected mechanical quantity is integrated over the deformation path. Because the latter is defined as the arc length of the displacement field, the new approach allows to consider the motion in its entirety. In this work, the internal energy was exemplarily employed to develop the basic motion design concept. Therefore, the cost of deformation is defined as the internal energy of the structure integrated over the deformation path, which then represents the measure that is to be minimized in the motion design problems presented in this thesis.

The problem formulation shows some apparent similarities to the brachistochrone problem. Hence, this historical task has been referred to in order to motivate the solution approach based on variational calculus. In doing so, the cost of deformation has been set as the underlying functional of motion design problems, and thus, its first variation could be derived. Applying a standard finite element discretization of the spatial domain led to a semi-discrete formulation, which was still continuous in the motion. However, the decisive aspect of this work is the discretization of this motion path, i. e., the deformation process. This means that the individual nodes of the finite element approximation of the path represent intermediate deformation states that are, in turn, interpolated by suitable shape functions over the entire motion. With this additional discretization, a nonlinear system of equations has been derived that could be solved using the

Newton-Raphson method and an accompanying consistent linearization. As a result, the problem is no longer solved incrementally, but all deformed states and, therefore, the whole deformation path are obtained in one go. This causes the primary adjusting variable that improves or deteriorates convergence in nonlinear analysis, the load step size, to disappear from the problem formulation. Nonetheless, the convergence behavior of motion design problems has been investigated and enhanced by various methods, such as using B-spline shape functions for the path discretization or a hierarchically improved predictor to reduce the total number of degrees of freedom. The introduced path finite elements were accompanied by the observation that the representation of motion paths is no longer unique in a discrete setting. Therefore, a regularization of the problem formulation with additional controls became necessary.

The Newton-Raphson method, which is applied as solution scheme for the nonlinear problem, can be interpreted as a second order optimization method using first and second derivatives of the objective function. Due to the particular structure of the functional, where a mechanical quantity is integrated over the motion path, these sensitivities can be calculated analytically. This merely requires the first and second derivative of exactly this underlying quantity. Using the internal energy, as it was done in this work, only quantities that are already available in nonlinear finite element software, such as the discrete internal forces and the tangent stiffness matrix, are required. But also in the case of many other possible functional definitions, which contain information about the internal stress or strain state of the structure, the first and second derivatives are often readily available in standard finite element procedures. This fact also opens up the possibility to employ any finite element formulation for the spatial discretization rather easily.

Consequently, the results computed with the novel motion design method are optimized motions between two geometric configurations with the objective of minimizing the chosen cost of deformation measure. Its implementation was verified by several benchmark problems for which the analytical solution is known. Additionally, the treatment of more complex motions, including instability and snap-through phenomena, with the prescribed functional was investigated in corresponding examples. The feasibility of the method for the design of inextensional deformations of shells was also demonstrated. The described procedure is inherently correlated with a large number of involved degrees of freedom. However, since the motion design method is primarily intended to give an idea and information on the first design concept of an adaptive structure, a coarse discretization of the spatial domain as well as the path is often appropriate. The results can then serve as a basis for subsequent high-fidelity analyses.

On closer inspection, it can be observed that the equilibrium conditions have not yet been considered in the basic motion design method. This means that the method yields,

as an additional output, the independent evolutions of the loads necessary to realize the resulting deformation path. For this purpose, the internal forces of the structure are recovered from the obtained displacement field in a postprocessing step. They are then set equal to the required actuation forces to guarantee an equilibrium state. However, this results in the major assumption that a point load can potentially be applied at every degree of freedom, which is typically not the case for most real-life engineering structures. Usually, only a certain, limited number of loads, load cases or actuators are available to realize the optimized motion. Therefore, the basic motion design method has been further extended by the introduction of additional constraints, which makes it more applicable for structures with limited actuation. This is accomplished by incorporating well-known constraint enforcement methods into the motion design concept, and thus, the forces at all degrees of freedom that are not accessible to actuation can be set to zero. The now additionally required first and second derivatives of the constraint equations, i. e., the affected internal forces, are given by the tangent stiffness matrix and its derivative, respectively. Despite being based on numerical differentiation, the exact value of the latter is obtained by the complex step method. Moreover, the conversion into a directional derivative helped to prevent a drastic decline in numerical efficiency. Further numerical experiments demonstrated the applicability of this approach. They showed that the constraints can be satisfied and that the functional value of constrained optimized motions increases compared to unconstrained optimized motions, as expected. Since actuator elements are commonly used as a type of load case for adaptive structures, they were also incorporated into the motion design method. For this reason, a new actuator element formulation, where a targeted actuator length change is introduced as an additional unknown parameter, has been developed. This actuator element formulation allowed a straightforward implementation into the presented method for motion design.

In the same way, other types of constraints have been applied to the optimized motion, such as enforcing a positive determinant of the tangent stiffness matrix with an inequality constraint. This guarantees a stable deformation process in a load-controlled scheme. The derivative of this much more intricate condition is again obtained numerically. In order to maintain a reasonable level of numerical efficiency, a modified Newton scheme is applied, where the second derivative of the constraint expression is omitted. However, the solution of the resulting extended system of equations might exhibit numerical instabilities in certain situations as the entries are characterized by a significant difference in magnitude caused by the value of the determinant. Nonetheless, the aim of this study was only to demonstrate the working principle of introducing such a constraint and its general feasibility has successfully been proven with simple structures. The described numerical problems still need to be tackled in further research if following this idea. Apart from that, both types of constraints can be combined. This allows designing an

optimized and stable motion that can be realized with a given limited number of loads, which has also been demonstrated with an exemplary structure.

Similarly, other inequality constraints on stress measures are thinkable. This way, it can be ensured that occuring stress values do not exceed any strength limits or requirements regarding local instability behavior, i. e., buckling of single truss elements, during the entire deformation process. Such constraints only require existing quantities in a nonlinear finite element code, and analytical sensitivities without the need for numerical differentiation can be obtained.

In summary, the new method of motion design developed in this thesis enables finding an optimized motion path for nonlinearly deforming adaptive structures in a purely formalized way based on the well-established concepts of variational calculus and finite element methods. It can be applied without providing any particular engineering expert knowledge besides the desired initial and target configurations of the structure. This supports an innovative design of motions for adaptive structures, where, for example, also instabilities can be exploited for the purpose of efficiency instead of avoiding them as it has conservatively been done in classical structural engineering. The basic method for motion design is particularly suitable for detecting and developing kinematic mechanisms as well as inextensional deformations of shells. This specific feature reveals a genuine potential for application to adaptive and deployable structures. For non-kinematic motions, the limiting assumptions regarding the actuation were handled and resolved by the introduction of constraints. Thus, the range of possible applications of the method has been extended to structures with a predefined actuation. These scenarios resemble actual technical implementations of real adaptive structures and further illustrate the potential of the new motion design approach for such complex design tasks.

Some further extensions of the motion design method have already been briefly studied. The initial and end geometry was always considered as being given so far. Even though large parts of the final deformed geometry were often left variable, the initial configuration was never part of the motion optimization process. This is different for the concept of designing compliant structures. However, both approaches, i. e., the design of compliant structures and the new motion design approach, aim at reducing the effort to deform a structure into a given target geometry. Therefore, a short study has been carried out, where shape optimization of the initial geometry and the motion design method were combined and different underlying objective functions were investigated. A further increase in efficiency, i. e., a reduction in the cost of deformation, could be achieved, which is an intriguing starting point for future research in this direction. Especially when considering the design of kinematic motions, which is already one of the major strengths of the presented method, new opportunities for improvement could be revealed. For example, an originally energy-inducing motion could be transferred into a

kinematic energy-free mechanism by the additional shape optimization step. The same principle also holds for inextensional deformations of shells. Consequently, shape optimization of the initial geometry could open up the possibility of finding an inextensional deformation through motion design. Pursuing this idea means that a procedure can be developed to identify geometries that are able to perform this kind of motion. However, more detailed studies on this topic need to be carried out.

In addition, the actuation can also be addressed to increase the efficiency of the motion. While the number and type of load cases has been predetermined so far, it can also be included in the design and optimization process. For this purpose, established algorithms for actuator placement have successfully been combined with the motion design method. Thus, the location of the most effective forces for the realization of energy-minimized motions could be found. However, this approach has been restricted to an actuation exclusively by point loads or discrete actuator elements. Future investigations could search for a relationship between these loads and identify possible clustering, for example. This would mean that fewer load cases have to be controlled independently to follow the optimized motion path of the structure. Moreover, other types of actuation, such as piezoelectric devices or shape-memory alloys, might be considered and studied as to whether they allow for realizing the desired shape change. It may, therefore, also become possible to search for the best type of actuation and not only for the best location of the actuating point loads.

Moreover, modifications of the underlying functional were presented. The motion design method was derived using the internal energy integrated over the motion path, i. e., the cost of deformation, as exemplary functional. Since this functional already contains relevant information about the structure, such as internal stress and strain states, it covers many types of possible demands for engineering structures. Furthermore, it offers the potential to be modified and varied using different weighting factors for stress or strain components or exponentiating of individual entries or entire functions. However, it is easily possible to replace the functional with other quantities. It was shown for structures with actuator elements that the actuation energy could be minimized, too. When a multistage motion incorporates a rigid body motion of an already pre-stressed structure, energy levels could be applied. Furthermore, a trivial functional was used to find the shortest deformation path. In contrast, the exponentiation of the internal energy within the motion integral enables a homogenization of the energy state. By combining the last two points, an approach for an incremental motion design process has been presented, which also allows the design of motions for more complex structures, which may exhibit convergence problems otherwise. In general, the underlying functional or objective function for the designed motion can be adapted to the requirements of the structure and application. The general applicability of the desired objective function

always has to be evaluated first, but it is precisely this flexibility that underlines and opens up further the potential of the new motion design approach.

Bibliography

ABDULLAH ET AL. 2001

    Abdullah, Makola M.; Richardson, Andy; Hanif, Jameel: Placement of sensors/actuators on civil structures using genetic algorithms. In: *Earthquake Engineering & Structural Dynamics* 30 (2001), No. 8, p. 1167–1184. – ISSN 0098-8847

ALBANESE AND RUBINACCI 1992

    Albanese, Raffaele; Rubinacci, Guglielmo: Numerical procedures for the solution of nonlinear electromagnetic problems. In: *IEEE Transactions on Magnetics* 28 (1992), No. 2, p. 1228–1231. – ISSN 00189464

ANONYMOUS 1697

    Anonymous: Epistola Missa ad Praenobilem Virum D. Carolum Montague Armigerum, Scaccarii Regii apud Anglos Cancellarium, et Societatis Regiae Praesidem: in qua Solvuntur duo Problemata Mathematica a Johanne Barnoullo Mathematico Celeberrimo Proposita - Letter sent to Charles Montague, President of the Royal Society, where two mathematical problems proposed by the celebrated Johann Bernoulli are solved. In: *Philosophical Transactions of the Royal Society of London* 19 (1697), p. 384–389

BAR-COHEN AND ANDERSON 2019

    Bar-Cohen, Yoseph; Anderson, Iain A.: Electroactive polymer (EAP) actuators—background review. In: *Mechanics of Soft Materials* 1 (2019), No. 1. – ISSN 2524-5600

BELYTSCHKO ET AL. 2014

    Belytschko, Ted; Liu, Wing K.; Moran, Brian; Elkhodary, Khalil I.: *Nonlinear finite elements for continua and structures.* Second edition. Hoboken, New Jersey : John Wiley & Sons Inc, 2014. – ISBN 978-1-118-63270-3

Bergman and Axehill 2018

Bergman, Kristoffer; Axehill, Daniel: Combining Homotopy Methods and Numerical Optimal Control to Solve Motion Planning Problems. In: *2018 IEEE Intelligent Vehicles Symposium (IV)*. Piscataway, NJ : IEEE, 2018. – ISBN 9781538644522

Bernoulli 1696

Bernoulli, Johann: Problema novum ad cujus solutionem Mathematici invitantur - New problem, to whose solution the mathematicians are invited. In: *Acta Eruditorum* (1696), p. 269

Bieze et al. 2018

Bieze, Thor M.; Largilliere, Frederick; Kruszewski, Alexandre; Zhang, Zhongkai; Merzouki, Rochdi; Duriez, Christian: Finite Element Method-Based Kinematics and Closed-Loop Control of Soft, Continuum Manipulators. In: *Soft robotics* 5 (2018), No. 3, p. 348–364

Boffi et al. 2013

Boffi, Daniele; Brezzi, Franco; Fortin, Michel: *Springer Series in Computational Mathematics*. Vol. 44: *Mixed finite element methods and applications*. Berlin and Heidelberg : Springer, 2013. – ISBN 978-3-642-36518-8

Campanile 2006

Campanile, Lucio F.: Shape-adaptive wings—the unfulfilled dream of flight. In: Liebe, R. (Eds.): *Flow Phenomena in Nature Volume 2* Vol. 2. WIT Press, 2006, p. 400–419. – ISBN 1-84564-095-0

Camprubí et al. 2004

Camprubí, Natalia; Bischoff, Manfred; Bletzinger, Kai-Uwe: Shape optimization of shells and locking. In: *Computers & Structures* 82 (2004), No. 29-30, p. 2551–2561. – ISSN 00457949

Carbone and Gomez-Bravo 2015

Carbone, Giuseppe; Gomez-Bravo, Fernando: *Motion and Operation Planning of Robotic Systems*. Vol. 29. Cham : Springer International Publishing, 2015. – ISBN 978-3-319-14704-8

Charpentier et al. 2017

Charpentier, Victor; Hannequart, Philippe; Adriaenssens, Sigrid; Baverel, Olivier; Viglino, Emmanuel; Eisenman, Sasha: Kinematic amplification strategies in plants and engineering. In: *Smart Materials and Structures* 26 (2017), No. 6, p. 063002. – ISSN 0964-1726

CHIRIKJIAN AND BURDICK 1994

Chirikjian, Gregory S.; Burdick, Joel W.: A hyper-redundant manipulator. In: *IEEE Robotics & Automation Magazine* 1 (1994), No. 4, p. 22–29. – ISSN 1070-9932

CLEGG 1970

Clegg, John C.: *Variationsrechnung.* Stuttgart : Teubner, 1970 (Teubner Studienbücher)

COTTRELL ET AL. 2009

Cottrell, J. A.; Hughes, Thomas J. R.; Bazilevs, Yuri: *Isogeometric Analysis: Toward Integration of CAD and FEA.* Chichester : Wiley a John Wiley and Sons Ltd. Publication, 2009. – ISBN 978-0-470-74873-2

DEL GROSSO AND BASSO 2010

Del Grosso, Andrea E.; Basso, Paolo: Adaptive building skin structures. In: *Smart Materials and Structures* 19 (2010), No. 12, p. 124011. – ISSN 0964-1726

ELBANHAWI AND SIMIC 2014

Elbanhawi, Mohamed; Simic, Milan: Sampling-Based Robot Motion Planning: A Review. In: *IEEE Access* 2 (2014), p. 56–77

ELSGOLC 1970

Elsgolc, Lev E.: *Variationsrechnung.* Mannheim : Bibliographisches Institut Mannheim, 1970 (BI-Hochschultaschenbücher). – ISBN 3411004312

EULER 1744

Euler, Leonhard: *Methodus inveniendi lineas curvas maximi minimive proprietate gaudentes, sive solutio problematis isoperimetrici latissimo sensu accepti – A method for finding curved lines enjoying properties of maximum or minimum, or solution of isoperimetric problems in the broadest accepted sense.* Lausannæ, Genevæ, apud Marcum-Michaelem Bousquet & socios, 1744

FIKE AND ALONSO 2011

Fike, Jeffrey; Alonso, Juan: The Development of Hyper-Dual Numbers for Exact Second-Derivative Calculations. In: *Aerospace Sciences Meetings.* Orlando, Florida, 2011. – ISBN 978-1-60086-950-1

FORTERRE ET AL. 2005

Forterre, Yoël; Skotheim, Jan M.; Dumais, Jacques; Mahadevan, L.: How the Venus flytrap snaps. In: *Nature* 433 (2005), No. 7024, p. 421–425. – ISSN 1476-4687

FRECKER ET AL. 1997
Frecker, Mary I.; Ananthasuresh, Gondi K.; Nishiwaki, Shinji; Kikuchi, Noboru; Kota, Sridhar: Topological Synthesis of Compliant Mechanisms Using Multi-Criteria Optimization. In: *Journal of Mechanical Design* 119 (1997), No. 2, p. 238–245. – ISSN 1050-0472

FRIEDMAN AND IBRAHIMBEGOVIC 2013
Friedman, Noemi; Ibrahimbegovic, Adnan: Overview of Highly Flexible, Deployable Lattice Structures Used in Architecture and Civil Engineering Undergoing Large Displacements. In: *YBL Journal of Built Environment* 1 (2013), No. 1, p. 85–103. – ISSN 2063-997X

FUJIWARA ET AL. 1993
Fujiwara, Koji; Nakata, Takao; Okamoto, Noriaki; Muramatsu, Kazuhiro: Method for determining relaxation factor for modified Newton-Raphson method. In: *IEEE Transactions on Magnetics* 29 (1993), No. 2, p. 1962–1965. – ISSN 00189464

GALILEI 1638
Galilei, Galileo: *Discorsi e dimostrazioni matematiche intorno a due nuove scienze – Discourses and Mathematical Demonstrations Relating to Two New Sciences: Discourses and Mathematical Demonstrations Relating to Two New Sciences.* Leiden : Elzevier, 1638

GELFAND AND FOMIN 2000
Gelfand, Izrail M.; Fomin, Sergej V.: *Calculus of variations.* Mineola, N.Y. : Dover Publications, 2000

GÖPPERT AND STEIN 2007
Göppert, Knut; Stein, Michael: A Spoked Wheel Structure for the World's largest Convertible Roof – The New Commerzbank Arena in Frankfurt, Germany. In: *Structural Engineering International* 17 (2007), No. 4, p. 282–287. – ISSN 1016-8664

GRAELLS ROVIRA AND MIRATS TUR 2009
Graells Rovira, Albert; Mirats Tur, Josep M.: Control and simulation of a tensegrity-based mobile robot. In: *Robotics and Autonomous Systems* 57 (2009), No. 5, p. 526–535. – ISSN 09218890

GUPTA ET AL. 2010
Gupta, Vivek; Sharma, Manu; Thakur, Nagesh: Optimization Criteria for Optimal Placement of Piezoelectric Sensors and Actuators on a Smart Structure: A Technical Review. In: *Journal of Intelligent Material Systems and Structures* 21 (2010), No. 12, p. 1227–1243. – ISSN 1045-389X

HASSE AND CAMPANILE 2009

Hasse, Alexander; Campanile, Lucio F.: Design of compliant mechanisms with selective compliance. In: *Smart Materials and Structures* 18 (2009), No. 11, p. 115016. – ISSN 0964-1726

HOLZAPFEL 2010

Holzapfel, Gerhard A.: *Nonlinear solid mechanics: A continuum approach for engineering.* Repr. Chichester : Wiley, 2010. – ISBN 978-0-471-82319-3

HOUSNER ET AL. 1997

Housner, George W.; Bergman, L. A.; Caughey, T. K.; Chassiakos, A. G.; Claus, R. O.; Masri, Sami F.; Skelton, R. E.; Soong, T. T.; Spencer, Billie F.; Yao, J. T. P.: Structural Control: Past, Present, and Future. In: *Journal of Engineering Mechanics* 123 (1997), No. 9, p. 897–971

HUGHES 2000

Hughes, Thomas J. R.: *The finite element method: Linear static and dynamic finite element analysis.* Reprint. Mineola, NY : Dover, 2000. – ISBN 0-486-41181-8

IBRAHIMBEGOVIC ET AL. 2004

Ibrahimbegovic, Adnan; Knopf-Lenoir, C.; Kučerov, A.; Villon, P.: Optimal design and optimal control of structures undergoing finite rotations and elastic deformations. In: *International Journal for Numerical Methods in Engineering* 61 (2004), No. 14, p. 2428–2460. – ISSN 0029-5981

IRSCHIK 2002

Irschik, Hans: A review on static and dynamic shape control of structures by piezoelectric actuation. In: *Engineering Structures* 24 (2002), No. 1, p. 5–11. – ISSN 01410296

KARAMAN AND FRAZZOLI 2010

Karaman, Sertac; Frazzoli, Emilio: Optimal kinodynamic motion planning using incremental sampling-based methods. In: *49th IEEE Conference on Decision and Control (CDC)*, IEEE, 2010, p. 7681–7687. – ISBN 978-1-4244-7745-6

KIENDL ET AL. 2009

Kiendl, Josef; Bletzinger, Kai-Uwe; Linhard, Johannes; Wüchner, Roland: Isogeometric shell analysis with Kirchhoff–Love elements. In: *Computer Methods in Applied Mechanics and Engineering* 198 (2009), No. 49-52, p. 3902–3914. – ISSN 0045-7825

KMET AND MOJDIS 2015

Kmet, Stanislav; Mojdis, Marek: Adaptive Cable Dome. In: *Journal of Structural Engineering* 141 (2015), No. 9, p. 04014225. – ISSN 0733-9445

KNIPPERS ET AL. 2013

Knippers, Jan; Jungjohann, Hauke; Scheible, Florian; Oppe, Matthias: Bio-inspirierte kinetische Fassade für den Themenpavillon "One Ocean" EXPO 2012 in Yeosu, Korea. In: *Bautechnik* 90 (2013), No. 6, p. 341–347. – ISSN 09328351

KNIPPERS AND SCHLAICH 2000

Knippers, Jan; Schlaich, Jörg: Folding Mechanism of the Kiel Hörn Footbridge, Germany. In: *Structural Engineering International* 10 (2000), No. 1, p. 50–53. – ISSN 1016-8664

KNIPPERS AND SPECK 2012

Knippers, Jan; Speck, Thomas: Design and construction principles in nature and architecture. In: *Bioinspiration & Biomimetics* 7 (2012), No. 1, p. 015002

KNOBLOCH 2012

Knobloch, Eberhard: Leibniz and the Brachistochrone. In: *Documenta Mathematica* (2012)

KORKMAZ 2011

Korkmaz, Sinan: A review of active structural control: challenges for engineering informatics. In: *Computers & Structures* 89 (2011), No. 23-24, p. 2113–2132. – ISSN 00457949

KÖRNER ET AL. 2018

Körner, Axel; Born, Larissa; Mader, Anja; Sachse, Renate; Saffarian, Sam; Westermeier, Anna S.; Poppinga, Simon; Bischoff, Manfred; Gresser, Götz T.; Milwich, Markus; Speck, Thomas; Knippers, Jan: Flectofold—a biomimetic compliant shading device for complex free form facades. In: *Smart Materials and Structures* 27 (2018), No. 1, p. 017001. – ISSN 0964-1726

KRUSKAL 1956

Kruskal, Joseph B.: On the Shortest Spanning Subtree of a Graph and the Traveling Salesman Problem. In: *Proceedings of the American Mathematical Society* 7 (1956), No. 1, p. 48. – ISSN 00029939

LAN AND CHENG 2008

Lan, Chao-Chieh; Cheng, Yung-Jen: Distributed Shape Optimization of Compliant Mechanisms Using Intrinsic Functions. In: *Journal of Mechanical Design* 130 (2008), No. 7. – ISSN 1050-0472

LAVALLE 2006

LaValle, Steven M.: *Planning algorithms.* Cambridge : Cambridge University Press, 2006. – ISBN 978-0-511-54687-7

Leibniz 1697

Leibniz, Gottfried: G.G.L. Communicatio suae pariter, duarumque alienarum ad edendum sibi primum a Dn. Jo. Bernoullio, deinde a Dn. Marchione Hospitalio communicatarum solutionum problematis curvae celerrimi descensus a Dn. Jo. Bernoullio Geometris publice propositi, una cum solutione sua problematis alterius ab eodem postea propositi – Leibniz' presentation of his solution and of those of J. Bernoulli and of Marquis de l'Hospital, to the problem published by Jo. Bernoulli, and at the same time, the solutions to his second problem. In: *Acta Eruditorum* (1697), p. 205–225

Liberzon 2012

Liberzon, Daniel: *Calculus of variations and optimal control theory: A concise introduction.* Princeton, NJ : Princeton Univ. Press, 2012. – ISBN 9780691151878

Lienhard et al. 2011

Lienhard, Julian; Schleicher, Simon; Poppinga, Simon; Masselter, Tom; Milwich, Markus; Speck, Thomas; Knippers, Jan: Flectofin: a hingeless flapping mechanism inspired by nature. In: *Bioinspiration & Biomimetics* 6 (2011), No. 4, p. 045001

Lu and Kota 2003

Lu, Kerr-Jia; Kota, Sridhar: Design of Compliant Mechanisms for Morphing Structural Shapes. In: *Journal of Intelligent Material Systems and Structures* 14 (2003), No. 6, p. 379–391. – ISSN 1045-389X

Marsden and Hughes 2012

Marsden, Jerrold E.; Hughes, Thomas J. R.: *Mathematical Foundations of Elasticity.* Newburyport : Dover Publications, 2012 (Dover Civil and Mechanical Engineering). – ISBN 0486678652

Martins et al. 2003

Martins, Joaquim R. R. A.; Sturdza, Peter; Alonso, Juan: The complex-step derivative approximation. In: *ACM Transactions on Mathematical Software (TOMS)* 29 (2003), No. 3, p. 245–262. – ISSN 0098-3500

Masching and Bletzinger 2016

Masching, Helmut; Bletzinger, Kai-Uwe: Parameter free structural optimization applied to the shape optimization of smart structures. In: *Finite Elements in Analysis and Design* 111 (2016), p. 33–45. – ISSN 0168874X

Masic and Skelton 2005

Masic, Milenko; Skelton, Robert E.: Path Planning and Open-Loop Shape Control of Modular Tensegrity Structures. In: *Journal of Guidance, Control, and Dynamics* 28 (2005), No. 3, p. 421–430. – ISSN 0731-5090

MATHWORKS, INC. 2018
The Mathworks, Inc. (Veranst.): *MATLAB version 9.5.0.944444 (R2018b).* 2018

MAUTE AND REICH 2006
Maute, Kurt; Reich, G. W.: Integrated Multidisciplinary Topology Optimization Approach to Adaptive Wing Design. In: *Journal of Aircraft* 43 (2006), No. 1, p. 253–263. – ISSN 0021-8669

MOHD JANI ET AL. 2014
Mohd Jani, Jaronie; Leary, Martin; Subic, Aleksandar; Gibson, Mark A.: A review of shape memory alloy research, applications and opportunities. In: *Materials & Design (1980-2015)* 56 (2014), p. 1078–1113. – ISSN 02613069

NEUHAEUSER ET AL. 2013
Neuhaeuser, Stefan; Weickgenannt, Martin; Witte, Christoph; Haase, Walter; Sobek, Werner: Stuttgart smartshell - A full scale prototype of an adaptive shell structure. In: *Journal of the International Association for Shell and Spatial Structures* 54 (2013), No. 178, p. 259–270. – ISSN 1996-9015

NOCEDAL AND WRIGHT 2006
Nocedal, Jorge; Wright, Stephen J.: *Numerical Optimization.* Second Edition. New York, NY : Springer Science+Business Media LLC, 2006 (Springer Series in Operations Research and Financial Engineering). – ISBN 978-0-387-30303-1

OH AND KOTA 2009
Oh, Young S.; Kota, Sridhar: Synthesis of Multistable Equilibrium Compliant Mechanisms Using Combinations of Bistable Mechanisms. In: *Journal of Mechanical Design* 131 (2009), No. 2. – ISSN 1050-0472

PAGITZ AND BOLD 2013
Pagitz, Markus; Bold, Jens: Shape-changing shell-like structures. In: *Bioinspiration & Biomimetics* 8 (2013), No. 1, p. 016010

PELLEGRINO 2015
Pellegrino, Sergio: Folding and Deployment of Thin Shell Structures. In: Bigoni, Davide (Eds.): *Extremely Deformable Structures* Vol. 562. Vienna : Springer Vienna, 2015, p. 179–267

POPPINGA ET AL. 2020
Poppinga, Simon; Correa, David; Bruchmann, Bernd; Menges, Achim; Speck, Thomas: Plant movements as concept generators for the development of biomimetic compliant mechanisms. In: *Integrative and Comparative Biology* (2020)

POPPINGA ET AL. 2016

Poppinga, Simon; Körner, Axel; Sachse, Renate; Born, Larissa; Westermeier, Anna S.; Hesse, Linnea; Knippers, Jan; Bischoff, Manfred; Gresser, Götz T.; Speck, Thomas: Compliant Mechanisms in Plants and Architecture. In: Knippers, Jan; Nickel, Klaus G.; Speck, Thomas (Eds.): *Biomimetic Research for Architecture and Building Construction* Vol. 8. Cham : Springer International Publishing, 2016, p. 169–193. – ISBN 978-3-319-46372-8

PREUMONT 2011

Preumont, André: *Solid mechanics and its applications.* Vol. 179: *Vibration control of active structures: An introduction.* 3. ed. Berlin : Springer, 2011. – ISBN 978-94-007-2032-9

RAJA AND NARAYANAN 2009

Raja, M. G.; Narayanan, S.: Simultaneous Optimization of Structure and Control of Smart Tensegrity Structures. In: *Journal of Intelligent Material Systems and Structures* 20 (2009), No. 1, p. 109–117. – ISSN 1045-389X

REKSOWARDOJO ET AL. 2020

Reksowardojo, Arka P.; Senatore, Gennaro; Smith, Ian F. C.: Design of Structures That Adapt to Loads through Large Shape Changes. In: *Journal of Structural Engineering* 146 (2020), No. 5, p. 04020068. – ISSN 0733-9445

RUS AND TOLLEY 2015

Rus, Daniela; Tolley, Michael T.: Design, fabrication and control of soft robots. In: *Nature* 521 (2015), No. 7553, p. 467–475. – ISSN 1476-4687

SACHSE AND BISCHOFF 2020

Sachse, Renate; Bischoff, Manfred: A variational formulation for motion design of adaptive compliant structures. In: *International Journal for Numerical Methods in Engineering* 122 (2020), No. 4, p. 972–1000

SACHSE ET AL. 2021a

Sachse, Renate; Geiger, Florian; Bischoff, Manfred: Constrained motion design with distinct actuators and motion stabilization. In: *International Journal for Numerical Methods in Engineering* 122 (2021), No. 11, p. 2712–2732

SACHSE ET AL. 2021b

Sachse, Renate; Geiger, Florian; von Scheven, Malte; Bischoff, Manfred: Motion design with efficient actuator placement for adaptive structures that perform large deformations. In: *Frontiers in Built Environment* (2021)

SACHSE ET AL. 2020

Sachse, Renate; Westermeier, Anna S.; Mylo, Max; Nadasdi, Joey; Bischoff, Manfred; Speck, Thomas; Poppinga, Simon: Snapping mechanics of the Venus flytrap (*Dionaea muscipula*). In: *Proceedings of the National Academy of Sciences of the United States of America* 117 (2020), No. 27

SAGGERE AND KOTA 1999

Saggere, Laxminarayana; Kota, Sridhar: Static Shape Control of Smart Structures Using Compliant Mechanisms. In: *AIAA Journal* 37 (1999), No. 5, p. 572–578. – ISSN 0001-1452

SANTER AND PELLEGRINO 2008

Santer, Matthew; Pellegrino, Sergio: Compliant multistable structural elements. In: *International Journal of Solids and Structures* 45 (2008), No. 24, p. 6190–6204. – ISSN 00207683

SANTER AND PELLEGRINO 2009

Santer, Matthew; Pellegrino, Sergio: Topological Optimization of Compliant Adaptive Wing Structure. In: *AIAA Journal* 47 (2009), No. 3, p. 523–534. – ISSN 0001-1452

SARGENT 2000

Sargent, Roger W. H.: Optimal control. In: *Journal of Computational and Applied Mathematics* 124 (2000), No. 1-2, p. 361–371. – ISSN 03770427

SAXENA AND ANANTHASURESH 2000

Saxena, Anupam; Ananthasuresh, Gondi K.: On an optimal property of compliant topologies. In: *Structural and Multidisciplinary Optimization* 19 (2000), No. 1, p. 36–49. – ISSN 1615-147X

SCHELLBACH 1851

Schellbach, Karl: Probleme der Variationsrechnung. In: *Crelle's Journal für die reine und angewandte Mathematik* 41 (1851), p. 293–363 + 1 table

SENATORE 2018

Senatore, Gennaro: Designing and Prototyping Adaptive Structures—An Energy-Based Approach Beyond Lightweight Design. In: Bier, Henriette (Eds.): *Robotic Building.* Cham : Springer International Publishing, 2018 (Springer Series in Adaptive Environments), p. 169–189. – ISBN 978-3-319-70865-2

SENATORE ET AL. 2018

Senatore, Gennaro; Duffour, Philippe; Winslow, Pete; Wise, Chris: Shape control and whole-life energy assessment of an 'infinitely stiff' prototype adaptive structure. In: *Smart Materials and Structures* 27 (2018), No. 1, p. 015022. – ISSN 0964-1726

SIGMUND 1997

Sigmund, Ole: On the Design of Compliant Mechanisms Using Topology Optimization*. In: *Mechanics of Structures and Machines* 25 (1997), No. 4, p. 493–524. – ISSN 0890-5452

SIMO AND RIFAI 1990

Simo, Juan C.; Rifai, M. S.: A class of mixed assumed strain methods and the method of incompatible modes. In: *International Journal for Numerical Methods in Engineering* 29 (1990), No. 8, p. 1595–1638. – ISSN 0029-5981

SOBEK 2016

Sobek, Werner: Ultra-lightweight construction. In: *International Journal of Space Structures* 31 (2016), No. 1, p. 74–80. – ISSN 0266-3511

SOFLA ET AL. 2009

Sofla, Aarash Y. N.; Elzey, Dana M.; Wadley, Haydn N. G.: Shape morphing hinged truss structures. In: *Smart Materials and Structures* 18 (2009), No. 6, p. 065012. – ISSN 0964-1726

SPENCER AND NAGARAJAIAH 2003

Spencer, Billie F.; Nagarajaiah, Satish: State of the Art of Structural Control. In: *Journal of Structural Engineering* 129 (2003), No. 7, p. 845–856. – ISSN 0733-9445

STEIN 2018

Stein, Erwin: Milestones of Direct Variational Calculus and its Analysis from the 17th Century until today and beyond – Mathematics meets Mechanics – with restriction to linear elasticity. In: *Computer Assisted Methods in Engineering and Science* 25 (2018), No. 4, p. 141–225

SUSSMANN AND WILLEMS 1997

Sussmann, Hector J.; Willems, Jan C.: 300 years of optimal control: from the brachystochrone to the maximum principle. In: *IEEE Control Systems* 17 (1997), No. 3, p. 32–44. – ISSN 1066-033X

SYCHTERZ AND SMITH 2018

Sychterz, Ann C.; Smith, Ian F. C.: Deployment and Shape Change of a Tensegrity Structure Using Path-Planning and Feedback Control. In: *Frontiers in Built Environment* 4 (2018)

VAN DE WIJDEVEN AND DE JAGER 2005

van de Wijdeven, Jeroen; de Jager, Bram: Shape change of tensegrity structures: design and control. In: *Proceedings of the 2005, American Control Conference, 2005*, IEEE, 2005, p. 2522–2527. – ISBN 0-7803-9098-9

VASISTA ET AL. 2012
   Vasista, Srinivas; Tong, Liyong; Wong, K. C.: Realization of Morphing Wings: A
   Multidisciplinary Challenge. In: *Journal of Aircraft* 49 (2012), No. 1, p. 11–28. –
   ISSN 0021-8669

VEUVE ET AL. 2017
   Veuve, Nicolas; Sychterz, Ann C.; Smith, Ian F. C.: Adaptive control of a deployable
   tensegrity structure. In: *Engineering Structures* 152 (2017), p. 14–23. – ISSN
   01410296

WAGNER ET AL. 2018
   Wagner, Julia L.; Gade, Jan; Heidingsfeld, Michael; Geiger, Florian; von Scheven,
   Malte; Böhm, Michael; Bischoff, Manfred; Sawodny, Oliver: On steady-state dis-
   turbance compensability for actuator placement in adaptive structures. In: *at -
   Automatisierungstechnik* 66 (2018), No. 8, p. 591–603. – ISSN 0178-2312

WEBSTER AND JONES 2010
   Webster, Robert J.; Jones, Bryan A.: Design and Kinematic Modeling of Constant
   Curvature Continuum Robots: A Review. In: *The International Journal of Robotics
   Research* 29 (2010), No. 13, p. 1661–1683. – ISSN 0278-3649

WEIDNER ET AL. 2018
   Weidner, Stefanie; Kelleter, Christian; Sternberg, Paula; Haase, Walter; Geiger, Flo-
   rian; Burghardt, Timon; Honold, Clemens; Wagner, Julia; Böhm, Michael; Bischoff,
   Manfred; Sawodny, Oliver; Binz, Hansgeorg: The implementation of adaptive el-
   ements into an experimental high-rise building. In: *Steel Construction* 11 (2018),
   No. 2, p. 109–117. – ISSN 18670520

WESTERMEIER ET AL. 2018
   Westermeier, Anna S.; Sachse, Renate; Poppinga, Simon; Vögele, Philipp; Adamec,
   Lubomir; Speck, Thomas; Bischoff, Manfred: How the carnivorous waterwheel plant
   (Aldrovanda vesiculosa) snaps. In: *Proceedings of the Royal Society B. Biological
   sciences* 285 (2018), No. 1878

YEKUTIELI ET AL. 2005
   Yekutieli, Yoram; Sagiv-Zohar, Roni; Aharonov, Ranit; Engel, Yaakov; Hochner,
   Binyamin; Flash, Tamar: Dynamic model of the octopus arm. I. Biomechanics of
   the octopus reaching movement. In: *Journal of neurophysiology* 94 (2005), No. 2,
   p. 1443–1458. – ISSN 0022-3077

ZHANG ET AL. 2017
   Zhang, Jiaying; Zhang, Chen; Hao, Lin; Nie, Rui; Qiu, Jinhao: Exploiting the

instability of smart structure for reconfiguration. In: *Applied Physics Letters* 111 (2017), No. 6, p. 064102. – ISSN 0003-6951

ZIENKIEWICZ AND TAYLOR 2006

Zienkiewicz, Olgierd C.; Taylor, Robert L.: *The finite element method.* 6. ed., repr. Amsterdam : Elsevier Butterworth-Heinemann, 2006. – ISBN 0-7506-6321-9

ZUK AND CLARK 1970

Zuk, William; Clark, Roger H.: *Kinetic Architecture.* New York : Van Nostrand Reinhold, 1970

Lebenslauf

Persönliche Angaben:

Name:	Renate Sachse, geb. Lehmann
Geburtsdatum:	9. Dezember 1989
Geburtsort:	Stuttgart

Schulische Ausbildung:

1996 – 2000	Steinbachschule, Stuttgart-Büsnau
2000 – 2008	Hegel-Gymnasium, Stuttgart-Vaihingen
2008	Allgemeine Hochschulreife

Akademischer Werdegang:

2008 – 2011	Bachelorstudium des Bauingenieurwesens an der Universität Stuttgart
2011	Bachelor of Science (B. Sc.)
2012	Auslandsstudium an der École Spéciale des Travaux Publics, du bâtiment et de l'industrie (ESTP), Paris
2012 – 2014	Masterstudium des Bauingenieurwesens an der Universität Stuttgart
2014	Master of Science (M. Sc.)
2014	Emil-Mörsch-Studienpreis für besondere Studienleistungen

Beruflicher Werdegang:

2009 – 2010	Werkstudententätigkeit bei Werner Sobek Stuttgart
2011	Praktikum bei Foster & Partners, London
2012 – 2013	Werkstudententätigkeit bei Werner Sobek Stuttgart
seit 2015	Akademische Mitarbeiterin am Institut für Baustatik und Baudynamik der Universität Stuttgart

Berichte des Instituts für Baustatik und Baudynamik der Universität Stuttgart

1 (1983) P. Osterrieder:
Traglastberechnung von räumlichen Stabwerken bei großen Verformungen mit finiten Elementen.

2 (1983) T. A. Kompfner:
Ein finites Elementmodell für die geometrisch und physikalisch nichtlineare Berechnung von Stahlbetonschalen.

3 (1983) A. Diack:
Beitrag zur Stabilität diskret längsversteifter Kreiszylinderschalen unter Axialdruck.

4 (1984) A. Burmeister, F.W. Bornscheuer, E. Ramm:
Traglasten von Kugelbehältern mit Stutzen und Formabweichungen unter Innendruck und Stützenlängskraft.

5 (1985) H. Stegmüller:
Grenzlastberechnungen flüssigkeitsgefüllter Schalen mit 'degenerierten' Schalenelementen.

6 (1987) A. Burmeister:
Dynamische Stabilität nach der Methode der finiten Elemente mit Anwendungen auf Kugelschalen.

7 (1987) G. Kammler:
Ein finites Elementmodell zur Berechnung von Trägern und Stützen mit offenem, dünnwandigem Querschnitt unter Berücksichtigung der Interaktion zwischen globalem und lokalem Versagen.

8 (1988) A. Matzenmiller:
Ein rationales Lösungskonzept für geometrisch und physikalisch nichtlineare Strukturberechnungen.

9 (1989) D. Tao:
Die Technik der reduzierten Basis bei nichtlinearen finiten Element–Berechnungen.

10 (1989) K. M. Weimar:
Ein nichtlineares Balkenelement mit Anwendung als Längssteifen axialbelasteter Kreiszylinder.

11 (1990) K.-U. Bletzinger:
Formoptimierung von Flächentragwerken.

12 (1990) S. Kimmich:
Strukturoptimierung und Sensibilitätsanalyse mit finiten Elementen.

13 (1991) U. Andelfinger:
Untersuchungen zur Zuverlässigkeit hybrid-gemischter Finiter Elemente für Flächentragwerke.

14 (1992) N. Büchter:
Zusammenführung von Degenerationskonzept und Schalentheorie bei endlichen Rotationen.

15 (1992) T. J. Hofmann:
Beitrag zur verfeinerten Balkentheorie.

16 (1994) D. de Mesquita Roehl:
Zur Berechnung von großen elastoplastischen Deformationen bei Flächentragwerken und Kontinua.

17 (1994) R. Reitinger:
Stabilität und Optimierung imperfektionsempfindlicher Tragwerke.

18 (1995) R. L. M. Suanno:
Ein dreidimensionales Simulationsmodell für Stahlbeton mit Plastizität und Schädigung.

19 (1995) M. Braun:
Nichtlineare Analysen von geschichteten, elastischen Flächentragwerken.

20 (1996) N. Rehle:
Adaptive Finite Element Verfahren bei der Analyse von Flächentragwerken.

21 **(1996)** **C. Haußer:**
Effiziente Dreieckselemente für Flächentragwerke.

22 **(1996)** **D. Kuhl:**
Stabile Zeitintegrationsalgorithmen in der nichtlinearen Elastodynamik
dünnwandiger Tragwerke.

23 **(1998)** **H. Schmidts:**
Zur effizienten Modellierung und Analyse von Hochhaustragwerken.

24 **(1998)** **H. Wang:**
Interaktion des lokalen und globalen Stabilitätsverhaltens dünnwandiger Stäbe.

25 **(1998)** **K. Maute:**
Topologie- und Formoptimierung von dünnwandigen Tragwerken.

26 **(1998)** **B. Maurer:**
Karl Culmann und die graphische Statik.

27 **(1998)** **F. Cirak:**
Adaptive Finite-Element-Methoden bei der nichtlinearen Analyse von
Flächentragwerken.

28 **(1998)** **M. Trautz:**
Zur Entwicklung von Form und Struktur historischer Gewölbe aus der
Sicht der Statik.

29 **(1999)** **H. Menrath:**
Numerische Simulation des nichtlinearen Tragverhaltens von Stahl-
verbundträgern.

30 **(1999)** **M. Bischoff:**
Theorie und Numerik einer dreidimensionalen Schalenformulierung.

31 **(1999)** **W. A. Wall:**
Fluid-Struktur-Interaktion mit stabilisierten Finiten Elementen.

32 **(2000)** **E. Kuhl:**
Numerische Modelle für kohäsive Reibungsmaterialien.

33 (2001) A. Maute:
Fehlerkontrolle bei Finite-Element-Methoden in der linearen Strukturdynamik.

34 (2001) S. Schwarz:
Sensitivitätsanalyse und Optimierung bei nichtlinearem Strukturverhalten.

35 (2001) A. Haufe:
Dreidimensionale Simulation bewehrter Flächentragwerke aus Beton mit der Plastizitätstheorie.

36 (2001) D. P. Mok:
Partitionierte Lösungsansätze in der Strukturdynamik und der Fluid-Struktur-Interaktion.

37 (2002) H. Steeb:
Fehlerschätzer für FE-Berechnungen bei entfestigenden Materialien.

38 (2002) K. Krausz:
Tragverhalten gemauerter Tonnengewölbe mit Stichkappen.

39 (2002) M. Hörmann:
Nichtlineare Versagensanalyse von Faserverbundstrukturen.

40 (2003) V. Gravemeier:
The Variational Multiscale Method for Laminar and Turbulent Incompressible Flow.

41 (2004) R. Kemmler:
Stabilität und große Verschiebungen in der Topologie- und Formoptimierung.

42 (2004) G. A. D'Addetta:
Discrete Models for Cohesive Frictional Materials.

43 (2004) M. Gee:
Effiziente Lösungsstrategien in der nichtlinearen Schalenmechanik.

44 (2004) T. Erhart:
Strategien zur numerischen Modellierung transienter Impaktvorgänge bei nichtlinearem Materialverhalten.

45 (2005) M. Leukart:
Kombinierte anisotrope Schädigung und Plastizität bei kohäsiven Reibungsmaterialien.

46 (2006) F. Huber:
Nichtlineare dreidimensionale Modellierung von Beton- und Stahlbetontragwerken.

47 (2007) A. Lipka:
Verbesserter Materialeinsatz innovativer Werkstoffe durch die Topologieoptimierung.

48 (2007) A. S. Hund:
Hierarchische Mehrskalenmodellierung des Versagens von Werkstoffen mit Mikrostruktur.

49 (2007) S. Hartmann:
Kontaktanalyse dünnwandiger Strukturen bei großen Deformationen.

50 (2007) T. M. Hettich:
Diskontinuierliche Modellierung zur Versagensanalyse von Verbundmaterialien.

51 (2007) C. Förster:
Robust methods for fluid-structure interaction with stabilised finite elements.

52 (2009) M. von Scheven:
Effiziente Algorithmen für die Fluid-Struktur-Wechselwirkung.

53 (2010) J. Kato:
Material Optimization for Fiber Reinforced Composites applying a Damage Formulation.

54 **(2010)** **C. F. Hilchenbach:**
Optimierung von Mehrphasenstrukturen mit lokalem Schädigungsverhalten.

55 **(2011)** **I. Bruss:**
Dreidimensionale Schädigungsmodellierung heterogener Materialien.

56 **(2012)** **B. J. Schneider:**
Polygonale diskrete Elemente zur Modellierung heterogener Materialien.

57 **(2012)** **R. Etlender:**
Modellierung und Simulation der Wellenausbreitung in flexiblen hydraulischen Leitungen.

58 **(2012)** **T. Cichosz:**
Stabile und konsistente Kontaktmodellierung in Raum und Zeit.

59 **(2013)** **R. Echter:**
Isogeometric analysis of shells.

60 **(2013)** **A. Tkachuk:**
Variational methods for consistent singular and scaled mass matrices.

61 **(2013)** **J. Irslinger:**
Mechanische Grundlagen und Numerik dreidimensionaler Schalenelemente.

62 **(2014)** **T. E. Pohl:**
Adaptive Methoden zur Pfadverfolgung bei Entfestigung.

63 **(2014)** **A. Sorg:**
Adaptive diskret-kontinuierliche Modellierung von Materialien mit Mikrostruktur.

64 **(2015)** **M. E. Matzen:**
Isogeometrische Modellierung und Diskretisierung von Kontaktproblemen.

65 (2016) V. M. Effinger:
Finite nichtlinear viskoelastische Modellierung offenzelliger Polymerschäume.

66 (2017) C. M. Wilking:
Effiziente Integration und verbesserte Kontaktspannungen für duale Mortar-Formulierungen.

67 (2018) B. Oesterle:
Intrinsisch lockingfreie Schalenformulierungen.

68 (2018) F. Neukamm:
Lokalisierung und Versagen von Blechstrukturen.

69 (2019) A.-K. Schäuble:
Variationally consistent inertia templates for speed-up and customization in explicit dynamics.

70 (2019) T. E. Willerding:
Multiscale simulation of phase transformation in metals.

71 (2020) S. Roth:
Algorithmen zur nichtlinearen Stabilitätsanalyse dünnwandiger Strukturen.

Renate Sachse

In this thesis, a novel approach to support the design of motions for adaptive structures is presented and gradually developed: the so-called method of motion design. It is based on the observation that, depending on the control of the actuation, the same deformation state of a structure can be reached through various motion processes. The method of motion design allows to calculate optimal deformation paths with defined properties between the initial geometry and a given deformed end geometry of a structure in a formalized way.

In order to motivate the efficiency of a movement and to make it mathematically quantifiable, the so-called cost of deformation is introduced as an exemplary target value based on the strain energy. By integration over the deformation path, the motion process is considered in its entirety in this optimization problem. The method of motion design is developed based on a variational formulation using the cost of deformation as underlying functional and the displacement field as the unknown function. One of the decisive features in this work is the discretization of the motion path, i.e., the deformation process.

Due to the special structure of the functional with the integration of the strain energy, analytical sensitivities can be calculated by using quantities that are generally available in finite element software. The presented basic method is particularly well suited for the identification and design of kinematic and energy-minimal motion mechanisms, which emphasizes the potential for application to deployable shape changing structures.

The motion design method is extended by the use of constraints such that the actuation can be prescribed, e.g., by actuator elements, or the entire motion can be stabilized.

Finally, possibilities for enhancement of the motion design method and combinations with other methods to increase the efficiency of adaptive structures are investigated. They include a combination with shape optimization of the initial geometry, an integration within an actuator placement algorithm and variations of the underlying objective function.